

PROCEEDINGS OF THE SIXTH ANNUAL PACIFIC CLIMATE (PACLIM) WORKSHOP

Asilomar, California – March 5-8, 1989

Edited by
Julio L. Betancourt and Ana M. MacKay

Technical Report 23
of the
Interagency Ecological Studies Program
for the
Sacramento-San Joaquin Estuary

February 1990

Copies of this report may be obtained from:

**California Department of Water Resources
P.O. Box 942836
Sacramento, CA 94236-0001**

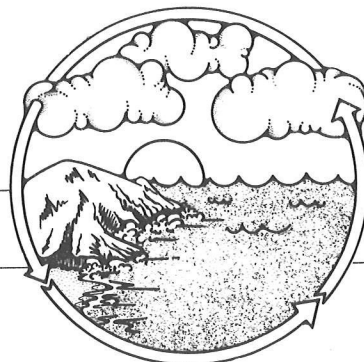
PROCEEDINGS OF THE SIXTH ANNUAL PACIFIC CLIMATE (PACLIM) WORKSHOP

Asilomar, California – March 5-8, 1989

Edited by
Julio L. Betancourt and Ana M. MacKay

Technical Report 23
of the
Interagency Ecological Studies Program
for the
Sacramento-San Joaquin Estuary

PACLIM



**Climate Variability
of the
Eastern North Pacific
and
Western North America**

The Sixth Annual Pacific Climate Workshop was sponsored by the

U.S. Geological Survey

Monterey Bay Aquarium Research Institute

National Oceanic and Atmospheric Administration,
Geophysical Data Center

Environmental Protection Agency, Global Change Program

California Department of Water Resources

Publication of this proceedings has been sponsored by the

Interagency Ecological Studies Program
for the
Sacramento-San Joaquin Estuary

A Cooperative Study by:

California Department of Water Resources
State Water Resources Control Board
U.S. Bureau of Reclamation

California Department of Fish and Game
U.S. Fish and Wildlife Service
U.S. Geological Survey

These proceedings were published by the Interagency Ecological Studies Program for the
Sacramento-San Joaquin Estuary (Interagency Program)
in a cooperative effort with the

U.S. Geological Survey Research Project Office, Tucson, Arizona.

Although the Research Project Office is not a member of the Interagency Program,
information generated by the PACLIM workshop provides the
Interagency Program with a climatological perspective that cannot be obtained from its own studies.
Views and conclusions contained in this publication do not necessarily reflect the opinions of the
Interagency Program or its member agencies.

Contents

Authors of Papers	vii
Introduction <i>Julio L. Betancourt</i>	1
Atmospheric Carbon Dioxide and the Climatic Record <i>Hugh W. Ellsaesser</i>	5
The Annual Course of Precipitation Over Much of the United States: Observed versus GCM Simulation <i>Ronald P. Neilson, George A. King, James Lenihan, and Robert L. DeVelice</i>	19
A Statistical Model of Climates in the Southwestern United States <i>Richard G. Craig and John F. Stamm</i>	27
Climate Signals in the Lower Stratosphere and Upper Troposphere <i>William D. Sellers</i>	33
1988 Summer Drought over the Great Plains: Some Causes and Predictions <i>Jerome Namias</i>	37
Current Water Supply Conditions in California <i>Maurice Roos</i>	43
Uncovering North American Temperature and Precipitation Patterns Associated with the Southern Oscillation <i>Chester F. Ropelewski and Michael S. Halpert</i>	47
Strong, Low Frequency (Decadal) Environmental Fluctuations During the 20th Century in the North Pacific Ocean, on the Washington Coast, and in Puget Sound <i>Curtis C. Ebbesmeyer and Carol A. Coomes</i>	49
Pacific Sea Surface Temperature Associations with Southwestern United States Summer Rainfall and Atmospheric Circulation <i>Andrew M. Carleton, Paul J. Weser, and Duane A. Carpenter</i>	55
Climatic Effects on Flood Frequency: An Example from Southern Arizona <i>Robert H. Webb and Julio L. Betancourt</i>	61
Time Series Analyses of Biological and Environmental Variables for Suisun Bay and the Sacramento and San Joaquin Rivers <i>Peggy Lehman</i>	67
Interpreting Long-Term Fish Landings Records: Environment and/or Exploitation? <i>Paul N. Sund and Jerrold G. Norton</i>	71
Solar-Cycle Modulation of ENSO: A Possible Source of Climatic Change <i>Roger Y. Anderson</i>	77

Rapid $\delta^{18}\text{O}$ and $\delta^{13}\text{C}$ Isotopic Shifts in Late Pleistocene Marine Varves on the California Margin	83
<i>Braddock K. Linsley, Roger Y. Anderson, and James V. Gardner</i>	
El Niño Reconstructions and Confirmation of a Pan-Californian Model via Radiolarian Evidence	87
<i>Richard E. Casey, Amy L. Weinheimer, Carl O. Nelson, Joseph B. Albin, David S. Beauchamp, David S. Carpenter, and Kevin M. O'Brien</i>	
Sediment Flux at Selected Coastal Sites: Proposed Time Series Measurement by Particle Traps	91
<i>A. Soutar, T.R. Baumgartner, R.E. Casey, J. Singleton, V. Ferreira-Bartrina, and C.O. Nelson</i>	
Climatic Changes Reflected in Laminated Santa Barbara Basin Sediments	97
<i>Arndt Schimmelmänn, Carina B. Lange, Joel Michaelsen, and Wolf H. Berger</i>	
A Modern Pollen Record from the Central Gulf of California	101
<i>K.H. Orvis, T.R. Baumgartner, R. Byrne, and L.D. Wright</i>	
A Pollen/Dinoflagellate Chronology for DSDP Site 480, Gulf of California	105
<i>Roger Byrne, Peta Mudie, and Andrew Soutar</i>	
Can a Climate Record Be Extracted from Giant Sequoia Tree Rings?	111
<i>M.K. Hughes, B.J. Richards, T.W. Swetnam, and C.H. Baisan</i>	
Interactions Between Climatic Variables Controlling Subalpine Tree Growth: Implications for Climatic History of the Sierra Nevada, California	115
<i>Lisa J. Graumlich</i>	
Holocene Fossil Pollen Records of Douglas Fir in Northwestern California: Reconstruction of Past Climate	119
<i>G. James West</i>	
Inferences from Tree Rings on Low Frequency Variations in Runoff in the Interior Western United States	123
<i>David M. Meko</i>	
El Niño-Southern Oscillation (ENSO) Phenomena and Forest Fires in the Southwestern United States	129
<i>Thomas W. Swetnam and Julio L. Betancourt</i>	
Tropical and Subtropical Moisture and Southerly Displaced North Pacific Storm Track: Factors in the Growth of Late Quaternary Lakes in the Mojave Desert	135
<i>Yehouda Enzel, Roger Y. Anderson, William J. Brown, Daniel R. Cayan, and Stephen G. Wells</i>	
Holocene History of the El Niño Phenomenon As Recorded in Flood Sediments of Northern Coastal Peru	141
<i>L.E. Wells</i>	
Changes in Mid-Troposphere Snow Accumulation on Mt. Logan, Yukon, over the Last Three Centuries	145
<i>Gerald Holdsworth</i>	

Authors of Papers

Sixth Annual Pacific Climate Workshop
Asilomar, California
March 5-8, 1989

Joseph B. Albin
University of San Diego
Alcala Park/Marine Studies
San Diego, CA 92110

Roger Y. Anderson
University of New Mexico
Department of Geology
Albuquerque, NM 87131

C. H. Baisan
University of Arizona
Laboratory of Tree-Ring Research
Tucson, AZ 85721

T. R. Baumgartner
Centro de Investigación Científica
y de Educación Superior de Ensenada
Ensenada, B.C., Mexico

David S. Beauchamp
University of San Diego
Alcala Park/Marine Studies
San Diego, CA 92110

Wolf H. Berger
Scripps Institution of Oceanography
University of California, San Diego
La Jolla, CA 92093-0215

Julio L. Betancourt
U.S. Geological Survey
300 West Congress, FB-44
Tucson, AZ 85701

William J. Brown
University of New Mexico
Department of Geology
Albuquerque, NM 87131

Roger Byrne
University of California
Department of Geography
Berkeley, CA 94702

Andrew M. Carleton
Indiana University
Department of Geography
Blomington, IN 47405

David S. Carpenter
University of San Diego
Alcala Park/Marine Studies
San Diego, CA 92110

Duane W. Carpenter
P.O. Box 14112
Anchorage, AK 99514-2112

Richard E. Casey
University of San Diego
Alcala Park/Marine Studies
San Diego, CA 92110

Daniel R. Cayan
Scripps Institution of Oceanography
University of California, San Diego
La Jolla, CA 92093-0215

Carol A. Coomes
Evans-Hamilton, Inc.,
6306 - 21st Avenue N.E.
Seattle, WA 98115

Richard G. Craig
Kent State University
Department of Geology
Kent, OH 44242

Robert L. DeVelice
NSI Tech Services Corporation /
U.S. Environmental Protection Agency
200 S.W. 35th Street
Corvallis, OR 97333

Curtis C. Ebbesmeyer
Evans-Hamilton, Inc.
6306 - 21st Avenue N.E.
Seattle, WA 98115

Hugh W. Ellsaesser
Lawrence Livermore National Laboratory, L-362
Atmospheric and Geophysics Science Division
Livermore, CA 94550

Yehouda Enzel
University of New Mexico
Department of Geology
Albuquerque, NM 87131

V. Ferreira-Bartrina
Centro de Investigación Científica
y de Educación Superior de Ensenada
Ensenada, B.C., Mexico

James V. Gardner
U.S. Geological Survey
345 Middlefield Road, MS 999
Menlo Park, CA 94025

Lisa J. Graumlich
University of Arizona
Laboratory of Tree-Ring Research
Tucson, AZ 85721

Michael Halpert
NWC/NWS/NOAA
Climate Analytical Center
World Weather Building, Room 605
Washington, DC 20233

Gerald Holdsworth
National Hydrology Research Institute
Surface Water Division
11 Innovation Boulevard
Saskatoon, Saskatchewan, Canada 57N 3H5

Malcolm K. Hughes
University of Arizona
Laboratory of Tree-Ring Research
Tucson, AZ 85721

George A. King
NSI Tech Services Corporation /
U.S. Environmental Protection Agency
200 Southwest 35th Street
Corvallis, OR 97333

Carina B. Lange
Scripps Institution of Oceanography, A-015
University of California, San Diego
La Jolla, CA 92093-0215

Peggy Lehman
California Dept. of Water Resources
3251 S Street
Sacramento, CA 95816

James Lenihan
Oregon State University,
U.S. Environmental Protection Agency
Environmental Research Laboratory
200 S.W. 35th Street
Corvallis, OR 97333

Braddock K. Linsley
University of New Mexico
Department of Geology
Albuquerque, NM 87131

David M. Meko
University of Arizona
Laboratory of Tree-Ring Research
Tucson, AZ 85721

Joel Michaelson
University of California, Santa Barbara
Department of Geography
Santa Barbara, CA 93106

Peta Mudie
Geological Survey of Canada
Atlantic Geoscience Centre
Box 1006
Dartmouth, N.S., Canada B2Y 4A2

Jerome Namias
Scripps Institution of Oceanography
University of California, San Diego
La Jolla, CA 92093-0215

Ronald P. Neilson
Oregon State University,
U.S. Environmental Protection Agency
Environmental Research Laboratory
200 Southwest 35th Street
Corvallis, OR 97333

Carl O. Nelson
University of San Diego
Alcala Park/Marine Studies
San Diego, CA 92110

Jerry G. Norton
National Marine Fisheries Service
Pacific Fish Environmental Group
P.O. Box 831
Monterey, CA 93942

Kevin M. O'Brien
University of San Diego
Alcala Park/Marine Studies
San Diego, CA 92110

K. H. Orvis
University of California
Department of Geography
Berkeley, CA 94720

B. J. Richards
University of Arizona
Laboratory of Tree-Ring Research
Tucson, AZ 85721

Maurice Roos
California Dept. of Water Resources
1416 Ninth Street
Sacramento, CA 94236-0001

Chester Ropelewski
NWC/NWS/NOAA
Climate Analytical Center
World Weather Building, Room 605
Washington, DC 20233

Arndt Schimmelmann
Scripps Institution of Oceanography
University of California, San Diego
La Jolla, CA 92093-0215

William D. Sellers
University of Arizona
Atmospheric Sciences, PAS 580
Tucson, AZ 85721

J. Singleton
Scripps Institution of Oceanography
University of California, San Diego
La Jolla, CA 92093-0215

Andrew Soutar
Scripps Institution of Oceanography
University of California, San Diego
La Jolla, CA 92093-0215

John F. Stamm
Kent State University
Department of Geology
Kent, OH 44242

Paul N. Sund
NOAA, National Marine Fisheries Service
Pacific Fish Environmental Group
P.O. Box 831
Monterey, CA 93942

Thomas W. Swetnam
University of Arizona
Laboratory of Tree-Ring Research
Tucson, AZ 85721

Robert H. Webb
U.S. Geological Survey
300 West Congress, FB-44
Tucson, AZ 85701

Amy L. Weinheimer
University of San Diego
Alcala Park/Marine Studies
San Diego, CA 92110

Lisa E. Wells
University of California
Department of Geography
501 Earth Sciences Building
Berkeley, CA 94720

Stephen G. Wells
University of New Mexico
Department of Geology
Albuquerque, NM 87131

Paul J. Weser
Geography Program
Scottsdale Community College
Scottsdale, AZ 85256

G. James West
3429 Oyster Bay
Davis, CA 95612

L. D. Wright
University of California (ret.)
Department of Paleontology
Berkeley, CA 94720

Julio L. Betancourt

In 1984, a workshop was held on "climatic variability of the eastern North Pacific and western North America." From it has emerged an annual series of workshops held each spring at the Asilomar Conference Center, Monterey Peninsula, California (Moore and others, 1986). These annual gatherings have come to be called PACLIM (Pacific Climate) Workshops, reflecting broad interests in the climatologies associated with the Pacific Ocean. Participants in the six workshops that have convened since 1984 have included atmospheric scientists, hydrologists, geologists, glaciologists, oceanographers, limnologists, and both marine and terrestrial biologists. A collective goal of PACLIM is to connect these various interests with common targets. One such target is the climate system associated with El Niño-Southern Oscillation (ENSO) and its physical and biological manifestations. Another is the behavior of this system on the scale of decades, centuries, and millennia, as recorded in high-resolution proxy data (i.e., annual ice layers, corals, sediment varves, and tree rings). Multidisciplinary collaborations fostered by previous PACLIM workshops are illustrated in Peterson (1989).

PACLIM Workshops have been sponsored largely by the U.S. Geological Survey (USGS) in cooperation with other federal and state agencies, as well as private institutions. PACLIM 89, which led to publication of this proceedings, was sponsored by USGS, the Monterey Bay Aquarium Research Institute (MBARI), the National Oceanic and Atmospheric Administration (NOAA-Geophysical Data Center), the Environmental Protection Agency (EPA-Global Change Program), and the California Department of Water Resources (CDWR). On behalf of the sponsors, we extend our gratitude to the various individuals responsible for the organization and planning of PACLIM 89. In particular, we thank Dave Peterson, USGS, and Dick Barber, MBARI, for co-chairing the workshop and Lucenia Thomas and Martha Nichols, USGS, for logistical and office support. We also thank Randy Brown, California Department of Water Resources, for arranging publication of this proceedings in the Technical Report Series of the Interagency Ecological Studies Program.

Papers in the proceedings are organized from the general to the specific, from observations based on instrumental data to inferences from the fossil record. The papers by Elsaesser, Sellers, and Namias represent the keynote addresses for PACLIM 89. Elsaesser's (this volume) skepticism about the magnitude of warming projected for doubled CO₂ stirred much debate at the workshop. He feels that too much is being expected of radiation transport theory in large-scale modeling of the CO₂ problem. For summer, general circulation models (GCMs) overestimate continental precipitation amounts and temperature variability. Miscalculations in radiation may also explain misplacement of continental heat lows during summer (i.e., in the eastern rather than southwestern United States). This problem is addressed

later in the proceedings by Neilson and others, who show that the GCMs distort actual rainfall seasonalities across the southern United States. Mesoscale models, such as the one constructed by Craig and Stamm (this volume) for the southwestern United States, could improve simulations of seasonality only if the general boundary conditions borrowed from GCM output are fundamentally correct. Elsaesser (this volume) also draws from Angell's (1988) synthesis of upper-air sounding data to show that cooling occurred in the polar zones, where the GCMs simulate maximum warming. In a similar light, Sellers (this volume) analyzes radiosonde data since 1957 for over 500 stations and suggests how temperature patterns in the lower stratosphere and upper troposphere might relate to the solar flux, ENSO, the quasi-biennial oscillation (QBO) and atmospheric CO₂.

Extreme droughts over the Great Plains in 1988 (Namias, this volume) and over northern California since the 1987 water year (Roos, this volume) raise some interesting questions. Though these droughts may have little connection to greenhouse effects, they bring to mind the societal impacts of more frequent droughts projected in some CO₂-climate scenarios. As usual, Namias' thoughtful relations to the oral presentations at PACLIM were worth the price of admission. In his paper, he again warns us against generalizations about El Niño and La Niña teleconnections (see earlier admonitions in Namias and Cayan, 1984). Rather than just the byproduct of La Niña conditions (Trenberth and others, 1988), the 1988 Great Plains drought resulted from evolution and development of the classical three upper-level anticyclonic anomalies over the north Pacific Ocean, north Atlantic Ocean, and continental United States, to interacting sea surface temperature (SST) patterns, and to very dry antecedent soil conditions.

Heeding Namias' warning, Ropelewski and Halpert (this volume) exercise great caution in uncovering North American temperature and precipitation patterns associated with extreme phases of the Southern Oscillation (SO). The consistent patterns are confined to the northwestern and southeastern parts of the continent. In the Pacific Northwest, precipitation patterns apparently depend on the precise evolution of each high or low SO-phase event and the prevailing atmospheric pressure patterns in the north Pacific Ocean, as gaged by the Pacific-North American (PNA) index (Ebbesmeyer and Coomes, this volume). Positive values of the PNA index, corresponding to an amplified wave pattern of 500 mb height with the Aleutian Low shifted eastward and an intensified sea level pressure gradient, are associated frequently, but not always, with the low-SO phase of El Niño. In Arizona, wet summers tend to follow the positive phase of the PNA-teleconnection pattern and/or low SO-phase of the antecedent winter (Carleton and others, this volume).

On a decadal scale, differences in the PNA and SO indices are reflected by hydrologic fluctuations. With the positive PNA-phase, streamflow into Puget Sound is reduced, the density difference across the entrance sill at Admiralty Inlet increases, and the fastest inflow in the Sound deepens toward the bottom (Ebbesmeyer and Coomes, this volume). On the larger streams of southern Arizona, the seasonality and magnitude of annual floods shift with the prevailing flow pattern of the upper-air westerlies and the frequency and intensity of ENSO events (Webb and Betancourt, this volume). Such climatic effects also are evident in biological productivity. Along the northern California coast, Lehman (this volume) notes that chlorophyll concentrations and populations of phytoplankton, zooplankton, and fish declined in the period 1977-1987, a decade bereft of La Niña conditions (Bradley and others, 1987) and with a consistently positive PNA index (Ebbesmeyer and Coomes, this volume). At Southern California ports, landings of swordfish increased after 1976, while those for other species decreased. Though these changes parallel warmer SSTs at the Scripps pier, they could also be attributed to developments in market and technology (Sund and Norton, this volume).

The second half of the proceedings volume is devoted to studies spanning centuries to millennia. Anderson's (this volume) contribution breaks new ground by exploring associations between solar and ENSO activities in the past four centuries. Of particular value is the pre-instrumental record of ENSO reconstructed from archives by Quinn and others (1987). Anderson attributes the reciprocal relation between ENSO frequency and sunspot number to modulation of a linear oscillator (ENSO; see Graham and White, 1988) by the changing amplitude of the 11-year solar cycle. During the Maunder Minimum, for example, ENSO might have approached the frequency of the quasi-biennial oscillation (QBO). Anderson suggests that the ocean's mixed layer should be sensitive to solar modulation of ENSO; a signal should be evident in the marine stratigraphic record.

On the continental slope off the coast of Northern California, Linsley and others (this volume) report alternating cycles of varved and bioturbated sediments between 45,000 and 12,000 YBP (years before present). These cyclic alternations indicate dramatic changes in wind-driven upwelling. Varved intervals reflect more upwelling and anoxic conditions in bottom waters of the oxygen minimum zone that discourage bioturbation by macrobenthos and thus help preserve varves. Linsley and others (this volume) suggest a connection between the rapid transitions in the cycles and climatic "jumps" identified for the same time in the Greenland ice cores (Broecker and others, 1988). These jumps are comparable in magnitude and duration to the Younger Dryas cold snap that, from evidence in the ice cores, apparently terminated abruptly (within 20 years) at ca. 10,700 YBP (Dansgaard and others, 1989). Continued development of marine varved chronologies will be critical to determine whether or not the Pacific Ocean responded as swiftly as the Atlantic, and to what extent the transition involved ENSO.

Casey and others (this volume) report on Neogene, Pleistocene, and Holocene varved sediments off the California coast. Interruptions in the varved series, representing bioturbation, are attributed to ENSO conditions, first identified ca. 5.5 MYA (million years ago). Radiolarian number and flux are used to indicate ENSO, calibrated from plankton tows and analysis of 20th century sediments in the Santa Barbara Basin. In the spirit of calibration, Soutar and others (this volume) propose methods for monitoring particle flux at coastal sites, partly to help understand varve formation. Based on the pioneering study by Soutar and Crill (1972), Schimmelman and others (this volume) extend the absolute chronology of laminated sediments in the Santa Barbara Basin to AD 1650. Their skillful dating of varves is essential in developing a precise history of the California El Niño that can be compared with other Pacific records of interannual resolution, such as marine varves from the Gulf of California (Juillet-Le Clerc and Schrader, 1987; Baumgartner and others, 1989a).

Most of the work with biological indicators in varves from the Santa Barbara Basin and Gulf of California has been with marine organisms. Charcoal counts from the Santa Barbara Basin varves have been used to reconstruct wildfire history in the coastal ranges of Southern California (Byrne and others, 1977). Orvis and others (this volume) and Byrne and others (this volume) now report pollen and dinoflagellate stratigraphies from the Gulf of California. Pollen influx bears directly on the processes of sediment transport and accumulation on the Guaymas slope. Pollen influx has remained the same over the past 200 years, despite artificial damming of rivers that flow into the Gulf (Orvis and others, this volume). This corroborates the claim by Baumgartner and others (1988b) that terrigenous flux in the Gulf is mostly eolian. Byrne and others (this volume) show the great potential awaiting full analysis of cores DSDP 479 and 480, which Glomar Challenger took in 1978 as part of the Deep Sea Drilling Project. Together these cores provide a complete sweep of the last million years in the Gulf of California, much of it laminated. Dating of these cores is still in question; calcareous foraminifera are not abundant enough in the Gulf sediment for development of an oxygen isotope chronology equivalent to stratigraphies now available from the deeper oceans.

Four papers in the proceedings draw from another high-resolution proxy record — tree rings in conifers from the western United States and northern Mexico. Hughes and others (this volume) resume earlier work on giant sequoia by tree-ring pioneer A.E. Douglass, and raise hopes for a 2,000-year chronology from the west slope of the Sierra Nevada. The surest climatic signal in the sequoia rings is the infrequent, severe drought. Severe drought frequencies comparable to those of the 20th century also happened during the 1500s and 1700s. Graumlich (this volume) uses response surfaces to show synergistic interactions of winter precipitation and summer temperature in producing tree rings of foxtail pines and western juniper in sub-alpine environments of the eastern Sierra Nevada. She proposes that response surfaces from multiple species may be necessary to derive quantitative reconstructions

of climate from tree rings. Response surfaces also may be useful in attaching climatic significance to large-scale changes in plant distribution. Such regression techniques have been used to simulate past vegetation from GCM output in the eastern United States (Bartlein and others, 1986). A similar approach could be taken to investigate climatic changes responsible for late Holocene expansion of Douglas fir into northeastern California (West, this volume).

Meko (this volume) uses tree rings to infer and compare low-frequency variations in runoff for the northern, central, and southern parts of the semi-arid interior of the western United States. These low-frequency variations seem to respond to both annual precipitation and evapotranspiration during the warm season. He also notes that downward trends in streamflow over the first half of this century are at least 250-year extremes and that asynchronicity between north and south occurs most commonly during ENSO events. In ponderosa pine forests of Arizona and New Mexico, fire activity is much reduced during ENSO events, primarily because of wetter winters and springs. Swetnam and Betancourt (this volume) identified ENSO effects in both fire statistics (1909-present) and fire-scar chronologies (1700-1900). Because teleconnections for fire climatologies are lagged one or two seasons, successful forecasting of extreme phases of the SO could improve fire readiness and scheduling of prescribed burning.

Two of the papers in the proceedings extract climatic meaning from rare and infrequent flood events evident in the fossil record. Enzel and others (this volume) link

perennial lakes in the Mojave Desert at ca. 3600 and 400 years ago to a persistent, southward displacement of the North Pacific storm track. As climatic analogs, they use historical flooding that led to formation of ephemeral lakes lasting several months to more than a year. On the hyperarid, northern coast of Peru, most evidence of catastrophic flooding during the Holocene, such as in 1982-1983, is believed to have resulted from ENSO (Wells, this volume). At present, however, the alluvial stratigraphic record is much too coarse and fragmentary for use in reconstructing past El Niño events (DeVries, 1987).

Finally, Holdsworth (this volume) presents a spectacular, interannual record of snow accumulation on Mt. Logan, Yukon, since AD 1700. Because of its location, this record is on equal par with ice core records from the Quelccaya ice cap in Peru (e.g., Thompson and others, 1984), which attracted much attention at early PACLIM workshops (Mooers and others, 1986). At 5340 m above sea level, Mt. Logan is located in the middle troposphere, near the limits of the circumpolar vortex, and along the preferred tracks of Rossby waves and major cyclones. It is thus not surprising, though still impressive, that net snow accumulation on Mt. Logan explains about 40 percent of the variance of precipitation in the northern Great Plains, the steppe of the Soviet Union, and Japan. Like the Quelccaya ice cap and marine varves from the Santa Barbara Basin and Gulf of California, the Mt. Logan record shows that Pacific climate changed dramatically at the end of the Little Ice Age. In many respects, twentieth century climate may be without analog in the past few centuries.

REFERENCES

- Angell, J.J., 1988, Variations and trends in tropospheric and stratospheric global temperatures, 1958-87: *Journal of Climate*, v.1, p.1296-1313.
- Bartlein, P.J., Prentice, I.C., and Webb, T., 1986, Climatic response surfaces based on pollen from some eastern North American taxa: *Journal of Biogeography*, v.13, p.35-57.
- Baumgartner, T.R., Ferreira-Bartrina, V., Cowen, J., and Soutar, A., 1989a, Reconstruction of a twentieth century varve chronology from the central Gulf of California, in Dauphin, P., and Simoneit, B., editors, *The Gulf and Peninsular Province of the Californias: American Association of Petroleum Geologists, Memoirs* (in press).
- Baumgartner, T.R., Ferreira-Batrina, V., and Moreno-Hentz, P., 1989b, Varve formation in the central Gulf of California: A reconsideration of the origin of the dark laminae from the twentieth century varve record, in P. Dauphin and B. Simoneit, editors, *The Gulf and Peninsular Province of the Californias: American Association of Petroleum Geologists, Memoirs* (in press).
- Bradley, R.S., Diaz, H.F., Kiladis, G.N., and Eischeid, J.K., 1987, ENSO signal in continental temperature and precipitation records: *Nature*, v.327, p.497-501.
- Broecker, W., Andree, M., Bonani, G., Wolfli, W., Oeschger, H., and Klas, M., 1988, Can the Greenland climatic jumps be identified in records from ocean and land: *Quaternary Research*, v.30, p.1-6.
- Byrne, R., Michaelsen, J., and Soutar, A., 1977, Fossil charcoal as a measure of wildfire frequency in southern California: A preliminary analysis: U.S. Department of Agriculture, Forest Service, General Technical Report, WO-3, p.361-367.

- Dansgaard, W., White, J.W.C., and Johnsen, S.J., 1989, The abrupt termination of the Younger Dryas climate event: *Nature*, v.339, p.532-534.
- DeVries, T.J., 1987, A review of geological evidence for ancient El Niño activity in Peru: *Journal of Geophysical Research*, v.92, p.14,471-14,479.
- Graham, N.E. and White, W.B., 1988, the El Niño cycle: A natural oscillator of the Pacific Ocean: *Science*, v.240, p.1293-1302.
- Juillet-Le Clerc, A. and Schrader, H., 1987, Variations of upwelling intensity recorded in varved sediment from the Gulf of California during the past 3000 years: *Nature*, v.329, p.146-149.
- Mooers, C.N.K., Peterson, D.H., and Cayan, D.R., 1986, the Pacific Climate Workshops: *EOS*, v.67, p.1404-1405.
- Namias, Jerome and Cayan, D.R., 1984, El Niño: The implications for forecasting: *Oceanus*, v.27, p.41-47.
- Peterson, D.H. (Editor), 1989, Aspects of climate variability in the Pacific and western Americas: *American Geophysical Union Monograph* 55.
- Quinn, W.H., Neal, V.T., and Antunez de Mayolo, S., 1987, El Niño occurrences over the past four and a half centuries: *Journal of Geophysical Research*, v.92, p.14,449-14,461.
- Soutar, A. and Crill, P.A., 1977, Sedimentation and climatic patterns in the Santa Barbara Basin during the 19th and 20th centuries: *Geological Society of America Bulletin*, v.88, p.1161-1172.
- Thompson, L.G., Mosley-Thompson, E., and Morales Arnao, B., 1984, El Niño-Southern Oscillation events recorded in the stratigraphy of the tropical Quelccaya ice cap, Peru: *Science*, v.226, p.50-53.
- Trenberth, K.E., Branstator, G.W., and Arkin, P.A., 1988, Origins of the 1988 North American drought: *Science*, v.242, p.1640-1645.

The views and conclusions contained in this publication are based on authors' studies or experiences and do not necessarily represent the official viewpoint or policy of any state or U.S. government agency.

Atmospheric Carbon Dioxide and the Climatic Record

Hugh W. Ellsaesser

ABSTRACT: This paper is an attempt to provide a summary review of conclusions from previous studies on this subject. They have been organized under the following subject headings.

- Conceptualization of the greenhouse effect.
- The climatic effect of doubled CO₂.
- Interpretation of the climatic record.
- Diagnosis of apparent and possible model deficiencies.
- The paleoclimatic record.

CONCEPTUALIZATION OF THE GREENHOUSE EFFECT

Sunlight, consisting of ultraviolet, visible and infrared radiation, reaches the Earth with a direct beam intensity of 1360 W/m², defined as the solar constant. Because of the Earth's rotation and spherical shape, the global average flux per unit area at the top of the atmosphere is only one fourth of this, or 340 W/m². The Earth's albedo, or fraction reflected, is 0.3 so that 238 W/m² is the average solar flux absorbed by the Earth and its atmosphere – and is the amount of energy which must be re-radiated to space if the Earth's temperature is to remain unchanged.

By the empirical and theoretical Stephan-Boltzmann Law (ideal), black bodies emit radiant energy at a rate proportional to the fourth power of the Kelvin (absolute) temperature of their surfaces.

$$R = \sigma T^4 [W/m^2] \quad (1)$$

Most solids and liquids do not depart very far from the black body curve. Gases, in contrast to solids and liquids, tend to absorb and radiate energy only at discrete wavelengths or bands, but their emission remains within the T⁴ limit for the wavelengths of concern.

Our sun radiates very nearly as a black body with a color temperature of 6000 K. The temperature determines not only the total energy output but also its spectral distribution and, in particular, the wavelength or color at which the energy is a maximum. These are given by Planck's law for the distribution of radiant energy as a function of wavelength and temperature and by Wien's displacement or color temperature law for the wavelength of peak radiation as a function of temperature. The latter may be expressed as:

$$\lambda_m T = 2897 [\text{micron degrees K}] \quad (2)$$

The surface temperature of the Earth averaged over all latitudes and seasons is very nearly 15°C or 288 K

(0°C = 273 K). A black body at this temperature would put out about 390 W/m² of radiant energy, i.e. 115% of the average solar flux or 165% of the absorbed solar energy, peaking at a wavelength near 10.6 microns in the IR (infrared) part of the spectrum. However, satellite measurements confirm that the outgoing radiation from the Earth averages only 238 W/m², i.e. matches the amount of sunlight absorbed. This corresponds to the radiation of a black body at a temperature of 255 K or -18°C. That is, the planet Earth radiates as would a black body that is 33°C colder than the average surface temperature of the Earth. This difference is attributed to the so-called greenhouse effect of our atmosphere.

Figure 1 (Luther and Ellingson, 1985) shows (above) the relative intensities of sunlight reaching Earth and the Earth's outgoing "light" as functions of wavelength. The sun's spectrum peaks in the visible, while the Earth's radiation is all in the IR, with very little overlap of the two spectra. The lower part of the figure shows the average percentage of absorption at each wavelength by the gases in the Earth's atmosphere and the gases responsible. The band of reduced absorption between 8 and 12.5 microns is the so-called atmospheric window. These are the only wavelengths at which IR radiation from the planet's surface can penetrate the atmosphere to outer space to any significant degree.

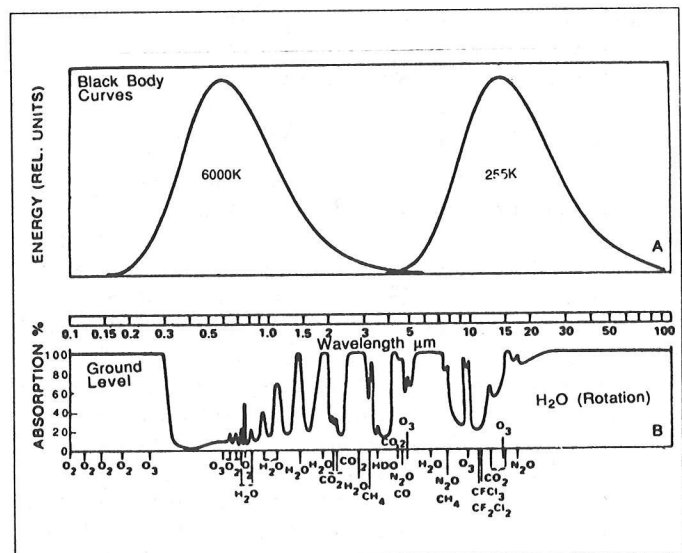


Figure 1. Radiant energy spectra of sun (at Earth distance) and Earth (above) and absorption bands of atmospheric gases (below). Wavelengths shown on center scale (from Luther and Ellingson, 1985).

In J.L. Betancourt and A.M. MacKay, editors, 1990. Proceedings of the Sixth Annual Pacific Climate (PACLIM) Workshop, March 5-8, 1989: California Department of Water Resources, Interagency Ecological Studies Program Technical Report 23.

This representation of the atmospheric window is a global average for beams originating at the surface and directed toward the zenith. The window becomes progressively more closed as the direction of the beam departs from the zenith and as the atmosphere becomes more moist. In the moist tropics, this window is completely closed by the so-called **continuum absorption** of water vapor (Kiehl and Ramanathan, 1982). One of the early explanations for surface warming due to increased CO₂ was that this would cause further spreading of the 15-micron absorption band of CO₂, narrowing the atmospheric window and, as a consequence, the surface would warm until it could radiate the same amount of energy up through the narrowed window. However, current estimates are that only about 7% of the surface emitted IR escapes through the window to space without reabsorption by the overlying atmosphere (Luther and Ellingson, 1985 Figure 2.8), so this effect must be a minor part of the greenhouse warming mechanism. But the atmosphere itself is also radiating — and in all directions, including up toward outer space and back toward the surface. At satellite altitude, most of the radiation observed coming from the planet Earth originates not from the planet's surface but from some higher level in the atmosphere.

Figure 2 (Lamb, 1972 p. 9) shows an averaged profile of temperature versus altitude in the Earth's atmosphere, along with the names given to various layers of the atmosphere. The lower part of the curve in which the temperature decreases with height is called the **troposphere**. The Earth's black body equivalent temperature of 255 K (-18°C) occurs at an altitude of about 6 km and this, in an averaged sense, is the level from which the Earth radiates to space. The **lapse rate** (average rate of decrease of temperature with altitude) between here and the surface is 5.5°C/km — 5.5°C/km times 6 km is 33°C, which added to the 6-km temperature of 255 K gives the surface temperature of 288 K (15°C).

This is a simplistic but physically valid explanation of how the atmosphere acts as a blanket or greenhouse to keep the surface of the planet warmer than it would be without an IR absorbing atmosphere. That is, the Earth does not lose energy by IR radiation from its surface, as would a bare black body; rather its black body radiation to space is actually emitted from the top of its greenhouse blanket, located, on average, about 6 km above the surface, where the average temperature is some 33°C (59°F) colder than the surface. The IR opacity of the atmosphere, which produces this greenhouse blanket, is due to liquid and solid particles, including clouds, and the IR absorbing gases: water vapor (20.6), carbon dioxide (7.2), ozone (2.4), nitrous oxide (1.4), methane (0.8), and freons (<0.8). (The numbers in parentheses are the individual contributions in degrees C to the total greenhouse effect of each gas calculated by Kondrat'yev, 1986, p.50).

If additional greenhouse gases are added to the atmosphere, it is logical to expect that the greenhouse blanket will thicken; i.e., the average altitude from which the atmosphere emits energy to space will rise above its present level of 6 km. But, since the absorbed solar

energy that has to be rejected remains essentially unchanged, the radiating temperature also must remain the same; i.e., average atmospheric temperature at the new higher level of the top of the greenhouse blanket must warm to the temperature existing now at the present top of the greenhouse blanket. If the lapse rate remains the same, then the temperature at Earth's surface will also warm. This is a somewhat simplistic, but physically valid, picture of the mechanism by which increases in the greenhouse gas content of the atmosphere will lead to climatic warming.

Unfortunately, this simple picture of how the greenhouse effect operates is of little help in quantifying the amount of warming to be expected. To see why this is so, examine Figure 3. This shows a terrestrial IR spectrum taken by Nimbus IV near Guam on 27 April 1970 on a background of temperature-labeled black body curves and with the wavelength range of the principal atmospheric IR absorbers (emitters) indicated. It is obvious that water, including the dimer, (H₂O)₂ — believed to be responsible for the continuum absorption (and emission) of water vapor, is the principle emitter, without even considering the effect of clouds, which are also composed of water. And since this spectrum is taken at latitude 15.1°N, it appears quite credible that the global average temperature of this emitter is 255 K. On the other hand, the IR flux from the CO₂ band centered near 15-microns, is both a small fraction of the total and is coming from an emitter with a temperature near 220 K (-50 to -55°C).

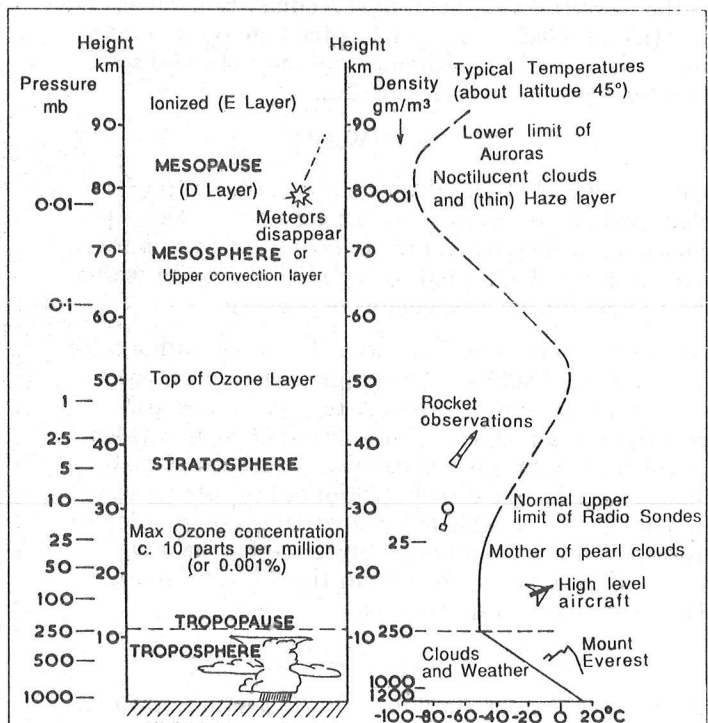


Figure 2. Typical vertical variation of temperature within the atmosphere and nomenclature for the various levels and layers (from Lamb, 1972, p.9).

Note: 3.048 km = 10,000 ft; 1.609 km = 1 mile.
Vertical divisions of the atmosphere.

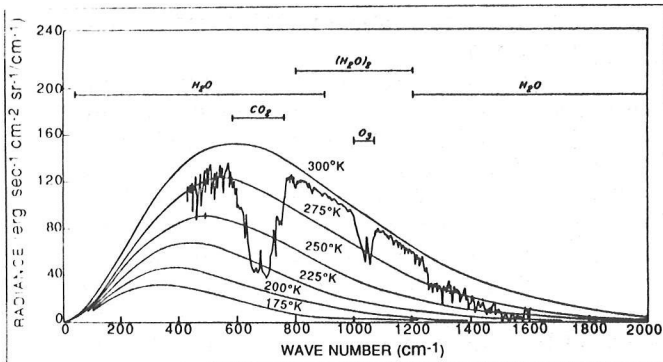


Figure 3. Terrestrial IR emission spectra recorded by IRIS-D on Nimbus IV near Guam at 15.1°N on 27 April 1970 (from Luther and Ellingson, 1985).

Returning to Figure 2, this temperature range is found in the altitude range 12 to 20 km. If the top of this CO₂ greenhouse blanket were to be raised, by the addition of CO₂, and maintained at constant temperature, this would have little or no effect on temperature at the surface and, if anything, might cause the surface to cool (i.e., if this radiating layer were pushed above 20 km).

THE CLIMATIC EFFECT OF DOUBLED CO₂

The National Academy of Sciences, in a series of reports (NRC, 1979, 1982, 1983), adopted 1.5 to 4.5°C (2.7 to 8.1°F) as the mean global surface warming to be expected from a doubling of CO₂ or an equivalent increase of all greenhouse gases. At the present time, the other greenhouse gases being added by man are supposed to have a warming effect about half that of the added CO₂. Current estimates for the time of equivalent doubling of preindustrial CO₂ greenhouse effect range from about 2020 to 2050 AD (Wigley, 1987). The most recent experiments by our most complex models have clustered in the upper part or even exceeded this range. It is my personal and professional opinion that our climate models are overestimating the warming due to CO₂ by at least a factor of 2 to 3.

Mike Schlesinger of Oregon State University has for several years been analyzing and reviewing model predictions of the climatic effect of a doubling of atmospheric carbon dioxide. Table 1, taken from his review for the U.S. Department of Energy State-of-the-Art

Table 1. RCM (radiative-convective model) analysis of the feedbacks in the GISS (Hansen et al., 1984) GCM simulation of (2xCO₂) - (1xCO₂) temperature changes (from Schlesinger and Mitchell, 1985).

Feedback Mechanism	(ΔT _s) i-1° °C	f*i
None	1.20	0.000
Water vapor amount	1.85	0.445
Water vapor distribution	0.90	0.216
Lapse rate	-1.10	-0.264
Surface albedo	0.38	0.091
Cloud height	0.51	0.123
Cloud cover	0.42	0.101
Total	4.16	0.712

Reports (Schlesinger and Mitchell, 1985) gives a breakdown of the model-computed temperature changes due to the doubling of carbon dioxide alone and to the various feed-backs expected to accompany such a doubling. Note that the doubling of carbon dioxide *per se* is calculated to produce a mean global warming of only 1.2°C (29% of the total of 4.16°C — Ramanathan (1981) computed this number to be only 0.5°C) while the calculated changes in water vapor amount and distribution are calculated to cause an additional warming of 2.75°C (66%) and calculated changes in lapse rate, surface albedo and cloudiness are credited with causing an additional warming of 0.21°C (5%). That is, the doubling of carbon dioxide is now calculated to produce a mean global warming 3.46 times greater than would occur if the carbon dioxide content of the atmosphere could be doubled with no other changes. The major portion of this amplification, a factor of 3.2, comes from the changes in the amount and distribution of the water vapor in the atmosphere predicted to occur as a result of the warming initiated by the increase in CO₂.

Note also that Item 4 in the table, "lapse rate", is calculated to contribute to a cooling. That is, the models are predicting doubled CO₂ to reduce the mean lapse rate of the troposphere below its present 5.5°C/km; i.e., the upper troposphere will warm more than the surface. As can be seen from Figure 2, if the slope of the temperature curve in the troposphere is decreased, while holding the temperature near 6 km constant, then the temperature at the Earth's surface will decrease. Aside from this one small item, all of the other feed-backs listed, resulting from predicted changes in the state and distribution of water, are positive; i.e., amplify the effect of increased CO₂.

INTERPRETATION OF THE CLIMATIC RECORD

For a long time it was believed that the preindustrial level of CO₂ was about 290 ppm and that the burning of fossil fuels such as coal, oil and gas contributed the only significant additions to atmospheric CO₂. These are estimated to have contributed about 180 GtonsC to date (1 gigaton C = 10¹⁵ grams or 10⁹ tonnes as carbon). In the past few years it has been realized that historical changes in land usage such as forest clearing and agriculture have probably released a cumulative total amount of CO₂ of about the same magnitude. To allow room for some fraction of this biospheric source of CO₂ to have remained in the atmosphere, the preindustrial level of CO₂ would have had to have been lower than 290 ppm. Estimates of various sorts have provided numbers from 240 to 280 ppm, with about 270 ppm now appearing most widely accepted. From these numbers we derive an estimate of the atmospheric increase of CO₂ due to this biospheric source of 10-50 ppm. Biospheric releases of CO₂ to the atmosphere were most probably in the range 90-180 GtonsC according to the Department of Energy State-of-the-Art Reports (Houghton et al., 1985). Using 58% for the fraction remaining in the atmosphere (determined from the fossil fuel releases during the period of the Mauna Loa record of CO₂),

this implies a CO₂ increase of 25-50 ppm due to the biospheric source. The extremes of these two estimates give percentage CO₂ increases of 3.5 to 21%, and assuming a warming of 3°C for a CO₂ doubling, these imply an equilibrium warming of 0.15 to 0.9°C due to the biospheric CO₂. The NH (Northern Hemisphere) land observations (see Figure 4) indicate a warming of about 0.6°C between 1881 and 1940. The data prior to 1881 are too sparse to be relied upon, but mainly indicate slight progressive cooling. Thus, they mainly indicate that the historical fact that our land record of temperature data starts in 1881 will tend to exaggerate the climatic warming derived from the record for the past century. (Note: I consider the record of NH land temperatures to be our most reliable estimate of climate change due to the unexpected and still unexplained variations shown by the more recently available SH and oceanic ship data.)

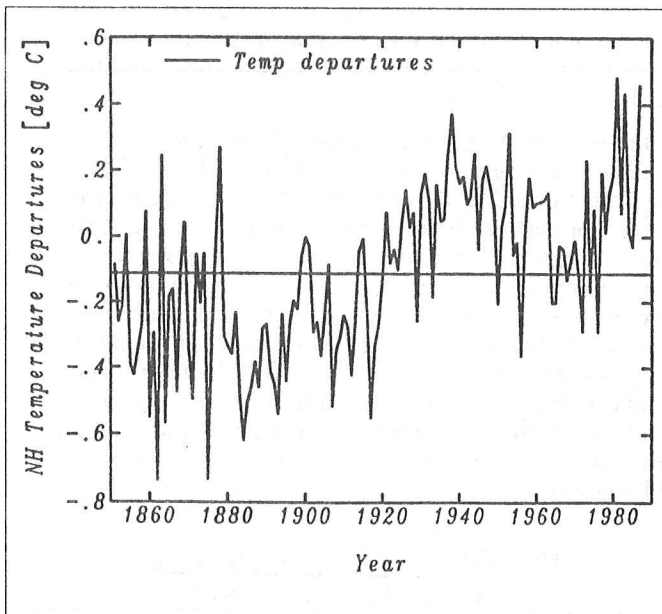


Figure 4. Northern Hemisphere surface air temperature annual mean departures from the 1951-1970 mean (replotted from Jones et al., 1986).

If we focus on 1938, the warmest year in the NH land data record prior to 1981, the burning of fossil fuels could have added no more than 15 ppm of CO₂ to the atmosphere by then (Pearman, 1980). This would have been a percentage increase of 5.2% and for a doubled CO₂ warming of 3°C would produce an equilibrium warming of no more than 0.22°C. Thus, the warming up to 1938, if due to carbon dioxide, had to be due to the biospheric source of CO₂. If the 45 ppm of fossil fuel CO₂ added to the atmosphere since 1938 has had no effect on temperature; then it is also unlikely that the 15 ppm released before 1938 had any effect either. Therefore the total CO₂ increase due to fossil fuels of about 60 ppm or 21%, which is now calculated to produce an equilibrium warming of at least 0.83°C (assumes 3° for a CO₂ doubling), presumably still lies ahead, even if we stop burning fossil fuels today. (Note: the calculated equilibrium warming is nearly doubled if the other increasing greenhouse gases such as methane, nitrous oxide, and ozone are included.)

Figure 5 was prepared to illustrate this problem: it is a plot of the NH temperature data from Figure 4 versus the atmospheric concentration of CO₂ at the time of the observation. The CO₂ concentrations used are those computed by the model of Pearman (1980), which assumed a preindustrial level of 290 ppm and used the fossil fuel CO₂ emission data of Rotty (1979) and the Mauna Loa observations as controls. This figure makes it clear that essentially all of the warming of the past 135 years had occurred by the time the first quarter of the fossil fuel CO₂ had been added to the atmosphere and that the addition of the remaining three-quarters of the fossil fuel CO₂ has had virtually no effect. Adding a lag for the thermal inertial of the oceans, as discussed below, simply pushes the warming farther in advance of the release of the fossil fuel CO₂. Again, inclusion of the other greenhouse gases increases the discrepancy.

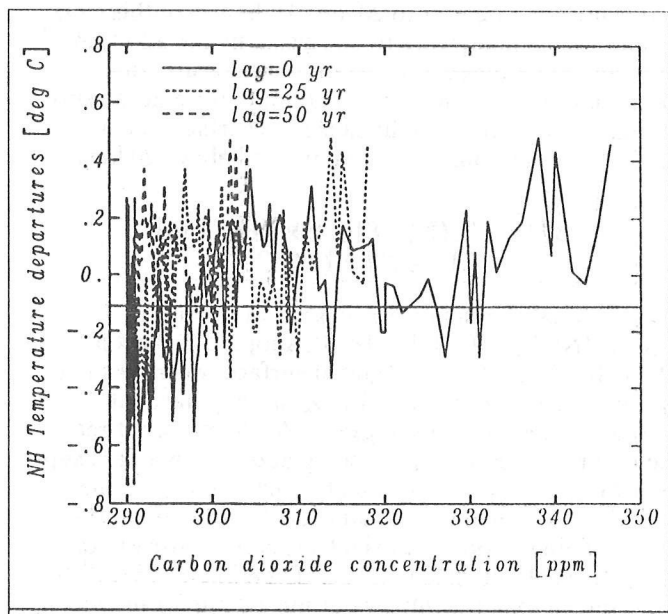


Figure 5. Plot of Northern Hemisphere temperature data from Figure 4 versus atmospheric concentration of CO₂ at the time of the observation based on Pearman's (1980) model.

The current explanation as to why we cannot identify the effect of fossil fuel CO₂ in the temperature record is the thermal inertia of the oceans. It has now been recognized that the atmosphere cannot warm until the underlying surface warms. But the implication drawn is that the ocean surface cannot warm until much of the deeper ocean is warmed. The time lag required to do this is decades to centuries, and this is presumed to be what is delaying the onset of a surface temperature rise due to fossil fuel CO₂.

Figure 6 from Hamon and Godfrey (1975 p.33) shows, as the typical temperature distribution in the ocean, a cross section along the 170°W meridian in the Pacific Ocean as a function of latitude and depth. Note how the warm surface water appears as a thin lens capping a very cold ocean. The thickness of the surface wind- and wave-stirred mixed layer varies seasonally and latitudinally and averages about 50 meters. Below it is the thermocline with a rapid drop in temperature to that

typical of the vast bulk of the ocean. Below a few hundred meters depth, the oceans are everywhere and always (relatively speaking) only a few degrees above the freezing point, which for sea water is about -2°C .

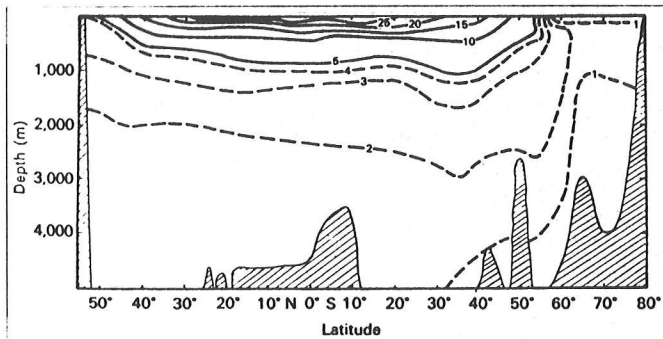


Figure 6. North-south section of water temperature ($^{\circ}\text{C}$) in the Pacific Ocean approximately along the 17°W meridian (from Hamon and Godfrey, 1975, p.33).

Figure 6 makes it obvious that the ocean surface can be warmed without warming the ocean to great depth. Physically, warming the ocean from above is like cooling the atmosphere from below — as soon as the process begins, the affected surface layer becomes progressively decoupled from turbulent mixing with the rest of the fluid due to differences in density, and the further the process progresses, the greater the inhibition of any mixing or overturning.

Each winter as polar sea ice is formed, dense cold brine is squeezed out of the ice and, being the densest water in the ocean, sinks to the bottom — unless diluted sufficiently in route. It is this process that has filled the oceans with water near the freezing point. And this process will continue as long as sea ice forms in winter at either pole. It is currently estimated that this so-called **bottom water** is formed at a rate sufficient to push the existing waters of the oceans upward at an average rate of 4 meters per year. The water sinking at the winter pole is replaced by warm surface water moving in from lower latitudes. This constitutes the so-called **thermo-haline circulation**, since it is driven by density differences due to differences in both temperature and salt content.

The warm lens of surface water overlying the cold oceans is due to the absorption of solar radiation by the oceans. The surface layer of the oceans strives to balance absorbed solar radiation with energy losses in the form of sensible heat and latent heat of water vapor evaporated into the atmosphere and black body IR radiation, most of which is reabsorbed at some level within the atmosphere. The temperature of the mixed layer accordingly undergoes a seasonal cycle that lags the sun in each hemisphere by about 30 days. The range between summer and winter temperatures is shown in Figure 7, from Panfilova (1972). It is largest in a belt near 40° latitude and is greatest in the North Pacific, where it reaches 14°C in a small area below Kamchatka. As the temperature in these bands rises in the spring, a new, shallow mixed layer of only 20 to 30 meters depth forms and gradually deepens as the summer gives way to fall and winter.

This warm mixed layer is less dense than the water below. Thus they can be mixed only by mechanical force such as wind stirring. If the surface layer were to be made warmer, as from increased CO_2 , it would resist mixing with the colder water below even more strongly. There appears to be no mechanism here to delay the heating of the mixed layer of the ocean much beyond the 30 days by which the temperature of the mixed layer is observed to lag the sun.

Even if there is such a lag mechanism, unless it exceeds a century, it should not have prevented warming due to the biospheric pulse of CO_2 from becoming apparent by now. Thus, if the model estimates are correct, then the warming of 0.3° to 0.5°C since The Little Ice Age (1430-1850 A.D.) must have been due to the biospheric pulse of CO_2 from forest clearing. As far as I am aware, only Alex Wilson of New Zealand has so far suggested such a connection. However, you can be certain that more and more people will jump on this band wagon unless they can somehow make the biospheric pulse of CO_2 go away. Why? Because, unless a warming due to the biospheric CO_2 pulse of 90-180 GtonsC can be identified, there is very little reason to believe what our climate models are now telling us about the effect of the fossil fuel pulse of CO_2 , which has now reached about 180 GtonsC.

Is the warming since The Little Ice Age due to the biospheric pulse of CO_2 ? I don't know. And I have been unable to think of a way in which the question can be answered definitively. I do not believe it was due to CO_2 , at least not entirely, for at least three reasons:

- I see no reason for ocean surface warming to lag more than a few years behind a flux increment; thus, if the warming we have detected was due to the biospheric CO_2 , why have we been unable to detect any warming from the fossil fuel CO_2 ?
- Warming of the present climate appears to be possible without increased CO_2 . Both the Climatic Optimum, centered about 6,000 years ago, and the Medieval or Little Optimum, centered about 900 years ago, are believed to have had mean surface temperatures 0.5° to 2°C warmer than that of today. While we do not know what caused these warmer periods, there is at present

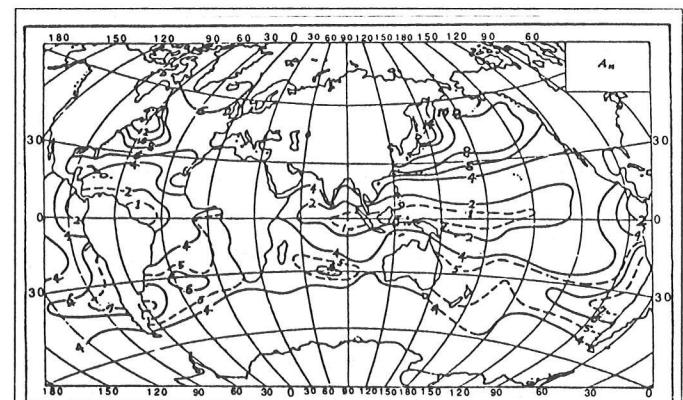


Figure 7. Map of the seasonal range in sea surface temperature in degrees C (adapted from Panfilova, 1972).

no reason to believe levels of CO₂ in the atmosphere then were different from its preindustrial value.

- Perhaps the most persuasive reason is the drastic difference between predicted and observed patterns of temperature change. Up to 1940, warming was a minimum near the equator and a maximum near the poles, but in most other respects it differed from what present models predict for increased CO₂. All patterns of surface temperature change, including that of 1881 to 1940, display cellular patterns of both warming and cooling; with few exceptions the models predict uniform monotonic warming for increasing CO₂. According to land observations from 1881 to 1940, the Northern Hemisphere warmed much more rapidly than did the Southern Hemisphere; the models indicate no such hemispheric asymmetry. The major fraction of Northern Hemisphere land data warming occurred in a discrete step of about 0.4°C between 1919 and 1921. A 7-year running average of the data in Figure 4, presented in Figure 8, illustrates this point. This is not at all the type of warming the models have led us to expect from a steadily increasing concentration of a greenhouse gas.

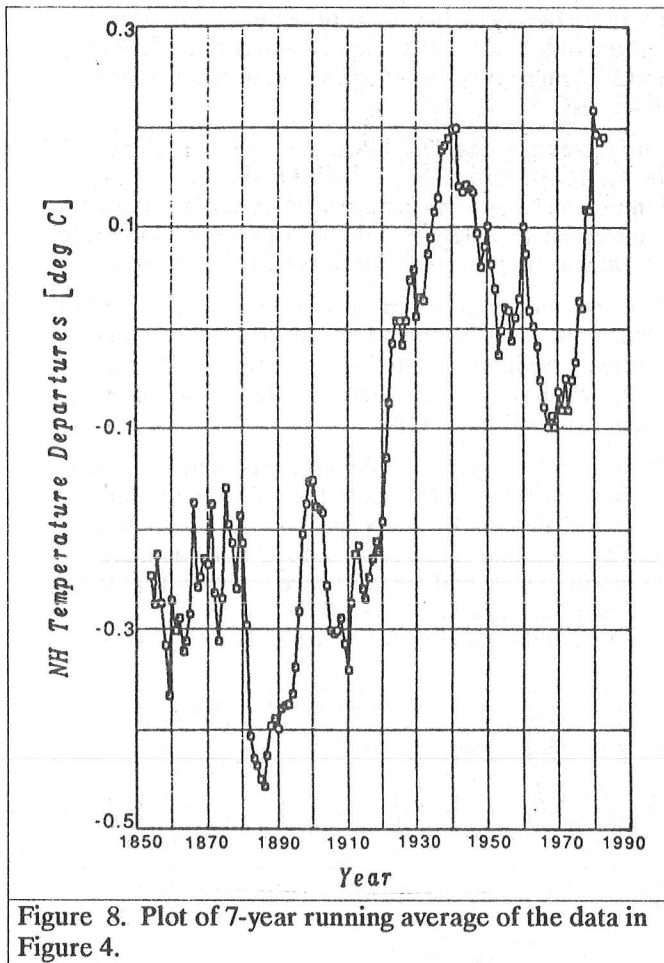


Figure 8. Plot of 7-year running average of the data in Figure 4.

There is another point to be made from Figure 8. We have heard much recently of how the climatic change predicted from increased CO₂ will be so rapid that both man and the natural biosphere will have trouble adjusting. Has anyone heard of any particular hardships caused by the apparent 0.4°C jump in Northern Hemi-

sphere land temperatures essentially between 1919 and 1921? To my knowledge, only a few of the specialists who have pored over the data are even aware of this abrupt "climate change" of this century.

While I am on this subject, I should point out that one of the strongest supporters of the contention that the warming of the past century has been due to CO₂ produced by man, Mikhail Ivanovich Budyko of the USSR State Hydrological Institute of Leningrad, has broken with most of his colleagues. While he still believes that doubled CO₂ will lead to a global warming of 3°C, he no longer believes this will be a climatic catastrophe. It is his view that while global warming will initially be accompanied by some drying in mid-latitudes, as the warming progresses, continental rainfall will increase almost everywhere and the planet will be a better place to live and produce crops for all of us. Rather than slowing the release of CO₂, he proposes that we speed up the process to hurry over the possibly unfavorable transition period (Budyko and Sedunov, 1988).

DIAGNOSIS OF APPARENT AND POSSIBLE MODEL DEFICIENCIES

I believe there are many reasons to be skeptical of the magnitude of the warming now being computed for the climatic effect of doubled CO₂. The most important ones are related to specific deficiencies which I see in the models and which I will discuss individually. Later I will summarize some more general problems which have been noted in the models.

Incorrect Handling of Tropical Convection

Over the approximately half of the Earth's surface constituting the tropics — roughly between 30°N and 30°S latitude — essentially all precipitation occurs in deep convection cells such as occur in the ITCZs (Intertropical Convergence Zones), monsoons, tropical cyclones (hurricanes, typhoons, etc.), easterly waves, and orographically induced thunderstorms. The first two of these, the ITCZs and monsoons, constitute the updraft leg of the Hadley circulation, which is a zonally symmetric planetary scale circulation with strong rising motion concentrated in relatively narrow bands near, but displaced from, the equator and slow broad-scale sinking motion or subsidence on either side covering the trade wind regions of both hemispheres and concentrated in the eastern and equatorward portions of the so-called subtropical anticyclones.

Each of the above types of deep convection, on their own space scales, sweeps warm moist air from the atmospheric boundary layer covering the tropical oceans and concentrates it into single cells or narrow bands of ascending air. If dry, the ascending air would cool at the so-called adiabatic lapse rate of 10°C/km (lapse rates any greater than this are statically unstable and will automatically cause overturning, like a layer of water on top of oil). But when saturated with water vapor, this cooling leads to condensation of the water vapor and release of latent heat, reducing the rate of cooling to about

6°C/km. This co-called **moist adiabatic** ascent is at very nearly the average lapse rate seen in the atmosphere – which in turn provides evidence that this is the mechanism that leads to the lapse rate we observe throughout most of the troposphere.

In deep convection, however, the latent heat released as water vapor is condensed and precipitated back to the surface; it is not mixed into the atmosphere at the level at which condensation occurs. Instead, the latent heat merely supplies the buoyancy that keeps the convective bubble or plume rising until it reaches a level in the atmosphere at which it is gravitationally stable; that is, that has the same density as the rising plume. While inertia may cause some overshooting of this level, the plume will soon settle back and spread out at its equilibrium level. The spreading tops of the convection cells or thunderstorms are visible as the so-called **anvils** of the thunderstorms. Around the convective updraft there will be volume conserving descent or subsidence, extending from the level at which the plume ceases to rise and spreads out horizontally all the way down to the level from which the updraft started. This descent will occur under dry adiabatic conditions; that is, it will warm at the rate of 10°C/km unless there are water drops present that can be evaporated. It is this mechanism that actually warms the atmosphere in regions of convection. Since the area of downdraft is very much larger than the area of ascent, the downward displacement for each individual convective plume is quite small. However, the process is cumulative. Each convection cell adds to the process, so most of the tropical troposphere above the trade wind inversion eventually is filled by air that has subsided from the altitude of the anvil tops of the deep convective cells. Since temperatures at that level are very low, -50° to -90°C, this subsided air is very dry.

What does this have to do with the climatic effect of increased CO₂? Climate models predict that increased CO₂ will lead to surface warming and, since warmer air can hold more water vapor, they predict a faster evaporation of water vapor, an acceleration of the hydrologic cycle leading to more precipitation and a general increase in the amount of water vapor in the atmosphere; that is, a deepening of the greenhouse blanket due to water vapor. As pointed out above, this is expected to amplify the greenhouse effect of increased CO₂ alone by a factor of 3.2. But over the tropics, which is about half the total area of the globe and where essentially all precipitation occurs in deep convection, acceleration of the hydrologic cycle also means acceleration of subsidence surrounding the deep convection cells – possibly including the global scale Hadley circulation. Any increase in water vapor in this part of the atmosphere will be restricted to the boundary layer and that small part of the area occupied by the ascending convective plumes. Over the vast bulk of the tropics, the stronger subsidence is more likely to lead to a drier tropical troposphere or a thinner, rather than thicker, greenhouse blanket of water vapor. Thus, over this half of the globe, which is also the warmest and most moist half, **feedback from water vapor** is likely to be **negative**, rather than positive. It does not appear likely that the expected

more than threefold amplification by water vapor of the added CO₂ greenhouse effect will occur here.

Figure 9 (Prabhakara et al., 1985) presents observational data from satellites showing that the acceleration of the hydrologic cycle and/or Hadley circulation in the eastern tropical Pacific during the El Niño of 1982 and 1983 produced exactly the moisture distribution changes I have described – i.e., a deeper moist layer (increase in precipitable water) in the enhanced ITCZ area near the equator and shallower moist layers (decreases in precipitable water) over the remaining tropical latitudes of both hemispheres. Such a distribution of vertical motion and precipitation anomalies was also found by Nicholson (1986) over Africa in those years that she classified as “stronger Hadley-type.”

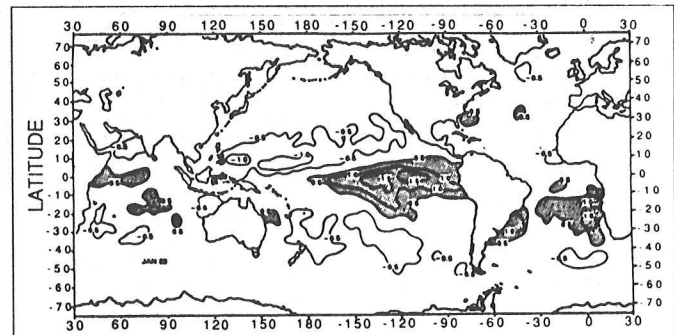


Figure 9. Map of January 1983 anomalies in precipitable water (g/cm^2) with respect to the 3-year mean, 1979-1981. Positive areas hatched (from Prabhakara and Short, 1985).

It is also of interest to note that the integrated upward IR flux at the top of the atmosphere, particularly in winter, peaks in the subtropics rather than at the equator. That is, IR emission can escape to space from lower and warmer altitudes because of the reduced optical thickness of the overlying column of water vapor, which occurs in the Hadley downwelling region of the subtropics compared to that near the equator (Charlock, 1984). Any strengthening of this subtropical downwelling would result in enhanced emission to space from an even lower and warmer top of the moist layer in these latitudes.

As the above analysis indicates, any acceleration of the hydrologic cycle in the tropics should augment the already sharp contrasts in precipitation observed there. That is, the wet regions should become wetter and the dry regions drier. However, any decrease in precipitation in the dry regions should be far more noticeable than slight increases in precipitation in the wet regions. This analysis leads to the conclusion that climatic changes such as the present Sahelian drought may be the first detectable evidence of climatic changes induced by increased CO₂ (Ellsaesser, 1987). Current climate model results tend to support this. They show generally an acceleration of both the hydrologic cycle and the Hadley circulation for a doubling of CO₂, and they all produce quite similar latitudinal profiles of percentage change in precipitation versus latitude. In the annual mean, the latter are peaked at the equator, show

minimal or even negative changes in subtropical latitudes of both hemispheres, and then percentage increases toward the poles. Thus, the climate models compute at least part of the climatic change from increased CO₂ by accelerating the intertropical convergence of the ITCZs even though they do not handle the convection within these circulation systems very well.

However, since the Hadley circulation is presumably driven by surface frictional drag on the trade winds — if increased CO₂ reduces zonal winds, as most models predict, the Hadley circulation itself will more likely decrease than increase as predicted by the models, even if the hydrologic cycle is accelerated. Evidence seems to indicate that the Hadley circulation was stronger during the period of stronger zonal winds of the last ice age and weaker during the warmer-than-present Altithermal of 6,000 YBP. Separation of the separate driving mechanisms of deep tropical convection and the Hadley cell is a problem that there is no hope of resolving until models can handle deep convection in a physically realistic manner. However, in two published studies of the energy balance of the equatorial trough, Riehl and Malkus (1958, 1979) concluded that the mass updraft in deep convection is at least twice that of the mean flow or Hadley updraft and that the excess is compensated by broadscale dry adiabatic descent and by near-cloud down drafts that are, at least in part, moist adiabatic.

Overestimation of Warming of the Tropical Oceans

In their analyses of recent doubled-CO₂ experiments with general circulation models (GCMs), Schlesinger and Mitchell (1985) noted that most of the models computed a warming of -2°C over the tropical oceans, but the GISS model (Hansen et al., 1984) computed a warming there nearly twice as great. I believe the problem is far more serious than mere disagreement among the models, which in itself is adequate reason for concern on this point.

The important point to remember is that the atmosphere cannot be warmed unless the underlying surface is warmed first. The present tropospheric lapse rate is much shallower than can be maintained by radiation transport alone. This means that each layer of the troposphere is now emitting more IR radiation than it absorbs from the overlying and underlying layers, including sunlight, and would therefore cool if radiation were the only process operating. All models since that of Manabe and Strickler (1964) compute a net radiative loss of energy from the lower atmosphere due to the three principal radiatively active gases in the atmosphere: water vapor (H₂O), carbon dioxide (CO₂), and ozone (O₃). The net radiation (solar plus IR) tends to show cooling throughout the troposphere, except below surface inversions in high latitudes, ranging up to 2.5°C/day and averaging 1.2°C/day for the whole troposphere (Dopplack, 1979). This cooling is not uniform but shows a maximum in a 2-km-thick warm moist surface layer extending over 30 to 50 degrees of latitude, which migrates seasonally with the sun, and another

maximum in a nearly continuous layer near 11 km, which is relatively uniform but does show a maximum at the summer pole and a minimum at the winter pole (Charlock, 1984). The apparent global mean radiating layer near 6 km and a temperature of 255K mentioned earlier is, obviously, in reality more structured.

For our principal greenhouse gas, water vapor, Doherty and Newell (1984) computed that the rate of radiative cooling increases throughout the troposphere as water vapor is increased to about 1.5 times the present level and, above 850 mb, the rate of cooling continued to increase up to the highest water contents tested, even though the changes were quite modest for a range of precipitable water content of 0.2 and 2.2 times the present. The only reason additional CO₂ does not also increase the tropospheric cooling rate is that increased CO₂ is uniformly mixed up into the stratosphere, where there is a temperature inversion; i.e., temperature increases with altitude. While increased CO₂ causes a cooling at these levels, it still results in an increase in the downward IR flux to the troposphere.

This analysis clarifies why the surface air cannot be warmed until the underlying surface is warmed. It also implies that, in contrast to current practice, climate models designed to compute surface air temperature changes should focus their attention on the lower boundary, particularly the surface or mixed layer of the oceans.

On a global basis, doubling the atmospheric content of CO₂ alone leads to an increase in IR flux to the surface of 1 to 1.5 W/m². (As pointed out above, this is actually a decrease in net outgoing flux from the surface.) In the tropics, Kiehl and Ramanathan (1982) computed almost no increase, because the moist surface layer is already essentially opaque to IR radiation due to the continuum absorption by water vapor. In addition, as temperatures rise, an increasing fraction of any enhanced flux to the surface will be used to evaporate more water from the ocean, as opposed to raising the temperature of the water.

From a study of maximum temperatures attained by plant foliage and the surface waters of tropical oceans, Priestley (1966) deduced that there should be a “rather sharply defined upper limit to which air temperature will rise above a well watered surface”. Using monthly averages of daily maximum temperatures, he identified the limiting temperature for land stations that had not exhausted their soil moisture as about 92°F (33.3°C). Priestly and Taylor (1972) found that the Bowen ratio (ratio of sensible to latent heat flux from the surface to the atmosphere) decreased monotonically with increasing temperature, suggesting that sensible heat flux became negative (flows from the atmosphere to the surface) at temperatures about 32°C. A reversal of the heat transfer between plant leaves and the air at about 33°C (i.e., heat moving from the air to the plant at temperatures above 33°C) was reported earlier by Linacre (1964). A review of the Bowen ratio data by Brutsaert (1982 Fig. 10.3) placed the apparent sign reversal near 30°C. Newell and Dopplack (1979) sought to illustrate the physics of this situation. Holding the surface atmospheric conditions fixed at 27°C and 65% relative

humidity, they computed a requirement of 30 W/m^2 incremental flux to warm the water 1°C . This paper has been widely and vehemently condemned as unrealistic for not allowing the air to warm and to increase its water vapor content. Since then, two papers have come to my attention that estimated the thermal inertia of the surface waters of the eastern Mediterranean (Assaf, 1983) and of the Tropical Pacific (Niiler, 1981) to be 40 W/m^2 per degree C. (Professor Newell told me that since the cited paper appeared, he and his colleagues have been essentially blackballed by those allotting climate research funds. It is my impression that the paper aroused great animosity in the climate research community — almost as great as that aroused by the papers of Idso [Luther and Cess, 1985].)

Flohn (1982) stated: “Above warm heated waters, the air is heated from below and thus unstable, water vapor is transported rapidly upward with atmospheric turbulence and the relative humidity cannot increase above a certain threshold (near 78 percent),” and that due to “the exponential increase of saturation vapor pressure with SST: above about 29°C (at a maximum 29.5°C) the available net radiation — see Hastenrath and Lamb (1978, 19[79]) — is no longer sufficient to maintain the process of evaporation.”

The palaeoclimatologists, Matthews and Poor (1980), proposed the working hypothesis that surface temperatures of the tropical oceans are tied to the solar constant and have maintained their present values back even through the Cretaceous — the period of warmest terrestrial climate yet documented (Barron et al., 1981). In its reconstruction of the climate of 18,000 YBP, CLIMAP (1976, 1981) found very little change in tropical ocean surface temperatures other than that attributed to stronger Chile and Benguela ocean currents and stronger equatorial upwelling.

All of these various types of information make it appear unlikely that doubling the atmospheric concentration of CO_2 will cause tropical ocean SSTs to warm by as much as 2°C , much less 4°C as predicted by the GISS model (Hansen et al., 1984), particularly since continuum water vapor absorption will prevent any significant increase in net downward radiation over these oceans from increased CO_2 (Kiehl and Ramanathan, 1982).

General Climate Model Deficiencies

Below is offered a general diagnosis of causes of some of the problems with the models cited above. These are, at best, educated guesses and could only be substantiated, if at all, by substantial additional model experiments. They are offered primarily as a stimulus to attract additional attention to this important problem. They are based primarily on comparative analyses of the four principal GCM models analyzed by Grotch (1988); i.e., the GCMs of the modeling groups at NCAR:

- CCM (Washington and Medehl, 1984),
- GFDL (Manabe and Wetherald, 1986; Manabe et al., 1981),

- GISS (Hansen et al., 1984), and
- OSU (Schlesinger, 1982).

Convection and Summer Precipitation — One rather broad generalization is that the models, as noted above, do not handle atmospheric convection, particularly deep convection, at all well. This shows up in the mainly convective precipitation of summer. To varying degrees (OSU most, GISS least), the models underestimate convective precipitation generally, as in the South Pacific Convergence Zone (which if Jaeger [1976] and Schutz and Gates [1971,1972] can be believed, is even stronger in the Southern Hemisphere winter than in summer), but particularly over land in summer. Outstanding examples of deficits in summer precipitation occur over Central America and northern and central South America, over the Caribbean in general, and along the Antarctic Convergence. On the other hand, the models tend to overestimate summer precipitation over continents. In their diagnoses of the GISS models, Strauss and Shukla (1988a,b) and Rind (1988) frequently note that discrepancies with observations are greater in summer and that continental precipitation is excessive in summer by a factor of 2. After experiments with models of different space resolutions, Rind (1988) reported: “Our true uncertainty in climate sensitivity is probably of the order of 100%”

Radiation Errors Suggested by Continental Summer Temperatures — A second broad generalization is that the models are quite diverse in their handling of radiative transport and, in so far as they disagree in this respect, they are probably all in error since no single model stands out as better than the others in this respect. The strongest evidence here is the poor agreement in computed land temperatures in summer (see Grotch, 1988). Inasmuch as the model agreements in sea surface temperature and in land surface temperatures in winter are more or less imposed by the essentially prescribed ocean temperatures on the one hand and the strong latitudinal temperature gradients in the winter hemisphere on the other, the weakness of the models is particularly discouraging. Hansen et al. (1988) pointed out that, despite the overall lesser variability of the models compared to observations — particularly in the upper troposphere and stratosphere, the models show unrealistically large surface temperature variability over the continents in summer. “The largest discrepancy in the [GISS] model is the overestimate of variability in continental areas during summer, with the model yielding a variability about twice as large as in the observations” (Hansen and Lebedeff, 1987; Hansen et al., 1988).

Additional evidence for this particular type of error is provided by the positions and intensities of continental summer heat lows. Both the CCM and GFDL models compute excessively strong continental heat lows, particularly over Australia (the smallest continent), and they also place the North American heat low in the eastern rather than southwestern United States (far east and north of its observed position). This latter error, in particular, would appear to be due to errors in the radiation calculations, possibly mediated by errors in water vapor and soil moisture distributions.

This comparative analysis of results of the four principal GCM models tends to cast doubt on validity of the GFDL (Manabe et al., 1981) prediction of reduced soil moisture in mid-latitudes as a result of doubled CO₂. As shown in Grotch (1988, Figs. 6-7, 6-8, and 6-9), for land areas of Africa, western Europe, and the United States, only GFDL computed a decrease of precipitation in summer for doubled CO₂. But, as shown in Grotch (1988, Fig. 5-17), GFDL also predicted the largest warming for Northern Hemisphere land areas in summer, particularly over North America and the United States. These higher summer temperatures will strongly affect soil moisture levels, and vice versa. However, there is little room for complacency here. That is, while the predicted decreases in soil moisture in mid-latitudes may not be believable, both the models and the theoretical analysis suggest greater aridity in the already dry subtropics with increased CO₂ (Ellsaesser, 1987). It should be noted that in discussions of soil moisture, few of the contributors on this subject have discussed, or even mentioned, the tendency of enhanced CO₂ to reduce the degree or daily period that plant stomata are open and thus to reduce evapotranspiration and the plant's water needs. This is particularly surprising since the theoretical basis for this effect is just as strong as that for enhancement of the greenhouse effect and the supporting experimental evidence is far greater (Idso and Brazel, 1984; Idso, 1988).

The OSU model appears to stand out in placing the subtropical anticyclones, or at least the areas of minimum precipitation usually associated with them, over (rather than to the west of) the subtropical continents. The cause for this is not apparent, but may again be a result of improper calculation of radiative transport.

Strong Band of Warming at 65°S — A third serious and general problem is revealed by the strong bands of warming, even in summer, computed for a doubling of CO₂ at approximately 6°S by all of the models except OSU. For the Northern Hemisphere summer, all models computed a doubled CO₂ warming of less than 2°C at the North Pole (see Grotch, 1988 Fig. 5-4), yet in the Southern Hemisphere summer (DJF), they computed warmings of 4° to 8°C at 60 to 70 degrees S (see Grotch, 1988 Fig. 5-3), a region where the current annual range in temperature is held to about 1°C due to deep oceanic overturning. This error suggests that the control model computed excess ice cover, which melted with doubled CO₂.

Disagreement with Observations — In addition to the differences in predicted and observed changes pointed out above, the more detailed observations of changes in atmospheric structure since 1957 show even stronger departures from the uniform monotonic polar-amplified type of warming suggested by the models. This is perhaps most apparent from Angell's (1988) analyses of upper air sounding data. During this later period, the Southern Hemisphere again warmed more at the surface than the Northern Hemisphere. However, most of the warming has been in low latitudes and Antarctica, such that the

equator-to-pole temperature gradient increased in the Northern Hemisphere while decreasing in the Southern Hemisphere. In the mid- to lower troposphere (850-300 mb) the meridional temperature gradient also increased in the Northern Hemisphere while remaining essentially unchanged in the Southern Hemisphere. During the most recent 15 years, 1973-1987, Angell's (1988) data indicate surface warming in all climatic zones except the two polar zones; i.e., cooling occurred in those zones where greenhouse warming is computed to be a maximum. This resulted in an increase in meridional temperature gradients in both hemispheres in this significant layer of the troposphere, again contrary to the expected effect of increased greenhouse gas.

Even more troubling is Angell's (1988) finding of cooling in the 300-100 mb layer, particularly in the tropics, where this layer is within the upper troposphere and where the models generally compute greater warming than at the surface. This has been cited as a "significant discrepancy" by several researchers, even though Angell (1988) himself called it a "neutral finding".

The Turf Factor

You are all no doubt aware of the tendency for each profession to find solutions to problems to lie within its own area of expertise; i.e. within its own turf. The CO₂ problem has actually been taken over by a specialty within a specialty — the specialists in radiation transport.

This is not particularly surprising. Radiation transport is a complex subject requiring a huge volume of detailed physical data of various types and specialized mathematical methods. Even now, comparatively few specialists are capable of reworking the CO₂ problem from the first principles. Those who could do so were given major roles in climate model development and for the most part emerged as the spokesmen of the climate modeling effort. This in itself would not be bad, except that the training requirements for excelling in the field and the demand for their special talents in most cases left little time for becoming comparably familiar with other important meteorological and climatic processes. As a corollary, many meteorologists, even though they have strong reservations about the model predictions, have remained silent rather than reveal or be accused of ignorance with regard to radiation transport. This combination of circumstances has led to a tendency to interpret all climatic processes in terms of radiation transport and, in particular, in the ongoing climatic debate to exaggerate the role of radiative transport compared to other processes of equal or even greater importance in climatogenesis.

THE PALAEOCLIMATIC RECORD

Based on several types of evidence, but mainly on variations in the isotope Oxygen-18 in drilling cores from the ocean floor, the climatic history of the Earth has been reconstructed in considerable detail (Crowley, 1983).

The Last 100 Million Years

Other than the estimated 10°C cooling from the Cretaceous peak about 100 million years ago, the outstanding feature of this history is the waxing and waning of continental glaciers over cycles about 100,000 years in duration. These cycles have been asymmetric, involving long periods of staged, multi-step glacial buildup (called the **glacials**), which last about 90,000 years each and are terminated abruptly by rapid transitions to warm periods (the **interglacials**), which last about 10,000 years each. Over the past 2 million years there have been at least 17 such cycles. The periods and phasing of the more regular records of the past 7 of these cycles have until recently (Winograd et al., 1988) appeared to be related to changes in received solar radiation due to the periodic variations in the Earth's orbit around the sun. But the quantitative relationships as to how such weak changes, mostly in seasonal and latitudinal distribution of sunlight, can cause such large climate variations remain a puzzle. These cycles have been accompanied by oscillations in average surface air temperature of the Earth estimated at 3° to 5°C in the global average, somewhat less in the tropics and 2 to 3 times greater near the poles (Crowley, 1983). The present interglacial, called the Holocene, is believed to have begun about 11,000 years ago (Crowley, 1983). Thus, evidence suggests that the onset of the next glacial is, if anything, overdue.

The Last 10,000 Years

The oceanic sediments from which the above climatic record was derived accumulated at rates of millimeters to centimeters per thousand years, so the records are greatly smoothed by the creatures living on the ocean floor and burrowing in the bottom ooze. Polar glaciers build up 10 to 1,000 times more rapidly than ocean sediments, have few burrowing life forms, and also have a temperature-indicative variation in Oxygen-18 about 5 times larger than that of ocean sediments. However, they are subject to other sources of confusion of the record — melting and glacial flow. Still, if cores are drilled at points perennially below freezing and forming a summit of the glacier, any flow should be outward in all directions so the layers below should be subject only to thinning, with no relative displacement from one layer to the next.

Ice cores from such sites in both the Greenland and Antarctic glaciers have given us an even more detailed reconstruction of climatic history back through the last

interglacial, or about the last 130,000 years. In addition to temperature changes indicated by Oxygen-18, the ice layers record past atmospheric levels of dust, radioactive tracers, chemicals such as sulfate, and even the greenhouse gases such as CO₂ and methane. While CO₂ levels appear to have varied from about 200 ppm during the glacials to 265 to 280 ppm during the interglacials, evidence suggests this is as much a result of the temperature changes as a cause of them.

Such reconstructions of the history of past temperature also show superimposed oscillations about 2,500 years in duration, with warmer periods centered about 1,000, 3,500, and 6,000 years ago and colder periods centered between them (Crowley, 1983). It was during the Medieval Little Optimum, centered about 1,000 years ago, that sea ice melted back in the North Atlantic and the Norsemen were able to settle Iceland and Greenland and may even have reached Labrador. Similarly, it was during the following cold part of the cycle, the Little Ice Age (usually assigned to 1430 to 1850 AD), that the Greenland colony died out and history recorded glacier advances and abandonment of farms and villages in parts of Europe. The Climatic Optimum (6,000 years ago) and the Medieval Little Optimum (1,000 years ago) apparently had mean temperatures 0.5° to 2°C warmer than today. Since evidence indicates that CO₂ was at the preindustrial level during those periods, higher levels of CO₂ are apparently not needed for the temperature to rise above the present level.

As noted above, in the present climatic epoch, there have been some 17 glacial/interglacial cycles, and the present interglacial is believed to have begun about 11,000 years ago. Thus, by present knowledge there is no reason not to expect the onset of the next cycle of 90,000 years of glaciation to begin at any time. In this context, I find it remarkable that one rarely hears the suggestion that increased carbon dioxide in the atmosphere is just what is needed to prevent or delay the onset of the next period of glaciation, which, if anything, is apparently already overdue! Also, on the longer time scale (100 million years), the Earth has been cooling and the atmosphere has been losing carbon dioxide. Most plants are not expected to survive at CO₂ concentrations below about 100 ppm — about half the levels reached during the most recent glacials. Yet no one seems to dare to suggest that man might be **fertilizing** rather than **fouling** his nest or that turning to consumption of fossil fuels was an act of such providential foresight for preservation of the biosphere that it could only have been **divinely inspired!**

REFERENCES

- Angell, J.J., 1988, Variations and trends in tropospheric and stratospheric global temperatures, 1958-87: *Journal of Climate*, v.1, 1296-1313.
- Assaf, G., 1983, Enhancement of precipitation via sea mixing: Paper presented at 12th International Conference on Unity of the Sciences, Chicago, IL, 24-27 November 1983.
- Barron, E.J., Thompson, S.L., and Schneider, S.H., 1981, An ice-free Cretaceous? Results from climate model simulations: *Science*, v.212, p.501-508.
- Brutsaert, Wilfried, 1982, *Evaporation into the Atmosphere*: Dordrecht, Holland, D. Reidel.
- Budyko, M.I., and Sedunov, Yu. S., 1988, Anthropogenic climate changes: Paper presented at the Climate and Development Conference, Congress Centrum, Hamburg (FRG), 7-10 November 1988.
- Charlock, Thomas P., 1984, Wavenumber dependent investigation of the terrestrial infrared radiation budget with two versions of the LOWTRAN5 Band Model: *Journal of Climate and Applied Meteorology*, v.23, no.1, p.25-33.
- CLIMAP (Climate: Long-Range Investigation, Mapping, and Prediction) Project Members, 1981, Seasonal reconstructions of the Earth's surface at the last glacial maximum: Map Chart Series, no.36, Geological Society of America, Boulder, CO.
- _____, 1976, The surface of the ice-age Earth: *Science*, v.191, p.1131-1137.
- Crowley, T.J., 1973, The geologic record of climatic change: *Review of Geophysics*, v.21, p.828-877.
- Davies, J.A., and Allen, C.D., 1973, Equilibrium, potential and actual evaporation from cropped surfaces in southern Ontario: *Journal of Applied Meteorology*, v.10, p.811-819.
- Doherty, G.M., and Newell, R.E., 1984, Radiative effects of changing atmospheric water vapor, *Tellus*: v.36B, p.149-162.
- Dopplick, Thomas G., 1979, Radiative Heating of the global atmosphere: Corrigendum: *Journal of Atmospheric Sciences*, v.36, p.1812-1817.
- Ellsaesser, H.W., 1987, The Sahelian drought – First evidence of a CO₂-induced Climatic Change? in *Proceedings of the Eleventh Annual Climate Diagnostics Workshop*: U.S. Department of Commerce, Climate Analysis Center, p.201-204, February 1987.
- _____, 1984, The climatic effect of CO₂: A different view: *Atmos. Environ.* v.18, p.431-434; 1495-1496.
- Ellsaesser, H.W., MacCracken, M.C., Walton, J.J., and Grotch, S.L., 1986, Global climatic trends as revealed by the recorded data: *Review of Geophysics*, v.24, no.4, p.745-792.
- Flohn, H., 1982, Oceanic upwelling as a key for abrupt climatic change: *Journal of Meteorological Society of Japan*, v.60, no.1, p.268-273.
- Grotch, Stanley L., 1988, Regional intercomparisons of general circulation model predictions and historical climate data, TRO41 DOE/NBB-0084: Springfield, VA, NTIS.
- Hamon, B.V., and Godfrey, J.S., 1975, The role of the oceans, in Pittock, A.B., Frakes, L.A., Jenssen, D., Peterson, J.A., and Zillman, J.W. (Eds.), *Climatic change and variability; a southern perspective*: Cambridge, Cambridge University Press, p.31-52.
- Hansen J., Fung, I., Lacis, A., Rind, D., Lebedeff, S., Ruedy, R., Russell, G., and Stone, P., 1988, Global climate changes as forecast by Goddard Institute for Space Studies three-dimensional model: *Journal of Geophysical Research*, v.93, v.D8, p.9341-9364.
- Hansen, J., Lacis, A., Rind, D., Russell, G., Stone, P., Fung, I., Ruedy, R., and Lerner, J., 1984, Climate Sensitivity: Analysis of feedback mechanisms, in *Climate Processes and Climate Sensitivity*: Washington, DC, American Geophysical Union, Maurice Ewing Series, No.5, p.130-163.
- Hansen, J. and Lebedeff, S., 1987, Global trends on measured surface air temperature: *Journal of Geophysical Research*, v.92, no.D11, p.13345-13372.
- Hastenrath, S., and Lamb, P., 1979, *Climatic atlas of the Indian Ocean, Part II*: Madison, University of Wisconsin Press.
- _____, 1978, *Heat budget atlas of the tropical Atlantic and eastern Pacific Ocean*: Madison, University of Wisconsin Press.
- Houghton, R.A., Schlesinger, W.H., Brown, S., and Richards, J.F., 1985, Carbon dioxide exchange between the atmosphere and terrestrial ecosystems, in *Atmospheric Carbon Dioxide and the Global Carbon Cycle*, DOE/ER-0239: U.S. Department of Energy, Carbon Dioxide Research Division, NTIS, p.113-140.
- Idso, S.B., 1988, Three phases of plant response to atmospheric CO₂ enrichment: *Plant Physiology*, v.87, p.5-7.

- Idso, S.B., and Brazel, A.J., 1984, Rising atmospheric carbon dioxide concentrations may increase streamflow: *Nature*, v.312, p.51-53.
- Jaeger, L., 1976, Monatskarten des Niederschlags für die ganze Erde: *Berichte des Deutschen Wetterdienstes*, No.139, p.1-38.
- Jones, P.D., Bradley, R.S., Diaz, H.F., Kelly, P.M., and Wigley, T.M.L., 1986, Northern hemisphere surface air temperature variations, 1851-1984: *Journal of Climate and Applied Meteorology*, v.25, p.161-179.
- Kiehl, J.T., and Ramanathan, V., 1982, Radiative heating due to increased CO₂: The role of H₂O continuum absorption in the 12-18 micron region: *Journal of Atmospheric Sciences*, v.39, p.2923-2926.
- Kondrat'yev, K. Ya., 1986, Natural and Anthropogenic Changes of Climate [In Russian]: *Itogi Nauki i Tekhniki, Meteorology and Climatology Series*, v.16, VINITI, Moscow.
- Lamb, H.H., 1964, *Climate: Present, Past and Future*, Vol. 1: London, Methuen and Co.
- Linacre, E.T., 1964, A note on a feature of leaf and air temperature: *Agricultural Meteorology*, v.1, p.66-72.
- Luther, F.M., and Cess, R.D., 1985, Review of the recent carbon dioxide-climate controversy, *in* Projecting the climatic effects of increasing carbon dioxide, DOE/ER-0237: NTIS, p.321-355.
- Luther, F.M., and Ellingson, R.G., 1985, Carbon dioxide and the radiation budget, *in* Projecting the climatic effects of increasing carbon dioxide, DOE/ER-0237: NTIS, p.25-55.
- Manabe, S., and Strickler, R.F., 1964, Thermal equilibrium of the atmosphere with a convective adjustment: *Journal of Atmospheric Sciences*, v.21, p.361-385.
- Manabe, S., and Wetherald, R.T., 1986, Reduction in summer soil wetness induced by an increase in atmospheric carbon dioxide: *Science*, v.232, p.626-628.
- Manabe, S., Wetherald, R.T., and Stouffer, R.J., 1981, Summer dryness due to an increase of atmospheric CO₂ concentration: *Climatic Change*, v.3, p.347-386.
- Newell, R.E., and Dopplick, T.G., 1979, Questions concerning the possible influence of anthropogenic CO₂ on atmospheric temperature: *Journal of Applied Meteorology*, v.18, p.822-825.
- Nicholson, Sharon E., 1986, The spatial coherence of African rainfall anomalies: Interhemispheric teleconnections: *Journal of Climatic and Applied Meteorology*, v.25, p.1365-1381.
- Niiler, P.P.(ed.), 1981, Tropical Pacific upper ocean heat and mass budget, Research Program Outline: Honolulu, Hawaii, Institute of Geophysics.
- NRC (National Research Council), 1983, *Changing Climate*: Washington DC (Board of Atmospheric Sciences and Climate), National Academy of Sciences.
- _____, 1982, *Carbon Dioxide and Climate: A Second Assessment*: Washington, D.C., National Academy of Sciences.
- _____, 1979, *Carbon Dioxide and Climate: A Scientific Assessment*: Washington, DC, National Academy of Sciences.
- Panfilova, S.G., 1972, Seasonal surface water temperature variations in the World Ocean: *USSR Academy of Science Oceanology*, v.12, no.3, p.333-344.
- Pearman, G.T., 1980, Preliminary studies with a new global carbon cycle model, *in* Pearman, G.I., editor, *Carbon dioxide and climate*: Canberra, Australian Research, Australian Academy of Science, p.79-91.
- Prabhakara, C., Short, D.A., and Vollmer, B.E., 1985, El Niño and atmospheric water vapor: Observations from Nimbus 7 SMMR: *Journal of Climate and Applied Meteorology*, v.24, p.1311-1324.
- Priestley, C.H.B., 1966, The limitation of temperature by evaporation in hot climates: *Agricultural Meteorology*, v.3, p.241-246.
- Priestley, C.H.B., and Taylor, J.R., 1972, On the assessment of surface heat flux and evaporation using large-scale parameters: *Monthly Weather Review*, v.100, p.81-92.
- Ramanathan, V., 1981, The role of ocean-atmosphere interactions in the CO₂ climate problem: *Journal of Atmospheric Science*, v.38, p.918-930.
- Riehl, H. and Malkus, J.S., 1958, On the heat balance in the equatorial trough zone: *Geophysical*, v.6(3-4), p.503-537.
- Riehl, H., and Simpson, J.S. (Malkus), 1979, The heat balance of the equatorial trough zone, revisited: *Contributions to Atmospheric Physics*, v.52, no.4, p.287-305.
- Rind, D., 1988, The doubled CO₂ climate and the sensitivity of the modeled hydrologic cycle: *Journal of Geophysical Research*, v.93, no.D5, p.5385-5412.

- Rotty, R.M., 1979, Energy demand and global climate change, in Bach, W., Pankrath, J., and Kellogg, W., (eds.), *Man's Impact on Climate*: Amsterdam, Elsevier Scientific Publishing Co., p.269-283.
- Schlesinger, M.E., 1982, Simulating CO₂-induced climatic change with mathematical climate models: capabilities, limitations and prospects, in *Proceedings: Carbon Dioxide Research Conference: Carbon Dioxide, Science and Consensus (CONF-820970)*: Springfield, VA, U.S. Department of Energy, Carbon Dioxide Res. Div., NTIS, p.III.3-143.
- Schlesinger, M.E., and Mitchell, J.F.B., 1985, Model projections of the equilibrium climatic response to increased carbon dioxide, in MacCracken, M.C., and Luther, F.M. (eds.), *DOE-ER-0237*: Springfield, VA, U.S. Dept. of Energy, Carbon Dioxide Res. Div., NTIS, p.81-147.
- Schutz, C., and Gates, W.L., 1971, Global Climatic Data for surface, 800 mb, 400 mb, January, Report R-915-ARPA: Santa Monica, CA, Rand Corporation, (available from Springfield, VA, NTIS (AD-760283)).
- _____, 1972, Global climatic data for surface, 800 mb, 400 mb, July, Report R-1029-ARPA: Santa Monica, CA, Rand Corporation, (Available from Springfield, VA, NTIS (AD-760283)).
- Straus, A.M., and Shukla, J., 1988a, A comparison of a GCM simulation of the seasonal cycle of the atmosphere with observations. Part I: Mean fields and the annual harmonic: *Atmosphere-Ocean*, v.26, no.4, p.541-574.
- _____, 1988b, A comparison of a GCM simulation of the seasonal cycle of the atmosphere with observations. Part II: Stationary waves and transient fluctuations: *Atmosphere-Ocean*, v.26, no.4, p.575-607.
- Washington, W.M., and Meehl, G.A. 1984, Seasonal cycle experiment on the climate sensitivity due to a doubling of CO₂ with an atmospheric general circulation model coupled to a simple mixed-layer ocean model: *Journal of Geophysical Research*, v.89, p.9475-9503.
- Wigley, T.M.L., 1987, Relative contribution of different trace gases to the greenhouse effect: *Climate Monitor*, v.16, no.1, p.14-28.
- Winograd, I.J., Szabo, B.J., Coplen, T.B., and Riggs, A.C., 1988, A 250,000-year climatic record from Great Basin vein calcite: Implications for Molankovitch theory: *Science*, v.242, p.1275-1280.

The Annual Course of Precipitation Over Much of the United States: Observed versus GCM Simulation

Ronald P. Neilson, George A. King, James Lenihan, and Robert L. DeVelice

ABSTRACT: General Circulation Models (GCMs) may be useful in estimating the ecological impacts of global climatic change. We analyzed seasonal weather patterns over the conterminous United States and determined that regional patterns of rainfall seasonality appear to control the distributions of the Nation's major biomes. These regional patterns were compared to the output from three GCMs for validation. The models appear to simulate the appropriate seasonal climates in the northern tier of states. However, the spatial extent of these regions is distorted. None of the models accurately portrayed rainfall seasonalities in the southern tier of states, where biomes are primarily influenced by the Bermuda High.

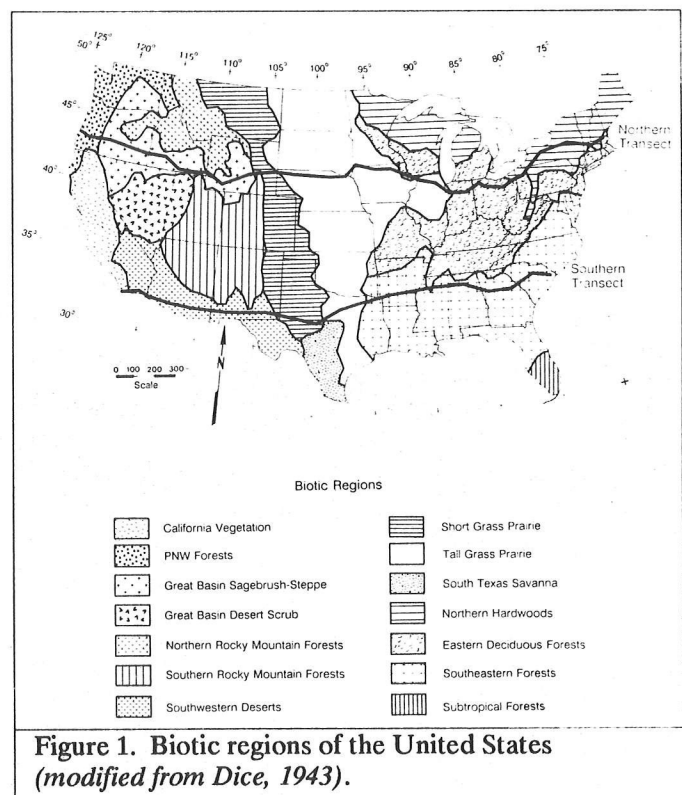
INTRODUCTION

The likelihood of global climatic change is receiving much attention from the scientific and lay communities (CES, 1989). Global increases in atmospheric concentrations of CO₂, CH₄, N₂O, and CFCs are now well documented (Wuebbles and Edmonds, 1988). General Circulation Models (GCM) are important in projecting the global climate impacts of these trace gas increases. These models are now expected to provide greater regional detail for the purpose of projecting ecological responses to climatic change (Environmental Protection Agency, 1989). Although the models reproduce zonal average temperature and rainfall patterns from the tropics to the poles reasonably well, their representation of regional patterns is more problematical (Grotch, 1988).

Additional difficulty arises in that ecologists still do not understand how the large-scale features of atmospheric circulation cause the geographic arrangement of different biotic regions such as grasslands, forests, and deserts. The objective of a related paper was to build mechanistic hypotheses causally relating regional climate, hydrology, and the distribution of major biomes in North America (King et al., in review). Having determined the apparent climatic drivers of biome distribution, we ask in this paper if the GCMs reproduce these drivers. This can be viewed as a component of validation for the use of these GCMs in projecting ecological consequences of climatic change.

METHODS

Precipitation data were obtained from U.S. Historical Climatology Network (HCN) Serial Temperature and Precipitation Data (Quinlan et al., 1987). Mean total monthly precipitation for selected stations was calculated for the 1941-1970 interval. HCN stations were selected along several east-west and north-south transects gridding the conterminous United States. Two east-west transects traversing the United States at latitudes of roughly 43° and 33°N (Figure 1) portray most of the climatic regionalization observed over the grid. Three-dimensional graphs were generated to portray spatial and seasonal gradients in observed precipitation along these transects (Neilson and Wullstein, 1983).



Station selection is stratified by elevation to suppress orographic complications. Stations were selected for the lower elevations within a region. When a mountain range was encountered, stations were selected from valleys on both sides of the mountain. The hypothesis is

In J.L. Betancourt and A.M. MacKay, editors, 1990. Proceedings of the Sixth Annual Pacific Climate (PACLIM) Workshop, March 5-8, 1989: California Department of Water Resources, Interagency Ecological Studies Program Technical Report 23.

that presence of the mountain range does not influence the general patterns of rainfall seasonality, only the amplitude. In some cases we find that the mountain influences the regional patterns and controls regional climatic boundaries. The coastal mountains and Rocky Mountains influence the seasonality of rainfall patterns over large regions (Bryson and Hare, 1974). The smaller mountains between these cordilleras have primarily local, orographic influences (Bryson and Hare, 1974). The Appalachians also produce a local influence on rainfall, but do not appear to control regional patterns of seasonality. The sampling approach described here allowed isolation of the specific mountain ranges that demarcate adjacent climatic regions.

The sampling design was intended to examine only horizontal climate patterns, rather than vertical zonation in mountains. Therefore, transects through the western United States pertain to the biomes that occupy the broad basins and were not intended to explain the forested zones at higher elevations within mountains.

U.S. Geological Survey (USGS) daily streamflow records (U.S. West, 1988) formed the basis for runoff data. Stream gages were selected to coincide with the two rainfall transects and were selected for watersheds between 100 and 200 km². Values for the selected gage stations were normalized by basin size and then converted to mean total monthly equivalent depths for comparison with the observed rainfall depths.

Simulated precipitation and runoff data were generated by three general circulation models:

- Goddard Institute for Space Studies (GISS) model (Hansen et al., 1988),
- Geophysical Fluid Dynamics Laboratory (GFDL) model (Wetherald and Manabe, 1988), and
- Oregon State University (OSU) model (Schlesinger and Zhao, 1988).

Model output was analyzed as total monthly precipitation and runoff depth. GCM output was compared to the real data along the two east-west transects.

In comparing the real and synthetic climates along the two transects, a word about resolution is appropriate. The selected weather stations are spaced about 2° of latitude, while the grid resolution of the GCMs is either 4°x5° or 8°x10°. Comparisons between models and the real values should be made at the same resolution, an exercise we have not included in this analysis. An equally important issue is that of translating coarse-grid information to a finer scale. Such scaling is required for the application of GCMs to ecological models. In this sense we feel it is instructional to compare the models to the real events in spite of the different resolution. This is useful in determining what needs to be done to rescale the GCMs to real situations.

RESULTS

The two east-west transects of climatic patterns display large regional climatologies associated with the major boundaries between the biomes in the conterminous

United States (Figures 2 and 3). These boundaries are primarily a result of changes in the seasonality of rainfall (King et al., in review). Specific mechanisms have been proposed that causally related these changes in rainfall seasonality to distributions of the biomes (King et al., in review). Temperature patterns will not be discussed.

The key features to be examined along each transect are the geographic sequence of precipitation seasonality and the locations of transitions from one pattern of seasonality to another. Thus, the northeast forested region receives high rainfall with virtually no seasonal pattern (Figure 2). The mid-continent grasslands along the northern transect are characterized by a strongly seasonal rainfall pattern with a mid-summer peak and a mid-winter minimum. The Great Basin receives low rainfall all year, with a significant winter precipitation peak. The west coast is dry in summer and very wet in winter. The transitions between biomes occur at ca. 87°, 103°, 107°, and 122° and are consistent with the regional transitions in rainfall seasonality (Figure 2b).

Comparison of the rainfall and runoff plots (Figures 2 and 3) suggests that streams in the northeast are drawn to low levels in summer, even though summer rainfall is quite high in both the grassland and forested regions. The persistence of runoff in summer in the forested region appears to result from the presence of high winter precipitation. This should recharge the deep soil layers during late winter and early spring snowmelt and runoff. Thus, a deep soil reservoir is apparently provided and allows tree transpiration, since summer rainfall apparently is not sufficient to balance the transpirational demand. The lack of sufficient winter rainfall in the grassland region apparently disallows the accumulation of a deep soil reservoir sufficient to maintain the water balance of trees on a regional scale. Note the lack of summer runoff in the grassland (Figure 3b). The sharpness of the spatial gradient in hydrology at the prairie-forest boundary, between 85° and 90° longitude (Figure 3b), is even more well defined than that in the rainfall gradient (Figure 2b).

The southern transect also displays large-scale regional rainfall patterns (Figure 4) that are similar to, but yet distinct from, those along the northern transect. The southeast forested region, like the northeast, receives high rainfall throughout the year. However, unlike the northeast, there are strong seasonal patterns of rainfall with winter and summer maxima. At the prairie-forest border (ca. 96°W, Figure 4b) the winter maximum has become a spring peak of rainfall, supplying necessary spring rains to the grasslands (Neilson, 1987; King et al., in review). Mid-summer rains in the southeast forested region become quite diminished at the border with the grasslands, leaving the prairie dry in mid-summer. The plains also receive a fall precipitation peak. The spring rainfall peak over the plains ceases at the Rocky Mountain/Sierra Madre Oriental axis (extending into Mexico) and becomes a spring drought in the southwest deserts (ca. 103°W). Southwest deserts are dominated by mid-summer rains, with spring and fall droughts and a mid-winter peak. The transition between the prairie

NORTHERN E-W TRANSECT, ACTUAL PRECIPITATION

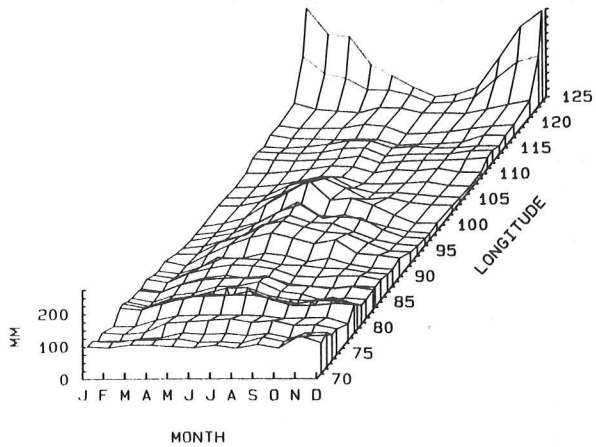


Figure 2a. Seasonality of precipitation across the northern transect. Locations of weather stations used to construct the graph are indicated by lines parallel to x-axis.

NORTHERN E-W TRANSECT, ACTUAL RUNOFF

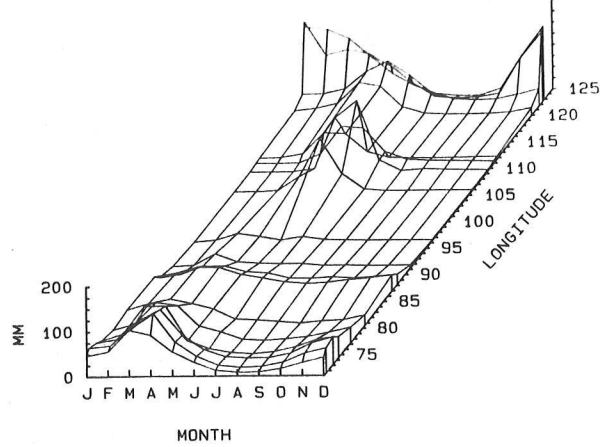


Figure 3a. Seasonality of runoff across the northern transect.

NORTHERN E-W TRANSECT, ACTUAL PRECIPITATION

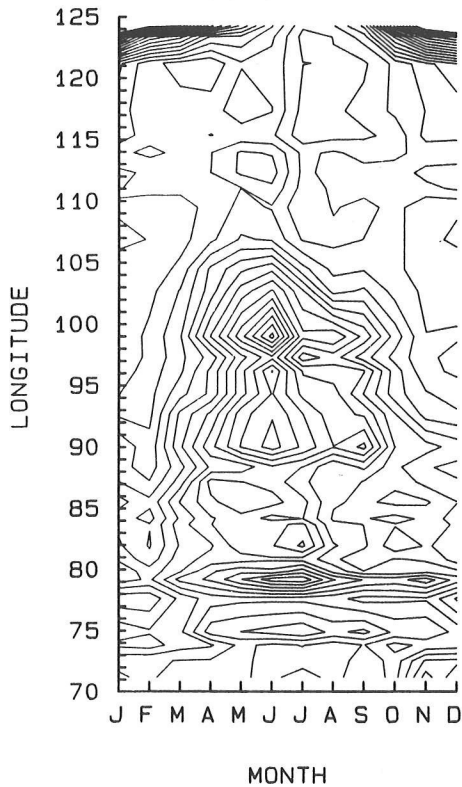


Figure 2b. Contour map of the surface in 2a. A particular contour represents seasonal distribution of a particular amount of precipitation. Contour interval is 10 mm, starting at 10 mm.

NORTHERN E-W TRANSECT, ACTUAL RUNOFF

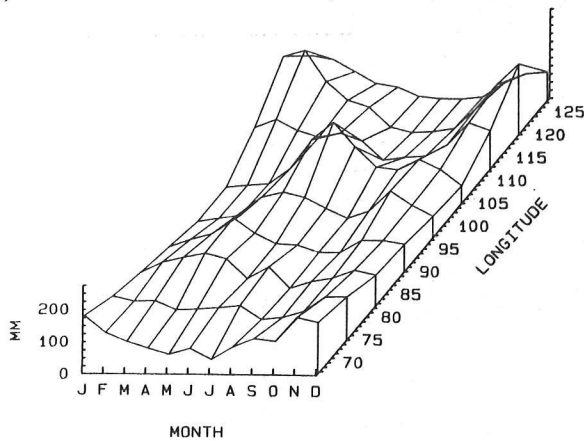


Figure 3b. Contour map of the surface in 3a. Contours as in 2b.

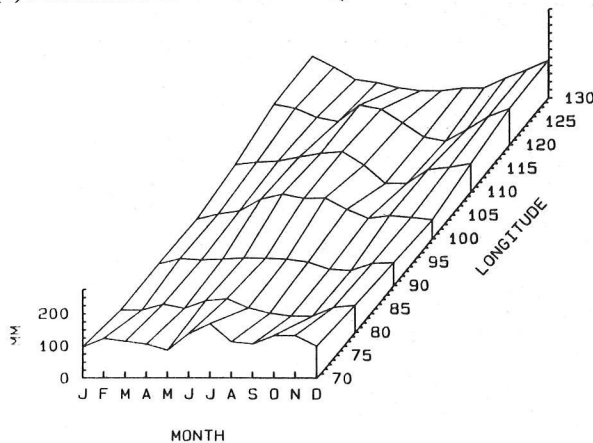
and desert climates is one of the few instances where a single mountain range controls a transition from one seasonal rainfall pattern to another (Bryson and Hare, 1974). The far-west coast is characterized by winter rains and mid-summer drought.

Seasonal runoff patterns along the southern transect (not shown) show similar patterns of regionalization. Again, the prairie-forest border is quite striking, with runoff all year in the forested region but only in spring in the grassland region. The hypotheses for explaining the seasonal runoff patterns and biome distributions are the same as for the northern transect.

(a) NORTHERN E-W TRANSECT, GFDL PRECIPITATION



(b) NORTHERN E-W TRANSECT, GISS PRECIPITATION



(c) NORTHERN E-W TRANSECT, OSU PRECIPITATION

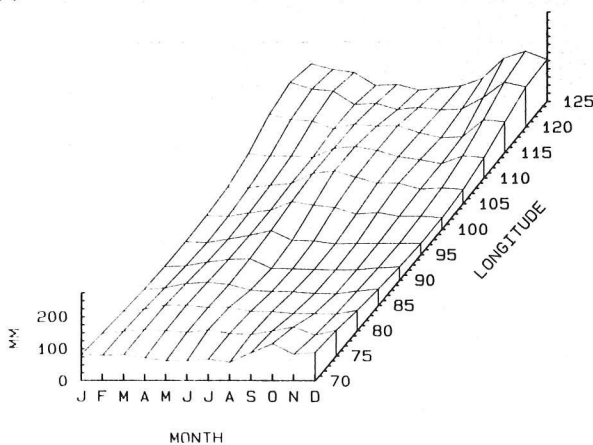


Figure 5. Seasonality of rainfall along the northern transect as produced by three General Circulation Models:

- a. GFDL
- b. GISS,
- c. OSU

We suggest that all these models have a reasonably correct spatial sequence of the seasonality of rainfall. However, the output appears to be spatially distorted. We hypothesize that this occurs in part because of the coarse representation of topography, being in part a function of the size of the grid-cells. For example, at an $8^{\circ} \times 10^{\circ}$ resolution, as in the GISS model, the coastal and Rocky mountains cannot be well resolved, likely producing the absence of the Great Basin climate. These spatial distortions appear to be artifacts of the topographic parameterization and should be stable within a model and between different model CO_2 runs, but different between models. Examination of $2 \times \text{CO}_2$ runs from the models (not shown) suggests that the spatial distortions are stable. The altered climate in the doubled CO_2 runs is apparent in the 3-dimensional plots as amplitude variation in the peaks and troughs. We propose that this stable distortion is one of the reasons the GCMs do not agree well in the regional rainfall patterns. However, the disagreement may not be as serious as previously thought. These distortions could be corrected in the calibration of the GCM output to the real data, but they never have been (Grotch, 1988).

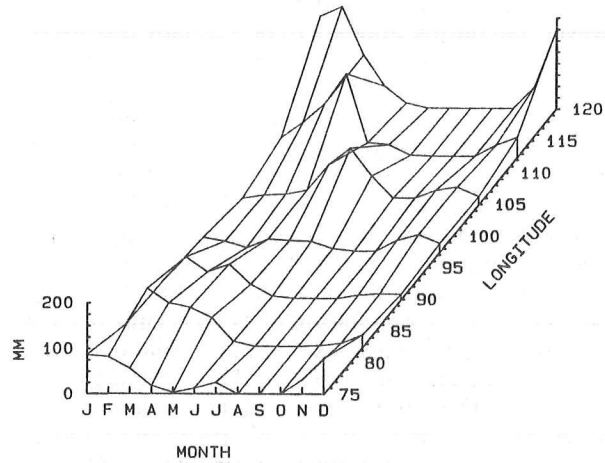
Although we suggest that the distortions in the models could be corrected, we recognize that this may not be consistent with the current representation of physics in the models. Variables such as winds, radiation, and clouds should also be analyzed in this way for consistency. Ground-surface interactions in the models may also be inconsistent with the suggested corrections. These are research questions.

The models also produce estimates of seasonal runoff. Comparison of Figure 3a with Figures 6a-c reveals considerable variation in fidelity of the models to the real data. The GFDL model comes the closest, followed by OSU and GISS.

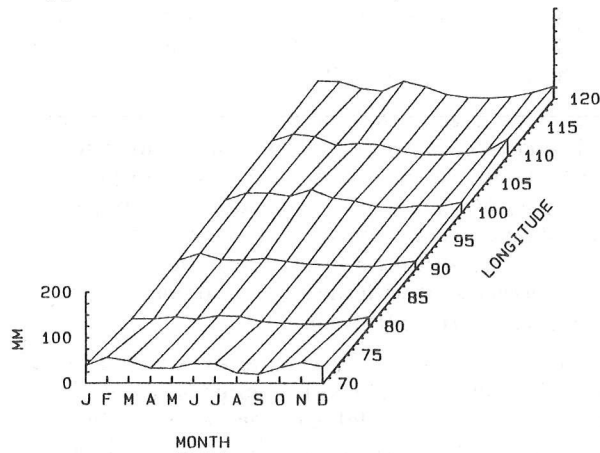
Turning attention to the southern transect, comparison of Figures 7a-c with Figure 4a reveals that there is no similarity between the modeled and real data in the spatial sequencing of seasonal rainfall patterns. This is a critical observation, given that the seasonality of rainfall along this transect appears to control the biotic distributions. Apparently the GCMs examined do not contain the large-scale features of the Bermuda High. Instead, they contain a circumglobal, subtropical high pressure belt, rather than three high pressure cells (Barry and Chorley, 1982). This would explain the lack of the appropriate storm tracks.

Runoff has been examined along the southern transect. However, since the rainfall seasonality bears little resemblance to the real data, the runoff plots are essentially meaningless and are not shown.

(a) NORTHERN E-W TRANSECT, GFDL RUNOFF



(b) NORTHERN E-W TRANSECT, GISS RUNOFF



(c) NORTHERN E-W TRANSECT, OSU RUNOFF

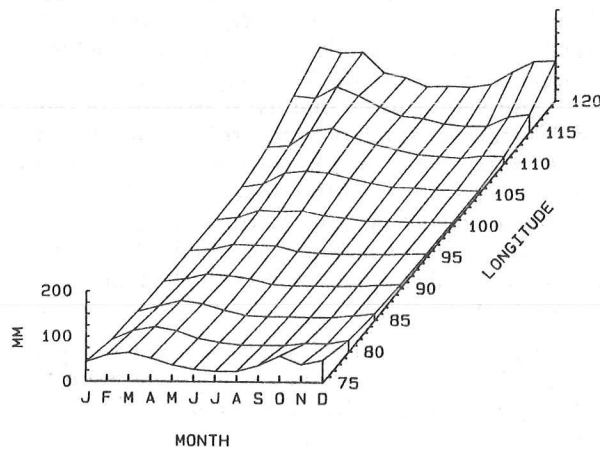
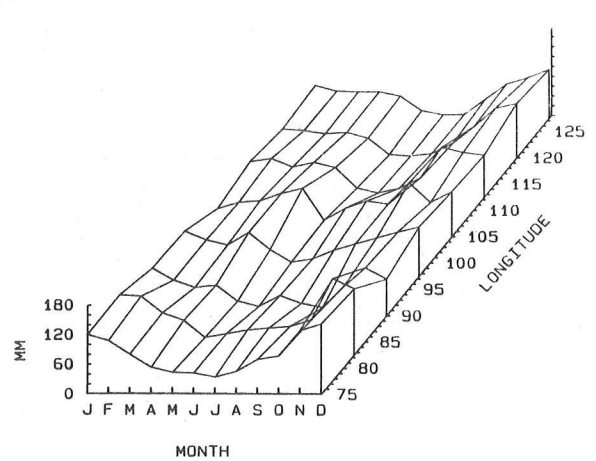


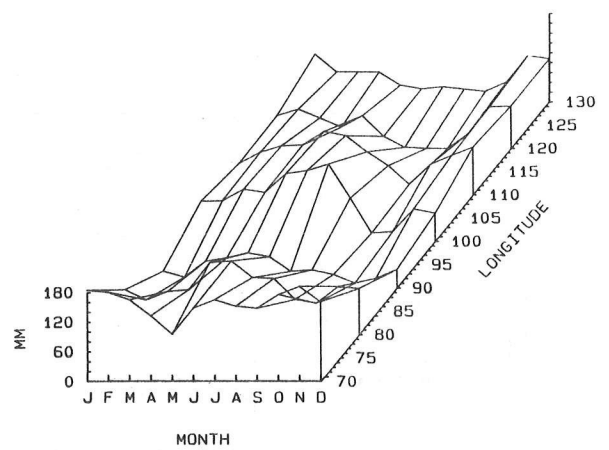
Figure 6. Seasonality of runoff along the northern transect as produced by three General Circulation Models:

- a. GFDL
- b. GISS
- c. OSU

(a) SOUTHERN E-W TRANSECT, GFDL PRECIPITATION



(b) SOUTHERN E-W TRANSECT, GISS PRECIPITATION



(c) SOUTHERN E-W TRANSECT, OSU PRECIPITATION

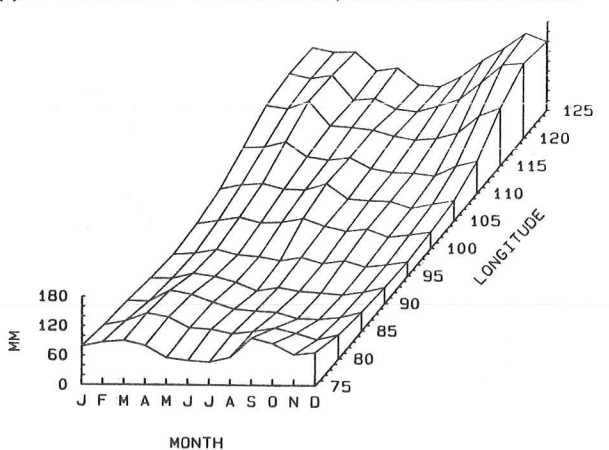


Figure 7. Seasonality of rainfall along the southern transect as produced by three General Circulation Models:

- a. GFDL
- b. GISS
- c. OSU

CONCLUSIONS

Analyses of weather patterns over the conterminous United States reveal relatively homogeneous climatic regions, defined from the rainfall seasonality. These regions coincide with the major biotic regions of the country and appear causative of the biome distributional patterns (Bryson and Hare, 1974; King et al., in review).

These analyses suggest that there are large zonal bands where the models are valid in reproducing seasonal rainfall patterns and large zonal bands where they are not valid in this sense. Where the models do appear valid, comparisons suggest that the regional rainfall patterns

are spatially distorted compared to the actual regional patterns. This implies that rules could be developed for calibrating model output to the actual spatial sequence of climates. This may have the effect of reducing discrepancies between models of regional rainfall patterns. Having made these corrections, the CO₂ driven anomalies should be examined for consistency between models.

The subtropical rainfall patterns do not appear to be valid in these models, suggesting the need for further model development. Potential areas of research are well recognized and consist of both sub-grid and large-scale processes, such as cloud parameterizations and feedbacks and ocean-atmosphere interactions.

REFERENCES

- Barry, R.G. and Chorley, R.J., 1968, *Atmosphere, Weather and Climate*: Methuen, 407p.
- Bryson, R.A. and Lowry, W.P., 1955, Synoptic climatology of the Arizona summer precipitation singularity: *Bulletin American Meteorological Society*, v.36, p.329-339.
- Bryson, R.A. and Hare, F.K., 1974, The climates of North America, in Bryson, R. and Hare, F., editors, *Climates of North America. World survey of climatology*, v.11: New York, Elsevier Scientific Publishing Company, p.1-47.
- Carleton, A.M., 1986, Synoptic-dynamic character of "bursts" and "breaks" in the south-west U.S. summer precipitation singularity: *Journal of Climatology*, v.6, p.605-623.
- CES, 1989, *Our changing planet: A U.S. strategy for global change research. A report by the Committee on Earth Sciences, to accompany the U.S. President's fiscal year 1990 budget.*
- Coleman, J.M., 1988, Climatic warming and increased summer aridity in Florida, U.S.A.: *Climatic Change*, v.12, p.165-178.
- Cry, G.W., 1967, Effects of tropical cyclone rainfall on the distribution of precipitation over the eastern and southern United States: U.S. Dept. Commerce, Environmental Science Service Administration, ESSA Professional Paper 1, 67p.
- Dice, L.R., 1943, *The biotic provinces of North America*: Ann Arbor, University of Michigan Press, 79p.
- Environmental Protection Agency, 1989, *The potential impacts of global climate change on the United States*: U.S. Government Printing Office.
- Grotch, S.L., 1988, Regional intercomparisons of general circulation model predictions and historical climate data: DOE/NBB-0084, 291p.
- Hales, J.E., 1974, Southwestern United States summer monsoon source—Gulf of Mexico or Pacific Ocean?: *Journal of Applied Meteorology*, v.13, p.331-342.
- Hansen, J., Fung, I., Lacis, A., Rind, D., Russell, G., Lebedeff, S., Ruedy, R., and Stone, P., 1988, Global climate changes as forecast by the GISS 3-D model: *Journal of Geophysical Research* (in press).
- King, G.A., Neilson, R.P., DeVelice, R.L., Lenihan, J.M., in review, Atmospheric circulation patterns and the control of major ecotones in the United States.
- Neilson, R.P., 1987, Biotic regionalization and climatic controls in western North America: *Vegetatio*, v.70, p.135-147.
- Neilson, R.P. and Wullstein, L.H., 1983, Biogeography of two southwest American oaks in relation to atmospheric dynamics: *Journal of Biogeography*, v.10, p.275-297.
- O'Connor, J.F., 1961, Mean circulation patterns based on 12 years of recent northern hemispheric data: *Monthly Weather Review*, v.89, p.211-228.
- Quinlan, F.T., Karl, T.R., and Williams, C.N. Jr., 1987, United States Historical Climatology Network (HCN) serial temperature and precipitation data: NDP-019, Carbon Dioxide Information Analysis Center, Oak Ridge National Laboratory, Oak Ridge Tennessee.
- Reyes, S. and Cadet, D.L., 1988, The southwest branch of the North American monsoon during Summer 1979: *Monthly Weather Review*, v.116, p.1175-1186.

- Rasmusson, E.M., 1967, Atmospheric water vapor transport and the water balance of North America: Part 1. Characteristics of the water vapor flux field: *Monthly Weather Review*, v.95, p.403-426.
- Schlesinger, M., and Zhao Z., 1988, Seasonal climate changes induced by doubled CO₂ as simulated by the OSU atmospheric GCM/mixed-layer ocean model: Corvallis, Oregon State University Climate Research Institute Report.
- Tang, M. and Reiter, E.R., 1984, Plateau monsoons of the northern hemisphere: a comparison between North America and Tibet: *Monthly Weather Review*, v.112, p.617-637.
- U.S. West, 1988, Hydrodata. USGS daily and peak values, user's manual and data: Version 2.0. Denver, U.S. West Optical Publishing.
- Wendland, W.M. and Bryson, R.E., 1981, Northern hemisphere airstream regions: *Monthly Weather Review*, v.109, p.255-270.
- Wetherald, R.T. and Manabe S., 1988, Cloud feedback process in a GCM: *Journal of the Atmospheric Sciences*, April 1988.
- Wuebbles, D.J. and Edmonds, J., 1988, A primer on greenhouse gases: Prepared for the U.S. Department of Energy. DOE/NBB-0083, Dist. Category UC-11.

A Statistical Model of Climates in the Southwestern United States

Richard G. Craig and John F. Stamm

ABSTRACT: We describe an empirical-statistical model of climates of the southwestern United States. Boundary conditions include sea surface temperatures, atmospheric transmissivity, and topography. Independent variables are derived from the boundary conditions along 1000-km paths of atmospheric circulation. Upper (400 mb) and lower level (800 mb) atmospheric independent variables describe available moisture and heat. Lower level atmospheric variables also describe orographic controls. Other independent variables represent climatic controls at the surface, such as elevation and slope. Mean monthly temperature and total monthly precipitation are the predicted variables. Canonical regression is applied to avoid problems of co-linearity. Predictor equations are derived over a larger region than the application area to allow for the increased range of paleoclimate. This larger region is delimited by the autocorrelation properties of climatic data.

INTRODUCTION

The level of climatic information required to understand the hydrologic system of the southwestern United States is difficult to reconstruct from general circulation model (GCM) output because of the coarse scale compared to the phenomena of interest (Kutzbach, 1983). Such models are of interest because they offer the advantage of providing information for any period for which the requisite boundary conditions can be specified (COHMAP, 1988). A possible supplement to GCM solutions is a statistical analysis that explicitly computes climate in terms of controlling factors in that area (Roberts, Craig and Stamm, 1989). We describe here an extension of that approach that more fully expresses the influence of the boundary conditions and allows greater flexibility in its application. In this study, we use canonical regression (Glahn, 1968). Such a modeling procedure has been successfully applied to paleoclimatic studies (Fritts, et al., 1971; Webb and Bryson, 1974).

THE STUDY AREA

We differentiate two tasks for this modeling: (1) solution of the climate equations, and (2) calibration of the equations. The area used to calibrate the equations is much larger than the area in which the equations are solved to ensure a robust set of equations as explained below.

The climate equations are solved at all points in the level II prediction area (Figure 1). These predictions draw upon information (to compute independent variables) from an area up to 1000 km upwind (the level I prediction area).

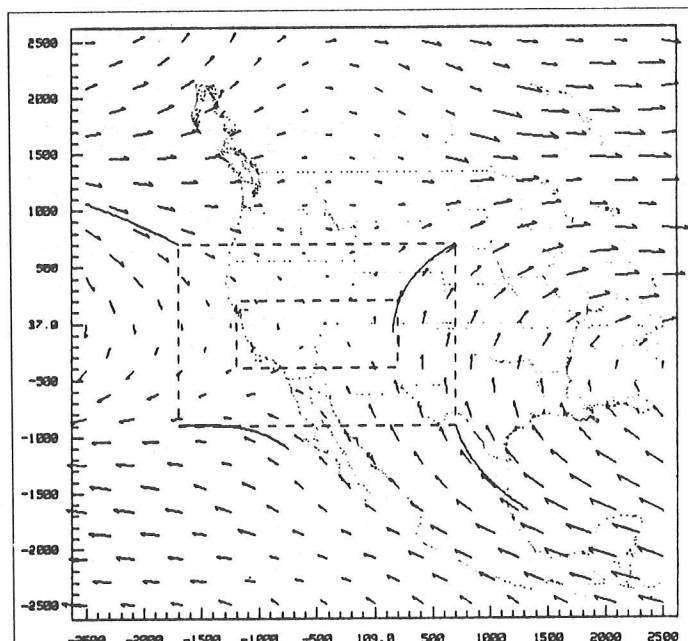


Figure 1. Level II calibration (*large dashed rectangle*) and solution (*small dashed rectangle*) areas. Arrows represent 800 mb July wind vectors interpolated from Schutz and Gates (1972). Curved lines represent wind trajectories along which independent variables are determined (axis units: km from central origin).

Winter 500 mb geopotential height departures from transient means (Figure 2) clearly show a decrease in the correlation between stations as the distance increases (Thiebaut and Pedder, 1987, p. 143). At about 1500 km distance, the averaged correlation values become negative. Because of the spread of the data, it is not clear that points more distant than about 1000 km are positively correlated. Therefore, trajectories of 1000 km are used to compile the independent variables.

To calibrate the climate equations, we select stations whose range of independent variables is considerably larger than that currently observed in the solution area. We assume that the most extreme climates to be

In J.L. Betancourt and A.M. MacKay, editors, 1990. Proceedings of the Sixth Annual Pacific Climate (PACLIM) Workshop, March 5-8, 1989: California Department of Water Resources, Interagency Ecological Studies Program Technical Report 23.

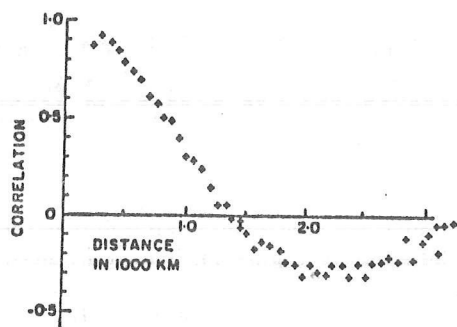


Figure 2. Correlation between geopotential height transient means as a function of distance of separation of stations (from Thiebaut and Pedder, 1987).

predicted are represented at stations within 1000 km upwind of the solution area. The area containing selected climate stations is called the **level II calibration area**.

The level I calibration area extends 1000 km upwind from the level II calibration area and is of sufficient size to provide boundary conditions needed to calculate independent variables in the level II calibration area. Figure 1 shows wind paths up to 1000 km upwind from the level II calibration area corners during July.

BOUNDARY CONDITIONS FOR CLIMATIC MODELING

Independent variables used in the climate equations are based on one or more of the following boundary conditions:

- Elevation
- Upper level (400 mb) winds, winter
- Upper level winds, summer
- Surface (800 mb) winds, winter
- Surface winds, summer
- Sea surface temperatures, winter
- Sea surface temperatures, summer
- Solar isolation

Elevation is represented by a digital elevation model (DEM) with a 10-km-square grid. This grid was interpolated from elevation and bathymetric data at a spacing of 5 minutes of latitude and longitude (National Geophysical Data Center, 1988).

Windfields for modern winter and summer are interpolated from first order U.S. Weather Bureau instrumental stations. We employ winds at two levels: near the surface (800 mb) and in the upper atmosphere (400 mb).

The windfield of the local climate model is interpolated with a 3-dimensional, objective-analysis mesoscale windfield model. This model was originally part of a meteorological data processor for an air quality monitoring program, MELSAR (MEsoscale Location Specific Air Resources) (Allwine and Whiteman, 1985). Given the horizontal velocity components at discrete points in the domain, the model generates an orthogonal polyno-

mial that represents horizontal velocity components continuously through the domain. Horizontal velocity components are then computed under constraint of conservation of mass. Figure 1 is an example of the output of the model.

Instrumental records allow direct calibration of the climatic equations with SST data representing the same years as the climatic data. We use those data to calibrate four polynomial equations. Two seasons, winter and summer, are used. Two functional surfaces are computed for each season, one for the Pacific Ocean and one for the Gulf of Mexico.

The polynomial equations provide a compact representation of SST, which minimizes storage requirements while accurately reproducing the original data. An R^2 of 99 percent is achieved, and the patterns of variability are well described. They allow estimation of SST at any point. This is important for applications along wind vector paths that do not lie at grid point locations. Sea surface temperatures are represented with CLIMAP (McIntyre, et al., 1981) and other data sources.

We limit our estimates of insolation to the top of the atmosphere and solve for daily insolation from orbital solutions based on the work of Berger (1978a). Inclusion of this term provides greater flexibility in considering climatic solutions for boundary conditions representing other climatic states.

We also use the orbital parameter calculations of Berger (1978b) to compute sun angle (declination and azimuth) and combine this information with slope derived from the DEM to determine the amount of solar energy received at each point of the level II area.

Heat energy added to an air mass upwind of a chosen point is approximated with an energy budget approach (Pease, 1987). The algorithm takes into account the incoming short-wave solar energy and long-wave energy emitted from the earth. This information is used to estimate the average air mass temperature along a 1000 km trajectory upwind of the point in question.

For this energy budget computation, certain assumptions must be made about the emissivity of the earth, the transmissivity of the atmosphere, certain partitioning fractions, and the density of cloud cover. A complete discussion is provided by Pease (1987). This model has the advantage of allowing adjustment for changes in the emissivity of the atmosphere such as could happen with a change in the concentration of carbon dioxide. This concentration has been shown to have varied in the Late Quaternary Period (Neftel et al., 1988). This concentration and the other partitioning fractions become parameters of the model.

Thermal energy input to the air mass from the upper level of the ocean is modeled by setting the surface energy in the energy balance model to the sea surface temperature. Planetary temperature and the non-radiative flux parameter, gamma, are adjusted to that SST.

INDEPENDENT VARIABLES

The canonical regression equation is based on independent variables representing the physical factors that can influence climate in the area while satisfying the constraint that they must be available for times in the geologic past. This constraint is exploited in other applications not discussed in this paper. We further constrain the independent variables to be calculated from boundary conditions within 1000 km of the calibration or solution point.

The independent variables are divided into three groups:

- Surface variables - calculated at the calibration or solution point.
- Lower-air variables - representing the influence of the boundary conditions from points up to 1000 km upwind from the calibration or solution point along the lowest conformal surface (~ 800 mb).
- Upper-air variables - representing the influence of the boundary conditions from points up to 1000 km upwind from the calibration or solution point along the upper conformal surface (~ 400 mb).

Considering that some variables are computed for each month, there are presently 72 independent variables used in the canonical regression procedure. The variables are described below.

Surface Variables:

- a. Climate station elevation interpolated from DEM.
- b. Maximum slope of the terrain surface.
- c. Normalized horizontal components of the maximum slope of the terrain surface.
- d. The angle between the horizontal wind direction and the azimuth of the maximum slope of the terrain surface.
- e. Vertical component of wind velocity.
- f. Surface temperature, from energy balance model.
- g. Planetary temperature, from energy balance model.
- h. Day length (sunrise to noon) at mid-month.
- i. Mid-month insolation.

Variables *d* and *e* are computed for both summer and winter, and variables *f* through *i* are computed for each month, yielding 54 independent variables.

Variable *a* represents the important effects of elevation. Variables *b* and *c* represent the microclimatic influence of slope. Variable *d* represents the angle of approach of a storm on terrain and the associated efficiency of precipitation. Variable *e* represents the potential for convective storms. Variables *f* through *i* represent the local effects of insolation.

Lower-Air Variables:

- a. Maximum [elevation/ln (distance to the elevation)] along upwind trajectory from the calibration/solution point.
- b. Maximum elevation along upwind trajectory from the calibration/solution point.

- c. Minimum elevation along upwind trajectory from the calibration/solution point and downwind from the location of variable *b*.
- d. Distance from calibration/solution point to variable *b*.
- e. Distance from calibration/solution point to variable *c*.
- f. Average surface temperature along trajectory using energy budget model.
- g. Percent distance over oceans/lakes along trajectory.

These variables are computed for both winter and summer, yielding 14 independent variables.

Variables *a*, *b*, and *d* represent the controls on orographic precipitation. Variables *c* and *e* represent adiabatic cooling that an air mass undergoes after it has passed an orographic depression. Variable *a* represents effects of local barriers, while variables *b* through *e* represent effects of distant barriers. Variable *f* represents possible horizontal advection of heat. Variable *g* represents the amount of moisture input from points upwind.

Upper-Air Variables:

- a. Average surface temperature along trajectory using energy budget model.
- b. Percent distance over oceans/lakes along the trajectory.

These variables are computed for both winter and summer, yielding four independent variables. These variables have the same physical representation as lower-air variables *f* and *g*.

STATUS

We have used a data set consisting of monthly mean maximum temperature and total monthly precipitation for 180 stations in the Great Basin (Wernstedt, 1972) to compute a canonical regression. For these stations, elevations ranged from -16 m to 2746 m, with a mean of 786 m and standard deviation of 734 m. Climatic variables, except for summertime precipitation, are highly correlated with one another (Table 1). We infer that at least two canonical variates must be employed.

Table 1. Squared multiple correlation of variables in the first set with all other variables in the first set.

	Temperature	Precipitation
January	0.99	0.99
February	0.99	0.98
March	0.99	0.98
April	0.99	0.97
May	0.99	0.97
June	0.99	0.92
July	0.99	0.89
August	0.99	0.88
September	0.99	0.82
October	0.99	0.98
November	0.99	0.98
December	0.99	0.98

Seventy-two independent variables were available for analysis. Because of co-linearity, only 26 independent variables were used in the canonical correlation procedure. Slope-related variables were not used, except for slope itself. Some mid-month day lengths were not used; summertime values were important. All insolation values except December were excluded. All planetary temperature variables were removed. Percent over ocean for surface variables were not needed.

Tests of the eigenvalues are reported in Table 2. Using Bartlett's test of sphericity, we found that seven canonical variates are significant (at the 0.01 level). Three were retained to develop regression coefficients, scores and loadings.

Table 2. Bartlett's test of number of eigenvalues needed.

	Chi-Square	d.f.	Tail Probability
	1999.34	624	0.0000
1	1518.60	575	0.0000
2	1102.34	528	0.0000
3	817.17	483	0.0000
4	643.39	440	0.0000
5	524.33	399	0.0000
6	426.37	360	0.0091
7	346.66	323	0.1748

Adjusted squared multiple correlations of temperature and precipitation with the chosen canonical variates (Table 3) ranged from 17 percent (September precipitation) to 82 percent (January and December temperatures). All adjusted R² values are significant at the 0.0005 probability level.

Table 3. Adjusted squared multiple correlations of each variable in the first set with chosen canonical variables of the second set. For all variables, the degrees of freedom are 26 and 153, and the F-statistic is significant at the 0.0005 level.

Variable	Adj. R ²	F-stat.	Variable	Adj. R ²	F-stat.
TJAN	0.82	33.22	PJAN	0.49	7.83
TFEB	0.79	27.59	PFEB	0.49	7.80
TMAR	0.75	21.86	PMAR	0.50	8.05
TAPR	0.70	17.85	PAPR	0.47	7.23
TMAY	0.66	14.89	PMAY	0.55	9.52
TJUN	0.62	12.33	PJUN	0.63	13.07
TJUL	0.53	8.82	PJUL	0.54	9.12
TAUG	0.54	9.33	PAUG	0.54	9.11
TSEP	0.58	10.67	PSEP	0.17	2.46
TOCT	0.68	15.84	POCT	0.38	5.38
TNOV	0.78	25.54	PNOV	0.44	6.59
TDEC	0.82	33.01	PDEC	0.50	8.11

Loadings of the independent variables on the canonical variates indicate that the first canonical variate has high loadings from nearly all variables. The second canonical variate has highest loadings from the day-length variables.

Wintertime temperatures tend to load highest on the first canonical variate. Of the precipitation variables, summer months tend to load highest on this variate (with negative loadings). Summer temperatures and all precipitations except June, July, and September load highest on the second canonical variate. Loadings on the third canonical variate are also high for summer temperatures and spring precipitation. Temperature loadings on that variate are negative and positive for all precipitation variables.

CONCLUSIONS

Empirical-statistical models capable of describing a significant portion of the variability of average monthly temperature and precipitation in the southwestern United States are feasible. These models can define the importance of various orographic and synoptic variables that can be solved from a fundamental set of boundary conditions, which can be specified by a GCM. The availability of a local climate model allows a meaningful comparison of climate forecasts to field observations.

ACKNOWLEDGEMENTS

This research has been supported by the Desert Research Institute of the University of Nevada, Reno through a grant from the National Science Foundation. We appreciate the support of personnel at DRI, including Cynthia Irwin-Williams, Jonathan Davis, Gil Cochran, and Peter Wigand.

REFERENCES

- Allwine, K.J. and Whiteman, C.D., 1985, MELGAR: A Mesoscale Air Quality Model for Complex Terrain. Volume 1 - Overview, Technical Description and User's Guide, Pacific Northwest laboratories, Battelle Memorial Institute. PNL-5460 v.1.
- Berger, A.L., 1978a, Long-term Variations of Daily Insolation and Quaternary Climatic Changes, *Journal of Atmospheric Sciences*, v.35, p.2362-2367.
- Berger, A.L., 1978b, A Simple Algorithm to Compute Long-Term Variations of Daily or Monthly Insolation (Contribution degree 18), *Universite Catholique De Louvain*, v.18.
- COHMAP Members, 1988, Climatic Changes of the Last 18,000 Years: Observations and Model Simulations, *Science*, v.241, p.1043-1052.
- Fritts, H.C., Blasing, T.J., Hayden, B.P., and Kutzbach, J.E., 1971, Multivariate Techniques for Specifying Tree-Growth and Climate Relationships and for Reconstructing Anomalies in Paleoclimate, *Journal of Applied Meteorology*, v.10, p.645-864.
- Glahn, J.R., 1968, Canonical Correlation and its Relation to Discriminant Analysis and Multiple Regression, *Journal of Atmospheric Sciences*, v.25, p.23-31.
- Kutzbach, J.E., 1983, Modeling of Holocene Climates, in Late-Quaternary Environments of the United States, ed., Wright, H.E. Jr., v.2, *The Holocene*, p.271-277.
- McIntyre, A., Cline, R. (Editor), Hayes, J., Prell, W., Moore, T., Kipp, N., Molino, B., Denton, G., Kukla, G., Matthews, R., Imbrie, J., and Hutson, W. (CLIMAP Project Members), 1981, Seasonal Reconstructions of the Earth's Surface at the Last Glacial Maximum, *The Geological Society of America Map and Chart Series*, MC-36.
- National Geophysical Data Center, 1988, Bathymetry/Topography Data, Newly Revised. Data Announcement 88-MGG-02.
- Neftel, A., Oeschger, H., Staffelback, T. and Stauffer, B., 1988, CO₂ record in the Byrd ice core 50,000-5,000 years BP, *Nature*, v.331, p.609-611.
- Pease, R.W., 1987, The Average Surface Temperature of the Earth: An Energy Balance Approach, *Annals of the Association of American Geographers*, v.77, no.3, p.450-461.
- Roberts, B.L., Craig, R.G., and Stamm, J.F., 1989, A Microcomputer Reconstruction of Paleoclimates, in *Microcomputer Applications in Geology*, v.II, J.T. Hanley and D.F. Merriam, editors, Pergamon Press.
- Schutz, R.P. and Gates, W.L., 1972, Global Climatic Data for Surface, 800mb, 400mb: July, ARPA, RAND 1029-ARPA, 180p.
- Thiebaux, H.J. and Pedder, M.A., eds., 1987, *Spatial Objective Analysis: With Applications in Atmospheric Science*: Academic Press, 299p.
- Webb, T. and Bryson, R.A., 1974, Late- and Postglacial Climatic Change in the Northern Midwest, USA: Quantitative Estimates Derived from Fossil Pollen Spectra by Multivariate Statistical Analysis, *Quaternary Research*, v.2, p.70-115.
- Wernstedt, F.L., 1972, *World Climatic Data, VI. North America*: Lemont, PA, Climatic Data Press.

Climate Signals in the Lower Stratosphere and Upper Troposphere

William D. Sellers

ABSTRACT: Empirical orthogonal function (EOF) analysis and regression analysis are used to investigate zonally averaged seasonal temperature anomaly patterns and trends in the lower stratosphere and upper troposphere. The first four EOFs explain 64 percent of the temperature variance and can be related, respectively, to the solar flux (SF) and El Niño/Southern Oscillation (ENSO), to the quasi-biennial oscillation (QBO), to atmospheric carbon dioxide (CO₂) and turbidity (TB), and to ENSO. The signal of the fourth EOF is modulated in January to March by the solar flux, with the sense of the modulation determined by the phase of the quasi-biennial oscillation.

INTRODUCTION

In a recent paper, Sellers and Liu (1988) suggested that clear signals due to solar emission variations, El Niño/Southern Oscillation (ENSO) events, the quasi-biennial oscillation (QBO) volcanic eruptions, and increasing atmospheric greenhouse gases are present in seasonal mean temperature data for pressure levels at and above 500 mbs. These signals were detected by using a combination of principal component (eigenvector) analysis and regression analysis. The basic data set consisted of

seasonal temperature anomalies for 114 seasons (summer 1957 through fall 1985) for six latitude belts (60-90N, 50-60N, 40-50N, 30-40N, 0-30N, and 0-90S), and four pressure levels (500, 300, 200, and 100 mbs). In this analysis all available radiosonde data for 511 stations were used.

There are advantages and disadvantages to working with upper-air data rather than surface data. The main advantages are that the confounding effect of clouds on the various climate signals is minimized and, at least in the case of increasing greenhouse gases, lag effects due to the slow response time of the oceans are not likely to be important. The disadvantages are the relative short record length and incomplete global coverage. About 40 percent of the stations, and many of those with the best, most complete records, are located on the 10 percent of the earth that is land covered and lie between 30° and 60°N.

RESULTS

In Sellers and Liu (1988), each of the first four eigenvectors derived from the basic data set seem to represent the response of the zonally-averaged temperature anomaly pattern to definite climate signals (Figure 1).

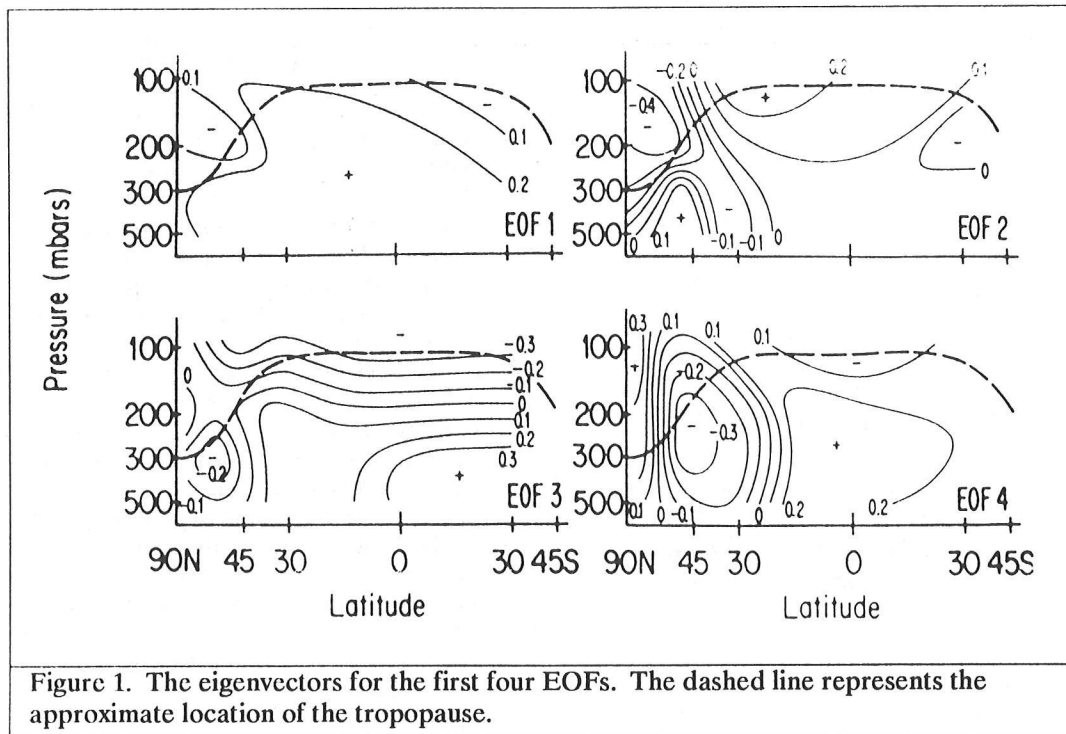


Figure 1. The eigenvectors for the first four EOFs. The dashed line represents the approximate location of the tropopause.

In J.L. Betancourt and A.M. MacKay, editors, 1990. Proceedings of the Sixth Annual Pacific Climate (PACLIM) Workshop, March 5-8, 1989: California Department of Water Resources, Interagency Ecological Studies Program Technical Report 23.

The first eigenvector or empirical orthogonal function (EOF), which explains 30.3 percent of the total variance of the temperature anomaly matrix, is characterized by anomalies of the same sign over the entire grid, with largest values in the upper troposphere between the equator and 30°N. In a given season, the sign of the anomalies is determined by the sign of the time-dependent amplitude of the EOF. If the amplitude, A_1 , is positive, the sign is as shown in Figure 1; if negative, the sign is reversed. The time series of the amplitudes, A_1 , of the first eigenvector (Figure 2) is positively correlated with the solar flux at 10.7 cm (SF) and the sea surface temperature off the west coast of the Americas (SST). The latter is a measure of the El Niño/Southern Oscillation phenomenon (ENSO). The maximum correlations, 0.616 for SF and 0.554 for SST, in both cases occur at a lag of 3 seasons, with A_1 lagging. The lag apparently represents the time it takes for surface heating to propagate upward to the upper troposphere and lower stratosphere, mainly through additional heat released by condensation.

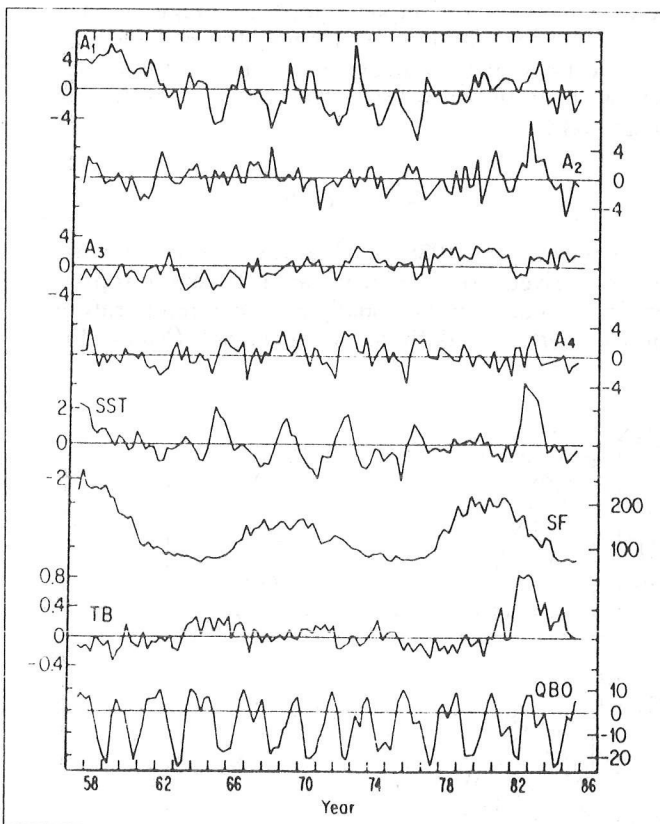


Figure 2. Time series of the amplitudes, A_1 , A_2 , A_3 , and A_4 , of the first four EOFs, SST (standardized values), SF (sfu; $1 \text{ sfu} = 10^{-22} \text{ W m}^{-2} \text{ Hz}^{-1}$), TB, and QBO (m sec^{-1}). The tic marks on the abscissa indicate the winter season.

The second eigenvector, which explains 14.1 percent of the variance, is most highly correlated with the quasi-biennial oscillation (QBO), a 26-month oscillation of the zonal wind at high elevations in the tropics. Using the 50 mb wind at Truk in the Caroline Islands as a measure of QBO, the maximum correlation with A_2 is 0.344 at a

lag of one season. The eigenvector pattern (Figure 1) is dominated by reversal of the sign of the temperature anomalies between polar latitudes and the subtropics in the lower stratosphere and upper troposphere. The pattern shown in the figure is associated with a strengthened polar vortex in the lower stratosphere and tends to occur when the QBO is in the west wind phase (A_2 positive), as noted also in analyses by Holton and Tan (1980, 1982), Wallace and Cheng (1982), and Van Loon and Labitzke (1987). The pattern of the second eigenvector in the troposphere is consistent with observations, since a colder stratosphere is usually associated with an increase in the height of the tropopause and a warmer troposphere. Thus, the pattern of the EOF in the troposphere is the reverse of that in the stratosphere.

The third eigenvector, which explains 10.1 percent of the variance, is dominated by a reversal of sign of the anomalies between the troposphere and stratosphere, with the strongest tropospheric signal in the Southern Hemisphere. This pattern is one commonly associated with increasing CO_2 and other greenhouse gases (Schlesinger and Mitchell, 1987) and, with the sign reversed (A_3 negative), with volcanic activity. Both of these signals show up in the time series of A_3 . Superimposed on the long-term upward trend of A_3 are decreases associated with increased volcanic activity between 1963 and 1968 (Agung and subsequent eruptions) and in 1982 and 1983 (El Chichón). A dip in A_3 also occurred in 1976 during the peak of the energy crisis, when fuel consumption was reduced. The correlation of A_3 with exponentially increasing CO_2 is 0.628 at zero lag. Although visually obvious in Figure 2, the correlation with volcanic activity, represented by the turbidity, TB, and Tucson, Arizona, is statistically insignificant due mainly to distortion of the turbidity record by the eruption of El Chichón in 1982.

The stratospheric cooling indicated by the third EOF and its amplitude is significant, aside from the cause of the cooling, because of the possible effect it might have on polar stratospheric clouds (PSCs) and stratospheric ozone concentrations. Recent evidence (Singer, 1988) has linked the PSCs, the frequency of which increases rapidly when the temperature drops below 195K, to the Antarctic ozone hole. If increasing CO_2 is the cause of the stratospheric cooling, as seems likely, then the cooling should be expected to continue and, along with it, ozone depletion. Since the magnitude of the cooling depends primarily on the radiative properties of the gases and clouds in the stratosphere, it is difficult to estimate the ultimate magnitude of the cooling and, likewise, the cooling and ozone depletion that might have occurred during periods in the geologic past when atmospheric CO_2 concentrations are believed to have been an order of magnitude larger than present concentrations. One can only speculate that ozone depletion might have played a role in the extinction of certain fauna and flora during these periods.

Perhaps the most interesting eigenvector is the fourth one, although it only explains 9.4 percent of the total variance. By comparing the curves for A_4 and SST in Figure 2, it is easy to see that the six major ENSO events

during the period are all accompanied by peaks in the A_4 curve. The maximum correlation between the curves is 0.385 at a lag of A_4 of one season. The pattern of the eigenvector is consistent with the so-called Pacific-North American (PNA) pattern, which is associated with ENSO events and is characterized by a wave train of alternating high and low pressure centers in the upper troposphere extending from the central equatorial Pacific, to the northern Pacific, to northern Canada, to the southeastern United States (Rasmusson and Wallace, 1983). That this signal appears in zonally-averaged data must be due to the disproportionately large number of stations in the North American sector.

The amplitude of the fourth EOF is also correlated with the solar flux and the quasi-biennial oscillation, but only in the boreal winter (January-March). Amplitude A_4 increases as the solar influx increases ($r = 0.680$) when

the QBO is in the west wind phase, and it increases as the solar flux decreases ($r = 0.464$) when the QBO is in the east wind phase.

These results and correlations are consistent with those obtained by Labitzke (1987), Labitzke and Van Loon (1988), and Van Loon and Labitzke (1988) using data for levels from the surface to 30 mbs. The fact that our correlations are with the PNA pattern (EOF4) and not with the stratospheric polar vortex pattern (EOF2), whose amplitude is positively correlated with the QBO, may be significant and may help shed some light on the cause of the phenomenon. However, the reality of this signal is very much in doubt, in spite of the rather strong evidence in its favor. The fact that it occurs only in the boreal winter makes it especially suspect. There seem to be one or more parts of the puzzle missing, which we hope will be uncovered through further research.

REFERENCES

- Holton, J.R., and Tan, H.C., 1980, The influence of the equatorial quasibiennial oscillation on the global circulation at 50 mb: *Journal of Atmospheric Science*, v.37, p.2200-2208.
- _____, 1982, The quasi-biennial oscillation in the Northern Hemisphere lower stratosphere: *Journal of Meteorological Society of Japan*, v.60, p.140-148.
- Labitzke, K., 1987, Sunspots, the QBO, and the stratospheric temperature in the north polar region: *Geophysical Research Letters*, v.14, p.535-537.
- Labitzke, K., and Van Loon, H., 1988, Associations between the 11-year solar cycle, the QBO and the atmosphere. Part I: The troposphere and stratosphere in the Northern Hemisphere in winter: *Journal of Atmospheric and Terrestrial Physics*, v.50, p.197-206.
- Rasmusson, R.M., and Wallace, J.M., 1983, Meteorological aspects of the El Niño/Southern Oscillation: *Science*, v.222, p.1195-1201.
- Schlesinger, M.E. and Mitchell, J.F.B., 1987, Climate model simulations of the equilibrium climatic response to increased carbon dioxide: *Review of Geophysics*, v.25, p.760-798.
- Sellers, W.D. and Liu, W., 1988, Temperature patterns and trends in the upper troposphere and lower stratosphere: *Journal of Climate*, v.1, p.573-581.
- Singer, S.F., 1988, Does the Antarctic ozone hole have a future? *EOS*, v.69, p.1588.
- Van Loon, H. and Labitzke, K., 1987, The Southern Oscillation. Part V: The anomalies in the lower stratosphere of the Northern Hemisphere in winter and a comparison with the quasi-biennial oscillation: *Monthly Weather Review*, v.115, p.357-369.
- _____, 1988, Association between the 11-year solar cycle, the QBO, and the atmosphere. Part II: Surface and 700 mb in the Northern Hemisphere in winter: *Journal of Climate*, v.1, p.905-920.
- Wallace, J.M. and Cheng, F.C., 1982, Interannual variability of the wintertime polar vortex in the Northern Hemisphere middle stratosphere: *Journal of Meteorological Society of Japan*, v.60, p.149-155.

1988 Summer Drought over the Great Plains: Some Causes and Predictions

Jerome Namias

ABSTRACT: The 1988 summer drought over much of the United States is described in terms of hemispheric mid-tropospheric flow patterns, temperature and precipitation anomalies, and sea surface temperature patterns. This drought was similar to earlier Great Plains droughts, although spatially more extensive than most. Three attempts to predict this drought from antecedent spring were moderately successful, though no one anticipated its severity and extent. Underlying reasons for the forecast made by the author and a colleague are cited, along with objective tools. Premonitory signs showed up in antecedent seasons, when deficient precipitation occurred, when climatological contingencies provided alerts, and when sea surface temperature patterns evolved in a conducive manner. A modified barotropic model iterating from a mean summer estimate of seasonal forcing from the May mid-tropospheric height pattern was reasonably successful in forecasting the drought. Sea surface temperature indications show that cold water (La Niña) along the equator subsequent to the 1987 El Niño, while contributory, cannot be considered a principal cause of the drought, since earlier cold water episodes did not produce drought, and other drought episodes occurred in the absence of cold equatorial waters.

INTRODUCTION

The great drought of the summer of 1988 brought home to the public once again the socioeconomic impact of short-term climatic fluctuations. It also brought to the fore warnings of global warming due to CO₂ and other gases, as well as scenarios wherein such droughts would become more frequent in years to come.

Like all major short-term climatic fluctuations, drought is never due to a single cause, but rather to multiple causes — usually involving synergistic factors. These factors involve numerous atmospheric teleconnections to and from the Great Plains, interactions between large-scale sea surface temperature (SST) anomalies and the atmosphere, and, equally important, air/land interactions in the domain afflicted by the drought.

DESCRIPTION OF THE DROUGHT, ASSOCIATED PHENOMENA, AND SOME PREDICTIONS

A clearly written discussion of the 1988 drought in particular and drought in general has been prepared for the

intelligent layman by the NOAA Climate Office under the supervision of W.A. Sprigg (1988). The 1988 drought has now been described by many scientists and laymen, as have equally severe episodes like the Dust Bowl droughts of the 1930s, the Southwest droughts of 1952-1954, the North Atlantic States droughts of 1962-1966, and the summer drought of 1980. Following is a thumbnail sketch, sufficient for our purpose, of the 1988 summer drought. Detailed statistics have been routinely published in *Weekly Climate Bulletins* and the *Weekly Weather and Crop Bulletin*, both published by NOAA in collaboration with the U.S. Department of Agriculture. A good summary has been provided by NOAA (1988).

Temperature and precipitation anomalies observed over the contiguous United States for the summer of 1988 are shown in Figure 1 (right), where three classes (terciles) have been employed. While these charts do not show the precise degree of abnormality, they do portray the signature of drought over most of the contiguous United States, especially in the Great Plains. Climatological frequency of occurrence of the extreme anomalies may be found in the NOAA publications cited above.

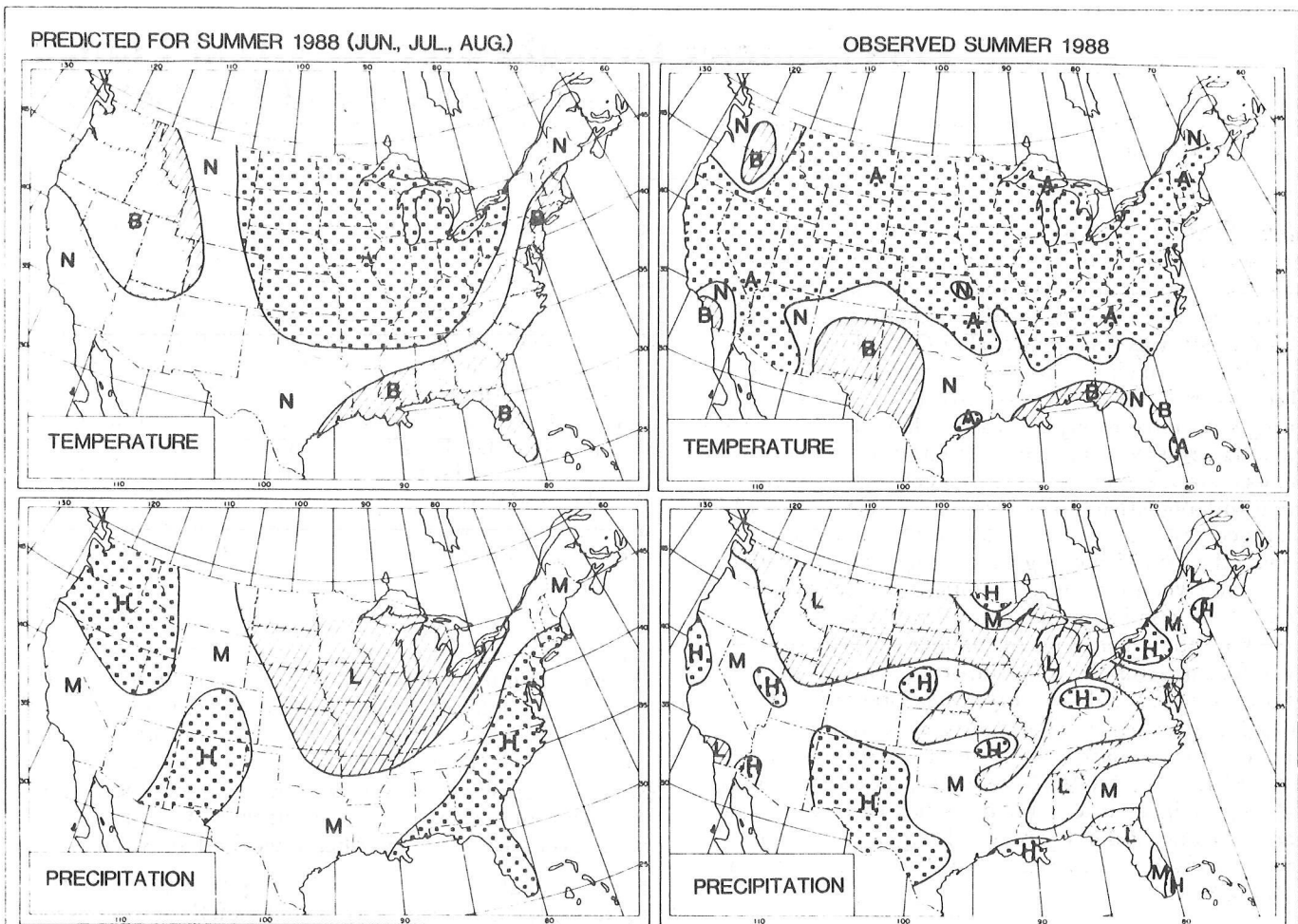
Experimental temperature and precipitation forecasts for one season in advance [Figure 1 (left)] are routinely made by the National Weather Service, of NOAA; by Daniel Cayan and me, of Scripps Institution of Oceanography; and by Arthur Douglas, of Creighton University. While generally warm, dry conditions were foreseen for much of the Nation, none of the forecasters foresaw the extent and severity of the drought — particularly the large area of deficient precipitation. Nonetheless, it was evident by late spring that summer drought in the Great Plains had become established. Using a verification at 99 stations over the Nation, the number of points forecast in the right category of three were:

- Scripps Institution of Oceanography,
44 for temperature and 48 for precipitation.
- Creighton University,
55 for temperature and 41 for precipitation.
- National Weather Service,
57 for temperature and 45 for precipitation.

Largely because of lack of space, only the Scripps Institution of Oceanography predictions are displayed in Figure 1.

While it is not possible in this short article to spell out all indications, a number of primary ones employed in making the forecast of Figure 1 are cited.

In J.L. Betancourt and A.M. MacKay, editors, 1990. Proceedings of the Sixth Annual Pacific Climate (PACLIM) Workshop, March 5-8, 1989: California Department of Water Resources, Interagency Ecological Studies Program Technical Report 23.



Completed Jun. 2, 1988 from data ending May 31, 1988 J. Namias/D. Cayan
 EXPERIMENTAL FORECAST. This forecast is made as a test of experimental procedures
 based on limited physical understanding and thus may have only marginal usefulness.

Figure 1. Observed and forecast temperature and precipitation anomalies for summer (June, July, and August) 1988. Both sets of charts are expressed in terciles (below, near, and above normal) computed from about 30 summers. The forecasts were made by J. Namias and D. Cayan of Scripps Institution of Oceanography.

First, the mid-tropospheric 700 mb height anomalies observed for the summer as a whole are reproduced in Figure 2, which forcefully brings to light the anomalously strong HIGH over the Plains, along with the often concomitant negative anomalies (troughs) off either coast and the stronger than normal upper level highs in the central North Atlantic and central North Pacific. This type of pattern has been found in many studies (e.g., Namias, 1983) to be characteristic of summer drought over the Plains. Subsidence in and below the continental high encouraged dryness and helped steer cyclonic systems away from the anticyclonic domain.

Teleconnections between the high cell over the core of the drought area and other remote areas in the Northern Hemisphere can be shown in a number of ways. Perhaps the best and most up-to-date method is to employ the work of J. Wagner and N. Maisel of the Long Range Prediction Group of the National Weather Service (personal communication, 1988). They selected key areas for large positive and negative anomaly centers from a

40-year series of monthly mean 700 mb charts with data from a 5x5 latitude-longitude grid, and cross-correlated all values over the hemisphere with values at these key points. Correlations were computed for individual months when the key area was a positive anomaly center over the Great Plains (like summer 1988).

Their teleconnection chart for July keyed on the positive anomaly center in the Plains that is shown in Figure 3. Note that on this chart, which corresponds to the anomaly center shown over the central plains in Figure 2, companion positive anomaly cells are indicated over the central North Pacific and central North Atlantic, separated by lesser or negative correlations along or off the west and east coasts.

The positive correlation center located north of Hawaii in Figure 3 is noteworthy inasmuch as Trenberth et al. (1988) have suggested that this cell was associated with the COLD equatorial water (La Niña) and a pool of warmer than normal water to its north following the strong El Niño of 1986-1987. Although this association

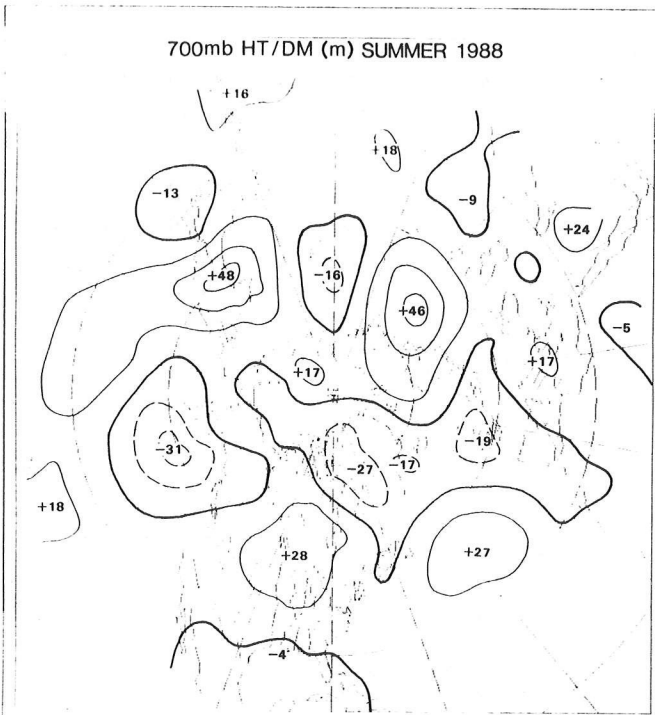


Figure 2. 700 mb height departures for summer 1988 from long-term (about 40 years) summer mean. Centers labelled in m, and isopleths drawn for every 15 m.

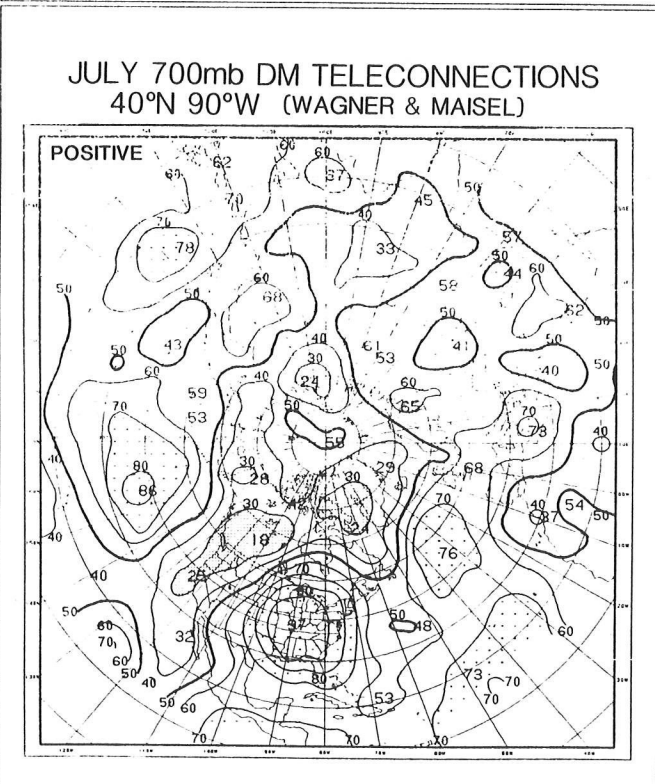


Figure 3. Teleconnections (cross-correlations) of 700 mb height anomalies keyed on 40N 90W (near the core of the drought upper level high pressure cell) for position centers in the Julys since 1947. Isopleths of correlation are drawn for every 0.10. Shaded and dotted areas indicate values exceeding ± 0.70 . (From Wagner and Maisel, National Weather Service).

probably played some part in generating and maintaining the high to the north and, through teleconnections, the downstream wave pattern of anomalies to which we have alluded, other factors in other summers of severe drought in the Plains have produced similar flow patterns without invoking La Niña. Besides, past years when cold water replaced El Niño were not associated with severe drought in the Plains.

Teleconnections in themselves do not prove cause and effect — they express linkages of abnormalities between parts of the general circulation. Hence, events in the North Atlantic — seat of one of the positive anomalies — might easily have been generated and maintained partly by the anomalously warm water mass seen there in summer 1988. Then again, regional soil/atmosphere interactions in the area of the drought, described later, could have been a key factor in its generation and maintenance, aside from the internal dynamics associated with teleconnections.

Both empirical and theoretical evidence strongly indicates that the character of the soil in the Plains, whether wet or dry, exerts a strong influence on overlying wind and weather patterns. It does this through latent and sensible heat alterations. When the soil is unusually dry, as it was in the spring of 1988, the increasing insolation as spring advances into summer is not used primarily to evaporate the moisture in and on the soil, but rather to directly heat the soil and overlying air — a process that encourages growth of an upper level high, decreases relative humidities, and inhibits cloud formation.

The author (Namias, 1960) pointed out these effects by constructing the contingencies shown in Tables 1 and 2. These contingency tables show that warm, dry springs in the western Plains states (nine states for springs and summers of about 70 years) are much more apt to be followed by warm and dry summers than by wet and cool or normal summers.

Shukla and Mintz (1982) confirmed these ideas in modelling experiments, as did Oglesby and Ericson (1988). It seems likely that the physical mechanisms suggested can operate most efficiently when the Plains high pressure cell is first generated by the teleconnection mechanisms suggested. It could be argued that the positive anomaly observed over the Great Plains in the summer of 1988 was as much a cause as a result of the positive anomaly north of Hawaii. Big droughts such as that in 1988 are manifestations of multiple effects in many branches of the general circulation and are not likely to be caused and maintained by a single factor.

Table 1. Summer temperature classes over the western Great Plains following different combinations of spring temperatures and precipitation. (Totals are underlined.)

Spring Temp.	Precip.	Following Summer Temperature			
		Cold	Normal	Warm	Total
Cold		<u>101</u>	<u>70</u>	<u>40</u>	
	Light	29	21	10	60
	Moderate	31	18	19	67
	Heavy	41	31	11	83
Normal		<u>53</u>	<u>74</u>	<u>81</u>	
	Light	12	18	34	64
	Moderate	18	33	27	78
	Heavy	23	23	19	65
Warm		<u>57</u>	<u>65</u>	<u>87</u>	
	Light	9	27	50	86
	Moderate	18	22	22	62
	Heavy	30	16	16	62

Summer temperature classes (terciles) over nine western Great Plains states as functions of combinations of antecedent spring temperature and precipitation. For example, of the 86 cases when spring was warm and dry (light precipitation), 9 were followed by cold summers, 27 by normal summers, and 50 by warm summers. Data involve seasons of the years 1900 to 1965.

OBJECTIVE ESTIMATES OF CIRCULATION PATTERN AND TEMPERATURE ANOMALIES FOR SUMMER 1988

The contingencies described in the previous section were employed as adjuncts in making the forecast illustrated in Figure 1. First, contingencies for individual states were used to obtain Figure 4(a), which shows probable summer temperature anomalies based on about 70 years of spring and summer data. The numbers indicate the excess over chance (33%) that the summer would be A (above normal), B (below normal), and C (near normal), based on the antecedent spring anomalies. Only values exceeding 10 percent above the 33 percent expected by chance are shown.

However, the situation with which we are dealing is highly abnormal, in that spring over the Plains was exceptionally dry over large areas. Hence, contingencies between spring precipitation and summer temperature were employed, as shown in Figure 4(b). Again, only values greater than 10 percent above chance are given. This contingency chart differs from Figure 4(a), which was based solely on temperature, by suggesting that much of the midwest and southeast would be apt to have above normal temperatures in summer.

The above described indications were used in conjunction with an estimate of the summer flow patterns at 700 mbs. Physically based mechanisms, such as the influences of wet or moist soil are likely to operate most efficiently when the continental high pressure anomaly cell is first established — chiefly by teleconnections. We now discuss some considerations that lead to the idea that the prevailing flow pattern of summer would

Table 2. Summer precipitation as related to temperature and precipitation of the preceding spring over the Great Plains of the United States. (Totals are underlined.)

Spring Temp.	Precip.	Following Summer Precipitation		
		Light	Moderate	Heavy
Cold		<u>53</u>	<u>74</u>	<u>85</u>
	Light	12	18	30
	Moderate	19	24	25
	Heavy	22	31	30
Normal		<u>70</u>	<u>73</u>	<u>65</u>
	Light	28	17	20
	Moderate	27	26	26
	Heavy	15	30	19
Warm		<u>87</u>	<u>63</u>	<u>58</u>
	Light	49	22	14
	Moderate	24	16	22
	Heavy	14	25	22

As in Table 1, except for precipitation as a function of antecedent spring temperature and precipitation classes. For example, dry summers tend to follow warm and dry springs.

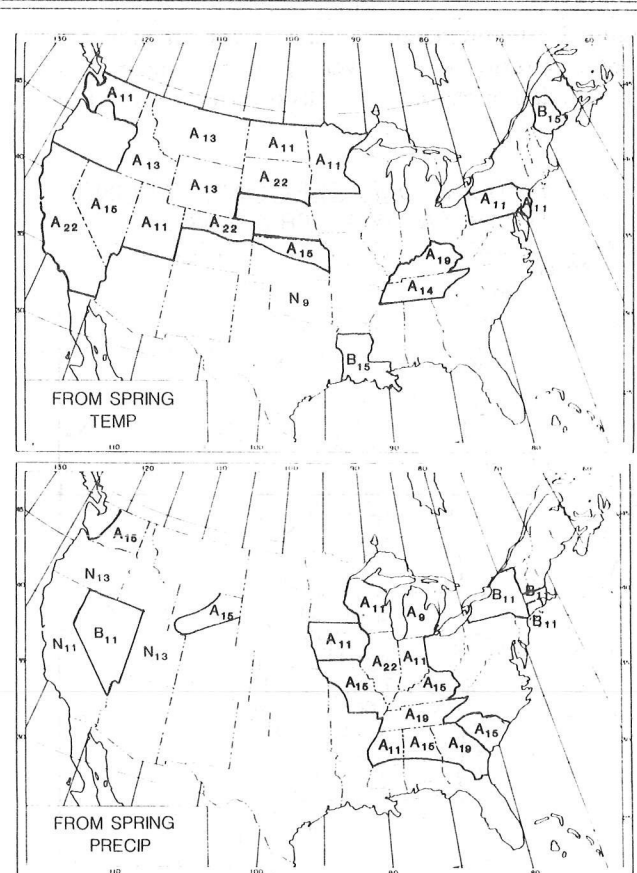


Figure 4. Above (a) Contingencies of summer temperature classes based on spring temperature anomalies. Numbers beside classes indicate excess over 33, the value expected by chance. Only excesses above 10 are shown. Below (b) Contingencies of summer temperature anomalies based on spring precipitation anomalies. Numbers give excess over chance (33) when greater than 10.

contain the anomalously strong continental upper level anticyclone and companion cells over the adjacent oceans.

Foremost among these indications was the concept that the final observed state of the flow pattern resulted from:

- A tendency of the existing 700 mb anomaly pattern of spring to persist into summer, and
- Anomalous boundary conditions, generated largely by spring air/sea/land interactions, would continue to operate in summer, and
- Normal seasonal changes in the strength of anomalies from spring to summer due to variability would be taken into account.

The third item was achieved by using persistence of **standardized** anomalies from spring to summer, rather than persistence of anomalies themselves. Furthermore, since large changes in flow pattern were taking place from month to month in spring, it was decided to apply this procedure using the latest month (in this case, May) as initial data. Thus, Figure 5 shows the hypothetical pattern of 700 mb height that would characterize summer if the standardized anomalies of May persisted, and then a modified barotropic model was applied.

The reason for this step is that, while the arrangement of anomalies that comprise the spring pattern may be stable for spring, it is unlikely to be stable for summer, so that instabilities due to internal dynamics must be adjusted to achieve a stable pattern. While there is no

simple method to do this, some experiments have suggested the use of a modified barotropic model (Namias, 1988) to apply to the hypothetical chart, which assumes conservation of standardized height anomalies from spring to summer. The model employed, supplied by John Roads of Scripps Institution of Oceanography, speeds up the velocities given in the initial hypothetical chart by a factor of two so as to offset the retrogression of long waves that might otherwise occur, then proceeds iteratively to predict patterns up to about a week. The choice of length of the prediction period is arbitrary, and it is assumed that the predicted pattern will recur persistently throughout the summer, recurrence that frequently takes place in nature. The final predicted pattern, shown in Figure 5 (top), resembles the observed chart for summer 1988, shown in Figure 3.

Before closing this paper, it is tempting to show Table 3, which shows contingencies like those shown earlier but for temperature anomalies in the Great Plains related to those of the following summer. Apparently there are interseasonal and interannual spells of persistence that cannot be ascribed to linear trend. Unless this circumstance is due to long period solar influences, it could indicate some conservative characteristics of the soil of the Plains or conservative properties of the sea underlying the oceanic high pressure cells (or both) that survive the changes of intervening seasons between summers.

These remarks are not meant to constitute a forecast for summer 1988 in the Great Plains; they do imply that drought in some parts of this area in 1988 should not be grounds for invoking the greenhouse effect.

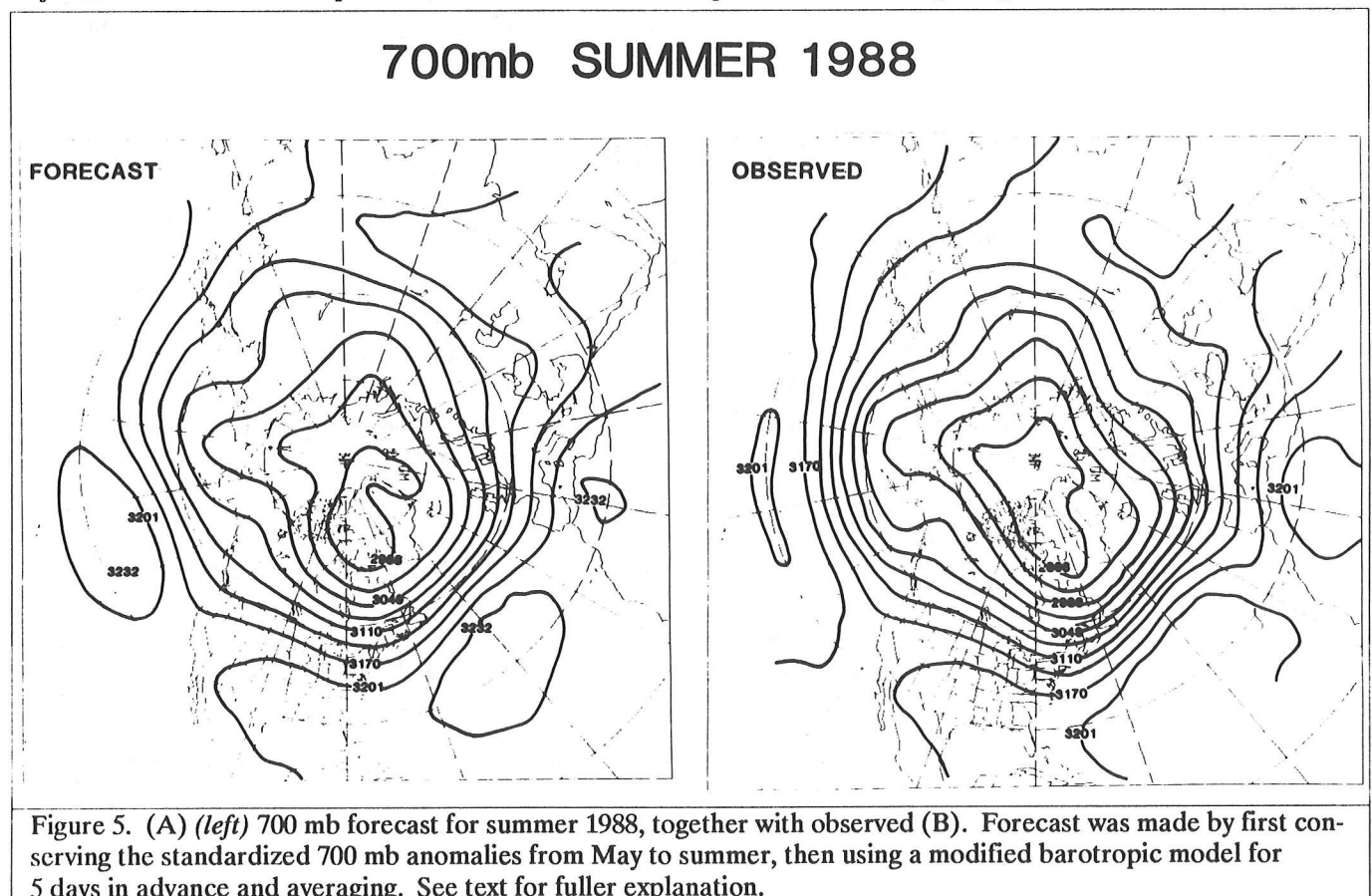


Table 3. Summer temperature over the Great Plains related to temperature and precipitation of the preceding summer. (Totals are underlined.)

Summer Temp.	Precip.	Following Summer Temperature			
		Cold	Normal	Warm	Total
Cold		<u>86</u>	<u>79</u>	<u>40</u>	<u>211</u>
	Light	11	13	7	31
	Moderate	30	17	22	69
	Heavy	45	49	17	11
Normal		<u>73</u>	<u>69</u>	<u>62</u>	<u>204</u>
	Light	16	18	23	57
	Moderate	30	30	18	78
	Heavy	27	21	21	69
Warm		<u>42</u>	<u>58</u>	<u>91</u>	<u>191</u>
	Light	18	33	59	110
	Moderate	16	19	23	58
	Heavy	8	6	9	23

As in Tables 1 and 2, except for summer temperature related to the preceding summer's temperature and precipitation. Note that warm summers tend to be preceded by warm, dry summers in the preceding year.

SUMMARY

Droughts of the summer of 1988 over the Great Plains of the contiguous United States has been described in the context of historical analysis of earlier droughts. The 1988 drought was ascribed to evolution and development of the classical three upper level anticyclonic anomalies over the North Pacific, North Atlantic, and continental United States, to interacting sea surface temperature patterns, and, perhaps most importantly, to the very dry soil developed in preceding seasons. Teleconnections among these areas appear to describe the main characteristics of the observed patterns. The influence of the tropics, especially the abnormally cold water along the equator in the aftermath of El Niño, may have contributed to the drought pattern, but in similar cold water episodes of past years, the tropical factor was by no means the major cause of such droughts.

Moderately successful predictions were made in late spring of 1988 for the observed midtropospheric flow pattern in the summer of 1988 as well as temperature and precipitation patterns. The anomalous circulation was predicted by applying a modified barotropic model to reasonable statistical estimates of seasonal forcing from the initial May.

ACKNOWLEDGEMENTS

I thank Ms. Marguerette Schultz, for preparing the illustrations and otherwise helping me assemble data, and Mrs. Mimi Bainto for programming assistance. The work was supported by the National Science Foundation under Grant ATM-8407891 and by the National Climate Program Office under Grant NA81AA-D-00054.

REFERENCES

- Namias, J., 1960, Factors in the initiations, perpetuation and termination of drought: Publication No. 51 of the IASH Commission of Surface Waters, p.81-94.
- Namias, J., 1988, Basis for the forecast for summer, 1987, following a non-persistent spring: *Weather and Forecasting*, 3, p.162-169.
- NOAA, 1988, Summary of conditions and impacts of the 1988 drought, a well illustrated report issued on September 18, 1988, by the Climate Analysis Center, Hydrological Services, and the National Climatic Data Center of NOAA.
- Oglesby, R.J. and Erickson, D.J. III, 1988, Moisture and persistence of mid-latitude drought; a GCM study: Presented at the American Geophysical Union Symposium on the 1988 Drought, San Francisco, December 7, 1988.
- Shukla, J. and Mintz, Y., 1982, Influence of Land-Surface Evapotranspiration on the Earth's Climate: *Science*, v.215, p.1498-1500.
- Sprigg, W. et al., 1988, U.S. Drought 1988: A climate assessment, a report issued by NOAA: U.S. Department of Commerce in July 1988.
- Trenberth, K.E., Branstator, G.W., and Arkin, P.A., 1988, Origins of the 1988 North American drought: Presented at the American Geophysical Symposium on the 1988 Drought, San Francisco, December 7, 1988.
- _____, 1988, Origins of the 1988 North American drought. *Science*, v.242, p.1640-1645.
- Wagner, A.J. and Maisel, N., 1988, Teleconnections among 700 mb height anomalies of the Northern Hemisphere by 15-day period.
- Unpublished work done at the Long Range Prediction Group of the Climate Analysis Center of the U.S. National Weather Service.

Current Water Supply Conditions in California

Maurice Roos

ABSTRACT: This paper contains a brief report on the status of the California water supply situation on March 1, 1989, including a review of the antecedent conditions of the past two dry water years.

CURRENT WATER SUPPLY CONDITIONS

On this first week of March, it is beginning to look like Northern California will endure an unprecedented third critically dry year in a row in 1989. Only about a quarter of the rainfall season is left. Unless precipitation patterns make a real turn-around, the outlook for water users this year is grim. Many farm and city users are facing curtailments of normal supply.

Some background information may be useful. All of you know that most of California's water is in the north. But I'm not sure many of us realize how strongly skewed the natural supply is. About three-fourths of our natural

runoff occurs north of Sacramento. Conversely about three-fourths of the water use is south of Sacramento. Those facts alone explain much about why we have such extensive water development in California.

It all starts with precipitation, or the lack of it in this case. The 3-part bar chart of Northern Sierra precipitation (Figure 1) tells its own story. In 1987, the first year of the current drought, the water year started very dry through December, then turned more normal. But the early season shortfall was just never made up.

In contrast, 1988 started off quite well with a good December and storms continuing halfway through January. Then the faucet was turned off, and we had a record dry February and March couplet. The rains came again in mid-April, but produced little gain in runoff from relatively dry watersheds. The big April storm was, however, a godsend to California's forests, which were already under stress.

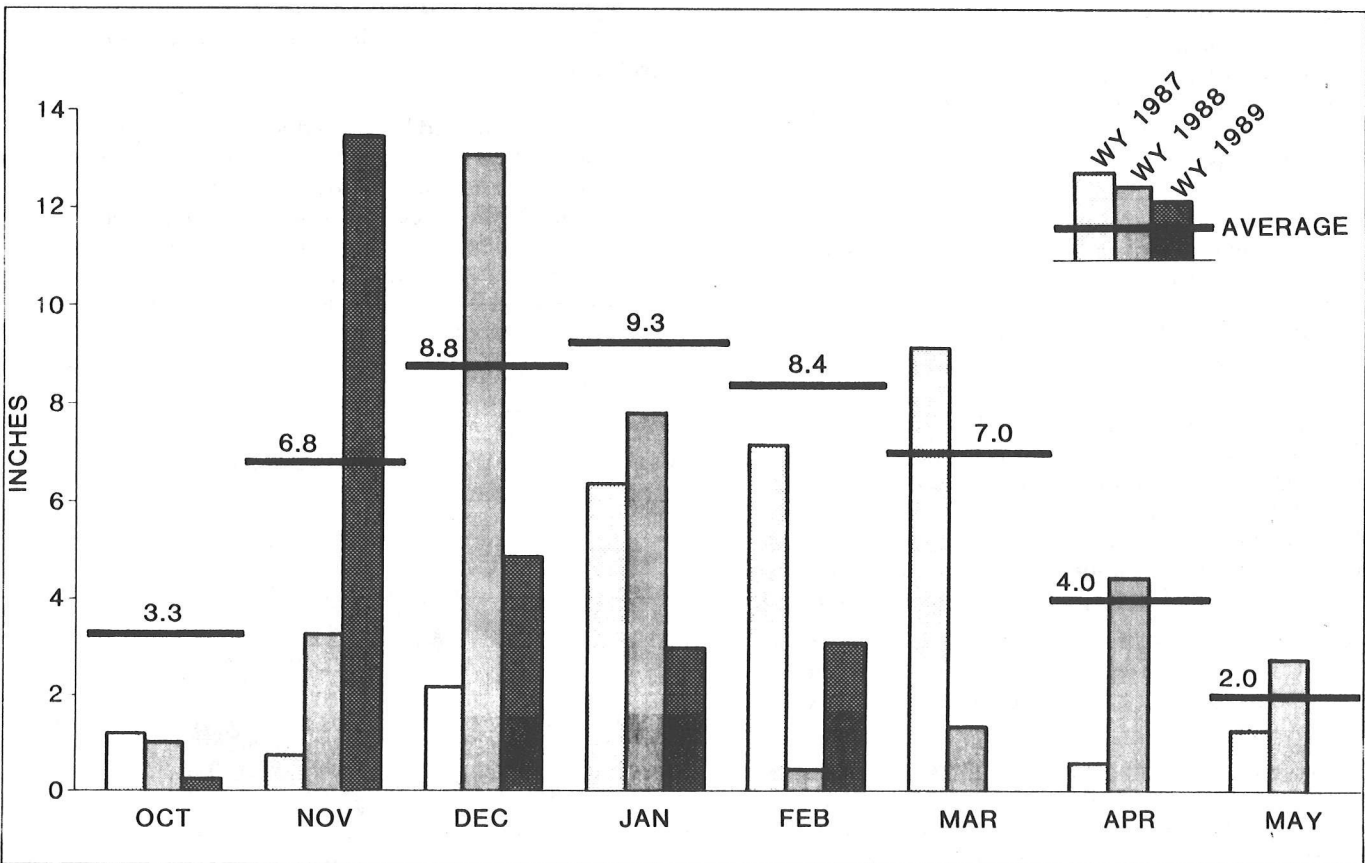


Figure 1. Sacramento River Index precipitation (eight station average, March 1, 1989).

In J.L. Betancourt and A.M. MacKay, editors, 1990. Proceedings of the Sixth Annual Pacific Climate (PACLIM) Workshop, March 5-8, 1989: California Department of Water Resources, Interagency Ecological Studies Program Technical Report 23.

This year, we got off to a good start in November, but the big three winter months turned out to be a bust, and we are not likely to make up the 30 percent chunk of normal water year precipitation lost in December through February, our primary rain season. Whether the month of March will see enough precipitation to eliminate Central Valley Project and State Water Project supply problems for this year is not yet known, but the historical odds of a super wet March are slim.

There was a loss in the strength of the orographic factor in northern Sierra precipitation in 1987 and 1988. This year it appears that the normal orographic pattern is back. This is shown by comparing the mile-high Blue Canyon weather station with Sacramento City rainfall, near sea level. The following tabulation compares precipitation at the two stations:

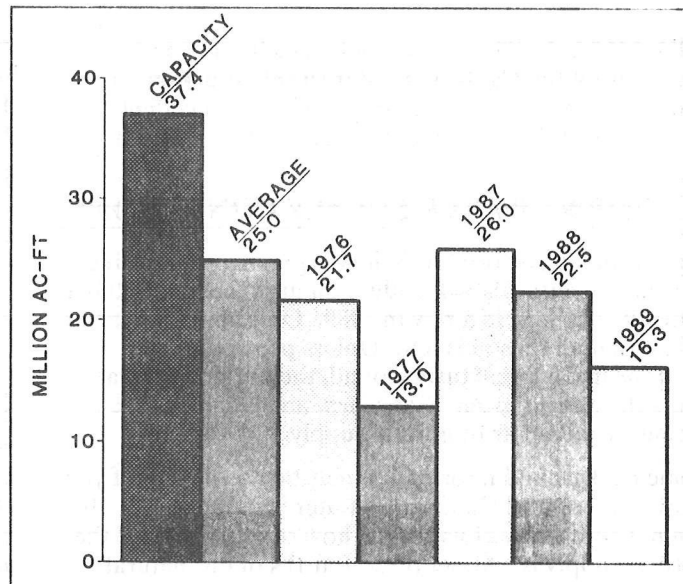
	Precipitation, in Percent of Average	
	Blue Canyon	Sacramento City
Water Year 1987	51	67
Water Year 1988	73	86
Water Year 1989, October-February	76	59

Snowmelt runoff (that is, April-July runoff) furnishes about 14 million acre-feet (MAF) on the average of Central Valley water supply. This is about 40 percent of current annual net water use of the entire state. Both 1987 and 1988 were dismal snowmelt runoff years, about 45 percent of average. The 1987 snowpack was just about nonexistent on January 1, to the distress of the winter snow sport operators. In 1988, snowline elevations were higher, but the higher elevation pack looked pretty normal until the end of January. Then little else happened. This year, we had a series of cold storms that had relatively dry snow, some down to a 20 to 1 ratio of water content. It was a better year, especially in the Central Sierra, and winter skiing was excellent. However, the water content was below average and, after a dry February, snow water content on March 1 was around 70 percent of average. This is better than last year, but not what we'd hoped for. Because of the cold air and dry antecedent conditions, early seasonal winter runoff was only about 40 percent of average on March 1, compared to 60 percent last year on March 1.

Water year runoff in 1987 and 1988 are strikingly similar, just under half average. Currently it looks like this year will be a little better, although the uncertainty level is pretty high yet.

California's water storage facilities proved their worth during the last two drought years (see Figure 2). At the end of 1986, storage was well over average (remember the February 1986 flood) — about 111 percent, even after a dry fall. Two years later, at the end of December 1988, major in-state reservoir water storage had fallen to 68 percent of average, down 5 million acre-feet (MAF) from the end of 1987 and over 9 MAF less than in 1986. On March 1, 1989, we were about 6 MAF behind last year and over 9 MAF behind two years ago. (Storage was still more than 3 MAF over the severe drought year

1977 levels, however.) With forecasted water year runoff heading toward the 50 percent mark, many agencies, including the SWP and CVP, are planning reductions in normal water deliveries.



Note: The 1987, 1988 and 1989 storage amounts include New Melones and Warm Springs Reservoirs which began operation after 1977.

Figure 2. Storage in 153 major California reservoirs on March 1, 1989.

We are often reminded how rapidly water conditions can change. In early February 1986 there were concerns about dryness. Then we had the Valentine's Day storm and the Presidential Weekend floods. Droughts are a gradual thing; flood and high runoff situations come suddenly. So there is still hope, particularly now when there are large storm systems in the Pacific not far from Northern California.

The pie chart on sources of California water use may be instructive (Figure 3). Last year the main segment affected was the 30 percent portion from local surface sources. This year shortages are expected to spread

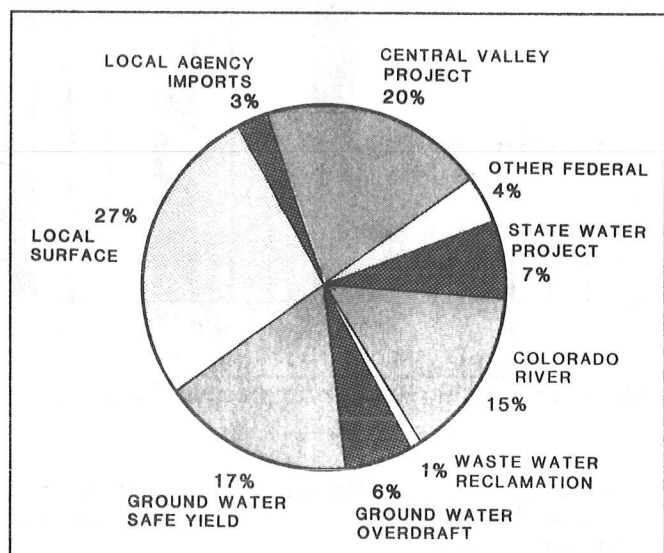


Figure 3. California water supply use in 1985.

over about 60 percent of the pie including the big state and federal water projects. Only the ground water and Colorado River segments are reasonably sure to be maintained.

There is hope that the good spring rains will enable the CVP and SWP to ease off their planned curtailments, but we will have to see how much. Even if full deliveries can be made this year, it does not look like there will be reservoir recovery, so California will still be vulnerable for a fourth dry year next fall.

ADDENDUM

March turned out to be a bountiful precipitation month, especially across the northern third of California. Sacramento River basin precipitation was 2-1/2 times average, with good runoff and reservoir storage increases. By April 1, statewide runoff had improved from 40 to 75 percent of average, and forecasted water year runoff was 75 percent of average. Major in-state reservoir storage had increased 5.8 MAF to 84 percent of the April 1 average. The two major water projects, the federal Central Valley Project and the State Water Project, announced they would be delivering full contract amounts of Northern California water in 1989. The wetness in March tapered off in central California, and some water problems continue in the central parts of the state.

Uncovering North American Temperature and Precipitation Patterns Associated with the Southern Oscillation

Chester F. Ropelewski and Michael S. Halpert

ABSTRACT: The extreme phases of the Southern Oscillation (SO) have been linked to fairly persistent classes of circulation anomalies over the North Pacific and parts of North America. It has been more difficult to uncover correspondingly consistent patterns of surface temperature and precipitation over much of the continent. The few regions that appear to have consistent SO-related patterns of temperature and precipitation anomalies are identified and discussed. Also discussed are regions that appear to have strong SO-related surface anomalies whose sign varies from episode to episode.

INTRODUCTION

The Southern Oscillation is the best documented and understood mode of interannual climate variability. While much remains to be learned about the evolution of individual warm SO episodes, research over the past two decades (e.g., Bjerknes, 1969; Rasmusson and Carpenter, 1982) has provided a fairly clear picture of the mean features associated with the warm extreme of the SO. Horel and Wallace (1981), through a spatial correlation analysis of geopotential height data, demonstrated that teleconnection patterns link the equatorial tropics with mid-latitude circulation anomalies over North America. These diagnostic studies were further bolstered by theoretical work, e.g., Opsteegh and Van den Dool (1980), which helped to explain the statistical teleconnection patterns in terms of Rossby wave propagation on a sphere.

We now envision the SO as a slowly evolving state of the climate system, which is manifested most clearly in the Pacific Ocean but includes the global atmosphere and may involve the other ocean basins as well. While the warm phase of the SO (also called the ENSO phase after El Niño/Southern Oscillation) has been studied extensively over the past decade, the appearance of extremely cold equatorial waters associated with an enhanced trade wind circulation early in 1988 has spurred renewed interest in the cold extreme of the SO. This phase of the SO has also been identified with high values of the Tahiti-Darwin SO index (Ropelewski and Jones, 1987), stronger than normal easterly trades across the Pacific, and strong 200 mb westerly wind anomalies over the equator (Ropelewski and Halpert, 1989). Since the SO tends to evolve slowly through both its extremes, the identification and tracking of SO has a promising potential for long-range (monthly, seasonal) prediction.

REGIONS WITH TYPICAL ANOMALY PATTERNS

Typical anomaly patterns of surface temperature and precipitation associated with the extremes of the SO have been identified (Ropelewski and Halpert, 1986, 1987, 1989). These studies indicate that consistent North American SO-related precipitation and temperature patterns are confined to the far northwestern reaches of the continent and to the southeastern Gulf regions (Figure 1).

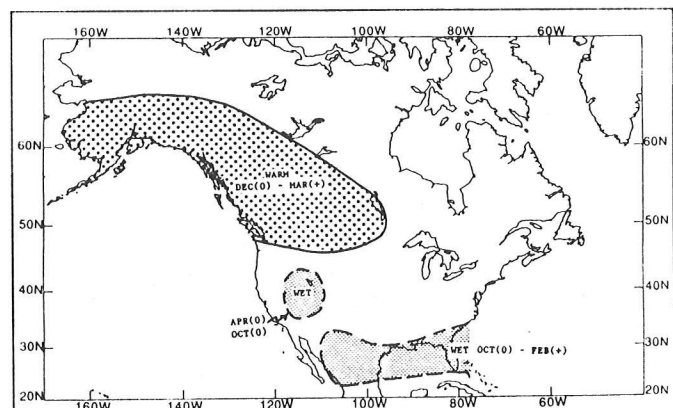


Figure 1. Schematic of areas with consistent SO-related precipitation and temperature anomalies. The anomalies are illustrated for the ENSO (warm phase of the oscillation). These anomalies have the opposite sign in association with the cold, high index, phase. The Great Basin shows a warm phase signal only. The Gulf/Mexico area also tends to be cool in ENSO episodes.

During the warm, or ENSO, phase of the oscillation, the northwestern sections of North America tend to exhibit positive temperature anomalies, while the southeastern region tends to be cooler than normal. The reverse-sign anomaly pattern tends to occur during the cold, or high index, phase of the SO (Table 1). The southeastern areas of North America, especially those adjacent to the Gulf of Mexico, tend to experience more than normal precipitation during the winter half of the year (October to March) during the ENSO phase of the oscillation and drier than normal conditions during the high index phase. There is also a tendency for the Great Basin to experience above normal precipitation over the April to October "season" during warm episode years. However, there appears to be no corresponding relationship

between Great Basin precipitation and the SO during the cold phase of the oscillation.

DISCUSSION OF OTHER REGIONS

While we could not find any consistent SO-temperature or SO-precipitation relationships for other regions of North America, this does not necessarily imply that the SO has no influence over monthly and seasonal climate anomalies in other regions. In fact, historical evidence suggests that the warm phase of the SO may be associated with precipitation anomalies of either extreme in the Pacific northwestern sections of the United States. Thus we are presented with the apparent paradox that in Oregon and Washington the ENSO phase can be linked with the dry winter conditions for 1951, 1965, 1972, 1976, 1986/7 and with the wet conditions of 1953, 1957, 1969, and 1982 (Karl and Knight, 1985). Likewise, the cold phase of the SO appears to be associated with anomalies of either sign.

To further complicate the issue, areas of precipitation anomalies very often, but not always, include Northern California. This suggests that SO-related precipitation patterns over the Pacific Northwest depend strongly on the detailed evolution of the individual ENSO and high index episodes. Thus, for the northwestern states, predictions (or even observations) of the initiation of ENSO episodes or of high index episodes are not very useful for predicting precipitation anomalies.

A further examination of monthly SO-precipitation patterns indicates that anomalies tend to be reasonably

Table 1. Number of positive/negative anomalies associated with ENSO and high index phase of the Southern Oscillation. (After Ropelewski and Halpert, 1986, 1989.)

Region	Precipitation			
	ENSO		High Index	
	Wet	Dry	Wet	Dry
Gulf/Mexico [Oct(0)-Mar(+)]	18	4	3	16
Great Basin [Apr(0)-Oct(0)]	9	2	4	4
Region	Temperature			
	ENSO		High Index	
	Warm	Cold	Warm	Cold
NW North America [Dec(0)-Mar(+)]	18	4	5	14
SE United States [Oct(0)-Mar(0)]	5	20	10	8

persistent within episodes; i.e., it appears that once a precipitation anomaly (and presumably a corresponding circulation anomaly) is initiated in conjunction with a particular SO episode, these anomalies tend to persist throughout the northwest's rainy season.

Numerical modeling is another arena that may provide some help in understanding and predicting precipitation anomalies associated with the SO. A promising example of this approach is the numerical simulation presented by Trenberth et al. (1988) to explain the spring and summer drought of 1988.

REFERENCES

- Bjerknes, J., 1969, Atmospheric teleconnections from the equatorial Pacific: *Monthly Weather Review*, v.97, p.163-172.
- Horel, J.D., and Wallace, J.M., Atmospheric phenomena associated with the Southern Oscillation: *Monthly Weather Review*, v.109, p.813-829.
- Karl, T.R., and Knight, R.W., 1985, Atlas of monthly and seasonal precipitation departures from normal (1895-1985) for the contiguous United States: Asheville, NC, National Climatic Data Center, Historical Climatological Series, 3-12.
- Opsteegh, J.D., and Van den Dool, H.M., 1980, Seasonal differences in the stationary response of a linearized primitive equation model: Prospects for long-range forecasting: *Journal of Atmospheric Science*, v.37, p.2169-2185.
- Rasmusson, E.M., and Carpenter, T.H., 1982, Variations in tropical sea surface temperature and surface wind fields associated with the Southern Oscillation/El Niño: *Monthly Weather Review*, v.110, p.354-384.
- Ropelewski, C.F., and Halpert, M.S., 1989, Precipitation patterns associated with the high index phase of the Southern Oscillation: *Journal of Climate*, v.2, p.268-284 (in press).
- _____, 1987, Global and regional scale precipitation patterns associated with the El Niño/Southern Oscillation: *Monthly Weather Review*, v.115, p.1606-1626.
- _____, 1986, North American precipitation and temperature patterns associated with the El Niño/Southern Oscillation: *Monthly Weather Review*, v.114, p.2352-2362.
- Trenberth K.E., Branstator, G.W., and Arkin, P.A., 1988, Origins of the 1988 North American drought: *Science*, v.242, p.1640-1645.

Strong, Low Frequency (Decadal) Environmental Fluctuations During the 20th Century in the North Pacific Ocean, on the Washington Coast, and in Puget Sound

Curtis C. Ebbesmeyer and Carol A. Coomes

ABSTRACT: At decadal period (10-20 years), dynamic linkage was evident between atmospheric low pressure systems over the North Pacific Ocean and circulation in a Pacific Northwest fjord (Puget Sound). As the Aleutian low pressure center shifts, storms arriving from the North Pacific Ocean deposit varying amounts of precipitation in the mountains draining into the estuarine system; in turn, the fluctuating addition of fresh water changes the density distribution near the fjord basin entrance sill, thereby constraining the fjord's vertical velocity structure. This linkage was examined using time series of 21 environmental parameters from 1899 to 1987. Covariation in the time series was evident because of the strong decadal cycles compared with long-term averages, interannual variability, and seasonal cycles.

INTRODUCTION

Long time series of environmental parameters typically contain prominent fluctuations at a number of periodicities. In this paper, dynamic linkage is examined between North Pacific Ocean atmospheric pressure and currents in a Pacific Northwest fjord (Puget Sound; Figure 1). Current measurements in Puget Sound have been made with internally-recording current meters for almost two decades. While examining the seasonal current cycle, it was apparent that the dominant subtidal signal was between decades at depth. Moreover, the variability of the atmosphere over the North Pacific Ocean is known to be reflected in the meteorology and hydrology of Puget Sound (Cayan and Peterson, 1989) and this undoubtedly affects the fjord's current structure (Figure 1). Identification of the strong, decadal fluctuations in North Pacific storms (Danielsen et al., 1957) and fjord currents led us to describe the linkage between a local estuary and large-scale atmospheric processes (see Ebbesmeyer et al., 1989, for additional explanation).

BACKGROUND

Atmospheric pressure fluctuations over the North Pacific Ocean previously have been correlated with environmental variability in the Pacific Northwest (Cayan and Peterson, 1989; Emery and Hamilton, 1985;

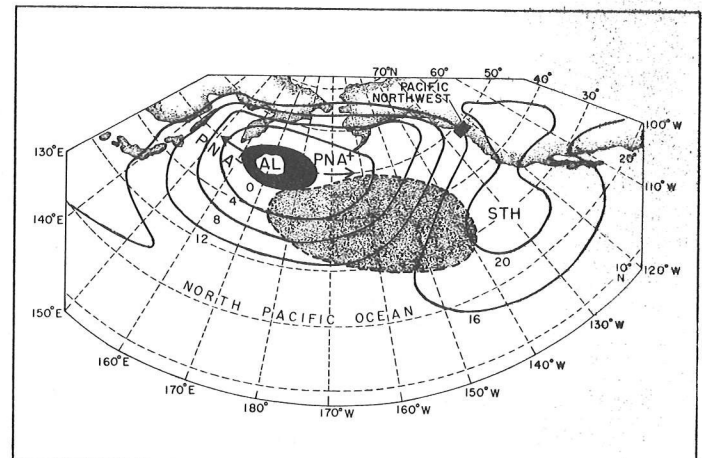


Figure 1. Study area (black rectangle) in relation to movement of the Aleutian Low (AL; blackened) shown by arrows at left and right of AL associated (respectively) with negative (PNA⁻) and positive (PNA⁺) values of the Pacific North American index (PNA): solid lines, January (1947-1985) mean sea level atmospheric pressure (Seckel, 1988) (SLP-1000 mb); stippled, area between Aleutian Low and Subtropical High (STH) pressure centers, where the correlation coefficient equals -0.50 to -0.63, computed between winter average SLP and the annual Pacific Northwest (PNW) index.

Wallace and Gutzler, 1981; and Yarnal, 1984). The Pacific North American (PNA) index (Wallace and Gutzler, 1981) quantifies the horizontal patterns of North Pacific sea level pressure (SLP) and the height of the 500 millibar-pressure surface. Negative values of the PNA index correspond to zonally oriented 500 mb height contours and an Aleutian Low pressure center displaced westward with a weak SLP gradient (G2) (Seckel, 1988) (Figure 1). Conversely, a positive PNA index corresponds to an amplified wave pattern of 500 mb height with the Aleutian Low shifted eastward and an intensified zonal SLP gradient.

The water masses of Puget Sound are contained within a system of glacially-carved channels appended to the primary estuarine system, the Strait of Georgia connecting through the Strait of Juan de Fuca to the North Pacific

In J.L. Betancourt and A.M. MacKay, editors, 1990. Proceedings of the Sixth Annual Pacific Climate (PACLIM) Workshop, March 5-8, 1989: California Department of Water Resources, Interagency Ecological Studies Program Technical Report 23.

©198-IEEE. Reprinted with permission from *Proceedings of Oceans 89*, Seattle, WA, September 18-21, 1989, p.242-246.

Occan (Barnes and Ebbesmeyer, 1978, and Ebbesmeyer and Barnes, 1980) (Figure 2). Prominent sills separate Puget Sound into several basins. This paper deals with water in the northern half of the central or Main Puget Sound Basin (hereafter Basin), which lies between sills located in Admiralty Inlet and The Narrows (Figure 2). Depths at mid-channel in the Basin average 200 m; approximately two-thirds of the Basin water column lies below Admiralty Inlet's sill depth (66 m).

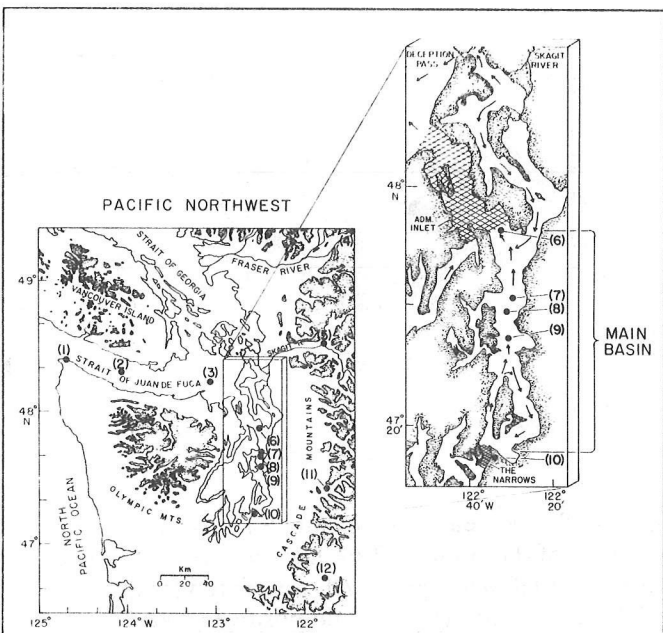


Figure 2. Puget Sound and approaches — sources of data: dots, sites 1-12; stippled, elevations greater than 2500 feet (762 m). Insert, Puget Sound Main Basin: stippled area, land; hatched areas, sill zones (Admiralty Inlet and The Narrows); arrows, direction of mean surface water flow.

Fresh water entering the Strait of Juan de Fuca is contributed primarily by the Strait of Georgia (~ 76 percent); the remainder comes from Puget Sound (~ 24 percent, Coomes et al., 1984, and Waldichuk, 1957). On an annual basis, the fresh water entering the Strait of Juan de Fuca is contributed in large part by snow from the Cascade Mountains. Seaward flowing snowmelt is mixed by strong tidal currents with the inflowing source water near the submerged banks in the eastern Strait of Juan de Fuca and the sills in Admiralty Inlet (Ebbesmeyer and Barnes, 1980).

Winds over the Basin are strongly constrained to northerly and southerly directions by the Olympic and Cascade mountains (Figure 2). During the year winds in winter are strongest, usually associated with Pacific storms that deposit most of the snow in the Cascade Mountains (Ebbesmeyer et al., 1989).

DATA

Observations at selected locations in the North Pacific Ocean and the Pacific Northwest were available during varying intervals from 1899 to 1987.

The atmospheric circulation over the North Pacific Ocean was characterized by SLP and 500 millibar height data. For the winters (Dec-Feb), the mean zonal gradient of SLP (G_2) along 50°N between 130°W and the Aleutian Low pressure center (AL) were available for 1947-85 (Seckel, 1988). The PNA index for the winters of 1946-84 was estimated from data at the U.S. Navy Fleet Numerical Oceanography Center (Ebbesmeyer et al., 1989). The frequency of wind velocities equaling Beaufort 8 or greater ($\geq 17.5 \text{ ms}^{-1}$; f_{B8}) was tabulated from ship reports in the region 45-60°N by 130-170°W for the months of January 1900 to 1938, as shown on historical weather maps for the northern hemisphere (Danielsen et al., 1957).

Available data (Ebbesmeyer et al., 1989) were collected at twelve sites in the Pacific Northwest (Figure 2):

Site 1: Coastal Temperature. Anomalies of monthly sea surface temperatures (McLain, 1984) (ΔT_c ; 1941-82) from the long-term mean seasonal cycle at Neah Bay, Washington, were averaged by calendar year for the Pacific Coast.

Site 2: Source Water in the Western Strait of Juan de Fuca. Temperature (T_s) and salinities (S_s) of the Pacific Ocean source water were averaged for yearly intervals from monthly observations, during 1934 to 1940 and 1953 to 1954, near mid-channel off Pillar Point at a depth of 140 m.

Site 3: Source Water in the Eastern Strait of Juan de Fuca. Temperature (ΔT_{AI}), salinity (ΔS_{AI}) and density ($\Delta \rho_{AI}$) differences were computed between two locations embracing Admiralty Inlet: 75 m at site 3, close to Admiralty Inlet's sill depth, and 100 m at site 6. The density difference was computed from monthly observations of temperature and salinity averaged at each site during four, 12-month intervals: 1/53-12/53, 1/54-12/54, 12/60-11/61, and 2/70-1/71. To reduce bias toward the decade of the 1950s, the annual values for 1953 and 1954 were averaged.

Sites 4, 5: Runoff. Monthly discharge values were averaged within calendar years from the two largest rivers influencing the Strait of Juan de Fuca: Fraser at Hope, British Columbia (RF; 1966-81; site 4), and Skagit at Concrete, Washington (RS; 1961-86; site 5).

Sites 6, 7: Basin Water Properties. Temperature (T_b), salinity (S_b), and density (ρ_b ; sigma-t) were averaged within 27, one-year intervals during 1934-1984, using monthly observations at 150 m depth from the vicinity of sites 6 and 7.

Sites 8, 9: Basin Currents. Current speed and direction were measured with Aanderaa current meters at sites 8 (1972-81) and 9 (1983-84). Tidally-induced, fortnightly fluctuations were filtered by averaging equally weighted along-channel speed from each observation over 28-day intervals.

Site 10: Wind. Hourly wind observations available for each month between 1972 and 1984 were tabulated by speed and direction. Monthly frequencies determined for southerly directions (f_{sw} ; 102° - 258° True) were averaged for winter months. Also, frequencies of wind speeds faster than 5.7 (f_{57}) and 8.7 ms^{-1} (f_{87}), regardless of direction, were determined for each winter.

Site 11: Precipitation. Annual (Jan-Dec) totals (PCL) were obtained for Cedar Lake (also known as Chester Morse Lake). Data were available for 1899-1987 (except for 1901, 1902).

Site 12: Snow Depth. Annual measurements of snow depth on 15 March of each year (SD) between 1916 and 1987 (except for 1949, 1950, 1952) were obtained at the Paradise Ranger Station. Fluctuations of snow depth and water equivalent are similar (Reid and Albright, 1981).

METHODS

The analysis of decadal period variability is simplified because temporal fluctuations of currents, temperature, salinity, and density at mid-depth in the Basin water column are representative of those at other depths, and decadal fluctuations can be characterized by the Pacific Northwest index computed from annual data (Ebbesmeyer et al., 1989). The along-channel speed profile pivots approximately about a fixed depth, dividing the water column into two depth ranges: Upper layer, 0 to ~ 56 m; lower layer, ~ 56 to 200 m. When mid-depth speed (U_m ; 90-116 m) exceeded a certain magnitude (0.06 ms^{-1}), speeds were slower near the bottom, whereas at lower magnitudes speeds were faster near the bottom. Annual average temperature, salinity, and density profiles were offset from year to year.

The Pacific Northwest (PNW) index, developed to provide a continuous record of decadal environmental fluctuation in the Pacific Northwest, apparently is amplified compared with parameters for the atmosphere over the North Pacific Ocean (Ebbesmeyer et al., 1989). The PNW index is expressed as the average of the standard normal deviates of three parameters: annual average coastal temperature anomaly; annual average basin temperature; and 15 March snow depth (Ebbesmeyer et al., 1989).

PNW index estimates for 1916-87 averaged within 5-year running blocks of time fluctuated at a period of approximately 18 years (twice the mean interval between zero-crossings) and accounted for 41% of the variance of the annual estimates. As 5-year averages (designated by overbars) of the standard normal deviates simplify visual comparison with the PNW index, 5-year averages for 1935-85 were computed for selected oceanic, coastal, and Pacific Northwest parameters: PNA and PNW indices, sea level atmospheric pressure gradient, coastal temperature anomaly, snow depth and basin temperature (Figure 3).

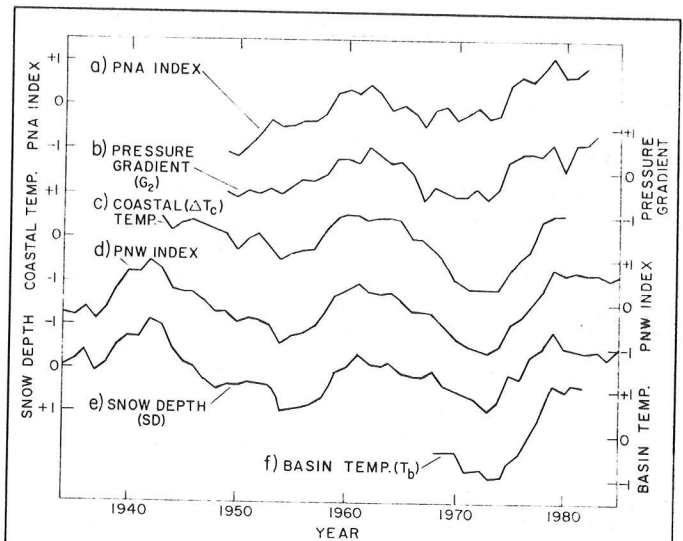


Figure 3. Low frequency fluctuations of oceanic, coastal, and Pacific Northwest environmental parameters, 1935 to 1985, based on five-year running averages of the standard normal deviates computed annually for (a)-(c), (e), (f):

- (a) Pacific North American (PNA) index;
- (b) Sea level atmospheric pressure gradient (G_2);
- (c) Coastal temperature anomaly (ΔT_c);
- (d) Pacific Northwest (PNW) index;
- (e) Snow depth (SD);
- (f) Puget Sound Main Basin temperature (T_b).

Note that the scale for snow depth has been inverted.

The similarities between decadal fluctuations of these parameters indicate qualitatively that the PNW index may be used to represent decadal environmental behavior. Moreover, a time series extending back to 1900 indicates that decadal fluctuation has persisted from the beginning of the 20th century (Figure 4).

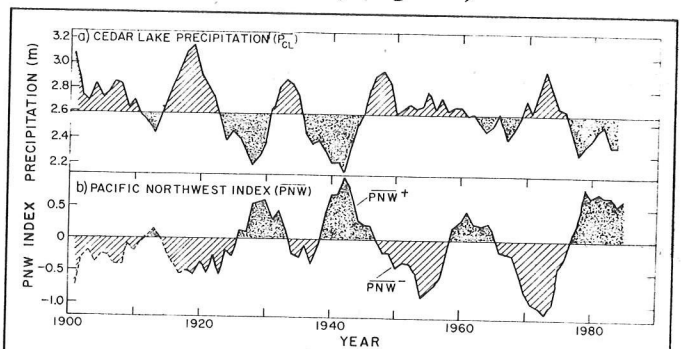


Figure 4. Five-year running averages of (a) Cedar Lake precipitations (PCL) and (b) Pacific Northwest (PNW) index, 1901-85: hatched area, precipitation above the long-term mean and negative PNW index (PNW⁻); stippled area, Cedar Lake precipitation below the long-term mean and positive PNW index (PNW⁺); dashed line in (b), PNW index estimated for 1900-17, using correlation with precipitation.

COVARIATION AND AMPLITUDE AT DECADAL PERIOD

The environmental parameters were compared at decadal period with the Pacific Northwest index; linear regressions were computed at zero time lag between the 5-year average PNW index and the environmental parameters (Table 1). The squared correlation coefficient averaged for seventeen regressions (not including Basin salinity, which is constant; Ebbesmeyer et al., 1989) equaled 0.75. This suggested that comparisons with the PNW index could be used to deduce the parameters' covariation at low frequency.

Amplitudes of the decadal fluctuations were compared with interannual variability, long-term averages, and seasonal cycles of 21 environmental parameters (Ebbesmeyer et al., 1989). For a given environmental parameter the dimensionless ratio of decadal amplitude to annual variability (a/σ) was computed, where σ represents the standard deviation of the annual value, and "a" the decadal fluctuation amplitude estimated by fitting a sinusoid to PNW and using the regressions in Table 1 (Ebbesmeyer et al., 1989). The dimensionless amplitudes of 21 environmental parameters vary by an order of magnitude between 0.1 to 1.1, with an average value of 0.67 (Figure 5.)

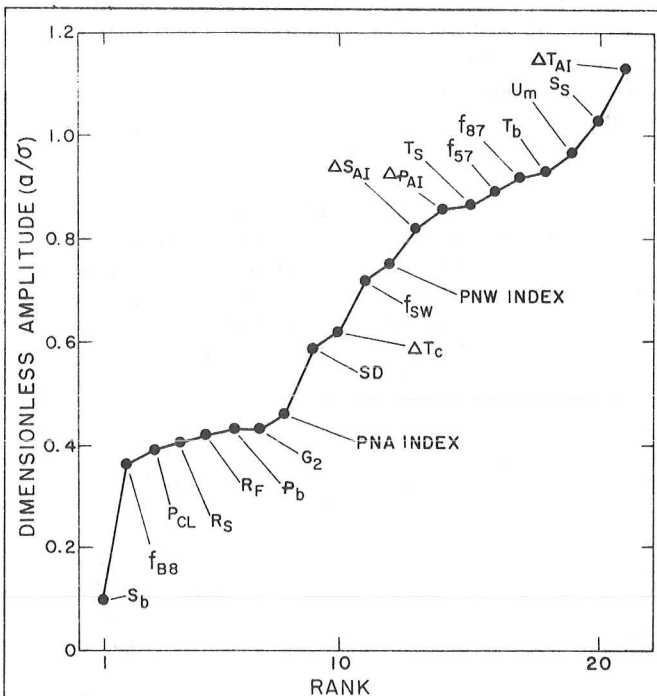


Figure 5. Dimensionless amplitude of decadal fluctuations for 21 environmental parameters ranked from lowest to highest. See text for abbreviations.

Amplitude of decadal fluctuation was compared to the long-term average for a given environmental parameter (Ebbesmeyer et al., 1989). In the North Pacific Ocean, the zonal sea level pressure gradient and degree of storm activity fluctuate by 37-49% of their mean values. In the Cascade Mountains, parameters of fresh water

Table 1. Linear regressions between environmental parameters and the 5-year average Pacific Northwest (PNW) index at decadal period. Overbars indicate 5-year averages. N = number of samples; r = correlation coefficient.

Regression	N	r
North Pacific Ocean Atmosphere		
$\overline{PNA} = 10.76 + 28.73 \overline{PNW}$	34	+0.66
$\overline{G_2} = 3.88 + 1.44 \overline{PNW}$	35	+0.81
$\overline{f_{BB}} = 0.058 - 0.0169 \overline{PNW}$	19	-0.49
Washington Coastal Temperature		
$\overline{\Delta T_c} = 0.31 + 0.415 \overline{PNW}$	38	+0.90
Western Strait of Juan de Fuca		
Source Water Temperature and Salinity		
$T_s = 7.11 + 0.281 \overline{PNW(a)}$	9	+0.91
$S_s = 33.52 - 0.126 \overline{PNW(a)}$	(a)	-0.20
Differences across Entrance Sill Zone (b)		
Density, salinity, temperature		
$\overline{\Delta \rho_{AI}} = 1.88 + 0.269 \overline{PNW}$	3	+0.96
$\overline{\Delta S_{AI}} = 2.082 + 0.271 \overline{PNW}$	3	+0.99
$\overline{\Delta T_{AI}} = -1.64 - 0.451 \overline{PNW}$	3	-0.99
Puget Sound Main Basin Salinity, Temperature, and Currents		
$S_b = \text{constant}$	(c)	27 +0.04
$T_b = 9.75 + 0.780 \overline{PNW}$	27	+0.82
$U_m = -0.0672 + 0.0439 \overline{PNW}$	28	+0.86
Winds over Puget Sound Main Basin		
$\overline{f_{SW}} = 0.558 - 0.0874 \overline{PNW}$	8	-0.98
$\overline{f_{57}} = 0.117 - 0.0868 \overline{PNW}$	8	-0.98
$\overline{f_{87}} = 0.0132 - 0.0137 \overline{PNW}$	8	-0.96
Fresh water in Cascade Mountains		
$\overline{R_F} = 2630 - 212.0 \overline{PNW}$	12	-0.88
$\overline{R_S} = 437 - 40.5 \overline{PNW}$	22	-0.85
$\overline{P_{CL}} = 2.59 - 0.258 \overline{PNW}$	67	-0.62
$\overline{SD} = 4.44 - 1.20 \overline{PNW}$	68	-0.92

- (a) Derived using T_s vs PNW and T_s vs S_s (see Ebbesmeyer et al., 1989). The annual values of PNW were used because the correlation between annual T_s and PNW ($r = +0.91$) was much larger than between five-year averages ($r = +0.52$).
- (b) Site 3 (75 m) - Site 6 (100 m).
- (c) See Ebbesmeyer et al., 1989.

fluctuate by 11-36%. Winds over Puget Sound vary by 21-140%. Differences across the entrance sill fluctuate by 19-37%. Finally, in the Basin, mid-depth current speed fluctuates by 87%.

The range of average monthly values was compared with that of decadal fluctuation for a number of parameters (Ebbesmeyer et al., 1989). To integrate the estimates of single strength, means for three comparison of decadal amplitude were computed:

- 0.67, the mean for 21 estimates of decadal amplitude divided by the standard deviation of annual values;
- 0.35, the mean for 17 estimates of the decadal range divided by the long-term average; and
- 0.57, the mean for 10 estimates of the decadal range divided by the range of the mean seasonal cycle.

Thus, several comparisons indicate that Basin currents, as well as the linkage to the North Pacific Ocean, have strong signals at decadal period.

DYNAMICS OF THE LINKAGE

Dynamics of the linkage between the North Pacific Ocean and Puget Sound at decadal period may be simplified as illustrated in Figure 6. As the Aleutian Low pressure center shifts position, storms from the Pacific Ocean deposit varying amounts of snow in the Cascade Mountains. Because snowmelt is a major source of fresh water for the Strait of Juan de Fuca, atmospheric pressure and storm patterns over the North Pacific Ocean therefore significantly regulate the addition of fresh water to the estuarine system. When the Aleutian Low moves eastward, storm winds become less frequent in the Gulf of Alaska and the Pacific Northwest; therefore smaller amounts of fresh water are available from the Cascade Mountains. In turn the density difference across Admiralty Inlet increases and the fastest inflow in the Basin deepens toward the bottom.

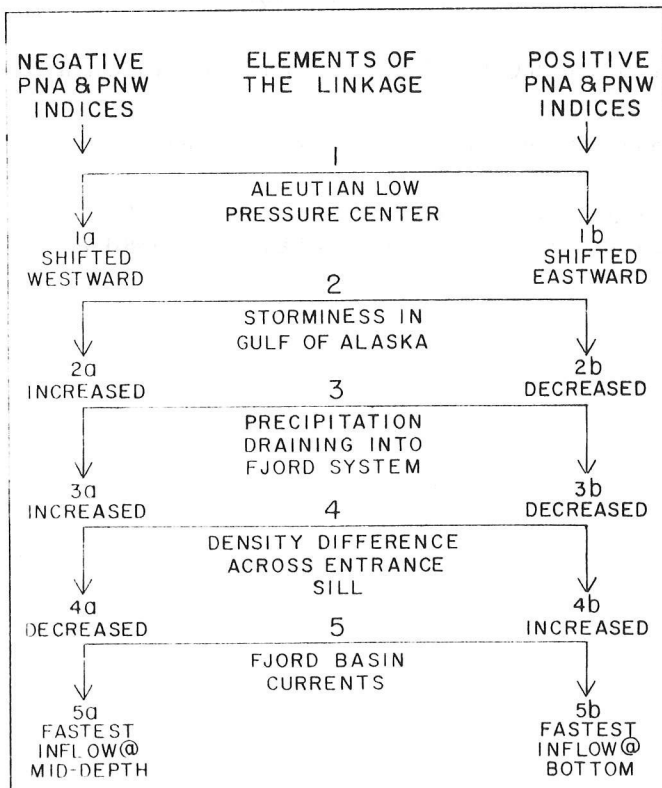


Figure 6. Schematic for the linkage between the Aleutian Low Pressure Center and the currents in Puget Sound's Main Basin (1-5); 1a-5a, negative PNA and PNW indices; 1b-5b, positive PNA and PNW indices.

CONCLUSION

Time series of environmental parameters indicate that approximately four decadal cycles occurred during 1900-1976 (Figure 4). If this phenomenon is continued, five cycles will have been completed in the twentieth century. The latest cycle, which began in 1977, might be expected to switch so that conditions associated with negative PNA and PNW indices would occur in most of the 1990s. For example, these conditions in the Pacific Northwest may lead to improved skiing at mountain resorts, more plentiful water supplies in Seattle, and increased hydroelectric power.

Decadal fluctuations of the linkage are apparently amplified in the Basin waters; therefore, the Basin may be viewed as a sensor for conditions across the North Pacific Ocean. Decadal fluctuations also may be amplified in the rings of certain Pacific Northwest trees sensitive to high elevation snow depth (Graumlich and Brubaker, 1986). Consequently, trees existing in the Cascade Mountains for the past 400 to 600 years might provide additional data describing the decadal variability of the meteorology, oceanography, hydrology, and ecology of the Pacific Northwest and the North Pacific Ocean.

REFERENCES

- Barnes, C.A., and Ebbesmeyer, C.C., 1978, Some aspects of Puget Sound's circulation and water inproperties, Kjerfve, B., editor, Estuarine Transport Processes: Columbia, University of South Carolina Press, p.209-228.
- Cayan, D.R., and Peterson, D.H., 1989, The influence of North Pacific atmospheric circulation on streamflow in the West, in Peterson, D.H., Editor, Aspects of climate variability in the Pacific and western Americas: American Geophysical Union Monograph v.55, p.375-398.
- Coomes, C.A., Ebbesmeyer, C.C., Cox, J.M., Helseth, J.M., Hinchey, L.R., Cannon, G.A., and Barnes, C.A., 1984, Synthesis of current measurements in Puget Sound, Washington - Volume 2: Indices of mass and energy inputs into Puget Sound: runoff, air temperature, wind, and sea level: National Oceanic Atmospheric Administration Technical Memorandum NOS OMS 4.
- Danielsen, E.F., Burt, W.V., and Rattray, M. Jr., 1957, Intensity and frequency of severe storms in the Gulf of Alaska: Transactions of the American Geophysical Union, v.38, no.1, p.44-49.
- Ebbesmeyer, C.C., and Barnes, C.A., 1980, Control of a fjord basin's dynamics by tidal mixing in embracing sill zones: Estuarine Coastal Marine Science, v.11, p.311-330.
- Ebbesmeyer, C.C., Coomes, C.A., Cannon, G.A., and Bretschneider, D.E., 1989, Linkage of ocean and fjord dynamics at decadal period, in Peterson, D.H., Editor, Aspects of climate variability in the eastern Pacific and western Americas: American Geophysical Union Monograph v.55, p.399-418.
- Emery, W.J., and Hamilton, K., 1985, Atmospheric forcing of interannual variability in the northeast Pacific Ocean: connections with El Niño: Journal of Geophysical Research, v.90, no.C1, p.857-868.
- Graumlich, L.J., and Brubaker, L.B., 1986, Reconstruction of annual temperature (1590-1979) for Longmire, Washington, derived from tree rings: Quaternary Research, v.25, p.223-234.
- McLain, D.R., 1984, Coastal ocean warming in the Northeast Pacific, 1976-1983, in Workshop Proceedings: The influence of ocean conditions on the production of salmonids in the north Pacific: ORESU-W-83-001, Oregon State University, Sea Grant College Program, p.61-83.
- Reid, R.J., and Albright, M.D., 1981, Report to Westours dated 23 July 1981.
- Seckel, G.R., 1988, Indices for mid-latitude north Pacific winter wind systems; an exploratory investigation: Geojournal, v.16, no.1, p.97-111.
- Waldichuk, M., 1957, Physical oceanography of the Strait of Georgia, British Columbia: Journal of Fisheries Research Board of Canada, v.14, p.321-486.
- Wallace, J.M., and Gutzler, D.S., 1981, Teleconnections in the geopotential height field during the northern hemisphere winter: Monthly Weather Review, v.109, no.4, p.784-812.
- Yarnal, B., 1984, Relationships between synoptic-scale atmospheric circulation and glacial mass balance in southwestern Canada during the International Hydrological Cycle, 1965-74: Journal of Glaciology, v.30, no.105, p.188-198.

Pacific Sea Surface Temperature Associations with Southwestern United States Summer Rainfall and Atmospheric Circulation

Andrew M. Carleton, Paul J. Weser, and Duane A. Carpenter

ABSTRACT: Pacific sea surface temperatures (SSTs) are examined for their associations with (1) summer rainfall, and (2) the latitude location of the mid-tropospheric subtropical high pressure ridge (STR) in the southwestern United States during 1945 to 1986. Extreme northward (southward) displacements of STR are associated with wet (dry) summers over Arizona and an enhanced (weakened) gradient of SST off the California and Baja coasts. These tend to follow winters marked by positive (negative) phases of the PNA, Pacific/North America, teleconnection pattern. Recent decadal variations of Arizona summer rainfall (1950s wet; 1970s dry) appear similarly related to southwestern United States synoptic circulation and eastern Pacific SSTs.

INTRODUCTION

Air/sea interaction is a continuing concern in climatic dynamics. SST variations have been implicated in the shorter-term (seasonal, interannual) variations of rainfall and temperature in both tropics and extratropics (e.g., Namias and Cayan, 1981). These often comprise the dominant mode of SST variability in the equatorial and North Pacific known as El Niño Southern Oscillation (ENSO) and its teleconnections (Chiu and Newell, 1983; Ropelewski and Halpert, 1987).

The southwest United States (principally Arizona) experiences a bimodal (winter, mid-summer) precipitation distribution. The summer rainfall singularity (or *monsoon*) dominates the months of July and August and stands in stark contrast to the aridity of the preceding months (Bryson and Lowry, 1955). Strong changes in mid-tropospheric circulation are associated with the arrival of subtropical moisture from the Gulf of California/eastern Pacific (Hales, 1974) and comprise a northward and westward shift of the STR. Within-season and interannual fluctuations in latitude location of STR have been correlated with changes in satellite-observed cloud cover over the southwestern United States (Carleton, 1985) and, accordingly, Arizona precipitation anomalies (Carleton, 1987).

A typing scheme of daily 500mb height patterns associated with southwestern U.S. summer cloud cover variations (Carleton, 1986) has been used to subjectively classify daily maps for summers 1945 through 1987. Figure 1 shows summer mean values of an index of the

STR. It is in ratio form and is given as the number of days of northward-displaced STR over the southwest (Four Corners High)/number of days of southward-displaced STR.

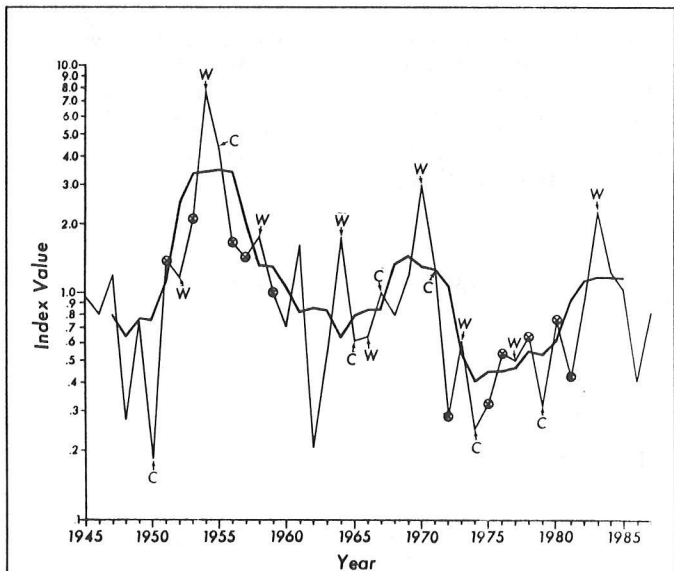


Figure 1. Individual and 5-summer moving averages of the circulation index STR ($= n$ of days anticyclonic north \div n of days anticyclonic south) for the southwestern United States, 1945-1987. Note the logarithmic scale on the vertical axis. Summers indicated "W" ("C") follow peak warm (cold) events of ENSO. Other summers (circled "X") are used in the *undisturbed decadal* composites of SST for the 1950s and 1970s (e.g., see Figure 7).

The STR index is significantly correlated with Arizona statewide summer rainfall over a 40-year period, especially for August ($r = 0.698$; $r^2 = 49\%$). Further, STR was consistently farther north in summers of the 1950s and farther south for much of the 1970s (Figure 1). The *persistence* (runs of days) of the anticyclonic types is similarly highly correlated with Arizona rainfall and also with the STR latitude index (Carleton, 1987).

This study examines the associations of Pacific SSTs with both Arizona summer rainfall variations and the STR index for the 1945-1987 period.

SUMMER STR / ARIZONA RAINFALL ASSOCIATIONS

Table 1 shows the selection of summers used for the composite analysis of Arizona rainfall and Pacific SST. In (a), wet (dry) summers are selected on the basis of at least 45% of Arizona rainfall stations having standardized summer rainfall departures equal to or exceeding + (-) 0.6 standard deviations from the long-term (1951-1980) means for July 1 to September 15 (Weser, 1985).

This results in 8 wet and 8 dry summers, a few of which repeat in Table 1(b). Composite (average) maps of rainfall departures were then derived. In Table 1(b), similar composite rainfall departure maps were derived, only in this case for summers of extreme northward: index values > 2.0 (southward: values < 0.4) STR (refer to Figure 1). The resulting composites (Figure 2) strongly resemble the maps derived using the years in Table 1(a) (not shown). They confirm the role of STR for Arizona summer rainfall variations.

Table 1. Stratification of extreme Arizona summer rainfall and circulation.

(a) 8 Wet and 8 Dry Summers, 1951-1980 ^a		(b) 5 STR(North) and 7 STR(South) Summers, 1945-1987 ^b	
Wet Summers	Dry Summers	STR (North)	STR (South)
1951	1952	1953	1948
1954	1956	1954	1950
1955	1962*	1955	1962
1963	1972*	1970	1972
1964	1973	1983	1974
1966	1978		1975
1967	1979*		1979
1970	1980		

- ^a Where at least 45% of stations exceed + (-) 0.60 standard deviations from the 30-year station means.
^b Where circulation index anticyclonic north/a-c south is greater (less) than 2.0 (0.4).

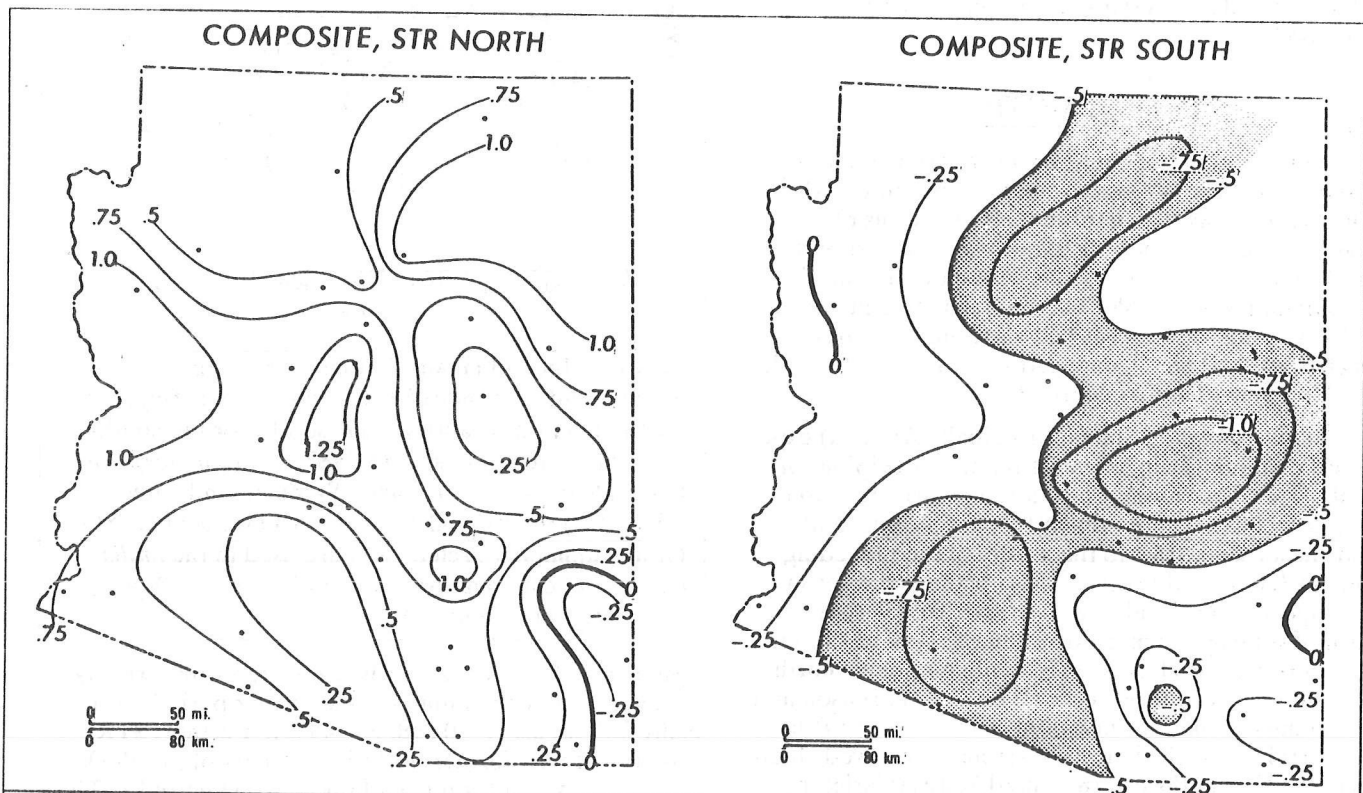


Figure 2. Composite normalized rainfall departure patterns for Arizona (standard deviation units) for summers of extreme northward STR (5 years: 1953, 1954, 1955, 1970, 1983) and extreme southward STR (7 years: 1948, 1950, 1962, 1972, 1974, 1975, 1979). The patterns appear very similar to those derived by compositing extreme rainfall summers in the 1951-1980 period (Table 1(a)).

PACIFIC SST / ARIZONA SUMMER RAINFALL ASSOCIATIONS

The Gulf of California and eastern Pacific are important for both *intraseasonal* variations (*bursts, breaks*) of Arizona summer rainfall (Hales, 1974) and the *inter-annual* variations of southwestern United States climate related to ENSO (Sheaffer and Reiter, 1985; Carleton, 1987; Andrade and Sellers, 1988). Thus, an examination of Pacific SST / Arizona rainfall / southwest U.S. circulation relationships is appropriate. Figure 3 shows the area covered by the COADS (*Cooperative Ocean-Atmosphere Data Set*, 10° lat./long. grids) and NODC (*National Oceanic Data Center*, 5° lat./long. grids) SST data of interest in this study. The NODC data are used to identify SST associations with Arizona summer rainfall for the years listed in Table 1(a), and the COADS is used for corroboration and also to identify broad-scale teleconnection patterns of SST that might be related to STR.

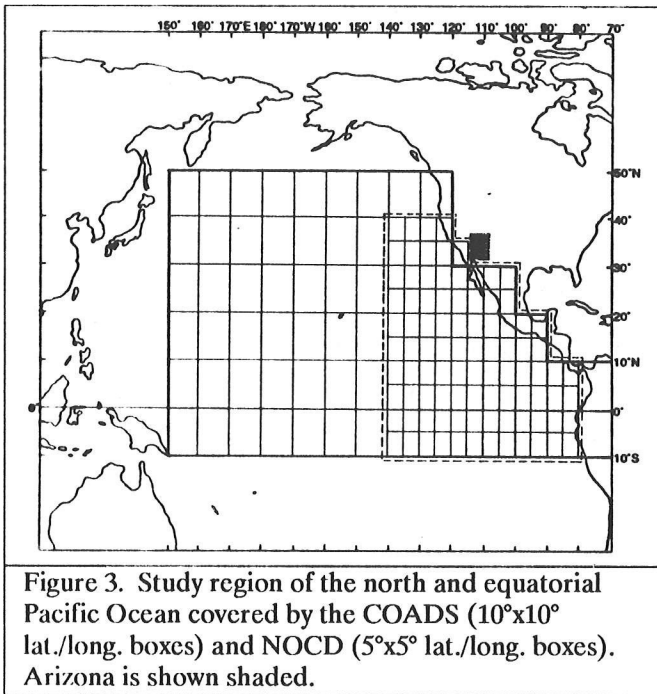


Figure 3. Study region of the north and equatorial Pacific Ocean covered by the COADS (10°x10° lat./long. boxes) and NODC (5°x5° lat./long. boxes). Arizona is shown shaded.

Compositing the NODC SST data separately for wet and dry summers, subtracting one composite from the other, and performing difference-of-means tests on the cell values reveals the pattern shown in Figure 4 (JJA only). The pattern is somewhat difficult to interpret, because of insufficient numbers of observations in near-equatorial cells and lack of significant differences in others.

However, the general appearance is one of lower SSTs in wet years in cells for which significant differences occur. This resembles broadly the composite difference map for MAM (not shown).

If one correlates the stratified (wet, dry summer) SSTs for six grid cells having acceptable numbers of observations with Arizona statewide rainfall, the results are as shown in Figure 5. Rainfall in the wet summer compos-

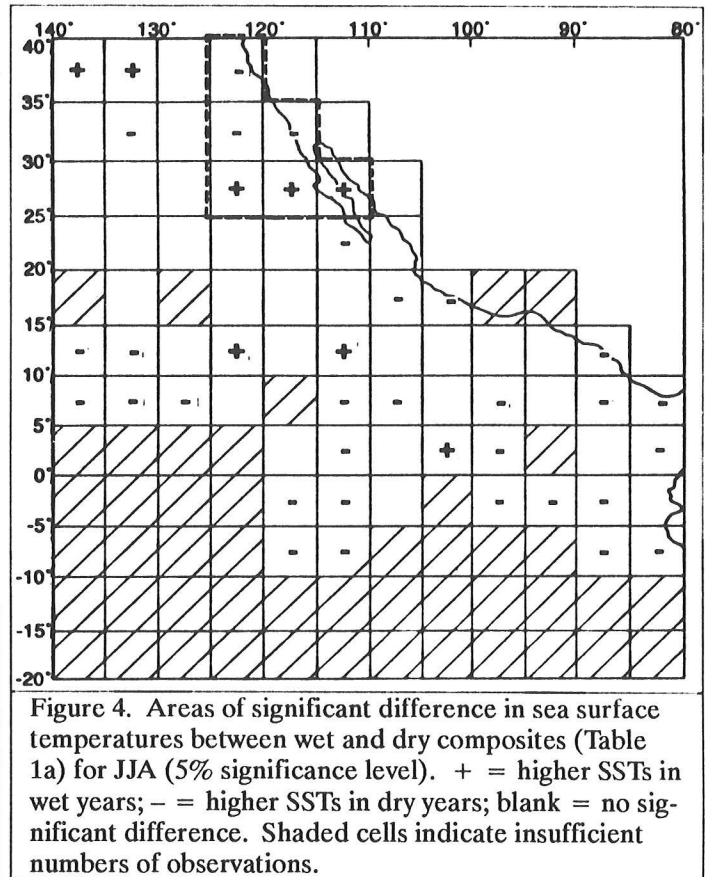


Figure 4. Areas of significant difference in sea surface temperatures between wet and dry composites (Table 1a) for JJA (5% significance level). + = higher SSTs in wet years; - = higher SSTs in dry years; blank = no significant difference. Shaded cells indicate insufficient numbers of observations.

ite is significantly negatively correlated with SSTs along the California/northern Baja coasts. SSTs in the Gulf of California are weakly positive. The enhanced longitudinal SST gradient in wet summers may favor a low-level wind anomaly from the southwest that facilitates transport of subtropical moisture into the desert southwest.

The lack of significant SST/Arizona rainfall correlations in dry summers and absence of a strong longitudinal SST gradient for this region may imply a weakened low-level wind that helps limit the northward penetration of moisture from the eastern Pacific/Gulf of California. This postulated link between the SSTs and wind fields of this region is being investigated.

PACIFIC SST / SUMMER STR ASSOCIATIONS

In an effort to compare the foregoing SST / rainfall results with the association between Pacific SSTs and the circulation (STR), seasonal composite difference maps of COADS SST were computed for summers of STR-north minus STR-south. Possible lead associations of SST over Arizona summer rainfall are considered by computing seasonal difference maps for spring-1 and winter-1. Broad-scale summer (i.e., contemporaneous) SST difference patterns are generally weakly defined (not shown); those for winter and spring are more strongly defined. The difference pattern for winter (Figure 6) resembles EOF number 1 of the nonseasonal

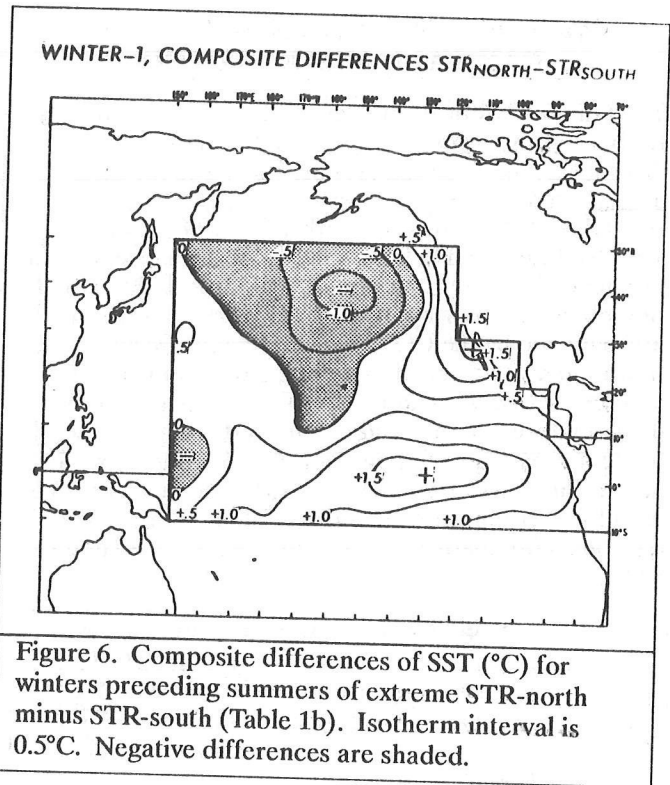
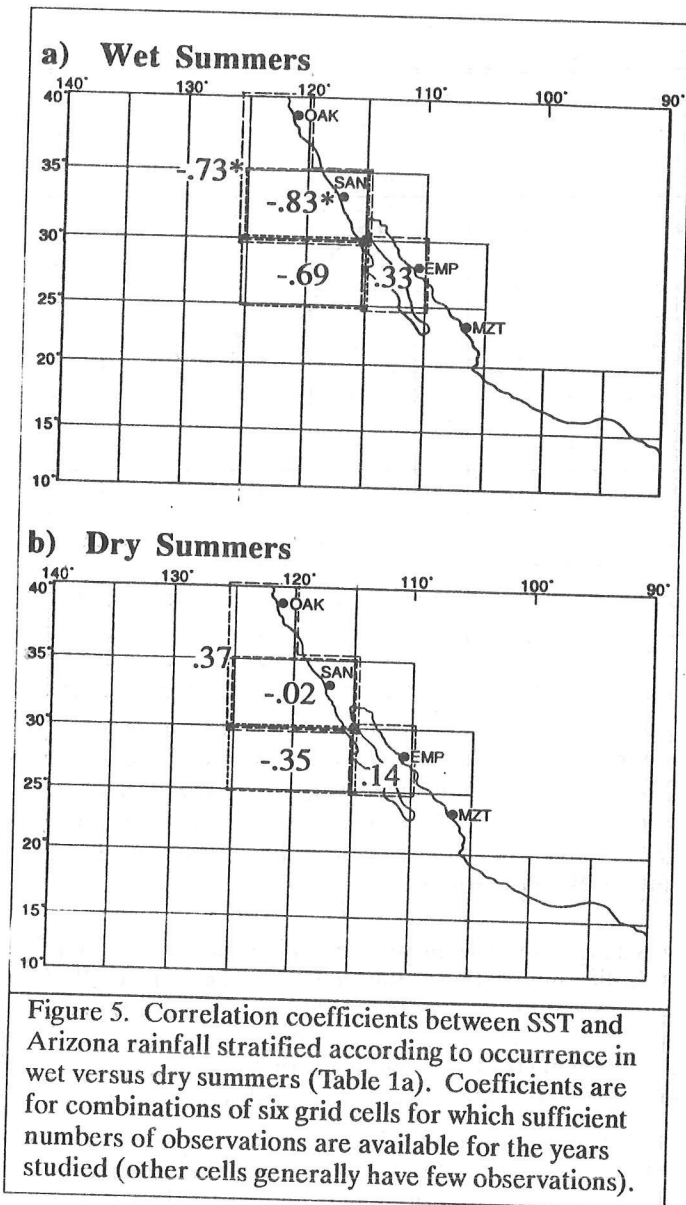


Table 2. Composite means and significance levels for circulation indices stratified according to extremes of Arizona summer rainfall.

(a) Wet vs. Dry Summers, 1951-1980

	STR	PI	PNA + SOI _{DJF} *	SOI _{MAM} *
Wet	2.48	1.99	0.28	4.53
Dry	0.71	0.95	-0.25	4.07
U-Stat.	12	9	16	27
Signif.	0.019	0.007	0.052	--

(b) STR-North vs. STR-South Summers, 1945-1987

	PI	PNA + SOI _{DJF} *	SOI _{MAM} *
STR-North	2.38	0.39	2.80
STR-South	0.55	-0.49	5.65
U-Stat.	0	4	3
Signif.	0.002	0.026	0.015

* Based on the non-normalized seasonal values of Parker (1983).

+ Based on the winter season values (DJF) provided

SST that is associated with ENSO (e.g., Chiu and Newell, 1983).

Such a pattern may favor (although not exclusively) the positive high amplitude phase of the PNA (Pacific-North America) teleconnection pattern. The role of antecedent winter PNA for the summer circulation and rainfall of the southwestern United States is demonstrated in Table 2. A significant difference exists in PNA winter values that precede extreme STR summers, and is such that a positive, high amplitude (negative, zonal) phase tends to precede STR-north (STR-south). A similar, although slightly weaker, relationship exists for summers composited on the basis of Arizona rainfall departures (Table 2a).

Since high amplitude PNA may occur in the absence of a negative extreme, or El Niño, of the Southern Oscillation Index, SOI (e.g., Hamilton, 1988), there are no significant differences found in the antecedent seasonal

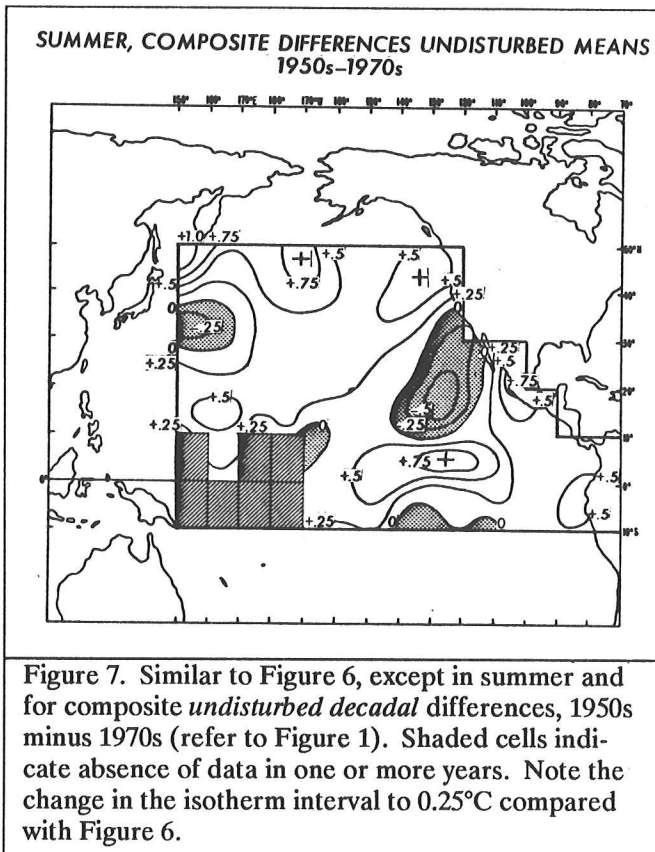
SOI and Arizona summer rainfall (Table 1a). This compares with the summer season results of Andrade and Sellers (1988). However, a significant difference is observed for winter SOIs and summer STR (Table 1b). Note also the consistent and significant differences in STR between summers of opposing Arizona rainfall anomalies (Table 1a).

DECADAL CHANGES IN PACIFIC SST/STR/ARIZONA RAINFALL

The foregoing results suggest strongly that wetter (drier) summers in Arizona are marked by generally northward (southward) displaced STR over the southwestern United States and an enhanced (weakened) SST gradient between the California/Baja coasts and Gulf of California. In addition, wetter (drier) summers seem to follow positive (negative) phases of PNA and associated broadscale SST patterns. Examination of Figure 1 reveals runs of summers in the 1950s (1970s) that were characterized by northward (southward) displaced STR. Similarly, a tendency toward decreasing summer rainfall in Arizona during the 1960s and 1970s has been noted elsewhere (e.g., Johnson, 1978). The question arises as to the possible changes in Pacific SST between the 1950s and 1970s that may have been, at least partly, responsible for these rainfall/circulation variations.

Difference patterns of the composite SSTs for summers of the 1950s (1951-1959) minus the 1970s (1972-1981) are spatially inhomogeneous (not shown). These arise, in part, from the presence of ENSO extremes in those decades (Figure 1). Removing these years and computing *undisturbed decadal* SST composites and difference fields for the remaining years of the 1950s and 1970s reveals more spatially homogeneous patterns. The difference pattern for summer, which is broadly similar to that for spring-1, is shown in Figure 7. Figure 7 suggests that the runs of wetter (drier) summers and northward- (southward-) displaced STR in the 1950s (1970s) were associated with an enhanced longitudinal gradient of SST between the Gulf of California and California/Baja coasts.

This may have influenced the transport of subtropical moisture at lower levels into the desert southwest in a similar way to that suggested for the multi-year cross-decadal composites computed earlier. Future studies hope to examine in more detail these decadal variations in SST and their impact on the atmospheric circulation of the southwestern United States.



REFERENCES

- Andrade, E.R. Jr., and Sellers, W.D., 1988, El Niño and its effect on precipitation in Arizona and western New Mexico: *Journal of Climatology*, v.8, p.403-410.
- Bryson, R.A., and Lowry, W.P., 1955, Synoptic climatology of the Arizona summer precipitation singularity: *Bulletin, American Meteorological Society*, v.36, p.329-339.
- Carleton, A.M., 1987, Summer circulation climate of the American Southwest, 1945-1984: *Annals, Association of American Geographers*, v.77, p.619-634.
- _____, 1986, Synoptic-dynamic character of "bursts" and "breaks" in the southwest U.S. summer precipitation singularity: *Journal of Climatology*, v.6, p.605-623.
- _____, 1985, Synoptic and satellite aspects of the southwestern U.S. summer "monsoon": *Journal of Climatology*, v.5, p.389-402.
- Chiu, L.S., and Newell, R.E., 1983, Variations of zonal mean surface temperature and large-scale air-sea interaction: *Quarterly Journal of Royal Meteorological Society*, v., 109, p.153-168.
- Hales, J.E., 1974, Southwestern United States summer monsoon source — Gulf of Mexico or Pacific Ocean: *Journal of Applied Meteorology*, v.13, p.331-342.
- Hales, K., 1988, A detailed examination of the extratropical response to tropical El Niño/Southern Oscillation events: *Journal of Climatology*, v.8, pp.67-86.

Climatic Effects on Flood Frequency: An Example from Southern Arizona

Robert H. Webb and Julio L. Betancourt

ABSTRACT: After 1960, the Santa Cruz River at Tucson, Arizona, an ephemeral stream normally dominated by summer floods, experienced an apparent increased frequency of flooding coincident with an increased percentage of annual floods occurring in fall and winter. This shift reflects large-scale and low-frequency changes in the eastern Pacific Ocean, in part associated with El Niño-Southern Oscillation (ENSO) phenomena. Using method of moments and a log Pearson type III distribution, the 100-year flood associated with ENSO conditions is double that for non-ENSO conditions. Statistical analysis of floods caused by different storm types yielded a 100-year flood for 1960-1986 that is about five times larger than that for 1930-1959. For 1960-1986, annual flood frequency above the 10-year recurrence interval is dominated by floods caused by dissipating tropical cyclones; for 1930-1959 annual flood frequency is dominated by floods caused by monsoonal storms. Questions are raised about the validity of standard methods of flood-frequency analysis to estimate regulatory and design floods.

INTRODUCTION

Statistical flood-frequency analysis is a commonly-used method for assessing flood hazards and risks in the United States (U.S. Water Resources Council, 1982). Data for flood-frequency analyses include the annual flood series, which is the array of the largest discharges (flood peaks) that occur each year at a gaging station. The annual flood series is used to estimate discharges associated with various recurrence intervals, such as 10, 50, 100 years; these estimated discharges form the basis for flood plain engineering and regulation. The societal importance of flood-frequency analysis is exemplified by the National Flood Insurance Program, which is based primarily on the area inundated by a 100-year flood.

Flood-frequency analysis requires certain assumptions about the statistical properties of the annual flood series. It is assumed that the floods were generated randomly from a single probability distribution with stable moments, such as the mean and the variance; i.e., that the floods in the annual series were derived from the same population. Climate is assumed to be invariant, and the effects of watershed changes on flood conveyance must be negligible (U.S. Water Resources Council, 1982). However, many of the assumptions required for flood-frequency analysis are not tested routinely and, thus, may be inappropriate. For example, mixed populations of floods, such as those caused by dis-

sipating hurricanes and runoff from snowmelt, may comprise the annual flood series.

Rivers in southern Arizona provide examples of annual flood series for which standard flood-frequency analyses yield inconsistent results. On the Santa Cruz River at Tucson, high stakes are involved in choosing design and regulatory floods on an increasingly urbanized flood plain. For example, a catastrophic flood in October 1983 caused \$100 million in damage to flood plain structures in Tucson (Saarinen et al., 1984). Past estimates of the 100-year flood for this river, using different methods and assuming different statistical properties of the series, range from 572 to 2,780 m³s⁻¹ in 1983 (Saarinen et al., 1984; Roeske et al., 1989), which at the time exceeded estimates of the 100-year flood. In addition, six of the eight largest floods in the annual series (1915-1986), including the 1983 flood, occurred after 1960 (see Figure 1).

The increasing magnitude of annual flood peaks on the Santa Cruz River, particularly since 1960, has been attributed to channel changes just upstream of Tucson (Reich, 1984). However, the most dramatic channel changes occurred just before the protracted low-flow period in the middle third of this century (Betancourt and Turner, 1988). Also, larger floods have affected the headwaters, which have experienced little geomorphic change. One alternative explanation is that decadal climates after 1960 favor a higher intensity and frequency of storms that cause floods. This may be reflected by shifts in the seasonality of annual floods (Figure 1). Against a background of predominantly summer floods, winter and fall floods account for 53 percent of annual peaks before 1930, only 3 percent from 1930 to 1959, and 39 percent after 1960. These apparent shifts in flood seasonality occurred elsewhere in southern and central Arizona, most noticeably Rillito Creek and the San Francisco, Gila, and San Pedro rivers. On these streams, summer flows are common, but the largest floods occur mostly in winter and fall. Heaviest regional flooding, such as in October 1983, happens when low pressure troughs or cutoff-low pressure systems steer moisture from Pacific tropical cyclones into Arizona.

Here we discuss how climatic variability affects flood frequency on the Santa Cruz River. We illustrate these effects by computing separate flood-frequency estimates for different storm types (monsoonal, frontal, and tropical cyclone), for El Niño-Southern Oscillation (ENSO) vs. non-ENSO conditions, and for discrete time periods (1930-1959, 1960-1986).

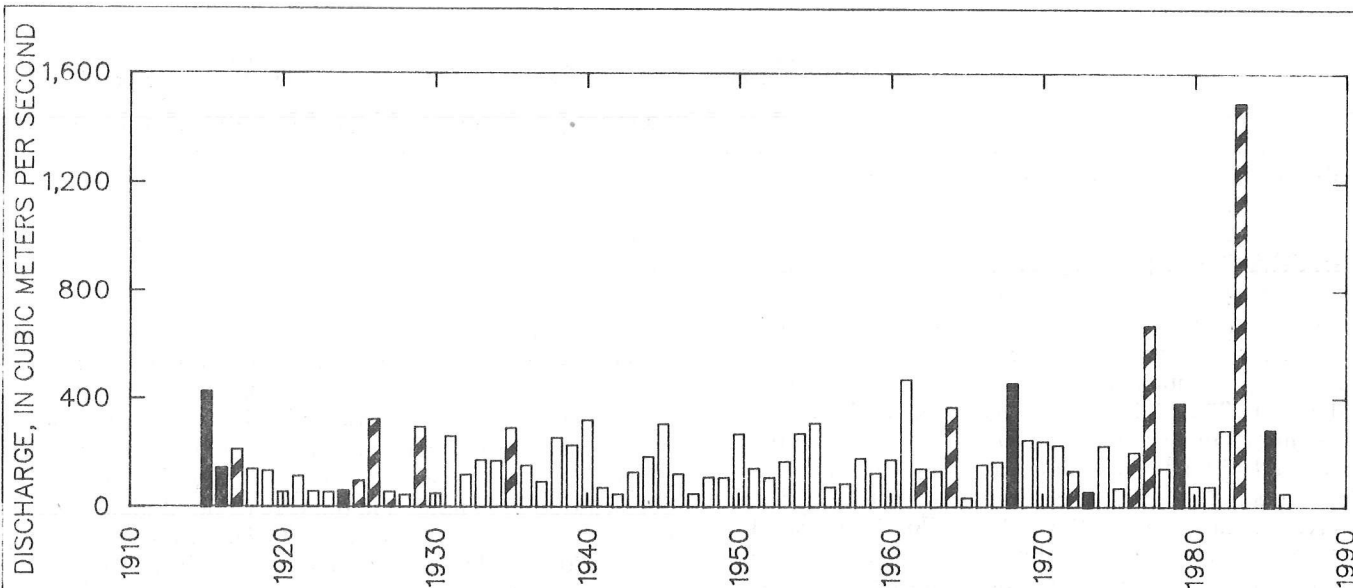


Figure 1. Annual flood series for the Santa Cruz River at Tucson, Arizona. Hydroclimatological year of November 1 to October 31; solid black bars indicate November to March floods; candy-striped bars indicate September and October floods; open bars indicate July and August floods.

METHODS

To compute flood-frequency estimates we employed several statistical techniques, including method of moments, maximum likelihood, and mixed-population analysis. Annual flood frequency during ENSO and non-ENSO conditions was determined using the method of moments (U.S. Water Resources Council, 1982).

Because the normally defined water year of October 1 to September 30 artificially separates the fall runoff season, we defined the hydroclimatic water year to be November 1 to October 31. We combined nine hydroclimatic classifications developed by Hirschboeck (1985) into monsoonal storms, frontal systems, and tropical cyclones. Floods above base discharge ($48 \text{ m}^3\text{s}^{-1}$) in the partial duration series were separated into the largest annual floods by storm type. The three resultant flood groups, which are treated as independent, are fit to the log-Pearson type III probability distribution using maximum-likelihood analysis with one censoring level (Stedinger and Cohn, 1986; Stedinger and others, 1988). A single distribution of annual floods was determined using mixed-population analysis (Kite, 1977).

Separate analyses of ENSO vs. non-ENSO conditions and the periods 1930-1959 and 1960-1986 are based on consideration of the hydroclimatology of southern Arizona. The tropical Pacific Ocean and southern Arizona are teleconnected seasonally; ENSO conditions enhance fall, winter, and spring precipitation in Arizona (Douglas and Englehart, 1984; Andrade and Sellers, 1988). With ENSO conditions, tropical cyclones in the eastern Pacific have an increased tendency to recurve from their normal west-northwest course to the northeast. Low pressure troughs or cutoff lows associated with recurvature of tropical cyclones may also act to steer the moisture into southern Arizona. Such conditions are ideal for producing major floods in the region, especially in

autumn (e.g., Claudia in September 1962, Norma in September 1970, Heather in October 1977, Octave in October 1983 — these and other tropical storms are described by Smith, 1983).

Partitioning of the flood series into 30-year periods assumes that the apparent shifts in flood seasonality around 1930 and 1960 track decadal climatic regimes. One such regime might consist of a more mixed distribution of flood-producing storm types during wet decades, especially when ENSO events are frequent. These regimes may have a global, as well as regional, expression. Below is a summary of large-scale shifts in oceanic conditions and atmospheric circulation that support separate treatment of pre-1930, 1930-1960, and post-1960 flood data.

In the Atlantic Ocean, before about 1925 and after the early 1960s, there was marked warming in the Southern Hemisphere and simultaneous cooling in the Northern Hemisphere (Folland et al., 1986). In the North Atlantic, oceanic cooling began in the 1950s (Cayan, 1986). The North Pacific Ocean also experienced cooling after the 1960s. This cooling coincided with negative 700-millibar (mb) anomalies in the central North Pacific and increases in the midtropospheric subtropical westerlies (Douglas et al., 1982; Balling and Lawson, 1982).

Precipitation records in certain parts of the world track these changes in atmospheric circulation and oceanic regimes. For example, summer rainfall in India (Mooley and Parthasarathy, 1984), western Africa (Ojo, 1987), and the Sahel (Folland et al., 1986) was scarce before 1930 and after 1960, but plentiful in the intervening period. Rainfall surges in the Line Islands of the central equatorial Pacific, which are considered a proxy for ENSO, were rare between 1930 and 1960, but frequent before and after. A quasi-biennial signal in Line Island rainfall only achieved significant amplitudes before 1930 and after 1960 (Reiter, 1983).

ENSO events have been least frequent in the middle one-third of this century. For this period, Elliott and Angell (1988) show reduced variances for sea surface pressures at Darwin, Tahiti, and Santiago, sea surface temperatures in the eastern equatorial Pacific, and Indian summer-monsoon rainfall. They also found reduced correlations between these variables and continental and marine hemispheric temperatures. Elliott and Angel's (1988) data end in 1973 and exclude the unusual period of 1975-1987, when La Niña conditions were virtually absent (Bradley et al., 1987) and several large fall and winter floods affected southern Arizona streams.

We subscribe to the notion put forth by Namias and others (1988) that low-frequency (decadal) climatic variability in western North America is driven by long-term increases in the subtropical westerlies and in the frequency of ENSO conditions. We suggest that, on the Santa Cruz River and other large streams in southern Arizona, this is reflected by increased magnitudes of annual floods in winter and fall before 1930 and after 1960.

RESULTS

Statistics describing the annual flood series for the periods 1915-1929, 1930-1959, and 1960-1986 and for ENSO and non-ENSO conditions appear in Table 1.

Period	N	\bar{Q}	S_Q	\bar{X}	S	G
All	71	199	198	2.17	0.319	0.222
1915-1929	15	147	117	2.05	0.321	0.441
1930-1959	30	166	85	2.16	0.248	-0.379
1960-1986	26	267	292	2.27	0.371	0.271
ENSO Years	27	226	288	2.18	0.368	0.616
Non-ENSO Years	44	181	111	2.17	0.288	-0.215

N = Number of years
 \bar{Q} = Mean discharge $m^3 s^{-1}$
 S_Q = Standard deviation $m^3 s^{-1}$
 \bar{X} = Logarithm of mean discharge
 S = Standard deviation of log discharge
 G = Skew coefficient

Mean discharges for the three periods, though they vary, are not significantly different. Variances for 1915-1929 and 1930-1959 are significantly less than the variance for 1960-1986. [Here and elsewhere in this report, significant differences between variances are reported at the 95 percent confidence level using the Squared Ranks Test (Conover, 1971).] The skew coefficient for the period 1930-1959 is -0.379, compared to 0.441 from 1915-1929 and 0.271 from 1960-1986. These results

suggest that the annual flood series at Tucson exhibits weak stationarity of order 1 (Box and Jenkins, 1971, p. 30); in other words, the mean may be time invariant, whereas the variance and possibly the skew coefficient change with time. The absence of significant trends within periods suggests that annual floods during the separate periods of 1930-1959 and 1960-1986 may represent homogeneous populations. The period 1915-1929 is not considered here because the partial duration series is available only since 1930, and flood-frequency analysis for only 15 annual events cannot provide meaningful results.

The annual flood series of the Santa Cruz River is affected by ENSO occurrences. Four of the five largest and six of the ten smallest annual floods at Tucson occurred during ENSO conditions. For ENSO conditions, the mean discharge and standard deviation for 27 annual floods are $226 \pm 288 m^3 s^{-1}$; for non-ENSO conditions, discharges decrease to $181 \pm 111 m^3 s^{-1}$ (Table 1). Only the variances are significantly different. The estimated 100-year flood for ENSO years is more than double that for non-ENSO years (Table 2 and Figure 2).

Table 2. Estimates of the 100-year flood for the Santa Cruz River calculated using different methods and based on different assumptions.

Years Considered	Methods	Assump-tions	100-Year Flood at Tucson ($m^3 s^{-1}$)
All	MM	A,B	872
ENSO	MM	A,B	1,300
Non-ENSO	MM	A	628
All	ML,MP	A,D	1,050
1930-1959	ML,MP	C,D	323
1960-1986	ML,MP	B,C,D	1,660

Methods:
 MM = Procedures specified in U.S. Water Resources Council (1982) and a generalized skew coefficient of -0.2.
 ML = Maximum likelihood analysis of type I censored data (Stedinger and others, 1988).
 MP = Mixed population analysis of floods caused by monsoonal storms, frontal systems, and dissipating tropical cyclones.

Assumptions:
 A Data are strictly stationary in time.
 B Discharge for 1983 flood is not considered as an historical peak.
 C Data are weakly stationary, but are considered stationary for the indicated period. Future flood potential is similar with conditions in the period.
 D Floods caused by different storm types are assumed to be independent.

To obtain stationary series for flood-frequency analysis, we assumed that populations of floods caused by frontal systems, dissipating tropical cyclones, and monsoonal storms are derived from different populations for the periods 1930-1959 and 1960-1986. Flood-frequency relations for floods caused by the three storm types differ drastically for the two periods (Figures 3 and 4). For the period 1930-1959, annual flood frequency is dominated by monsoonal floods, and the estimated 100-year flood at Tucson is $323 \text{ m}^3\text{s}^{-1}$. After 1960, annual flood frequency above the 10-year interval is dominated by floods caused by dissipating tropical cyclones, and the estimated 100-year flood is $1,660 \text{ m}^3\text{s}^{-1}$ (Table 2).

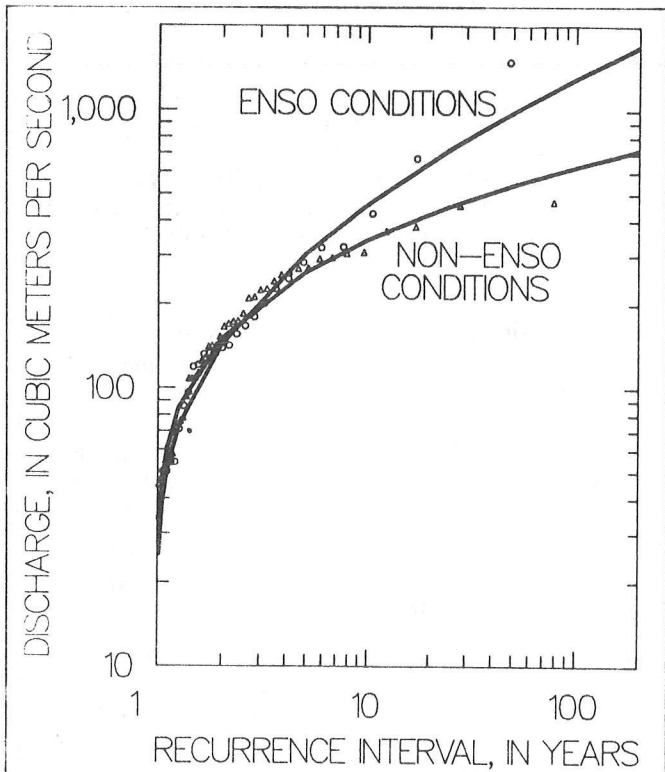


Figure 2. Flood frequency on the Santa Cruz River at Tucson, Arizona during ENSO and non-ENSO years. The skew coefficient is weighted using a generalized skew coefficient of -0.2 and a mean-squared error of 0.303 for the generalized skew coefficient.

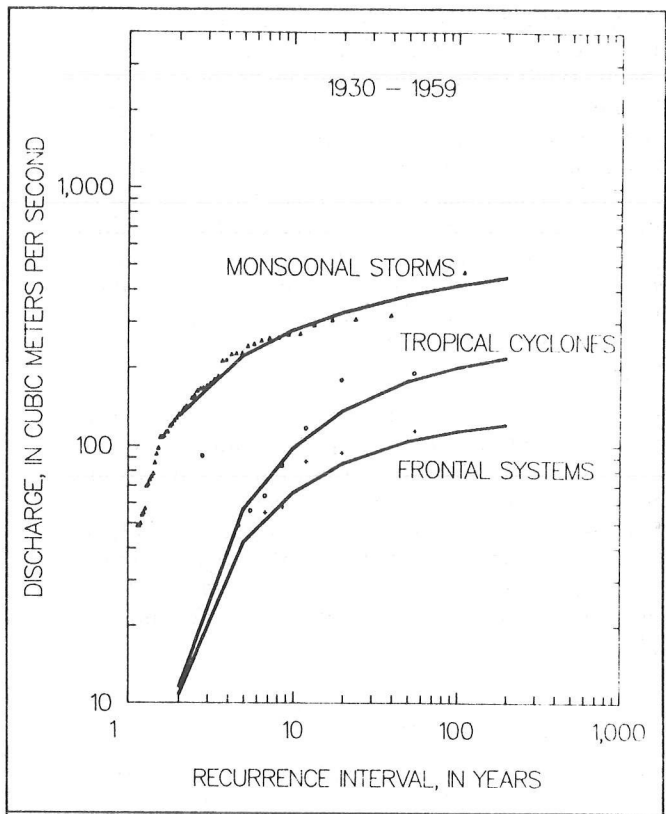


Figure 3. Comparison of fitted probability distributions for floods between 1930 and 1959 on the Santa Cruz River at Tucson caused by three storm types.

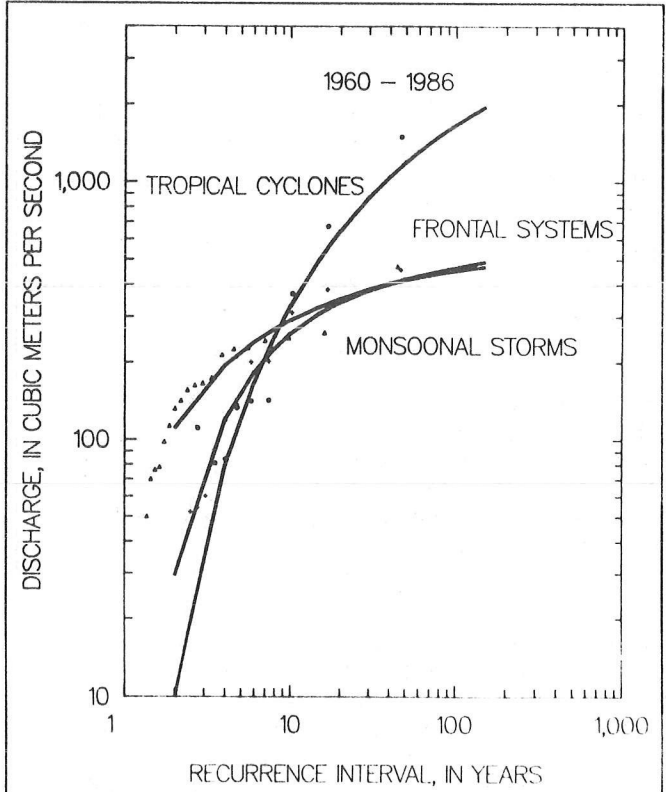


Figure 4. Comparison of fitted probability distributions for floods between 1960 and 1986 on the Santa Cruz River at Tucson caused by three storm types.

CONCLUSIONS

Hydroclimatic flood-frequency analyses underscore a likely cause for increased frequency of flooding on the Santa Cruz River. The probability for floods caused by dissipating tropical cyclones, by frontal systems, and, to a lesser extent, by monsoonal storms changed during the twentieth century.

One pitfall with mixed-population analysis is the inability to assign uncertainties to discharges at given recurrence intervals. Presently, there is no method available for estimating standard errors of estimate or confidence limits for mixed populations. Second, the assumption that floods are stationary for ENSO or non-ENSO conditions or during each of the periods may be incorrect. For example, transitions in decadal climates may be gradual instead of abrupt; subjective partitioning of the flood series may contribute further to uncertainties in flood-frequency analysis. Nevertheless, divergent flood frequencies for ENSO vs. non-ENSO, different storm types, and for the three periods in the twentieth century

show that climatic effects are time variant. Consequently, some of the assumptions needed for standard flood-frequency analysis may not be valid.

Judicious use of hydroclimatic flood-frequency analyses, such as those summarized here, requires prediction of future decadal climates, which may or may not be possible in years to come. Flood-frequency estimates for the Santa Cruz River should be used cautiously in design applications, and alternative nonstatistical methods of assessing flood hazards, such as rainfall/runoff models (Ponce et al., 1985), ought to be considered.

Effects of decadal climatic variability on flood frequency probably are not unique to the Santa Cruz River. Hydroclimatic flood-frequency analyses are recommended for other streams where mixed populations of floods affect flood magnitude and frequency. We envision application of these methods elsewhere in the subtropics where the annual frequency and intensity of flood-producing storms like hurricanes are highly variable.

REFERENCES

- Andrade, E.R., and Sellers, W.D., 1988, El Niño and its effect on precipitation in Arizona: *Journal of Climatology*, v.8, p.211-219.
- Balling, R.C., and Lawson, M.P., 1982, Twentieth century changes in winter climatic regions: *Climatic Change*, v.4, p.57-69.
- Betancourt, J.L., and Turner, R.M., 1988, Historic arroyo-cutting and subsequent channel changes at the Congress Street crossing, Santa Cruz River, Tucson, Arizona, in Whitehead, E.E., Hutchinson, C.F., Timmermann, B.N., and Varady, R.G., eds., *Arid Lands Today and Tomorrow*: Boulder, Colorado, Westview Press, p.1353-1371.
- Box, G.E.P., and Jenkins, G.M., 1971, *Time series analysis*: San Francisco, Holden-Day, 553p.
- Bradley, R.S., Diaz, H.F., Kiladis, G.N., and Eischeid, J.K., 1987, ENSO signal in continental temperature and precipitation records: *Nature*, v.327, p.497-501.
- Cayan, D.R., 1986, North Atlantic seasonal sea surface temperature anomalies and associated statistics: La Jolla, California, Scripps Institution of Oceanography, SIO Reference No. 85-19, 89p.
- Conover, W.J., 1971, *Practical nonparametric statistics*: New York, John Wiley, 493p.
- Douglas, A.V., Cayan, D.R., and Namias, Jerome, 1982, Large-scale changes in North Pacific and North American weather patterns in recent decades: *Monthly Weather Review*, v.110, p.1851-1862.
- Douglas, A.V., and Englehart, P.J., 1984, Factors leading to the heavy precipitation regimes of 1982-1983 in the United States: Washington, D.C., U.S. Department of Commerce, National Oceanic and Atmospheric Administration, *Proceedings of the Eighth Annual Climate Diagnostics Workshop*, p.42-54.
- Elliott, W.P., and Angell, J.K., 1988, Evidence for changes in Southern Oscillation relationships during the last 100 years: *Journal of Climate*, v.1, p.729-737.
- Folland, C.K., Palmer, T.N., and Parker, D.E., 1986, Sahel rainfall and worldwide sea temperatures, 1901-1985: *Nature*, v.320, p.602-606.
- Hirschboeck, K.K., 1985, *Hydroclimatology of flow events in the Gila River basin, central and southern Arizona*: Tucson, University of Arizona, Ph.D. dissertation, 335p.
- Kite, G.W., 1977, *Frequency and risk analyses in hydrology*: Littleton, Colorado, Water Resources Publications, 224p.
- Mooley, D.A., and Parthasarathy, B., 1984, Fluctuations in all India summer rainfall during 1871-1978: *Climatic Change*, v.6, p.287-301.
- Namias, Jerome, Yuan, Xiaojun, and Cayan, D.R., 1988, Persistence of North Pacific sea-surface temperature and atmospheric flow patterns: *Journal of Climate*, v.1, p.682-703.

- Ojo, Oyediran, 1987, Rainfall trends in west Africa, 1901-1985, in Solomon, S.I., Beran, M., and Hoff, W., editors, The influence of climatic change and climatic variability on the hydrologic regime and water resources: International Association of Hydrological Sciences Publication No. 168, p.37-43.
- Ponce, V.M., Osmolski, Zbig, and Smutzer, David, 1985, Large basin deterministic hydrology, a case study: Journal of Hydraulic Engineering, American Society of Civil Engineers, v.111, p.1227-1245.
- Reich, B.F., 1984, Recent changes in a flood series: Journal of the Arizona-Nevada Academy of Science, v.14, p.231-238.
- Reiter, E.R., 1983, Surges of tropical Pacific rainfall and teleconnections with extratropical circulation patterns, in Street-Perrott, F.A., Beran, M. and Ratcliff, R., editors, Variations in the Global Water Budget: Drodrecht, The Netherlands, D. Reidel Publishing Company, p.285-299.
- Roeske, R.H., Garrett, J.M., and Eychaner, J.H., 1989, Floods of October 1983 in southeastern Arizona: U.S. Geological Survey Water Resources Investigations 85-4225-C, 77p.
- Saarinen, T.F., Baker, V.R., Durrenberger, Robert, Maddock, Thomas, Jr., 1984, The Tucson, Arizona flood of October 1983: Washington, D.C., National Academy Press, 112p.
- Smith, Walter, 1986, The effects of eastern north Pacific tropical cyclones on the southwestern United States: Salt Lake City, Utah, U.S. Department of Commerce, National Oceanic Atmospheric Association, Technical Memorandum NWS WS-197, 229p.
- Stedinger, J.R. and Cohn, T.A., 1986, Flood frequency analysis with historical and paleoflood information: Water Resources Research, v.22, p.785-793.
- Stedinger, J.R., Surani, Rafiq, and Therivel, Riki, 1988, Max users guide, a program for flood frequency analysis using systematic-record, historical, botanical, physical paleohydrological and regional hydrologic information using maximum-likelihood techniques: Ithaca, New York, Cornell University, Department of Environmental Engineering, 51p.
- U.S. Water Resources Council, 1982, Guidelines for determining flood flow frequency: Washington, D.C., U.S. Water Resources Council, Hydrology Subcommittee, Bulletin 17B, 28p.

Time Series Analyses of Biological and Environmental Variables for Suisun Bay and the Sacramento and San Joaquin Rivers

Peggy Lehman

ABSTRACT: Arima analysis was used to compute cross-correlations between principal component axes that described environmental variables, chlorophyll concentration and zooplankton density for the Sacramento and San Joaquin rivers and Suisun Bay. For all three regions, chlorophyll anomalies were significantly cross-correlated with a principal component axis that was inversely related to streamflow at lag 1 and water transparency at lag 0. Zooplankton anomalies were significantly cross-correlated with a principal component axis that was inversely related to water transparency at lag 1 for the Sacramento and San Joaquin rivers. Cross-correlations among the time series may provide information about links between environmental and biological variables within the estuary and the possible influence of climate.

INTRODUCTION

For data collected within Suisun Bay and the Sacramento and San Joaquin rivers between 1968 and 1988, phytoplankton, zooplankton and fish populations have declined and experienced shifts in species composition. Since 1977, chlorophyll concentrations have decreased among regions and dominance has shifted from *Skeletonema*, *Cyclotella*, and *Thalassiosira* to *Melosira granulata*. Zooplankton density also decreased after 1977 and coincided with increased abundance of newly introduced species from China. Changes in both of these communities are important because they affect the striped bass food chain. Striped bass are a major sport fish in the Bay/Delta and, like other organisms in their food chain, they declined sharply after 1977.

The cause(s) of the decline in estuarine populations at all levels of the food chain are unknown. The cause(s) may be natural or produced by mankind, and they may or may not be related. The purpose of this study is to use time series analyses to determine if there are correlations among the environmental and biological variables measured over time and to use this information to gain insight into possible causes of the observed changes in estuarine populations.

DATA

Physical, chemical and biological data were collected from seven sites located in Suisun Bay and the Sacramento and San Joaquin rivers by the California Department of Water Resources, California Department of Fish and Game, and U.S. Bureau of Reclamation between 1971 and 1987 on a semi-monthly or monthly basis (Figure 1). The data include measurements of chlorophyll concentration, zooplankton abundance, Sacramento and San Joaquin River flow, Delta export flow, secchi disc depth, suspended solids, turbidity, pH, specific conductance, nitrate, phosphate and silicate concentration, air and water temperature, and wind velocity.

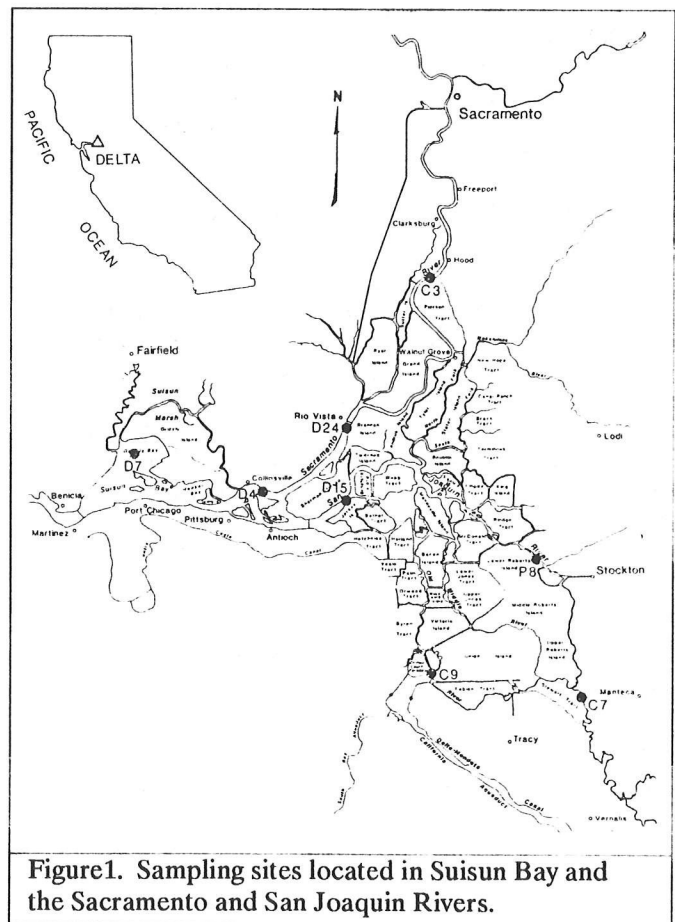


Figure 1. Sampling sites located in Suisun Bay and the Sacramento and San Joaquin Rivers.

DATA ANALYSIS

Principal component (PCA) and autoregressive integrated moving average (ARIMA) analyses were computed using the Statistical Analysis System (SAS) programming packages. Before analysis, average monthly data for each site were standardized by conversion to anomalies. Anomalies were calculated as the monthly mean minus the average monthly mean over time divided by the standard deviation of the monthly mean over time. Anomalies were then averaged for each region. Using anomalies, PCA axes were computed for the suite of 14 environmental variables measured for each region. PCA axes were cross-correlated with chlorophyll and zooplankton anomaly data using ARIMA analysis. Since data analyses conducted for each site were the same for each region, only the region data are presented. Representative anomaly values are shown in Figure 2 for the Sacramento River.

RESULTS

The first two PCA axes extracted from the set of environmental data were similar for all three regions. The first axis (axis 1) described streamflow and was negatively associated with Sacramento and San Joaquin River flow and positively associated with nutrient concentration and specific conductance. The second axis (axis 2) described water transparency and was positively associated with turbidity and suspended solids and negatively associated with secchi disc depth. Together the first two axes described between 51% and 53% of the variation within the environmental data sets for each region.

Chlorophyll anomalies were significantly cross-correlated with both axis 1 and axis 2. Chlorophyll anomalies had a significant positive cross-correlation with axis 1 and lag 1 for all three regions (Table 1). The cross-correlations implied that higher chlorophyll concentrations were associated with slower streamflow and higher specific conductance during the previous month. Chlorophyll anomalies were also significantly cross-correlated with axis 2 and lag 0 for all regions and suggested that chlorophyll concentration and water turbidity covaried.

Table 1. Cross-correlations between chlorophyll (*Chloro*) and zooplankton (*Zoo*) anomalies for Suisun Bay and the Sacramento and San Joaquin Rivers.

Region	Variable	Axis	Lag	r	Signif.	n
Suisun Bay (D07)	Chloro	1	1	.155	.05	202
		2	0	.422	.01	202
	Zoo	-.	-.	-.	-.	-.
Sacramento River (D04, D24, C03)	Chloro	1	1	.213	.01	202
		2	0	.165	.05	202
	Zoo	1	2	.218	.01	144
San Joaquin River (D15, P08, C07)	Chloro	1	1	.161	.05	202
		2	0	.202	.01	202
	Zoo	2	1	.187	.05	144

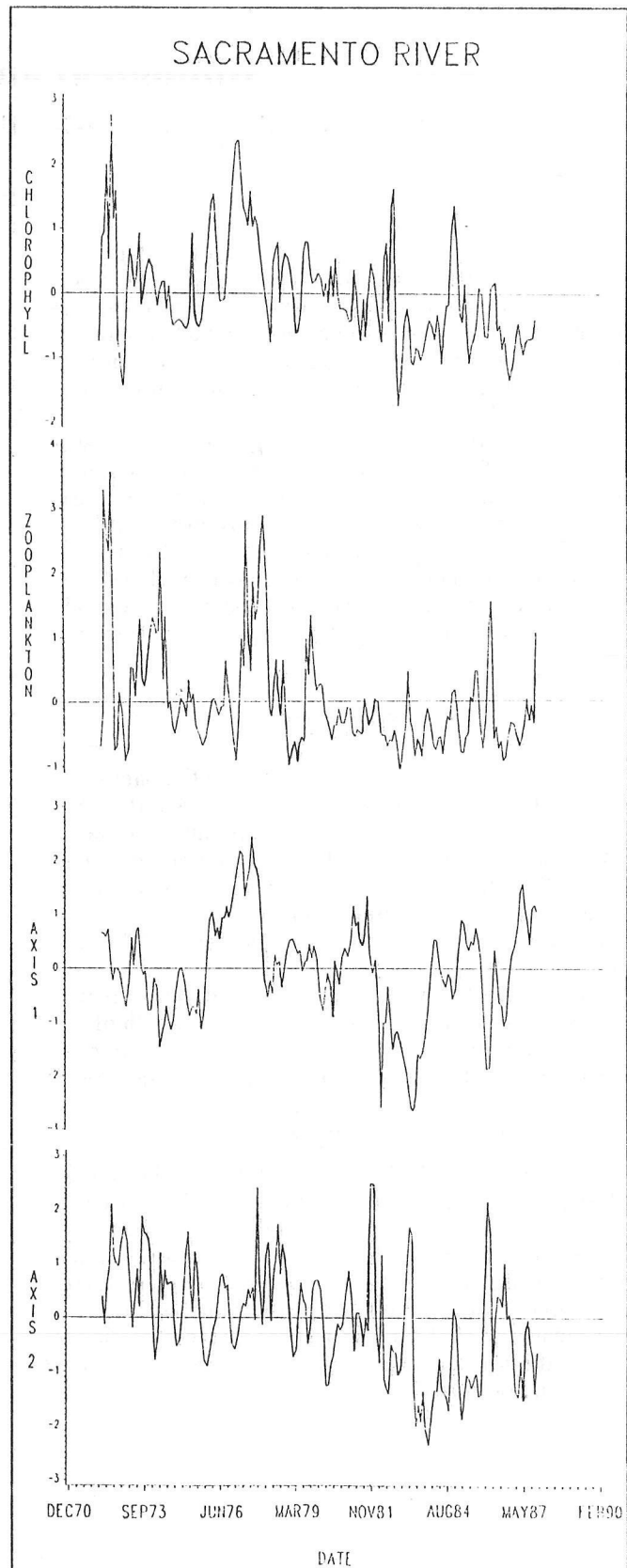


Figure 2. Monthly anomaly values calculated for chlorophyll concentration, zooplankton density, and two principal component axes that describe environmental variables in the Sacramento River.

Zooplankton anomalies were significantly cross-correlated with axis 2 at lag 1 for the Sacramento and San Joaquin rivers. The positive cross-correlation suggested that zooplankton abundance was associated with the amount of particulate matter in the water column during the previous month. In addition, a significant positive cross-correlation was calculated between zooplankton anomalies and axis 1 and lag 2 for the Sacramento River.

The cross-correlations between the PCA axes and chlorophyll or zooplankton anomalies were significant and low. Most of the cross-correlations were marginally significant and accounted for, at most, 16% of the variance. The low cross-correlations were produced by high autocorrelation within the data.

DISCUSSION

The significance and consistent behavior of the associations among the PCA axes and biological time series among regions using time domain analyses are encouraging because they describe a logical pattern among the variables. Higher zooplankton populations would occur when the suspended materials within the water column, including phytoplankton and organic and inorganic matter, are high during the previous month. Accumulation

of chlorophyll biomass would depend on sufficiently low streamflows during the previous month. By extrapolation, zooplankton would be somewhat dependent on the streamflow two months before. This conclusion was supported for the Sacramento River by the significant correlation between zooplankton anomalies and axis 1 at lag 2.

The significant and consistent cross-correlations between chlorophyll anomalies and axis 1, which describes streamflow, are also encouraging because they suggest a link between climate and plankton. Associations between plankton and climatic variables have been suggested by other long-term data sets. Zooplankton abundance or biomass was associated with changes in westerly weather for the North Sea (Colebrook, 1986) and water temperature and large-scale flows along the California coast (Chelton et al., 1982). Phytoplankton production was associated with large-scale flows along the California coast (Tont, 1976) and the Gulf of California (Baumgartner et al., 1985).

For the Suisun Bay and the Sacramento and San Joaquin rivers, the low cross-correlations among the PCA axes and the biological variables may limit their predictive value. Additional analyses will examine the correlation patterns as a function of frequency and development of a transfer function model.

REFERENCES

- Baumgartner, T., Ferreira-Bartina, V., Shrader, H., and Soutar, A., 1985, A 20-year varve record of silicious phytoplankton variability in the central gulf of California. *Marine Geology*, v.64, p.113-129.
- Colebrook, J.M., 1986, Environmental influences on long-term variability in marine plankton: *Hydrology and Biology*, v.142, p.309-325.
- Chelton, D.B., Bernal, P.A. and McGowan, J.A., 1982, Large-scale interannual physical and biological interaction in the California Current: *Journal of Marine Research*, v.40, p.1095-1125.
- Tont, S., 1976, Short-period climatic fluctuations: effects on diatom biomass. *Science*, v.194, p.942-944.

Interpreting Long-Term Fish Landings Records: Environment and/or Exploitation?

Paul N. Sund and Jerrold G. Norton

ABSTRACT: The California Department of Fish and Game data base of California commercial fish landings for the period 1928 to 1985 has been assembled in computer accessible form at the Pacific Fisheries Environmental Group in Monterey, California. Time series for fishes whose landings are known to vary during periods of ocean warming were compared to time series of sea surface temperature. Expected patterns of variation were confirmed in the seasonal cycle, but were less clear on the interannual scale. When interannual variation was considered, the most serious hindrance to interpretation of the landings series appeared to be the continued reduction of the fish stocks due to commercial exploitation; other factors are discussed. Landings data contain information potentially useful in climatological studies, but problems should be anticipated in their use.

INTRODUCTION

Fish landings data are one of few types of marine biological data that exist for periods of time sufficient for climatological investigations. This report announces the digitization and archiving of 58 years of commercial fish landings data from California Department of Fish and Game (CDF&G) records. It discusses a preliminary investigation into the value of this data set as a source of information on temporal variation in the marine ecological system, and it gives examples of problems encountered in extracting useful information from them.

The approach used here to test the utility of the data set has been to state a well known hypothesis relating landings variability to ocean warming; to test this hypothesis using a subset of the data; and then to examine the results of the test from two points of view. First, how well is the hypothesis demonstrated? Second, identify factors other than the one hypothesized that influence variability in landings.

Previous studies have shown that increased commercial and sport landings of albacore, bonito, barracuda, bluefin tuna, skipjack tuna, swordfish, and white seabass along the California coast vary simultaneously with warming of the coastal waters (Walford, 1931; Hubbs, 1948; Radovich, 1960, 1961, 1975; MacCall et al, 1974; Squire, 1987.) This well established relationship is the known hypothesis to be tested below using the newly archived data. Our results may not be expected to be new, but they will amplify past work and will provide a framework for discussion of some of the problems encountered in the use of landings data.

DATA

The newly archived data series for the 1928 to 1985 period was obtained from the CDF&G. For the years 1928 to 1977, these data are in publications of the CDF&G *Fish Bulletin* series. The data since 1978 have not been published, but corresponding records for 1978 to 1985 were obtained from the Monterey, CA, office of CDF&G. These all have been archived digitally at the Pacific Fisheries Environmental Group for the six California statistical regions shown in Figure 1. This report uses data from the Santa Barbara, Los Angeles, and San Diego statistical regions. The species of fish selected for consideration are commonly known to have their presence and/or levels of abundance related to warming (*op cit*) of the coastal ocean environment.

The Scripps pier temperature data set is one of few environmental time series of length comparable to the fish landings time series. It is used as an index of conditions in the Southern California region (Mooers et al., 1986; Smith and Eppley, 1982; Fiedler, 1984).

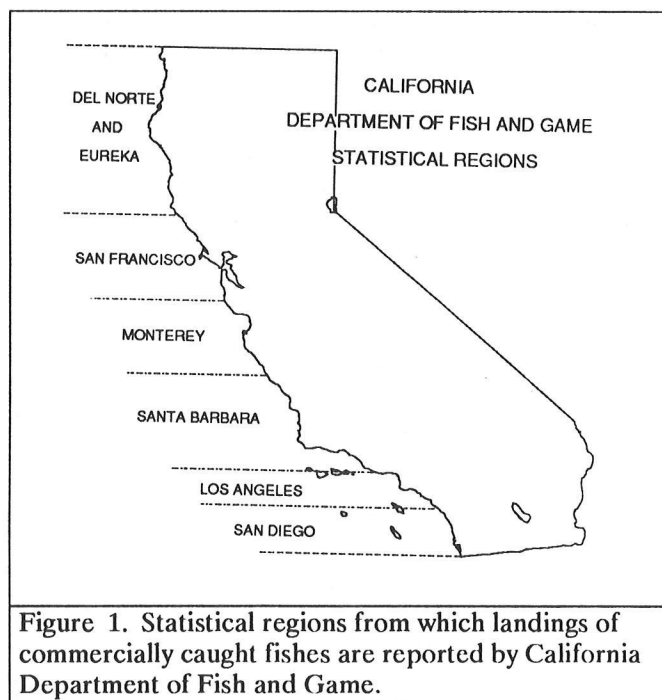


Figure 1. Statistical regions from which landings of commercially caught fishes are reported by California Department of Fish and Game.

PROBLEMS AND EXAMPLES

A representative time series plot of monthly landings (Figure 2) shows that the seasonal cycle is conspicuous, as are interannual variations and multi-year trends in the level of landings.

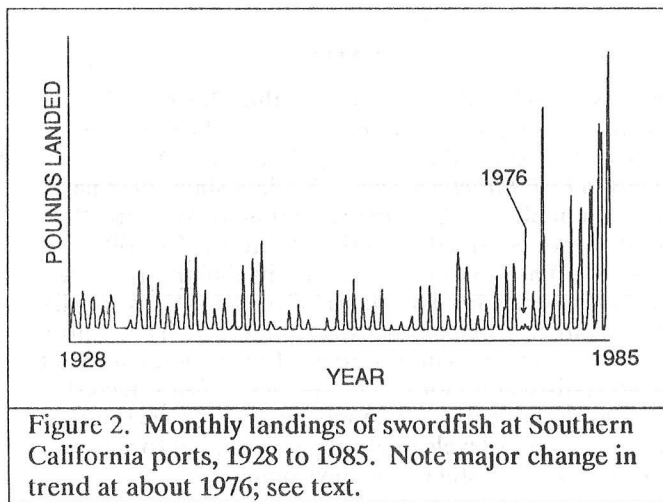


Figure 2. Monthly landings of swordfish at Southern California ports, 1928 to 1985. Note major change in trend at about 1976; see text.

Plots of long-term average monthly landings (annual seasonal cycle) of selected warm-water species (Figure 3) illustrate that albacore, bluefin, skipjack, white seabass, bonito, and swordfish landings peak in August and September (skipjack landings have an additional minor peak in April). Barracuda landings peak in June and July. The principal peaks of landings of all the species except barracuda occur when the Scripps pier SST is at

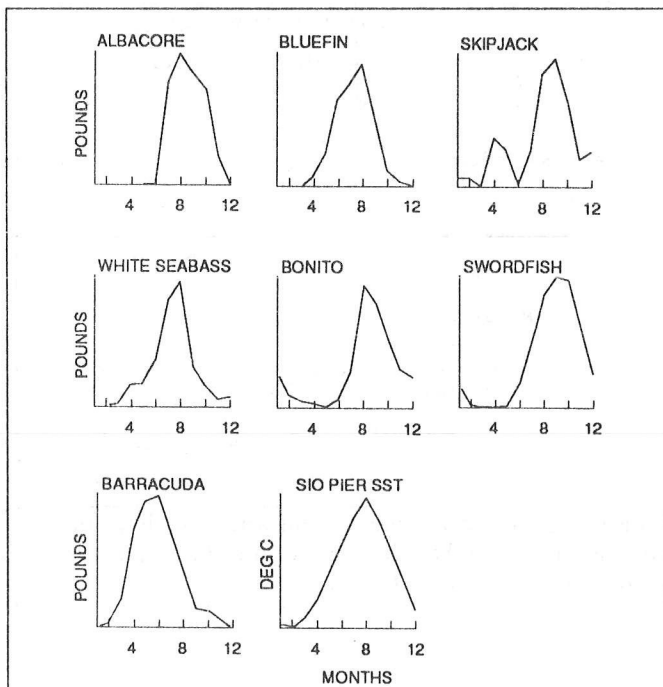


Figure 3. Long-term average monthly landings of warm-water fishes in the Southern California bight. Plots show types of seasonal patterns in landings. Vertical axes are not labeled because each panel is scaled to give the maximum value full scale.

a maximum (last panel, Figure 3). The composited (normalized and summed) long-term monthly mean landings and SST correlate at $r=0.96$, and all except barracuda are individually correlated at significance levels over 99% (r over 0.69). In terms of seasonality then, the hypothesis that the test species are associated with periods of warm water is well validated by the commercial landings data set. The correlation of $r=0.96$ shows a close seasonal phase relationship between the warm-water species and the ocean temperature indicator.

We next made an exploratory test of the interannual relationship between summed annual landings and SST. The annual total landings for the test species were normalized to standard deviation units and summed for each year; the data were combined for all species then were compared to Scripps pier SST. This simple approach of summing the annual landings for each species for each year and correlating this with SST gives a seemingly correct association, $r=0.61$, between fish landings and warm ocean conditions on the interannual scale (MacCall et al., 1974; Radofich, 1961, 1975). However, the SST time series pattern is dominated by four warm-water periods at 1931, 1941, 1957-60, 1982-84 (see smoothed SST curve, Figure 4), seemingly related to the timing of major warm (El Niño Southern Oscillation, or ENSO) events. And the landings data show trends and shifts in levels that are due to natural and anthropogenic causes. Factors such as these partly obscure the environmental influence on landings and contribute to reducing the effective degrees of freedom ($n = 58$) by introducing autocorrelation.

When the species are tested individually against SST, it is noted that only skipjack has an r -value comparable to the composite series ($r=0.51$; Figure 4). Further examination of the individual series shows conspicuous overall trends in all the fish landings time series plots except albacore and skipjack.

The plot of annual albacore landings for the three southern regions may be misleading, because albacore landings distributions change between Southern California waters and the region from Northern California to British Columbia. Albacore apparently enter those northern regions from the west. Thus the plot presented may not reflect the coastwide landings of albacore. The other species appear to enter the Southern California region from the south or southwest.

White seabass landings show a general decline. An exceptional increase in landings occurred during the 1957-59 ENSO event, in which they reached an all time peak of 3.4 million pounds. Increases of lesser magnitudes also occurred at the times of warm events in 1931, 1941 and 1972-73.

Barracuda landings show an even more abrupt decline. Increases in landings, apparently associated with the 1957-59 ENSO event, as well as the prior major event in 1940-41, are evident.

The bluefin tuna landings time series shows noticeable maxima during the 1941 and 1957-59 warm water events.

COMMENTS AND DISCUSSION

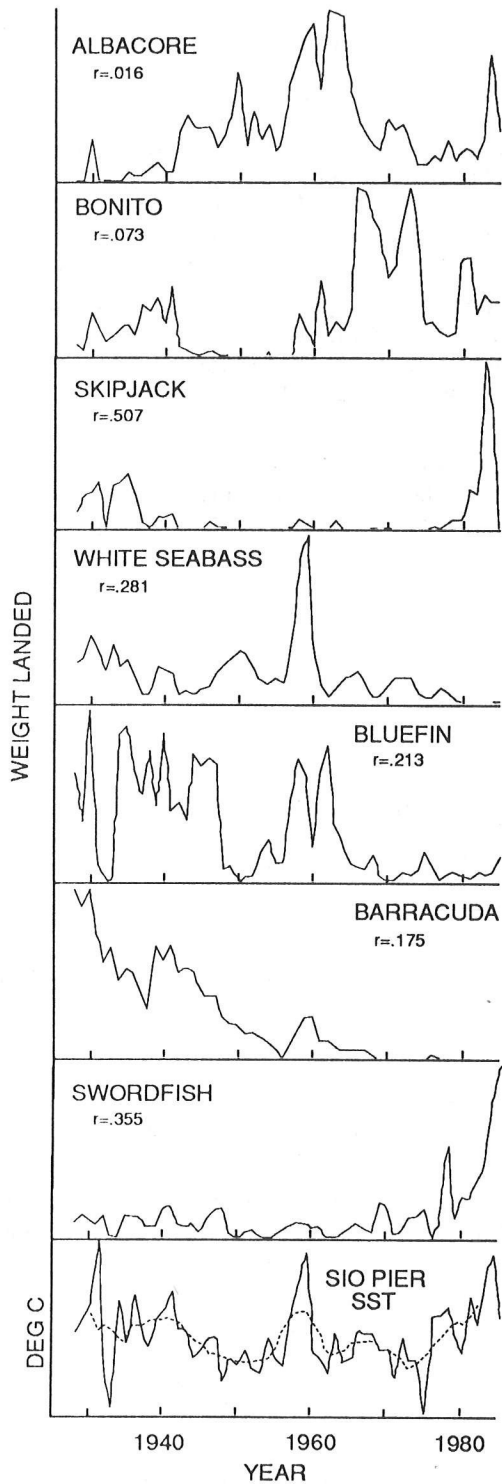


Figure 4. Time series plots of annual landings of warmwater fishes and Scripps pier surface temperature, 1928-1985. Correlation coefficients (r) for each species and SST are given in each panel. Vertical axes are not labeled because each panel is scaled to give the maximum weight landed full scale. Dashed line in SST panel is 5-year running mean.

Commercial fish landings statistics are one of only few kinds of data on biological variation in the ocean available over periods of time of sufficient length to permit their use in bioclimatological investigations. To make good use of these data, however, requires considerably more information. Data concerning any resource highly impacted by man's economic or other activities are likely to have variability in amplitudes and frequencies that are greater than those induced by non-anthropogenic factors. This appears to be demonstrated by the commercial fish landing data.

Bluefin tuna and barracuda have generally declined in abundance over the 58-year period studied. Commercial fishing probably has been an important factor contributing to this decline. Reduction in stock size may have occurred during periods of increased availability to the commercial fisheries.

Episodic increases in landings followed by declines may mean that the total populations were more accessible to fishing during warming events, but not necessarily more abundant at those times. Landings for barracuda and white seabass declined rapidly after reaching peaks occurring simultaneously with warmings (Figure 4). This may explain why the association between the landings of the fishes studied herein and warm water is not as evident during the warm events that occurred since 1959; there may not have been sufficient stocks size for an expression of the environmental relationship to be evident.

There has been an increase in swordfish landings (Figures 2 and 4) that began simultaneously with the onset of an ocean climate shift in 1976 (Norton et al., 1985; PACLIM Abstracts, 1986, 1987, 1988). Because the swordfish market demand usually exceeds supply, all fish landed can be sold. In the mid-1970s it was discovered that swordfish could be caught more easily with gillnets than by the traditional harpoon method (Bedford and Hagerman, 1983). The catch by harpooning has remained about constant (*ibid*), but introduction of the new gillnet gear made it possible to extend the fishery into waters that had been unsuitable for harpooning. This expanded the area subject to fishing and also extended the time fish were available to exploitation. The result has been a major increase in landings that occurred simultaneously with a major environmental shift. The connection between ocean climate (SST) and catch is, at this point, unclear because the new fishing methods were introduced coincidentally with the onset of the environmental change.

Various methods for combining data from different sources are being developed. Independent scientific surveys of adults may be used to determine species abundance. This approach has been used for sablefish, rockfish, and some species of wet fish. Other surveys might monitor changes in numbers of eggs, larvae and juveniles. From these surveys, fisheries independent estimates of stock abundance may be possible.

Combination of sport and commercial catch records may help to interpret trends. These two data sets are controlled by somewhat different variables. Sportfishing is not for profit, whereas commercial fishing is profit driven; but a certain level of success is necessary in either case.

In a recent report to the Pacific Fisheries Management Council, Methot and Hightower (1988) combined information from scientific surveys and tagging experiments to arrive at estimates of current and previous sablefish stock sizes.

We have explored the climatological variations in the relationship of SST and commercial fish landings. The expected linkage seems confirmed; but we demonstrated that users of landings data should be aware of the presence and possible effects of other factors on landings variability. These include:

- Autocorrelation introduced by extreme environmental events,
- Depletion of the species,
- Fishing gear changes,
- Merchandising demand factors,
- Availability of market replacement species, etc.

SUMMARY

- Commercial fish landing data compiled by the CDF&G have been refined into a uniform, computerized data base at the PFEG.
- These data have been tested with a commonly accepted hypothesis relating ocean warming and landings variability. The data strongly support the hypothesis on the inter-monthly or seasonal scale, but the relationship is less decisive on the interannual scale. That linkage is partially obscured by the interplay of numerous factors.
- Declines in fish landings over time, as a possible result of high exploitation during warm water periods and high abundance, is thought to be a major factor which confuses simple interpretation of these commercial landings data.
- Other data sources and data processing techniques will be used to obtain additional information on the marine ecosystem from the commercial fish landings data set.

REFERENCES

- Bakun, A., and Parrish, R., 1980, Environmental inputs to fishery population models for eastern boundary current regions, *in* Sharp, G., Ed., Workshop on the effects of environmental variation on the survival of larval pelagic fishes: Paris, Intergovernmental Oceanographic Commission, UNESCO, IOC Workshop Report, v.28, p.67-104.
- Bedford, D.W., and Hagerman, F.B., 1983, The billfish fishery of the California Current: CalCOFI Report, v.XXIV, p.7078.
- Cayan, D.R., McLain, D.R., and Nichols, W.D., *In prep.*, The PACLIM Monthly Time Series Atlas: U.S. Geological Survey Open File Report.
- Fiedler, Paul C., 1984, Effects of El Niño on the northern anchovy: California Cooperative Fishery Investigation Report (CalCOFI), v.25, p.53-58.
- Hubbs, C.L., 1948, Changes in the fish fauna of western North America correlated with changes in ocean temperature: *Journal of Marine Resources*, v.7, p.459-482.
- Jordan R.S., 1983, Variabilidad de los recursos pelagicos en el Pacifico sudeste, *in* Proceedings of the expert consultation to examine changes in abundance and species composition of neuritic fish resources: FAO Fisheries Report No. 291, v.2, p.113-129.
- MacCall, A.D., Stauffer, G.D., and Troadec, J.P., 1974, Stock assessments of Southern California recreational and commercial marine fisheries: U.S. Department of Commerce, NOAA, NMFS, Southwest Fisheries Center, Admin. Report LJ-74-24, 144p.
- Mendelsohn, R., and Cury, P., 1987, Fluctuations of a fortnightly abundance index of the Ivoirian coastal pelagic species and associated environmental conditions: *Canadian Journal of Fish. Aquatic Sciences*, v.44, p.408-421.
- Methot, Richard, and Hightower, Joseph, 1988, Status of the Washington - Oregon - California sablefish stock in 1988 (submitted to the Pacific Fisheries Management Council, Portland, Oregon, October 1988), Northwest and Alaska Fishery Center, National Marine Fisheries Service, 7600 Sand Point Way, NE, Seattle, WA 98115, and Southwest Fisheries Center, Tiburon Laboratory, 3150 Paradise Drive, Tiburon, CA 94920.
- Mooers, Christopher N.K., Peterson, D.H., and Cayan, Daniel R., 1986, The Pacific Climate Workshops: EOS - Transactions, American Geophysical Union, v.67, no.52, p.1404-1405.
- Murphy, G.I., 1966, Population biology of the Pacific sardine (*Sardinops caerulea*): *Proceedings California Academy of Sciences*, v.34, no.1, p.1-84.

- Norton, J., McLain, D., Brainard, R., and Husby, D., 1985, The 1982-83 El Niño event off Baja and Alta California and its climate context, *in* Wooster, W., and Fluharty, D., Eds., *El Niño North*: Seattle, Washington Sea Grant Program, University of Washington, p.44-72.
- Norton, J., 1987, Ocean climate influences on groundfish recruitment in the California current, *in* *Proceedings of the International Rockfish Symposium*, October 20-22, 1986: Fairbanks, Alaska Sea Grant College Program, University of Alaska.
- Parrish, R., Nelson, C., and Bakun, A., 1981, Transport mechanisms and reproductive success of fishes in the California current: *Biology of Oceanography*, v.1, no.2, p.175-203.
- Radovich, J., 1975, Water temperature and fish distribution: An epilogue to the warm water years, *in* *Rec. Proceedings of 13th Pacific Science Congress*, Aug. 18-30, 1975: Vancouver, University of BC, v.1, p.264-265.
- _____, 1961, Relationship of some marine organisms of the northeast Pacific to water temperatures: California Department of Fish and Game, *Fish Bulletin* 112, 62p.
- _____, 1960, Redistribution of fishes in the eastern north Pacific Ocean in 1957 and 1958, *in* *California Coop. Oceanic Fish. Investigation Report* 7, p.163-171.
- Smith, Paul E., and Eppley, R.W., 1982, Primary production and the anchovy population in the Southern California Bight: Comparison of time series: *Limnology of Oceanography*, p.27, 1-17.
- Squire, J.L., 1987, Relation of sea surface temperature changes during the 1983 El Niño to the geographical distribution of some important recreational pelagic species and their catch temperature parameters: *Marine Fisheries Review*, v.49, no.2, p.44-57.
- Walford, L.A., 1931, Northward occurrence of southern fish off San Pedro in 1931: *California Fish Game* 17, p.401-405.
- Wooster, W.S., and Fluharty, D.L., Editors, 1985, *El Niño North*, Niño effects in the eastern subarctic Pacific Ocean: Seattle, Washington Sea Grant Program, University of Washington.

Solar-Cycle Modulations of ENSO: A Possible Source of Climatic Change

Roger Y. Anderson

ABSTRACT: An association between long-term changes in the solar cycle and the frequency of El Niño events has been identified in historical records of El Niño and sunspot number. Although no known mechanism can explain the apparent relationship, the association is strong. A possible coupling between the sun and the ocean's mixed layer, involving ENSO, is worthy of further study.

INTRODUCTION

Varved (annually layered) marine sediments off Northern California contain evidence that El Niño circulation regimes have alternated with an anti-El Niño (La Niña) regimes since the late Pleistocene (Anderson et al., 1989 and in press). The sediment record shows that ENSO regimes persist for decades to millennia (Anderson et al., in press). Quinn, Neal, and Antunez de Mayolo (QNA) (1987) observed that the frequency of El Niño events changed systematically over time, and Enfield (1988) noted that the QNA record of El Niño contained a centennial cycle.

A search for an explanation of long-term ENSO cycles in the geologic record prompted a comparison of the record of sunspot number with the historical record of El Niño events compiled by QNA. The comparison revealed what appears to be an extraordinary association between sunspot number and the frequency of occurrence of El Niños. This contribution to the PACLIM Workshop describes the association and briefly considers known mechanisms that might explain the observed association.

SOLAR/EL NIÑO ASSOCIATION

QNA used ships logs of pirates, privateers, and explorers, as well as other information, to assemble a remarkable record of the occurrence and intensity of El Niño events since 1525. Their qualitative data were numerically transformed and compared with the Southern Oscillation Index (SOI) since 1880 and with the record of sunspot number since 1700. Frequency of occurrence of El Niño events (QNA event-date) was transformed by calculating a symmetrical, linearly weighted moving average (e.g., $[a + 2b \dots 2d + e]$) for various moving time intervals (e.g., 5, 11, and 19 years). The same rank was assigned to all events and expressed as number of events per year. More frequent events appear as values above the mean in proportion to the number of events in

the assigned moving interval, and length of the interval is not critical (Figure 1).

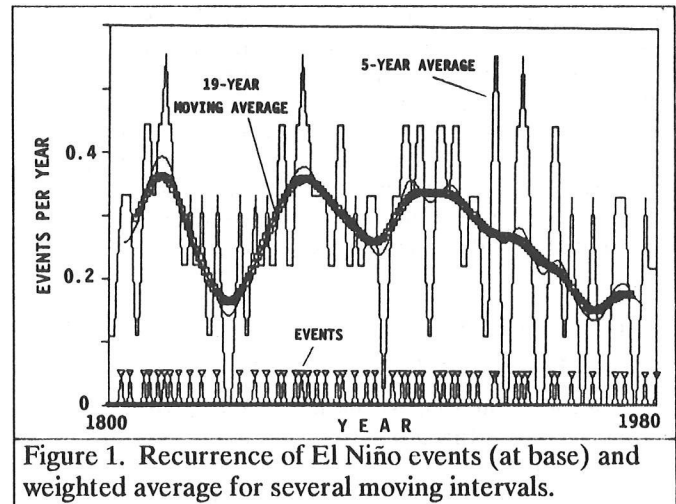


Figure 1. Recurrence of El Niño events (at base) and weighted average for several moving intervals.

The pattern of recurrence was compared to QNA estimates of the strength of El Niño events by assigning a value of 6 to their very strong events, 5 to strong events, etc. and determining the relationship between frequency of occurrence and strength of event. For the historical period after 1880 when data became available, the strength of El Niño events was further estimated by scaling the negative departure from zero of monthly maxima of the SOI in the NOAA Climate Analysis Center Index (Ropelewski and Jones, 1987; e.g., the 1982-83 departure was assigned a value of -2.9).

Comparison of QNA ranking with the SOI revealed inconsistency in ranking the strength of events. Prior to 1800, stronger El Niño events appear to be associated with less frequent El Niños (Quinn et al., 1987). Thereafter, the opposite is the case. Therefore, only the QNA frequency term is used to examine the behavior of El Niño. Comparison of El Niño frequency and sunspot number was done in sets of data organized, younger to older, into four time-series of increasing length but decreasing reliability. The four series include:

- Data for El Niño recurrence and sunspot number from 1880 to 1986 ($n = 36$), this series also includes the SOI.
- Data for El Niño recurrence and sunspot number from 1800 to 1986 based on the full set of QNA observation ($n = 50$).

- Data for El Niño recurrence and sunspot number from 1700 to 1986 based on only strong and very strong events ($n = 28$).
- El Niño recurrence since 1525, also based on only strong and very strong events ($n = 47$).

Because of the scarcity of data and the subjective nature of the QNA compilation, minimal processing of the transformed data seemed advisable. Associations were identified and further clarified with simple measures of correlation and cross-correlation. In three sets of data for the interval after 1700, when systematic observation of sunspots began, Pearson correlation was used as an estimator of relative association between sunspot number and El Niño recurrence. The solar/El Niño association is observable through only three long solar cycles, and correlation coefficients are used only as a relative measure of association in records of different quality; they are not intended to imply that an association is real.

El Niño Association with ~90-Year Solar Cycles

Examination of the longest but least reliable time-series (Figure 2) reveals three ~90-year cycles in El Niño recurrence after 1650. Power spectral density in this same record since 1650 confirms a ~90-year cycle. The maxima of the two older cycles correspond, approximately, to the Maunder and Dalton minima in sunspot number. The maximum of the most recent ~90-year cycle in El Niño frequency corresponds to a lesser minimum in sunspot number that centers around the year 1900.

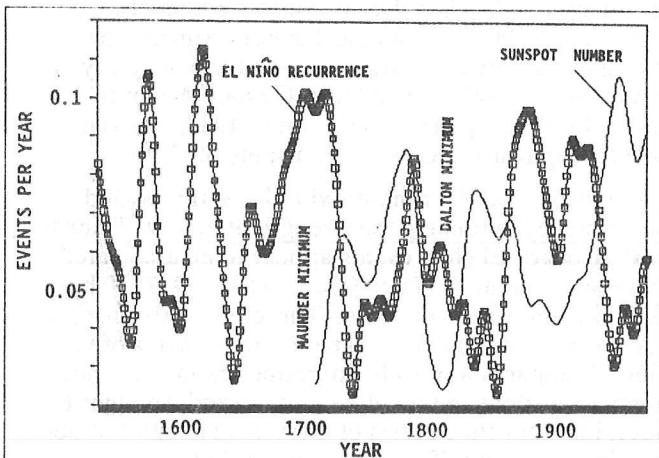


Figure 2. Recurrence of strong and very strong El Niño events since 1525 and sunspot number since 1700. Smoothed time-series. Note that more El Niño events occur during the Maunder Minimum.

The record for strong and very strong events shifts out of phase in the Dalton Minimum. However, a sequence containing more events (Figure 3) confirms a negative association with the Dalton Minimum, and the phase shift in Figure 2 is an artifact of less reliable data. The strongest association and greatest recurrence of El Niño events after 1650 occurs during the Maunder Minimum,

an interval of very low sunspot activity (Eddy, 1976; Stuiver and Quay, 1980).

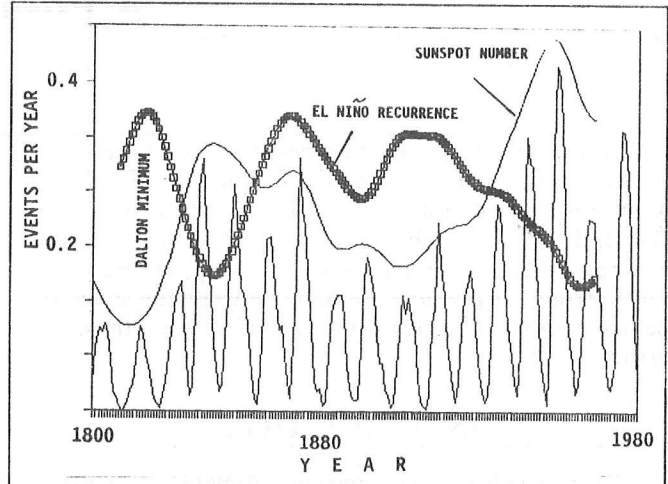


Figure 3. Association between El Niño frequency and sunspot number for all ranks of El Niño events since 1800. Note that the Dalton Minimum has a negative association not apparent in Figure 2 and that fewer El Niño events occur at times of high sunspot number.

The correlation coefficient for El Niño events and sunspot number of an iterated 19-year moving average of the combined record of all El Niño events since 1700 is $r = -0.45$. The coefficient for the time-series since 1800 ($r = -0.59$) is increased to $r = -0.65$ when the El Niño record lags by 4 years. The coefficient for sunspot number and El Niño recurrence since 1880 (see Figure 3) is $r = -0.85$. Coefficients are lower for 11-year and 5-year moving averages.

A more complete picture of the relationship between sunspot number and El Niño recurrence can be seen in the time-series for all QNA El Niño events after 1800 (Figure 3). The negative association in the Dalton Minimum repeats the stronger effect observed during the Maunder Minimum. A strong 11-year solar cycle after 1930 is accompanied by fewer El Niño events, and the weak 11-year solar cycle between 1880 and 1930 is a time of more frequent El Niños with an equivocal relationship in the transition after the Dalton Minimum. Correlation coefficients, which increase as information improves in newer records, support the visual observation (Figures 2 and 3) that occurrence of El Niños is approximately doubled at times of low sunspot number in ~90-year solar cycles.

El Niño Association with the 11-year Solar Cycle?

The QNA record since 1800 contains a sufficient number of El Niño events for a 5-year moving average to define the temporal position of groupings of several events (Figures 1 and 4). A detrended 5-year moving average of events after about 1890 shows a cross-correlation with the sunspot record (Figure 4, second half). In contrast, the record before 1890 does not correlate (Figure 4, first half).

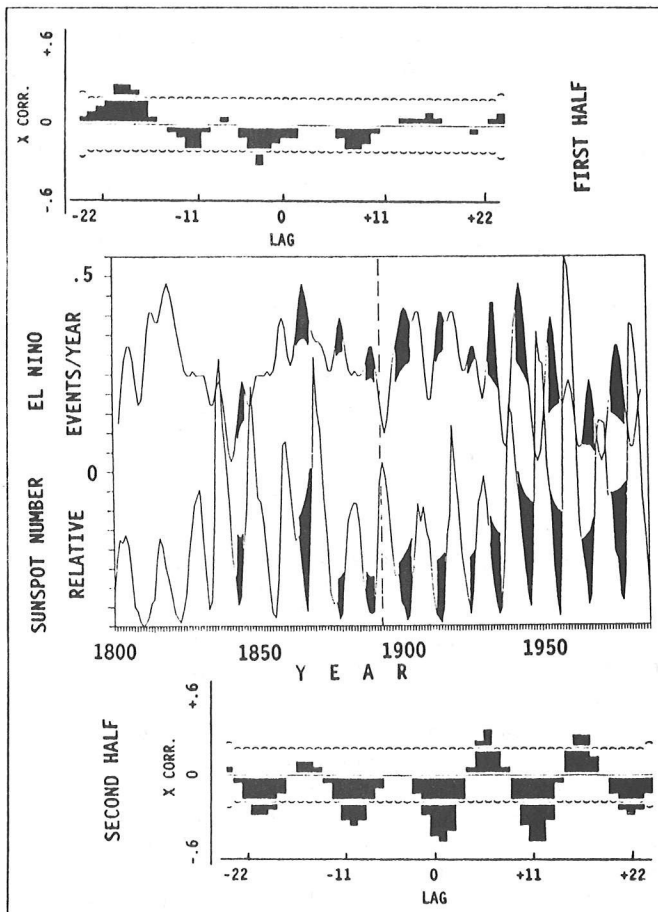


Figure 4. Recurrence of El Niño events and annual sunspot number since 1800 and cross-correlations for first and last half of the record. High coefficients at an 11-year lag in the last half of the record show that El Niño recurrence is aligned with low sunspot number when the 11-year sunspot cycle is strongest.

A stronger correlation in the second half of the record can be attributed to greater alignment between minima of sunspots and maxima in El Niño recurrence. As a test of this supposition, the same number of El Niño events as occur in the second half of the time-series were artificially spaced ~ 11 years apart so that three events occurred within the lowest part of each 11-year sunspot minimum. The coefficient for this contrived association ($r = -0.68$), compared to the coefficient actually observed ($r = -0.51$) confirms that alignment of maxima and minima (negative association between El Niño recurrence and sunspot number) is responsible for the correlation and for the regular 11-year spacing of the lag cycles (Figure 4, second half). The lag of 11 years is largely the result of a strong solar cycle. Nevertheless, the second half of the record, when both the 11-year solar cycle and El Niño recurrence have their greatest amplitude, has a higher correlation coefficient, and more El Niño maxima are visually aligned with sunspot minima (Figure 4).

Changes in the strength of El Niños, as measured by the SOI, appear to have a weak association with sustained changes in sunspot number. For example, before ~ 1930 , sunspot number was low when El Niño events

were generally stronger (Figure 5). The reverse situation holds after ~ 1930 . A correlation of this weak negative association between SOI values and corresponding annual sunspot number for individual events since 1880 is $r = -0.27$ ($n = 53$; $p = 0.05$; extreme outliers from the mean were removed from the detrended series). Reduced amplitude of SOI corresponds to low amplitude variations of sea surface temperature in the quasi-biennial band, which for the same historical period, occur at times of high solar activity (Barnett, 1989).

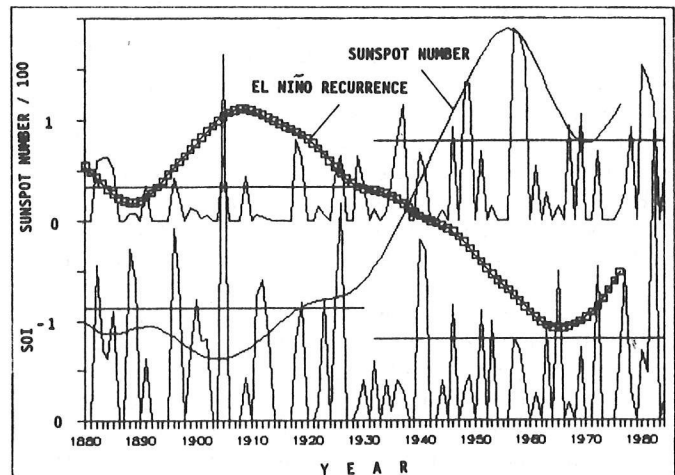


Figure 5. Changes in amplitude of the southern oscillation index (SOI) and corresponding annual sunspot number for all El Niño events after 1880. Shift to lower mean SOI values (straight lines) after 1930 shows that weaker El Niño events occur when the 11-year sunspot cycle is strongest.

Relationship Between El Niño Strength and Frequency

After 1880, the strength of El Niño events, as measured by the SOI, is reduced when El Niño events are less frequent. The association can be observed visually by comparing the first and second half of the post-1880 SOI and sunspot records (Figure 5). For example, before ~ 1930 , SOI values are high when El Niños are generally more frequent. The opposite relationship holds after ~ 1930 , suggesting a positive association between higher frequency and strength.

In contrast to the relationship defined by the SOI (more frequent El Niños = stronger El Niños), QNA estimates for the interval before 1880 indicate that El Niño events are weaker when more frequent than the mean frequency. These comparisons show that the relationship between the frequency of recurrence and strength of El Niño events is either unclear or is changeable over time.

In summary, the frequency of occurrence of El Niño events approximately doubles when sunspot number is low. When the 11-year solar cycle is strongest, the spacing between El Niño events increases. The amplitude of El Niño events appears to weaken with a stronger 11-year solar cycle, but the association between frequency and amplitude is equivocal and may change over time.

MODULATION OF ENSO BY THE SOLAR CYCLE?

The solar/El Niño association described above suggests that unrecognized mechanisms may link ENSO to the solar cycle. However, a specific physical mechanism is required to show that the association is more than a curiosity and to explain why a more active, irradiant sun might be associated with effects that lengthen the period of ENSO and that possibly reduce its amplitude (more sunspots accompany increased irradiance; Kerr, 1987, 1988; Lean, 1989).

ENSO, with an average period of 3 to 4 years for El Niño events, is believed by some observers to be a natural, self-regulating, linear oscillator, with nonlinear effects (Graham and White, 1988). The well understood behavior of linear oscillators indicates that modulation of ENSO by an 11-year solar cycle would lengthen ENSO's period and reduce its amplitude. This heuristic explanation agrees with the observed relationship that El Niño events are less frequent at times of strong 11-year solar cycles. Assuming modulation of a linear oscillator, the historical record suggests that the higher frequency of ENSO would prevail and approach the frequency of the quasi-biennial oscillation when the 11-year solar cycle is weak, as during the Maunder Minimum. The period would lengthen to about 4 years when a strong 11-year solar cycle modulates ENSO. The historical El Niño record is not clear as to whether weaker or stronger El Niños go with more frequent events. However, the SOI record suggests that frequent El Niños are stronger.

Several possible mechanisms for converting solar variability to changes in climate are known (see review in Landscheidt, 1987). A survey of physical processes, however, has failed to identify a mechanism that might explain the solar/El Niño association. Direct transfer of solar energy via heating of the ocean's mixed layer is apparently ruled out by weak changes in solar irradiance that accompany the 11-year solar cycle (about 0.08%; Lean, 1989) and longer solar cycles (about 0.14%; Kerr, 1987).

Without a specific mechanism, the solar/El Niño association described above joins many other earth-based phenomena that have an interesting but unproven relationship to the solar cycle. Is there a chance, however, that the association could be real?

A poor understanding of ENSO and the origin of the oscillation leave open the possibility that the solar/El Niño association may ultimately be explained by as yet unknown mechanisms operating in the larger ocean/atmosphere system. For example, the 11-year solar cycle has been linked through the QBO to upper tropospheric winds and storm tracks and to changes in regional temperature (van Loon and Labitzke, 1988; EOS, 1988). Also, temperature anomalies in the upper troposphere and lower stratosphere contain both a solar and an El Niño signal (Sellers, this volume).

Barnett (1989) apparently has extended the 11-year solar/QBO/atmosphere association identified by van

Loon and Labitzke to include an association between the solar cycle and sea surface temperature (SST). The solar/QBO/SST association, in a record that extends to 1884, is strongest after ~1930 when the sun is most active and in the central and eastern equatorial Pacific where El Niño is best developed. In addition, low amplitude variations in the quasi-biennial band coincide with high solar activity, a relationship that matches the solar/El Niño association after 1880 (Figure 5) and the expected response of a linear oscillator.

ENSO and the QBO are closely related, if not part of the same phenomenon, and with the addition of Barnett's (1989) analysis to that of van Loon and Labitzke, a solar/El Niño association in QNA data appears to be a reasonable extension of that relationship, as well as a further indication that solar-related changes occur in the ocean's mixed layer.

MIXED-LAYER RESPONSE TO ENSO COUPLING

Transforming the historical record of El Niño events (QNA) into a numerical estimate of El Niño frequency has revealed an interesting association with changes in the ocean's mixed layer and with Pacific climate. For example, a record of $\delta^{18}\text{O}$ in the planktonic Foraminifera *Globigerina bulloides* reconstructed from the Santa Barbara Basin by Dunbar (1983) shows that isotopic changes in near-surface waters are coincident with the changes in El Niño frequency in cycles of 50 or more years (Figure 6). Changes in $\delta^{18}\text{O}$ after 1750 consistently and closely parallel the frequency of occurrence of El Niño events. Dunbar (1983) suggested that $\delta^{18}\text{O}$ in *G. bulloides* is an estimator of near-surface temperature, in which case more frequent El Niños occur when the surface layer in the Santa Barbara Basin is cooler.

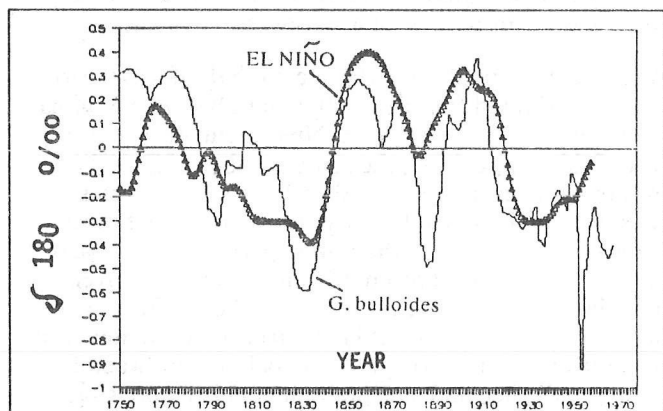


Figure 6. Recurrence of strong and very strong QNA El Niño events and $\delta^{18}\text{O}$ in *G. bulloides* after 1750 in Santa Barbara Basin. El Niño record is shifted slightly to adjust for errors in varve chronology.

The validity of *G. bulloides* as an indicator of temperature and the regional extent of a cooler mixed layer must be documented with additional study. However, even without demonstrating the specific nature of the association, the remarkably close agreement between the oxygen isotope and El Niño records in the Santa Barbara

Basin (Figure 6) suggests that a long-term response by the mixed layer is tied to the frequency of El Niño events. If so, the moving-average transformation used to characterize El Niño frequency in historical data is a useful device for examining responses to long-term changes in El Niño. Also, this example suggests that the QNA methodology is reasonably valid and improves prospects that the solar/El Niño association observed in the long historical record is real.

CONCLUSIONS

The historical record contains an unmistakable association between the solar cycle and the frequency of occurrence of El Niño events, but the record is not long

enough to confirm that the association is real. However, evidence is accumulating that the ocean carries the solar signal and that ENSO, along with the QBO, may be part of the mechanism. Potential involvement of the mixed layer suggests that marine paleoclimate records may be an important source of information about the long-term response of El Niño to solar variability and associated changes in climate.

ACKNOWLEDGMENTS

Supported by National Science Foundation grant ATM8707462. B. Allen, Y. Enzel, S.P. Heustis, L.H. Koopmans, and B.K. Linsley, University of New Mexico, provided critical comments.

REFERENCES

- Anderson, R.Y., Gardner, J.V., and Hemphill-Haley, E., 1989, Variability of the late Pleistocene-early Holocene oxygen minimum zone off northern California, *in* Peterson, D.H., Editor, Aspects of climate variability in the Pacific Ocean and western Americas: American Geophysical Union Monograph v.55, p.75-84.
- Anderson, R.Y., Linsley, B.K., and Gardner, J.V., in press, Expression of seasonal and ENSO forcing in climate variability at lower frequencies: Evidence from Pleistocene marine varves off California, *in* Benson, L.V., and Myers, P.A. (eds.), Paleoclimates: The record from lakes, ocean, and land: Palaeo., Palaeo., Palaeo.
- Barnett, T.P., 1989, A solar-ocean relation: Fact or fiction?: Unpublished manuscript, 5p.
- Dunbar, R.B., 1983, Stable isotope record of upwelling and climate from Santa Barbara Basin, California: *in* Thiede, J., and Seuss, E. (eds.), Coastal Upwelling, Part B: New York, Plenum Press, p.217-245.
- Eddy, J.A., 1976, The Maunder Minimum, *Science* v.192, p.1189-1202.
- Enfield, D.B., 1988, Is El Niño becoming more common?: *Oceanography*, v.1, p.23-27.
- EOS, 1988, Storms and the solar cycle: v.69(20), p.594.
- Graham, N.E., and White, W.B., 1988, The El Niño cycle: A natural oscillator of the Pacific Ocean-atmosphere system: *Science* v.240, p.1293-1302.
- Kerr, R.A., 1988, Relax, the sun is brightening again: *Science* v.240, p.1734.
- _____, 1987, How the sun faded even as its sunspots did: *Science* v.236, p.1624-1625.
- Landscheidt, T., 1987, Long range forecasts of solar cycles and climate change: *in* Rampino et al. (eds.), Climate: History, Periodicity, and Predictability: New York, Van Nostrand Reinhold, p.421-445.
- Lean, J., 1989, Contribution of ultraviolet irradiance variations to changes in the sun's total irradiance: *Science* v.244, p.197-200.
- Quinn, W.H., Neal, V.T., and Antunoz de Mayolo, S.E., 1987, El Niño occurrences over the past four and a half centuries: *Journal of Geophysical Research* v.92(C3), p.14449-14461.
- Ropelewski, C.F., and Jones, P.D., 1987, An extension of the Tahiti-Darwin southern oscillation index: *Monthly Weather Review*, v.115, p.2161-2165.
- Stuiver, M., and Quay, P.D., 1980, Changes in atmospheric carbon-14 attributed to a variable sun: *Science* v.207, p.11-19.
- van Loon, H., and Labitzke, K., 1988, Association of the 11-year solar cycle, the QBO, and the atmosphere. Part II: surface and 700 mb on the northern hemisphere in winter: *Journal of Climate* v.1, p.905.

Rapid $\delta^{18}\text{O}$ and $\delta^{13}\text{C}$ Isotopic Shifts in Late Pleistocene Marine Varves on the California Margin

Braddock K. Linsley, Roger Y. Anderson, and James V. Gardner

ABSTRACT: Upper Pleistocene sediments on the continental slope off Northern California contain alternations of varves and bioturbation produced by fluctuations in intensity of the coastal upwelling system. Stable isotopic analyses of benthic Foraminifera across a particularly well developed varve/bioturbation sequence deposited $\sim 26,000$ years ago reveal rapid shifts of $\sim 0.25\text{‰}$ in $\delta^{18}\text{O}$ and $\sim 0.4\text{‰}$ in $\delta^{13}\text{C}$. The $\delta^{18}\text{O}$ shift occurs within a varved section. Based on varve counts, the isotopic change occurred in less than 100 years. Timing and magnitude of the shift coincide with similar shifts observed in almost all other high-resolution $\delta^{18}\text{O}$ records that have been interpreted as primarily representing global in-volume fluctuations.

INTRODUCTION

High-resolution sedimentary records in oceanographically sensitive areas offer the potential to examine oceanographic variability at a higher frequency than with open-ocean records. On the California margin, where sediment accumulation rates are in excess of 30cm/Kyr , cyclic alternations of varves with zones of bioturbation are found in upper Pleistocene sediments. The intermittently varved and bioturbated sediments reveal an oceanographic and climatic regime vastly different from that of the Holocene (Linsley et al., 1987; Anderson et al., in press). Periodic intensifications of the wind-driven coastal upwelling system resulted in a depletion of dissolved oxygen in the oxygen-minimum zone (OMZ) and the resultant development of anoxic or extreme dysacrobic conditions at the sediment surface. These conditions allow the seasonal signal of sedimentation to be preserved as varves. Bioturbated intervals resulted from a relaxation of wind stress and upwelling, which allowed dissolved oxygen levels in the OMZ to rise above some critical threshold.

Radiocarbon dating has constrained the age of varve/bioturbation cycles to between 12,000 and 45,000 years ago. Although no single core contains this entire time interval, a suite of cores has preserved portions of the time 12,000 to 45,000 years ago.

The marine varves are best preserved at a water depth of about 700 m. This depth corresponds to the lowest concentration of dissolved oxygen found in the present oxygen-minimum zone (Gardner and Hemphill-Haley, 1986). The diatomaceous clay-rich sediments are not continuously varved, but contain alternations of varves

and bioturbation. Varved intervals have biogenic silica mass accumulation rates (MAR, in gm/cm^2) and bioturbation. Varved intervals have biogenic silica mass accumulation rates (MAR, in $\text{gm/cm}^2/\text{Ka}$) of $\sim 0.9\text{--}2.0$ $\text{gm/cm}^2/\text{Ka}$ and organic carbon accumulation rates of $\sim 0.3\text{--}0.39$ $\text{gm/cm}^2/\text{Ka}$ (Figure 1).

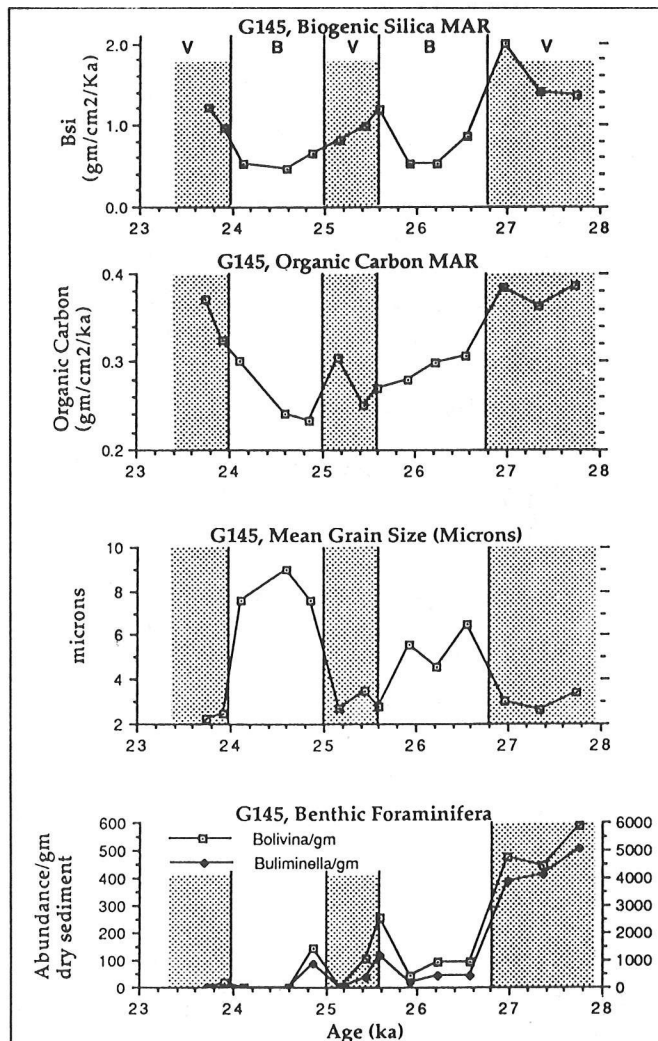


Figure 1. Mass accumulation rates (MAR) of Biogenic Silica, organic carbon, benthic Foraminifera per gram, and mean grain size in varve/bioturbation cycles in core G145 collected at 700m off the Russian River, northern California margin. Varved intervals are indicated by shading.

Diatom abundance patterns in the varved sections are indicative of deposition under an intensified coastal upwelling system. Species of benthic Foraminifera known to favor low dissolved oxygen and/or high organic carbon content are also generally more abundant in the varved intervals. Enrichment of the metals Fe, Ba, Ni, Cu, Li, along with elemental sulfur, in the varves also supports the interpretation that the laminae are preserved under reducing and low dissolved oxygen conditions (Figure 2). The compositional relationships observed in G145 are also found in several other varved cores from within the OMZ on the California margin.

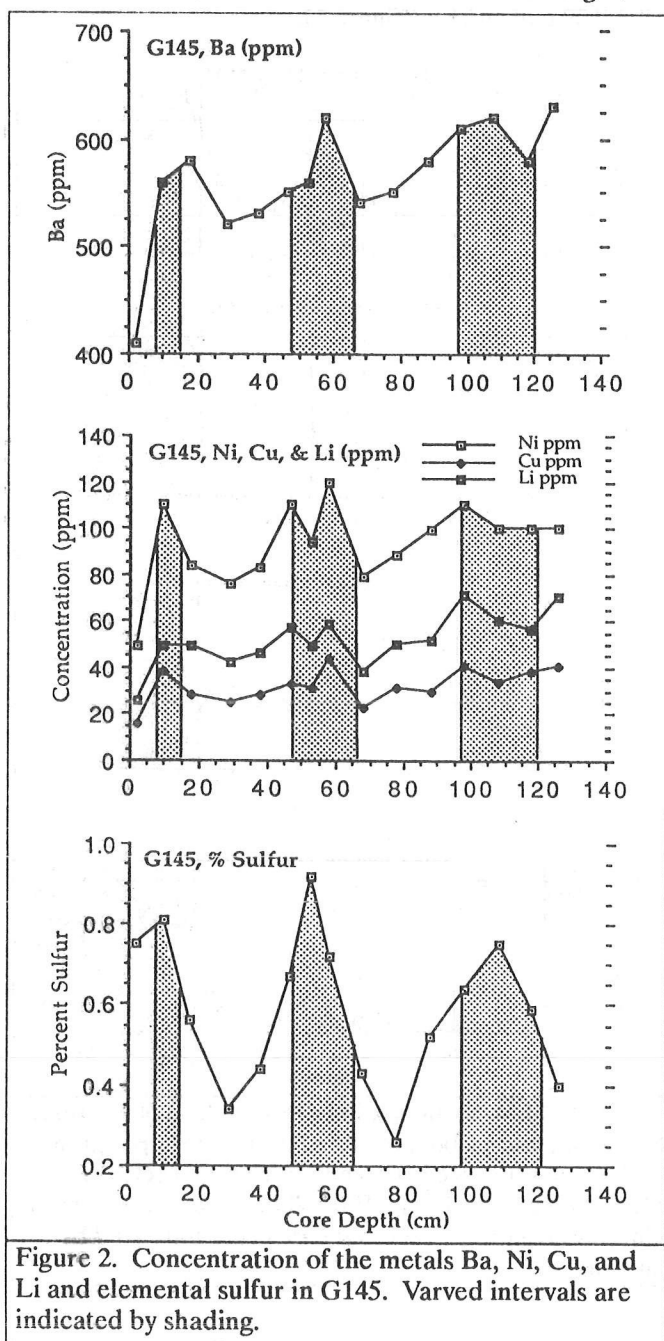


Figure 2. Concentration of the metals Ba, Ni, Cu, and Li and elemental sulfur in G145. Varved intervals are indicated by shading.

In contrast, bioturbated sediments generally have lower accumulation rates of both biogenic silica ($\sim 0.4\text{-}0.6 \text{ gm/cm}^2/\text{Ka}$), and organic carbon ($0.23\text{-}0.28 \text{ gm/cm}^2/\text{Ka}$) (Figure 1), and contain large burrow structures. Relative to the varves, the bioturbated intervals are not enriched in metals or forms of benthic Foraminifera tolerant of low dissolved oxygen.

There is evidence of a minor component of reworked, off-shelf sediment in both the varved and bioturbated intervals. In G145, a few individuals of benthic Foraminifera indicative of neritic, shallow-water environments (Quintero and Gardner, 1987) are found in the assemblages from both varved and bioturbated sections. However, a robust tychoelatic diatom *Stephanopyxis* comprises 50-60% of the diatom flora in the bioturbated intervals is $\sim 1.3 \text{ gm/cm}^3$ compared to 0.8 gm/cm^3 in the varves. This evidence may suggest that winnowing or a greater component of off-shelf transport has occurred during formation of the bioturbated intervals. However, the benthic foraminiferal assemblages, large bioturbation structures, and lack of apparent hiatuses support the conclusion that off-shelf transport was a relatively minor component throughout the deposition of G145.

Recent attention has focused on a series of North Atlantic climatic "jumps" recorded in Greenland ice cores during the time interval 60,000 to about 20,000 years ago (Dansgaard et al., 1985; Hammer et al., 1985; Beer et al., 1985; Broecker et al., 1988). So far these events have not been conclusively documented outside of Greenland, although there is some evidence in North Atlantic cores and European Bog sediments (Broecker et al., 1988). The varve/bioturbation cycles on the California margin occurred during the same time as the Greenland climatic shifts and, based on our partially complete record, appear to have a similar frequency. This would suggest that the millennial changes in wind stress, upwelling, and productivity recorded by the varve/bioturbation cycles may be more than regional in extent. However, the association between the climatic oscillations on the California margin and the Greenland climatic shifts is tentative.

STABLE ISOTOPIC ANALYSES

The stable isotopic composition of the benthic Foraminifera *Bolivina spissa* and *Uvigerina peregrina* were analyzed in a sample series across the middle varve/bioturbation cycle in Figure 1 (core G145, 700 m water depth). Foraminifera were ultrasonically cleaned, roasted at 250°C , and analyzed on a Micromass 602 ES at the Department of Geology and Geophysics at Rice University. Due to inconsistent abundance of *Uvigerina peregrina*, specimens of *Bolivina spissa* were also analyzed in separate samples. There appears to be good correspondence between both species in duplicate samples. The analytical precision for the NBS-19 carbonate standard was $\pm 0.034 \text{ ‰}$ for $\delta^{18}\text{O}$, and $\pm 0.050 \text{ ‰}$ for $\delta^{13}\text{C}$.

RAPID ISOTOPIC SHIFTS

The isotope analyses show a rapid and significant shift in benthic $\delta^{18}\text{O}$ and $\delta^{13}\text{C}$ shortly after 26,000 years ago (Figure 3). The $\sim 0.25\text{‰}$ shift in $\delta^{18}\text{O}$ occurs within a varved interval and is slightly preceded by a $\sim 0.4\text{‰}$ shift in $\delta^{13}\text{C}$. Both changes occur at the onset of increased organic carbon and biogenic silica preservation, interpreted as a time of intensified upwelling and productivity.

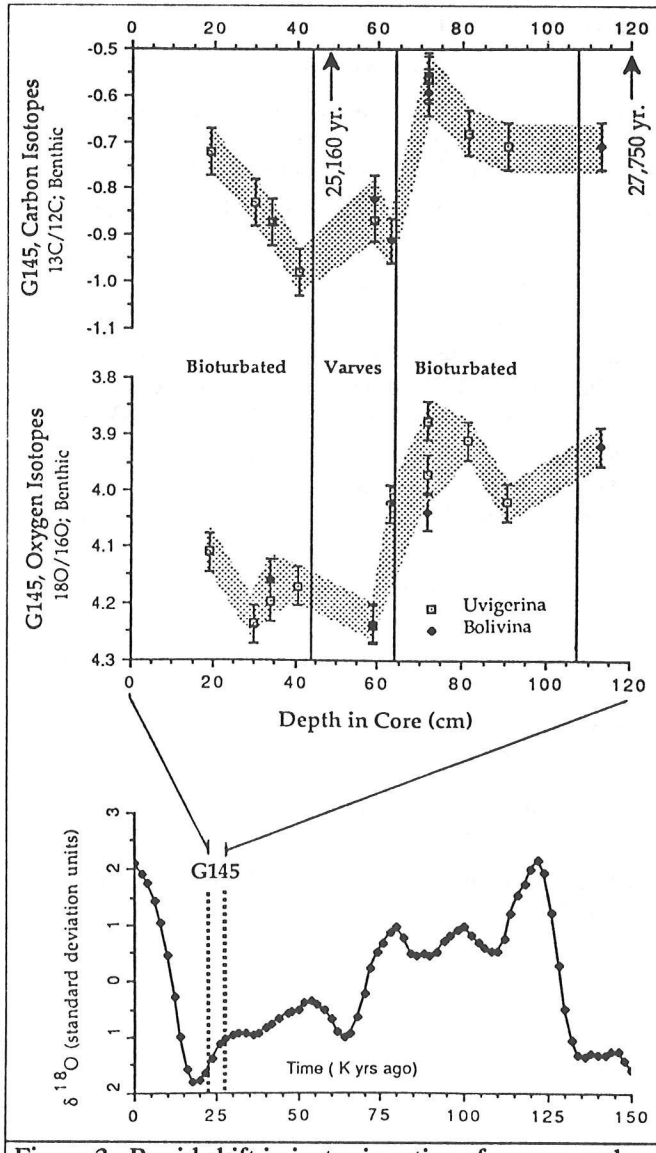


Figure 3. Rapid shift in isotopic ratios of oxygen and carbon in benthic Foraminifera species *Uvigerina peregrina* and *Bolivina spissa* from core G145. The oxygen isotopic shift occurs in less than 100 varve years. Note that the shift corresponds to a shift of similar magnitude in the stacked, smoothed planktonic foraminiferal isotopic record compiled by Imbrie et al. (1984).

The carbon isotopic composition of benthic Foraminifera tends to reflect the $\delta^{13}\text{C}$ of the total dissolved inorganic carbon (TDC) of the water in which they form. In general, the $\delta^{13}\text{C}$ of TDC in oceanic water masses is a function of the relative age of the water mass (Deuser and Hunt, 1969; Craig, 1969; Kroopnick et al., 1972). The organic matter oxidation signals dominate the $\delta^{13}\text{C}$ of TDC (average $\delta^{13}\text{C} = \sim -20$ to -25‰) (Sackett et al., 1965), such that the $\delta^{13}\text{C}$ will progressively decrease as a water mass ages and as organic matter is added. Therefore, the consumption of dissolved oxygen through oxidation of organic matter and a decrease in $\delta^{13}\text{C}$ should accompany one another (Kroopnick et al., 1972; Kroopnick, 1974). The $\sim 0.4\text{‰}$ $\delta^{13}\text{C}$ change across the varved zone in G145 (Figure 2) is apparently reflecting the addition of isotopically light organic matter or aging water mass conditions, which resulted from increased upwelling driven productivity. Furthermore, the $\delta^{18}\text{O}$ shift is preceded by the shift in $\delta^{13}\text{C}$, suggesting that whatever forced the $\delta^{18}\text{O}$ signal lags the intensification of upwelling.

The 0.25‰ enrichment in $\delta^{18}\text{O}$ values observed within a varved interval in G145 is coeval and of almost the same magnitude as a shift found in almost all high-resolution $\delta^{18}\text{O}$ records. Timing of the $\delta^{18}\text{O}$ enrichment appears during buildup to maximum ice-volume conditions during the last glacial maximum. Given the > 1000 -year mixing time of the oceans, it is intriguing that such a rapid shift ($< \text{years}$ in G145) in benthic $\delta^{18}\text{O}$ should occur synchronously in cores widely separated oceanographically and geographically. The similar magnitude of the shifts in cores from widely separated regions of the world's oceans suggests that local temperature or salinity changes on the California margin may not be the sole contributing factors and that some global ice-volume signal was preserved in this relatively shallow-water locale.

The sudden shift in G145 could be due to enhanced upwelling effects that occurred during this time of rapid ice buildup to the last glacial maximum. Identification of similar rapid isotopic shifts in other alternately varved and bioturbated cores will be a priority of future studies on the California margin. We will continue to concentrate on separating local from regional effects in an attempt to test whether climatic oscillations responsible for the varve/bioturbation cycles are more than regional in extent, and perhaps related to the North Atlantic Greenland climatic "jumps" and other fluctuating global climatic phenomena.

ACKNOWLEDGEMENTS

The National Science Foundation (ATM 8707462) and the U.S. Geological Survey Paleoclimate Program have supported the research used in this discussion. We are indebted to Walter E. Dean and Eileen Hemphill-Haley for their efforts in discovery of the varved sediments and for contributing data to the project.

REFERENCES

- Anderson, R.Y., Linsley, B.K., and Gardner, J.V., in press, Expression of seasonal and ENSO forcing in climatic variability at lower frequencies in Benson, L.V., and Meyers, P.A., Paleoclimates, the record from Lakes, Ocean and Land: Palaeogeography, Palaeoclimatology, Palaeoecology, 20p.
- Beer, J., Andree, M., Oeschger, H., Stauffer, B., Balzer, R., Bonani, G., Stoller, Ch., Suter, M., Wolli, W., and Finkel, R.C., 1985, ^{10}Be variations in polar ice cores, in Langway, C.C., Oeschger, H., and Dansgaard, W., Eds., Greenland Ice Core: Geophysics, Geochemistry, and the Environment, American Geophysical Union Monograph 33, p.66-70.
- Broecker, W.S., Andree, M., Bonani, G., Wolli, W., Oeschger, H., and Klas, M., 1988, Can the Greenland climatic jumps be identified in records from ocean and land: Quaternary Research, v.30, p.1-6.
- Craig, H., 1969, Abyssal carbon and radiocarbon in the Pacific: Journal of Geophysical Research, v.75, p.5491-5506.
- Dansgaard, W., Clausen, H.B., Gunderstrup, N., Johnsen, S.J., and Rygner, C., 1985, Dating and climatic significance of two deep Greenland ice cores, in Langway, C.C., Oeschger, H., and Dansgaard, W., Eds., Greenland Ice Core: Geophysics, Geochemistry, and the Environment: American Geophysical Union Monograph 33, p.71-76.
- Deuser, W.G., and Hunt, J.M., 1969, Stable isotopic ratios in dissolved inorganic carbon in the Atlantic: Deep-Sea Research, v.16, p.221.
- Gardner, J.V., and Hemphill-Haley, E., 1986, Stronger oxygen minimum zone in the late Pleistocene off central California: Geology, v.14, p.691-694.
- Hammer, C.U., Clausen, H.B., Dansgaard, W., Neftel, A., Kristinsdottir, P., and Johnson, E., 1985, Continuous impurity analysis along the Dye 3 deep core, in Langway, C.C., Oeschger, H., and Dansgaard, W., Eds., Greenland Ice Core: Geophysics, Geochemistry, and the Environment: American Geophysical Union Monograph 33, p.90-94.
- Imbrie, J., Hayes, J.D., Martinson, D.G., McIntyre, A., Mix, A.C., Morley, J.J., Pisias, N.G., Prell, W.L., and Shackleton, N.J., 1984, The orbital theory of Pleistocene climate: Support from a revised chronology of the marine $\delta^{18}\text{O}$ record, in Berger, A., Imbrie, J., Hays, J., Kukla, G., and Saltzman, B., Eds., Milankovitch and Climate, part 1: D. Reidel Publishing, p.269-305.
- Kroopnick, P., 1974, The dissolved O_2 - CO_2 - ^{13}C system in the eastern equatorial Pacific: Deep-Sea Research, v.21, p.211-227.
- Kroopnick, P., Weiss, R.F., and Craig, H., 1972, Total CO_2 , ^{13}C , and dissolved oxygen- ^{18}O at GEOSECS II in the North Atlantic: Earth Planetary Science Letter, v.16, p.103-110.
- Linsley, B.K., Hemphill-Haley, E., Gardner, J.V., and Anderson, R.Y., 1987, Late Pleistocene varve-bioturbation sediment cycles, northern California continental margin (abs): EOS v.68, p.1332-1333.
- Quinterno, P.J., and Gardner, J.V., 1987, Benthic Foraminifers on the continental shelf and upper slope, Russian River area, northern California: Journal of Foramin. Research, v.17, no.2, p.132-152.
- Sackett, W.M., Eckelmann, W.R., Bender, M.L., and Be' A.W., 1965, Temperature dependence of carbon isotope composition in marine plankton and sediments: Science, v.148, p.235.

El Niño Reconstructions and Confirmation of a Pan-Californian Model via Radiolarian Evidence

Richard E. Casey, Amy L. Weinheimer, Carl O. Nelson, Joseph B. Albin,
David S. Beauchamp, David S. Carpenter, and Kevin M. O'Brien

ABSTRACT: Radiolarian number and/or flux rates extracted from Holocene and fossil sediments are used to help detect the presence of, type of (weak or strong), and exact location of the depocenter under an El Niño. These data, along with the known provenances of certain radiolarians, support an earlier model that suggests a weak El Niño is a northern and coupled expression of a more southerly strong component dominated by eastern tropical Pacific water underlain by California current and gyre water.

INTRODUCTION

Holocene varved sediments from Santa Barbara Basin, Pleistocene varved sediments from the mid-California continental slope, and Neogene sediments from the Eel River Basin (Figure 1) all contain records of El Niño or El Niño-like events. Increased radiolarian flux into the Santa Barbara Basin appeared to be an indicator of the strong 1983 El Niño (Lange et al., 1987). A similar, although less dramatic, flux increase appeared to indicate the weak 1964 El Niño (Weinheimer et al., 1986). During both of these El Niños, physical oceanographic and radiolarian material from plankton tows suggest different configurations and dynamics for the California Current System (Casey et al., 1989). In fact, a model was developed that coupled weak and strong El Niño dynamics into a single related system. This system apparently shifts up and down the California coast, depending on the strength of the entire California El Niño "system" (Casey et al., 1989). We test this model by comparing it to the radiolarian flux and number record of the Pleistocene mid-California shelf sediment and those of the Neogene Eel River Basin sediment. Both are considered to represent deposition under El Niño conditions and would contain a record of the northern, or *weak*, El Niño portion of the El Niño System.

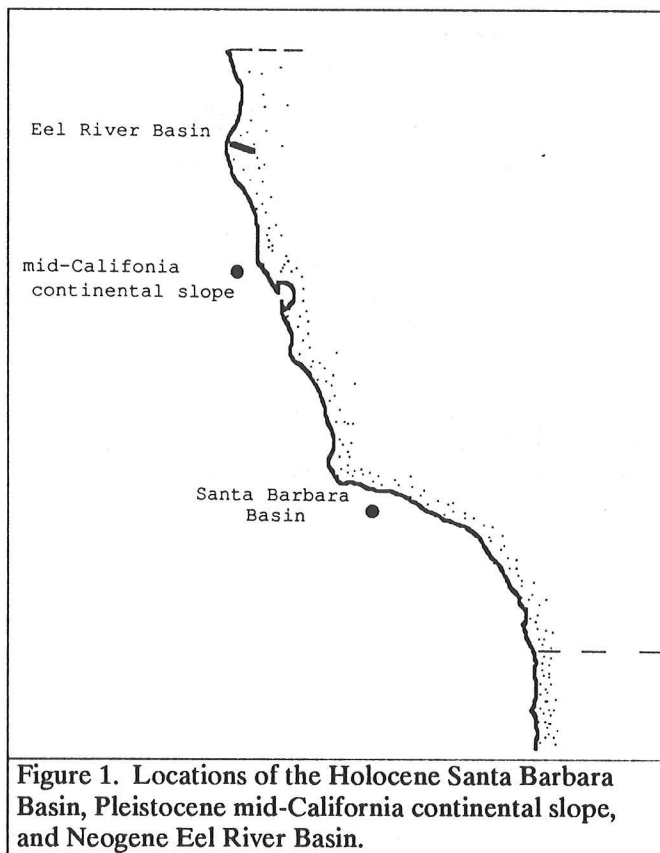


Figure 1. Locations of the Holocene Santa Barbara Basin, Pleistocene mid-California continental slope, and Neogene Eel River Basin.

PREVIOUS STUDIES

Using radiolarian data from plankton tows and Santa Barbara Basin sediments, and physical and chemical data from the water column, a reconstruction of oceanographic conditions off the California coast were made for the 1964 California El Niño by Weinheimer et al. (1986) (Figure 2). Using the same type of data, a similar reconstruction was made for the 1983 California El Niño by Casey et al. (1989) (Figure 3). Casey et al. suggest that weak El Niños (like 1964) and strong El Niños (like 1983) are actually coupled events, with the weak El Niño being a northern manifestation (extension) of the strong El Niño (Figure 3). The investigation of more northerly samples during periods of paleo-El Niños is used to test this coupled El Niño model.

METHODS

Pleistocene sediments were collected via core at about 500m off mid-California (Figure 1). These sediments are varved for the most part and interrupted by minor intervals of El Niño conditions, which appear to be representative of El Niño conditions. Neogene sediments, dated at 5.5 mya (Nelson, 1986), were collected from land-based outcrops in the exposed Eel River Basin (Figure 1). These sediments are nonlaminated, believed to be representative of El Niño conditions (Nelson, 1986), and recently reinterpreted as indicative of the first true El Niño conditions in the Pacific (Casey et al., 1989).

The Pleistocene varved and bioturbated sediments from the mid-California slope were subsampled at what was considered an annual level. This subsampling was done taking into account the surface area of the paleowater-sediment interface to determine flux rates by the same method as that used to determine those of the Holocene Santa Barbara Basin samples. The nonlaminated Neogene sediments from the Eel River basin were weighed before processing to determine radiolarian number (the number of radiolarians per gram of dry sediment). Although radiolarian number is not considered as accurate an indicator of El Niño conditions as radiolarian flux (since a high terrigenous input could influence the number), it was considered our most comparable parameter due to the nonlaminated nature of the Eel River samples.

All the depocenters considered are at a depth of approximately 500m. These are the actual depths of the Santa Barbara Basin and mid-California slope sites and the reconstructed depth of the Eel River Basin site (Nelson, 1986). Because the Eel River Basin site is one of considerable terrigenous sedimentation, in attempting to compare the radiolarian number from that site to radiolarian flux rates from the other sites, the radiolarian numbers from Eel River were multiplied by 100. The conversion factor of 100 was determined upon observing that the Eel River radiolarian numbers at 500m were two orders of magnitude less than the average radiolarian number of Cleveland and Casey (1986).

RESULTS

Radiolarian fluxes of the 1964 and 1983 El Niños (and corresponding anti-El Niños) from Santa Barbara Basin are shown on Figure 4. The flux peaks from Holocene Santa Barbara Basin correlate to El Niños and the troughs to anti-El Niños. Explanations for these peaks during El Niños (and, therefore, troughs during anti-El Niños) have been that high radiolarian density central gyre and intermediate waters invade the region during these periods (Weinheimer et al., 1986; Casey et al., 1989). Pleistocene and Neogene sediments, on the other hand, exhibit a trough during a suspected El Niño and a peak during a suspected anti-El Niño (Figure 4). Magnitude of the El Niño peak decreases from south to north; anti-El Niños to the north exhibit, in general, a similar flux or radiolarian number, respectively, to those of the Southern California location (Figure 4).

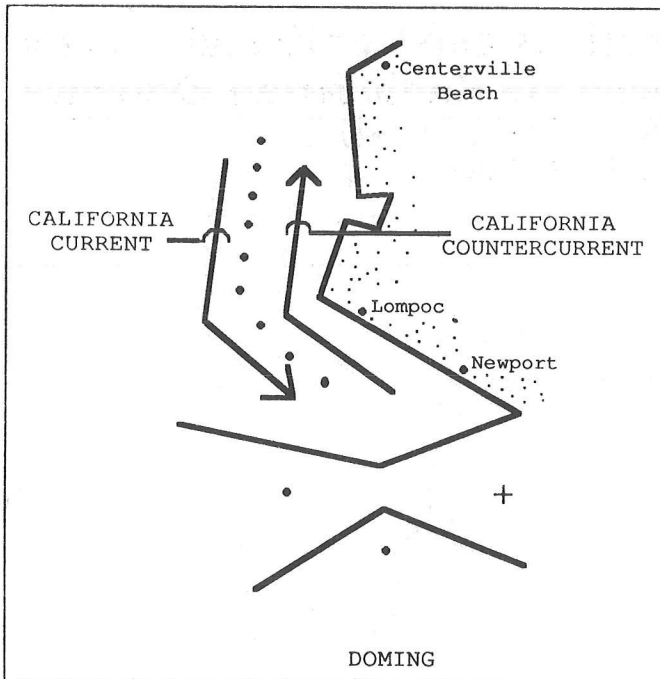


Figure 2. Model of the California Current System during a weak El Niño phase (modified from Weinheimer et al., 1986).

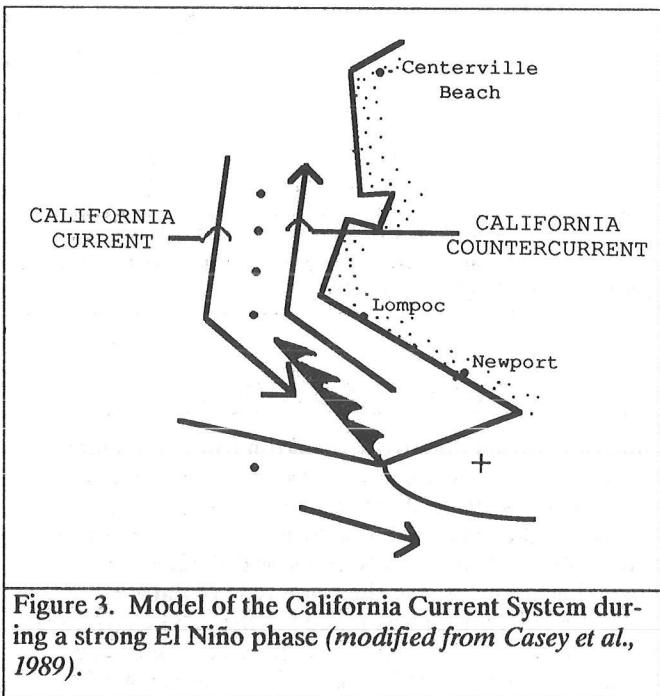


Figure 3. Model of the California Current System during a strong El Niño phase (modified from Casey et al., 1989).

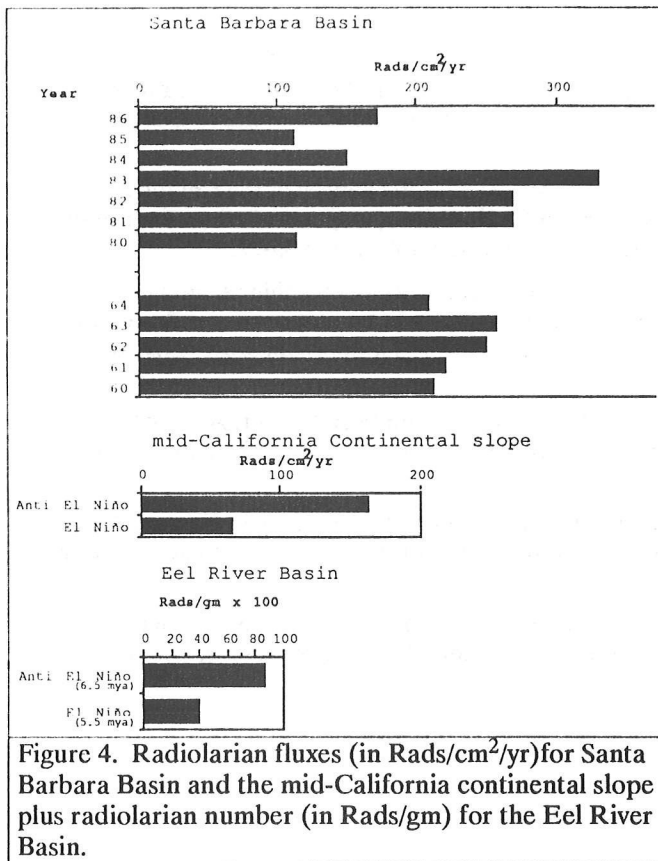


Figure 4. Radiolarian fluxes (in Rads/cm²/yr) for Santa Barbara Basin and the mid-California continental slope plus radiolarian number (in Rads/gm) for the Eel River Basin.

DISCUSSION AND CONCLUSIONS

Although the results exhibited in Figure 4 and related in the previous section appear to be incompatible, they in fact give credence to the model under test when the entire model is examined and provenances and densities of the radiolarians inherent to that model are included. Not only do the fluxes into the Santa Barbara Basin differ in magnitude (greater during stronger El Niños; see Figure 4), but the composition of the fluxed radiolarians also differs. The strong 1983 El Niño exhibited a greater flux of radiolarians from the California Current and gyre provenances than did the weak 1964 El Niño (Casey et al., 1989).

The reasons for these greater fluxes from those provenances can be seen by comparing Figures 2 and 3. A major portion of the California Current and its entrained California Current and gyre province radiolarians invaded the Santa Barbara Basin during the strong 1983 El Niño (Figure 3). Since the gyre provenance contains the highest standing crops of radiolarians of all potential contributing provenances, it appears to account for the high radiolarian flux peak (Casey et al., 1989). During the weak 1964 El Niño, the less dramatic radiolarian flux peak appears to be related mainly to an influx of high standing crops of intermediate and deep radiolarians in southerly moving waters under the divergence shown in Figure 2.

The provenance exhibiting the lowest standing crop during El Niño conditions would be from the eastern tropical Pacific, which should invade the area as the coastal countercurrent shown on both Figures 2 and 3. Waters of the eastern tropical Pacific have been found to exhibit the lowest radiolarian standing crops (Carson, 1986) of any of the potential invading radiolarian provenances. Therefore, should waters from the eastern tropical Pacific (the coastal countercurrent) overlie a depocenter, they should contribute little in radiolarian flux to that depocenter.

The Pleistocene mid-California depocenter is currently 30 kilometers from shore. The Neogene Eel River site is taken from a section that did not contain a known paleo-shoreline, but was deposited at a depocenter having a reconstructed paleodepth of 500m (Nelson, 1986). If this depth is *hung* on the current bathymetry off Eel River (a technique used by Nelson (1986) in his reconstructions of that area), the 500m site in question would be 29 kilometers offshore at the 5.5mya datum.

Since both the Pleistocene and Neogene sites suggest deposition under northern components of strong El Niños, they should be compared to a weak or northern component of an El Niño like the 1964 El Niño. The width of the coastal countercurrent during the 1964 El Niño (eastern tropical Pacific) measured along CalCOFI Line 90 is 153 kilometers (from Weinheimer et al., 1986). Both the Pleistocene and Neogene locations would be sites of deposition underlying the coastal countercurrent and, therefore, subjected to low radiolarian fluxes. This supports the model, suggesting that weak and strong El Niños are coupled and that there is evidence for the northern component (weak) of the El Niño imprinting the Eel River Basin at least 5.5mya. Further evidence is suggested by the decreasing flux of the El Niño peaks from south to north (Figure 4).

Additional support comes from the fluxes during known or suspected anti-El Niños. The similarity of these fluxes at the northern and southern sites suggest that the El Niño differences are real (Figure 4).

ACKNOWLEDGMENTS

All authors are members of the Marine Studies Program at the University of San Diego. Samples from the Pleistocene mid-California slope were collected by Roger Anderson and James Gardner under support from NSF Grant ATM-8707462. Support for the authors' research was partially provided by National Science Foundation Grant OCE-86-20446. Acknowledgement is also made to the donors of the Petroleum Research Fund administered by the American Chemical Society and to the W.M. Keck Foundation for partial support of these studies.

REFERENCES

- Carson, T.L., 1986, Radiolarian response to the 1983 California El Niño, *in* Casey, R.E., and Barron, J.A., editors, Siliceous microfossil and microplankton studies of the Monterey formation and modern analogs: Los Angeles, SEPM Pacific Section, p.9-19.
- Casey, R.E., Weinheimer, A.L., and Nelson, C.O., 1989, California El Niños and related changes of the California current system from recent and fossil radiolarian records, *in* Peterson, D.H., Editor, Aspects of climate variability in the Pacific and western Americas: American Geophysical Union Monograph v.55, p.85-92.
- Cleveland, M.N., and Casey, R.E., 1986, Radiolarian indices of physical and chemical oceanographic phenomena in recent sediments of the Southern California continental borderland, *in* Casey, R.E., and Barron, J.A., editors, Siliceous microfossil and microplankton studies of the Monterey formation and modern analogs: Los Angeles, SEPM Pacific Section, p. 9-19.
- Lange, C.B., Berger, W.H., Burke, S.K., Casey, R.E., Schimmelmann, A., Soutar, A., and Weinheimer, A.L., 1987, El Niño in Santa Barbara Basin: Diatom, radiolarian, and foraminiferan responses to the 1983 El Niño event: *Marine Geology*, v.78, p.153-160.
- Nelson, C.O., 1986, Radiolarian paleoceanographic studies of the Humbolt Basin and adjacent area, *in* Casey, R.E., and Barron, J.A., editors, Siliceous microfossil and microplankton studies of the Monterey formation and modern analogs: Los Angeles, SEPM Pacific Section, p.9-19.
- Weinheimer, A.L., Carson, T.L., Wigley, C.R., and Casey, R.E., 1986, Radiolarian responses to recent and Neogene California El Niño and anti-El Niño events: *Palaeogeography, Palaeoclimatology, Palaeocology*, v.53, p.3-25.

Sediment Flux at Selected Coastal Sites: Proposed Time Series Measurement by Particle Traps

A. Soutar, T.R. Baumgartner, R.E. Casey, J. Singleton,
V. Ferreira-Bartrina, and C.O. Nelson

ABSTRACT: Particle flux in the ocean reflects ongoing biological and geological processes operating under the influence of the local environment. Estimation of this particle flux through sediment trap deployment is constrained by sampler accuracy, particle preservation, and swimmer distortion. Interpretation of specific particle flux is further constrained by indeterminate particle dispersion and the absence of a clear understanding of the sedimentary consequences of ecosystem activity. Nevertheless, the continuous and integrative properties of the particle trap measure, along with the logistic advantage of a long-term moored sampler, provide a set of strategic advantages that appear analogous to those underlying conventional oceanographic survey programs. Emboldened by this perception, several stations along the coast of Southern California and Mexico have been targeted as coastal ocean flux sites (COFS).

INTRODUCTION

Over the past few years PACLIM discussion has included natural time series that, among other things, can serve as a proxy for pre-instrumental climate (PACLIM Workshop Reports, 1985-1988; Baumgartner et al., 1989). In the case of time series derived from marine sediment, emphasis has been on high resolution varve sequences such as those found in the Santa Barbara Basin and the Gulf of California. However, as with all proxy records, the series are fixed and have only limited potential for expansion; furthermore, appreciation of how such records form and their significance is constrained by availability of meaningful environmental and ecological information.

Two limitations of "high resolution" sediment records are their geographic rarity and their inherent resolution of one year. These limitations may, in part, be circumvented through use of sediment trap devices configured to intercept particles within the water column. While there is continuing community discussion as to the effectiveness of such devices for specific purposes (e.g., measuring carbon flux in surface waters), it is clear that sediment traps do provide insight into the ocean process that is otherwise unavailable (Deusser et al., 1981; Knauer et al., in prep).

PERCEPTIONS

An operational framework and justification for deployment of sediment traps in coastal waters can be derived from the following perceptions.

- **Under certain circumstances, sediment traps provide a reasonably accurate measure of inorganic and biogenic particle flux in the ocean.**

It is perhaps self evident that most upwardly concave structures placed in a still water environment (or carried along with no relative motion) will reliably intercept settling particles. One of the simplest shapes is an open mouth cylinder, and work continues in flues and field to understand the hydromechanics of particle collection in the more common case of water movement past a moored collector (Hawley, 1988; Butman, 1968; Gardner, 1980; Lau, 1979). An alternative collection mechanism utilizing a grid surface to intercept particles essentially suspended in horizontal flow has been suggested (Soutar et al., 1977; Dymond et al., 1981).

Ideally sediment trap devices should be evaluated in natural sedimentation regimes that are essentially deterministic. That is to say: synoptic, independent, and reliable measures of particle flux should be available for comparison to sediment trap catch. Placing sediment traps near the bottom in regions of annually layered sediments provides one reasonable approach to the ideal. Indeed, regions of varved sedimentation can be considered as unusually large sediment traps that sequence twice a year and have fairly good sample preservation.

A 2-year deployment of grid-surface collectors configured as paired cones (see Figure 1) in the Santa Monica Basin indicates a collection efficiency of 96% relative to contemporary bottom accumulation adjusted for silica dissolution and organic matter decomposition (R. Janke, pers comm; see Table 1). This result, coming after a number of intermittent attempts (Soutar et al., 1977; Bruland et al., 1981), provides a relatively clear operational pathway for interpretation of trap samples collected in the deep Santa Monica basin and environments having similar current and particle characteristics.

In J.L. Betancourt and A.M. MacKay, editors, 1990. Proceedings of the Sixth Annual Pacific Climate (PACLIM) Workshop, March 5-8, 1989: California Department of Water Resources, Interagency Ecological Studies Program Technical Report 23.

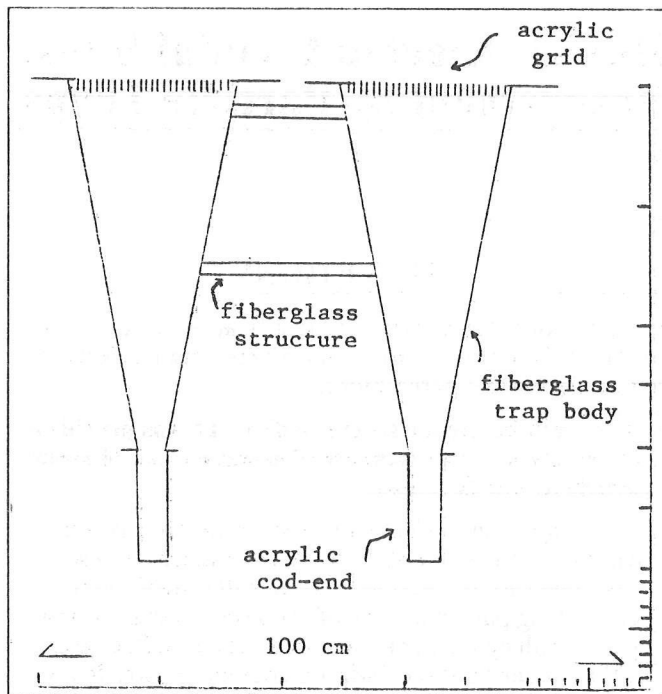


Figure 1. Cross section of paired cone configuration of open grid-surface sediment trap. Collection area of each trap is 0.06 m^2 , grid cells are $1 \times 4 \text{ cm}$ deep, and the angle of funnel wall is 7° off vertical.

Table 1. Santa Monica central basin deployment (50 m above 890 m bottom, 734 days between February 1986 and February 1988 [76% of time]; 1986 average current speed, 2 cm/sec, max. $< 10 \text{ cm/sec}$ [Hickey, 1986]).

Bottom (net) mass flux (a)	*440 $\text{mg/m}^2/\text{day}$
Measurement inferred mass out-flux of recycled opal and organic matter (b)	*210 $\text{mg/m}^2/\text{day}$
Gross bottom sediment mass flux (a + b)	650 $\text{mg/m}^2/\text{day}$
Gross sediment trap mass flux	625 $\text{mg/m}^2/\text{day}$

*R. Janke, pers comm

- The passive particle flux gathered by sediment traps in coastal regions is a continuous and integral measure on predominantly local spatial and temporal scales and, thus, serves as a selective index to geological, chemical, and biologic activity and may serve as an indirect index to environmental and climatic change.

Certainly, a reasonably accurate collection of mass particle flux implies a capability of assessing geologic and geochemical processes within the water column. Furthermore, extrapolation to time scales shorter than one year and to regions distant from the bottom may be contemplated. Limitations of time scale resolution involve realistic assessment of particle formation, particle interaction and particle descent rate factored into water movement at depth. In terms of biological processes, Takahashi (1986), working with sequential trap samples

collection at separate depths, was able to estimate an aggregate diatom sinking speed of 175 m/day. Similar settling in 900-meter coastal waters would imply a 5-day response time, with perhaps a 10 km to maximum 60 km dispersion after particle injection (Table 2). However, surface water advection (e.g., coastal Davidson current) of live and temporarily buoyant particles (such as diatoms and radiolarians having lifespans of days to weeks) could lead to occasional dispersions on the order of 100 to 500 km. Taken at face value, these conjectures would suggest that material from month or longer sampling intervals would tend to be drawn from a wide, though only generally determinate, area.

Table 2. Horizontal dispersion of surface injected particles in a sea with a very simple hypothetical current structure and a particle fall velocity of 175 m/day.

Depth (meters)	Current Velocity (cm/sec)	Dispersion (Uniform) (km)	Dispersion (Alternate) (km)
0-100	50	24.6	24.6
100-200	25	12.3	-12.3
200-400	10	9.8	9.6
400-900	5	12.4	-12.4
Total		59.1	9.7

Local interpretation of biogenic sediment trap flux in terms of productivity can be equivocal. Takahashi (1986; 1987) considers diatom, radiolarian and foraminiferal fluxes at depth direct indicators of productivity in the overlying North Pacific waters. Baumgartner (1988) indicates an increase in measured primary productivity during the 1982-1983 ENSO event and increased diatom flux to the sediments during previous such events. Lang et al. (1988) indicate an increase in radiolarian deposition in the sediments during the 1982-1983 ENSO period that is in opposition to the ENSO related general decline of zooplankton stock and productivity in the Southern California bight emphasized by McGowan (1985). This productivity index reversal is not limited to the recent event, but consistently extends back through past ENSO events (Weinheimer, 1987) and also includes planktonic forms (Dunbar, 1981).

- Active particle flux (swimmer organisms) can occur during sediment trap deployment.

Placement of sediment traps in near-surface waters not only increases exposure to much higher current regimes but also exacerbates the problem of swimmer entry into collectors (Lee et al., 1988). This action may routinely interfere with accurate estimation of organic carbon and nutrient flux in such waters; however, there is the potential of continuously monitoring and indexing the standing crop of "problem" organisms.

- The uncertainty of sediment trap flux interpretation due to lack of sufficient information on water movement, particle interaction and particle settling velocity does not intuitively appear greater than:

- The uncertainty associated with either continuous but surface limited or continuous but widely spaced point measures (temperature, salinity, current) associated with physical oceanography and
- The uncertainty associated with the occasional point measures (nutrients, productivity, standing crop) associated with chemical and biological oceanography.

In this regard, it is interesting to note that the present CalCOFI program conducts quarterly cruises to the Southern California bight and utilizes about 65 unreplicated standard stations to characterize the physical and biological condition of the region. In terms of area, this amounts to one station for every 3700 square kilometers. Characterization of the biological character is made more difficult by strong day-night differences and patchiness in near-surface waters. Allowing a sampling to remain representative for 0.5 day might suggest an uncontested description for 2 days out of the year. It is perhaps a tribute to the persistence of both the system and the investigators that identifiable bio-oceanographic patterns emerge.

- The number and scope of parameter measurement that should be carried out as part of a comprehensive program to understand a regional ecosystem and its sedimentary consequences greatly exceed most combinations of physical-economic restraint and technical capability.

If one sits down with an interdisciplinary group of people to plan an ecosystem dynamics program, it is not long before the chalkboard overflows with a *wish list* of field and analytical items. Probably quite a few such programs have been planned, and at least one approximation has been attempted. The CUE (*Coastal Upwelling Experiment*) program of the 1970s comes to mind. Such a program can run into the tens of millions of dollars, can only be sustained for a few years, and can only be carried out occasionally in a very few deserving regions.

- Some measurement is better than no measurement in that:
 - Predictive efforts in complex natural systems appear, for the foreseeable future, to be limited at best to elegant descriptions of eventlike processes; therefore, it will be necessary to carry out measurements to maintain a realistic image of such systems;
 - Substantial environmental measures (atmospheric pressure, temperature, rainfall, sea level, satellite overview) and occasional oceanographic measures (nutrients, productivity, standing crop) will continue to be available. These provide an opportunity base for continuous study of coastal marine ecosystems;
 - Sediment trap sampling in definable circumstances can, at the least, provide a broad range of indices that are equivalent to otherwise unobtainable measures of ocean activity.

We live in a world where persistence and surprise are the rule. The seasons progress and return with mathematical certainty; however, the seasonal excursions of weather and climate are often sufficient to cause dis-

comfort and disaster. A substantial arrangement of resources in the form of the weather service provides perhaps a 2-week warning of either. The oceans have a familiar pattern of flow. In coastal regions of high latitude, the sign of the new year is the return of sunlight, keying phytoplankton production. No one can say how intense the resultant blooms will be. Nevertheless, just as hurricanes are tracked and the possibilities for land-fall broadcast, so now in the ocean is the development of an ENSO condition dutifully followed. We know more hurricanes and El Niños will come. We would like to think an historical perspective could lead someone to guess just how many to expect. We are quite sure that no one knows when they will occur or how substantial they will be.

If the predictive grasp on highly visible events such as hurricanes and El Niño is marginal, then certainly the situation for most regional seas should be tenuous. CalCOFI (a fundamental fisheries program) has been operating at varying levels off California for 40 years. This has resulted in a considerable body of information on the physical and biological makeup of the California current. Aside from the dominating effect of local ENSO development (Bernal, 1981; Chelton, 1981), nothing has appeared to suggest how the system will develop from year to year. Rather, there are suggestions that even this substantial effort is programmatically wanting. Smith and Moser (1988), commenting on the CalCOFI fish-related time series, note that the extensive egg surveys carried out in conjunction with the physical and biological measurements, though a good measure to spawning population, are not sufficient to predict the success of a fish year class. In coastal fishery regions having no tradition of time series, the verdict on year class success must, in parallel fashion, await catch landings.

PROGRAM

An informal cooperative project designed to provide time series of particle flux in regional coastal waters is advocated (*acronym: COFS, Coastal Ocean Flux Sites*). Presently, some institutional and individual resources have been diverted to a local program.

A southern California and central Mexico group (composed of at least the authors) is targeting a few sites (three off southern California, one off southern Baja California, and one off Guaymas, the Gulf of California) for development of sediment flux time series (see Figure 2). The group will attempt to deploy sediment traps more or less continuously at two of the sites (San Diego basin and Guaymas slope). With the exception of the San Diego Basin, all sites have laminated deposition that could provide, in retrospect, a hard confirmation of findings.

The start-up moorings will be at a single depth of 40 meters off the bottom, and recycling will be on a seasonal basis. Eventually, electromechanical sequences will be added to the collectors, and recovery intervals could extend to 6 months or greater, with a 1-month or less sampling resolution. On-site work (monthly at San

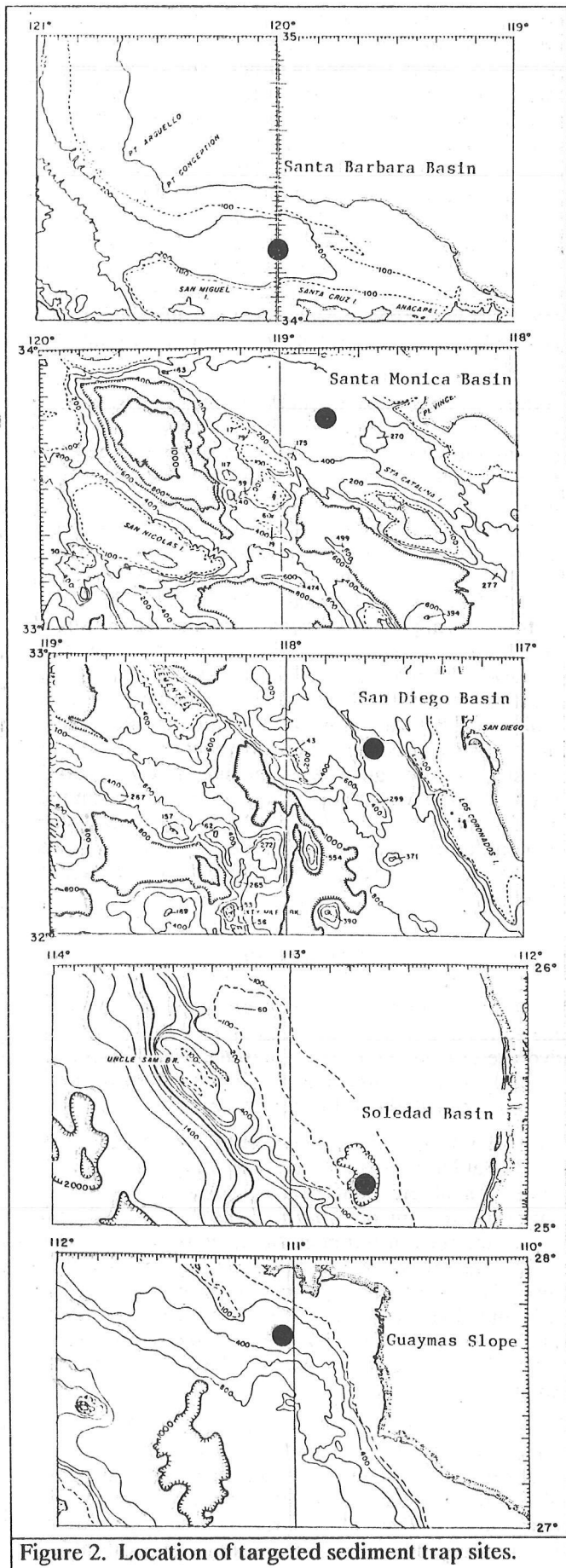


Figure 2. Location of targeted sediment trap sites.

Diego and seasonally at Guaymas) can include CTD/transmissometer cast and microplankton hauls. The San Diego site, at the southern end of the CalCOFI surveys, will benefit from their physical and nutrient/productivity information. Process and distributional studies in the central gulf could provide a similar, though less consistent, oceanographic context for the Guaymas deployment.

PRODUCT

We have attempted to convey the idea that the serial accumulation of sediment particles is, in effect, an index of the local state of the sea. Since a substantial portion of the index signal is composed of biological information and in view of the fact that frequent and comprehensive biological characterization of the sea is one of the more elusive of tasks, we will aim to assemble an ongoing view of local ocean activity placed within the framework of available environmental information.

This roughly translates as an ongoing presentation of seasonal flux rates of selected fish, zooplankton, and phytoplankton species-specific particles, along with mass fluxes and eventually (though analytical and sampling problems intrude), including something on organic carbon, carbonate, nitrogen, phosphorus, silica, and the trace elements. Given the systemic delay due to deployment/recovery and follow-on analysis, an eventual goal of a 6-month lag for key indicators is suggested.

We hope a number of important environmental parameters will be available through the auspices of PACLIM members and others for presentation in parallel form. We also hope the inauguration of camera-ready manuscripts for PACLIM might provide a continuing incentive and forum for reporting such efforts. In this regard, it seems that the ongoing patterns of climate in its broadest sense is of interest to an equally broad audience; and although our efforts in isolation might appear narrow, they are impacted by forces of hemispheric scope. A clear and well commented presentation of the ongoing Pacific climate picture would be of benefit to many.

ACKNOWLEDGEMENTS

Appreciation is expressed to the Marine Life Research Group, Scripps Institution of Oceanography (A. Soutar, J. Singleton), the Centro de Investigacion Cientifica y de Educacion Superior de Ensenada (T. Baumgartner, V. Ferreira-Bartrina), and the Marine Studies Program, University of San Diego (R. Casey, C.O. Nelson) for their support. Santa Monica trap samples that constitute Table 1 were collected under a Department of Energy, West Coast grant.

REFERENCES

- Baumgartner, T., 1987, High resolution Paleoclimatology from varved sediments of the Gulf of California: Ph.D. thesis, Oregon State University, Corvallis, OR, 287p.
- Baumgartner, T., Michaelsen, J., Thompson, L.G., Shen, G.T., Soutar, A., and Casey, R.E., 1989, The recording of inter-annual climate change by high-resolution natural systems: tree-rings, coral bands, glacial ice layers, and marine varves, *in* Aspects of Climate Variability in the Pacific and Western Americas: American Geophysical Union Monograph v.55, p.1-14.
- Bernal, P.A., 1981, A review of the low-frequency response of the pelagic ecosystem in the California Current: CalCOFI Reports, v.22, p.34-48.
- Bruland, K.W., Franks, R.P., Landing, W.M., and Soutar, A., 1981, Southern California inner basin sediment trap calibration: Earth and Plant Science Letter, v.53, p.40-408.
- Butman, C.A., 1986, Sediment trap biases in turbulent flows: results from a laboratory study: Journal of Marine Research, v.44, p.645-693.
- Chelton, D.B., 1981, Interannual variability of the California current-physical factors: CalCOFI Reports, v.22, p.34-48.
- Dauser, W.G., Ross, I.H., and Anderson, R.F., 1981, Seasonality of the supply of sediment to the deep Sargasso Sea and implications for the rapid transfer of matter to the deep ocean: Deep-Sea Research, v.28A, p.494-505.
- Dunbar, R.B., 1981, Sedimentation and the history of upwelling and climate in high fertility areas of the northeastern Pacific Ocean: Ph.D. thesis, Scripps Institute of Oceanography, Univ. California at San Diego, CA, 234p.
- Dymond, J.D., Fisher, K., Clausen, M., Clobler, R., Gardner, W., Richardson, M.J., Berger, W., Soutar, A., and Dunbar, R., 1981, A sediment trap intercomparison study in the Santa Barbara Basin: Earth and Planet Science Letter, v.53, p.409-418.
- Gardener, W.D., 1980, Sediment trap dynamics and calibration: a laboratory evaluation: Journal of Marine Research, v.38, p.41-52.
- Hawley, N., 1988, Flow in cylindrical sediment traps: Journal of Great Lakes Research, v.14, p.76-88.
- Hickey, B., 1986, Circulation over the Santa Monica/San Pedro Basin and shelf: D.O.E. West Coast Environmental Program, California Basin Study (CaBs), Progress Report III.
- Knaur, G., In prep, Report on the NSF-GOFS "Sediment Trap Vagaries" Workshop: Ocean Springs, University of Southern Mississippi, Nov. 1988.
- Lange, C.B., Berger, W.H., Burke, S.K., Casey, R.E., Schimmelman, A., Soutar, A., and Weinheimer, A.L., 1987, El Niño in Santa Barbara Basin: diatom, radiolarian and foraminiferan responses to the 1983 El Niño event: Marine Geology, v.78, p.153-160.
- Lau, Y.L., 1979, Laboratory study of cylindrical sedimentation traps: Journal of Fish. Res. Board Canada, v.36, p.1288-1291.
- Lec, C., Wakeham, S.G., and Hedges, J.I., 1988, The measurement of oceanic particle flux — are "swimmers" a problem?: Oceanography, v.1, p.34-36.
- McGowan, J.A., 1985, El Niño 1983 in the southern California bight, *in* Wooster, W.S., and Fluharty, D.L., eds., El Niño North — Niño Effects in the Eastern Subarctic Pacific Ocean: Seattle, Washington Univ. Press, p.166-184.
- PACLIM Reports, 1985-1988, Workshop of the eastern Pacific and western North America Workshops, Asilomar, CA: Abstracts.
- Smith, P.E., and Moser, H.G., 1981, CalCOFI time series: an overview of fishes: CalCOFI report, v.29, p.1-13.
- Soutar, A., Kling, S.A., and Duffrin, E., 1977, Monitoring the marine environment through sedimentation: Nature, v.266, p.136-139.
- Takashaki, K., 1987, Radiolarian flux and seasonality: climatic and El Niño response in the subarctic Pacific, 1982-1983, 1987: Global Biogeochemical Cycles, v.1, p.213-231.
- _____, 1986, Seasonal fluxes of pelagic diatoms in the subarctic Pacific, 1982-1983: Deep-Sea Research v.33, p.1225-1251.
- Weinheimer, A.L., Carson, T.L., Wigley, C.R., and Casey, R.W., 1986, Radiolarian responses to recent and neogene California El Niño and anti-El Niño events: Palaeogeography, Palaeoclimatology, Palaeoecology, v.53, p.3-25.

Climatic Changes Reflected in Laminated Santa Barbara Basin Sediments

Arndt Schimmelfmann, Carina B. Lange, Joel Michaelsen, and Wolf H. Berger

ABSTRACT: Dating of annually varved sediments of Santa Barbara Basin down to AD 1650 in absence of precise radiometric methods was achieved by (1) counting varves and determining mean annual sedimentation rates from x-radiographs, and (2) correlation with historical rainfall and tree-ring records.

INTRODUCTION

In the ca. 590-meter-deep center of the Santa Barbara Basin 34°11'-34°16'N; 120°01'-120°05'W), about 120 m below sill depth, low oxygen concentrations in near-bottom water exclude bioturbation by macrobenthos. With a high sedimentation rate of about 4 mm per year at the surface, millimeter-scale laminae of alternating light and dark sediment are chronologically deposited and preserved (Soutar and Crill, 1977). Their value as record keepers of the environmental history has long been recognized (see Lange et al., 1987, and references therein).

Precise subsampling of 1-2 mm intervals and core-to-core correlation of partially overlapping, up to 1.5-m-long sediment cores is necessary to recover interannual climate-related information (Schimmelfmann et al., 1989). Lange et al. (1987) and Lange et al. (1989) reported the presence of El Niño deposits of the past 30 years, based on diatom and foraminifera assemblages within the sediment layers, on a year-to-year resolution. They also found a drastic decrease in the diatom flux between the periods AD 1954-1969 and 1970-1986, which reflects large-scale climatic changes in the eastern North Pacific (Lange et al., 1989).

RESULTS AND DISCUSSION

Building upon Soutar and Crill's (1977) pioneering methods and time-scale (spanning 1820-1972), we report here an extended (1650-1987) year-to-year time scale for sediments from the center of the basin, to permit transformation of sediment data into time-series. Sequential counting of annual varves and determination of their thickness on x-radiographs (Figure 1) allows the reconstruction of mean annual sedimentation rates for five large continuous intervals of sediment (Figure 2), using four correlated sediment cores.

Varves could not be counted between ca. 56 to 58 cm depth in core, because burrowing macrobenthos disturbed the record preceding the "AD 1835" pelecypod shell layer (Soutar and Crill, 1977). We set this bioturbated interval to 1831-1834.

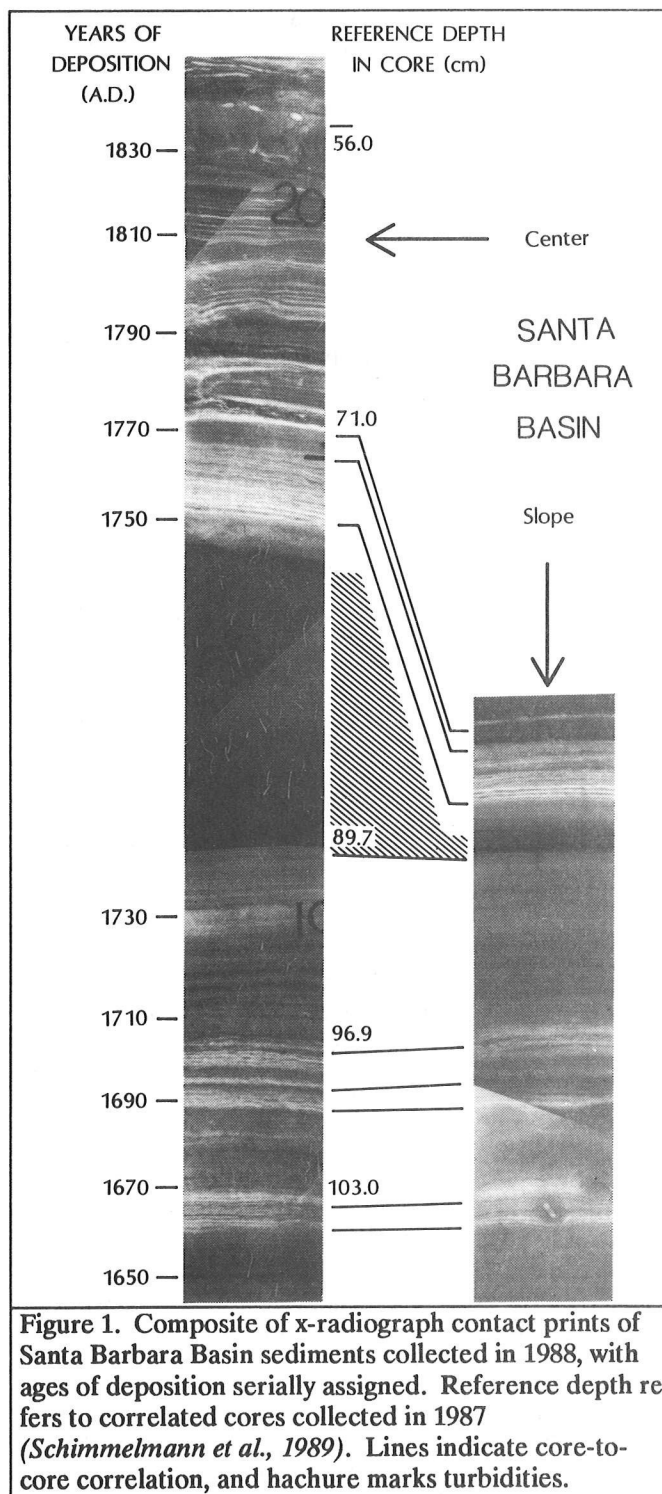


Figure 1. Composite of x-radiograph contact prints of Santa Barbara Basin sediments collected in 1988, with ages of deposition serially assigned. Reference depth refers to correlated cores collected in 1987 (Schimmelfmann et al., 1989). Lines indicate core-to-core correlation, and hachure marks turbidities.

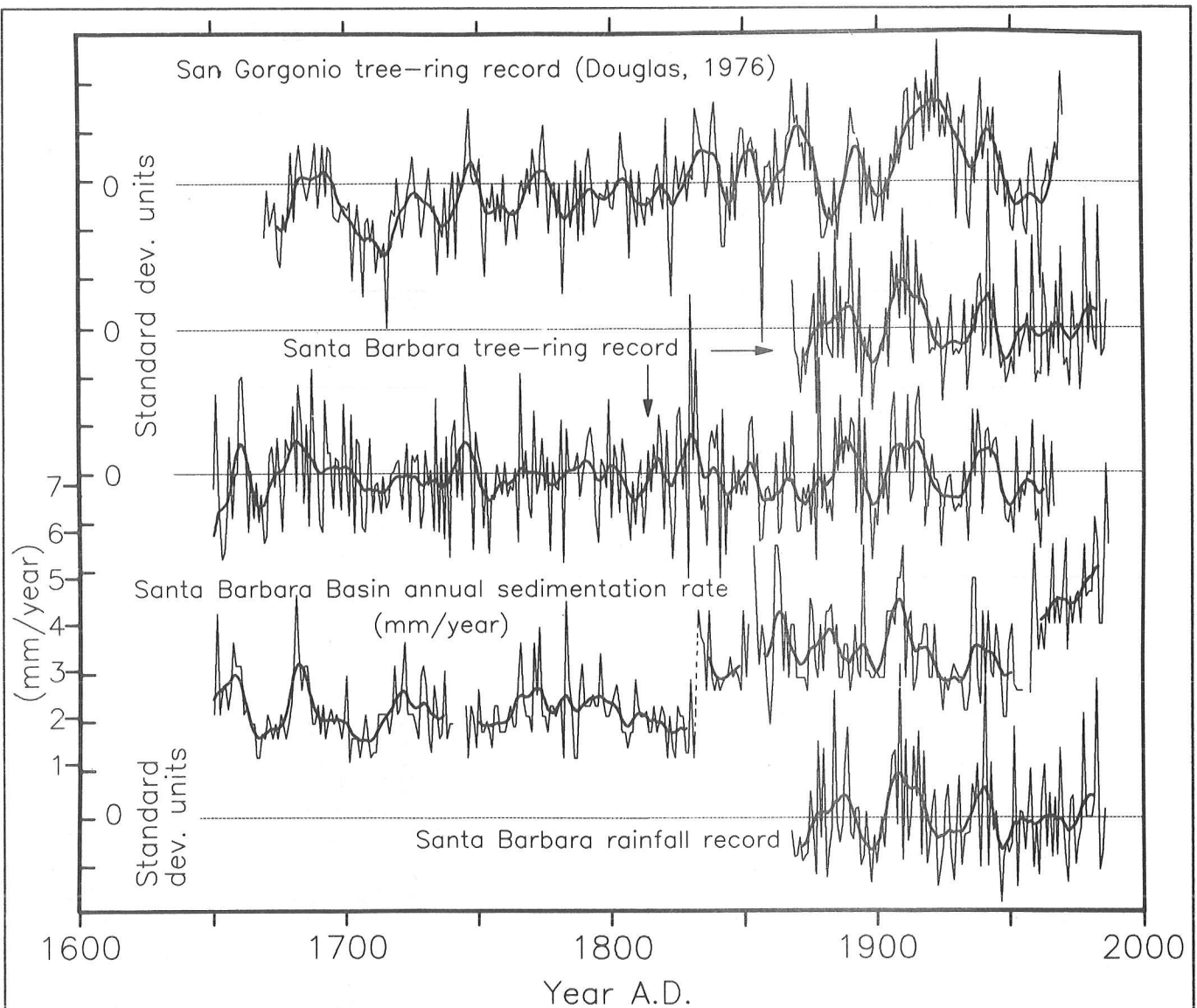


Figure 2. Time series of tree-ring data and historical annual rainfall (all in standard deviation units of the means), and of annual sedimentation rates (in mm/year; determined in cores collected in 1964 by A. Soutar, SIO, and on cruise SABA 88-2). The thickness of a varve decreases through time as water is expelled from the aging sediment, thus causing the long-term trend toward sedimentation rates.

Furthermore, x-radiographs show a lamination-free interval between ca. 78 and 89 cm depth in the center of the basin (34°13.89'N, 120°01.05'W, 580 m isobath). Its color is olive-grey (5/4, on Munsel Soil Color Chart #5Y). Diatom abundances are in the same order of magnitude as in laminated intervals (108×10^5 to 206×10^5 g^{-1} dry sediment). The corresponding lamination-free interval in a core from the northern slope (34°17.82'N, 120°00.02'W, 560 m isobath) measures only 0.7-0.8 cm (Figure 1). With the sedimentation rates of the laminated sediments above and below this layer being about equal in both cores, we agree with Thornton's (1986) diagnosis of its turbiditic origin. We therefore disregard it in the year-counts of our time-series.

The annual sedimentation rates derived from five blocks of continuously varved sediment are further refined by calibration with historical Santa Barbara rainfall records (U.S. Weather Bureau, 1931; National Climatic Data Center, 1985) and with tree-ring records from Santa Barbara County (Michaelsen et al., 1987) and San Bernardino County (Douglas, 1976; Figure 2). The assumption is that tree growth and sedimentation are directly related to precipitation and that there is a lag effect in both (3-7 years; Soutar and Crill, 1977). In this manner, we assign ages to the annual varves. A superimposed running mean (9-notch triangular filter) facilitates comparison of decadal signals.

CONCLUSIONS

Out extended high-resolution time-frame for Santa Barbara Basin sediments down to A.D. 1650 is fundamental for our ongoing efforts:

- To establish a record of historic and prehistoric El Niño events affecting the dynamics of this coastal ecosystem, and
- To produce a long-term record of productivity fluctuations.

This work was supported by NSF grants OCE86-08407 and ATM 87-23024.

REFERENCES

- Douglas, A.V., 1976, Past air-sea interactions over the Eastern North Pacific Ocean as revealed by tree-ring data: Ph.D. dissertation, Tucson, University Arizona, p.196.
- Lange, C.B., Berger, W.H., Burke, S.K., Casey, R.E., Schimmelmann, A., Soutar, A., and Weinheimer, A.L., 1987, El Niño in Santa Barbara Basin: Diatom, Radiolarian and Foraminiferan responses to the 1983 El Niño event: *Marine Geology*, v.78, p.153-160.
- Lange, C.B., Burke, S.K., and Berger, W.H., 1989, Biological production off Southern California is linked to climatic change: ms submitted.
- Michaelsen, J., Haston, L., and Davis, F.W., 1987, 400 years of central California precipitation variability reconstructed from tree-rings: *Water Resources Bulletin*, v.23, p.809-817.
- Munsell Soil Color Charts, 1971, Baltimore, Munsell Color Co., Inc.
- National Climatic Data Center, 1985, Tape data file 3220, summary of the month element digital file: Asheville, North Carolina.
- Schimmelmann, A., Lange, C.B., and Berger, W.H., 1989, Climatically controlled marker layers in Santa Barbara Basin sediments, and fine-scale core-to-core correlation: ms submitted.
- Soutar, A., and Crill, P.A., 1977, Sedimentation and climatic patterns in the Santa Barbara Basin during the 19th and 20th centuries: *Geological Society of America Bulletin*, v.88, p.1161-1172.
- Thornton, S.E., 1986, Origin of mass flow sedimentary structures in hemipelagic basin deposits: Santa Barbara Basin, California Borderland: *Geological-Marine Letters*, v.6, p.15-19.
- U.S. Weather Bureau, 1931, Summary of climatological data for the United States: *Bulletin W*, Second Edition.

A Modern Pollen Record from the Central Gulf of California

K.H. Orvis, T.R. Baumgartner, R. Byrne, and L.D. Wright

ABSTRACT: As one facet of an effort to tie the pollen record of central Gulf of California deep cores (Byrne et al., this volume) to modern analogs, pollen was analyzed in the uppermost 150-200 years of varved core 7807-1410 taken nearby. Sampling at 2- to 8-year resolution yielded a noncomplacent record, suggesting pollen in these sediments may be a potential high resolution proxy record of short-term climatic events. The pollen spectrum as a whole matches that of uppermost DSDP Site 480 (means of all samples). Lack of a ratio or influx shift following damming of local rivers and a surplus of low-spine Compositae pollen relative to mainland sites support Baumgartner's theory that terrigenous influx to the site is largely acolian and also suggest that a significant fraction of the pollen influx may come from Baja California.

INTRODUCTION

Cores taken at Deep Sea Drilling Project Sites 479 and 480 (Byrne et al., this volume) have yielded a rich pollen record extending to the mid-Pleistocene. Much of the length of those cores is varved, potentially allowing high resolution analysis. To bring the fossil record up to the present and to tie it to modern marine (Cross et al., 1966) and mainland (Orvis, 1985) pollen surface samples, analysis was undertaken of samples from similarly varved short core 7807-1410 taken nearby (Figure 1) in 1978 by Baumgartner and others, using an open-vented box corer (Soutar, 1978).

Objectives of the study were twofold:

- First, to see whether higher resolution analysis of pollen from these varved sediments could provide any information regarding patterns of pollen production and processes of sediment transport and accumulation on the Guaymas slope.
- Second, to see whether modern human disturbance has greatly altered the regional pollen spectrum. (If it has, the applicability of modern surface pollen studies would be called into question.)

METHODS

Samples were taken from a 43-cm column about 3x1 cm, at an outside corner of the core, and were cut along varve boundaries as nearly as possible. Samples were prepared routinely according to procedures adapted to the long core material (Byrne, 1982), with *Lycopodium* tracers added to allow influx calculations. Unfortunately

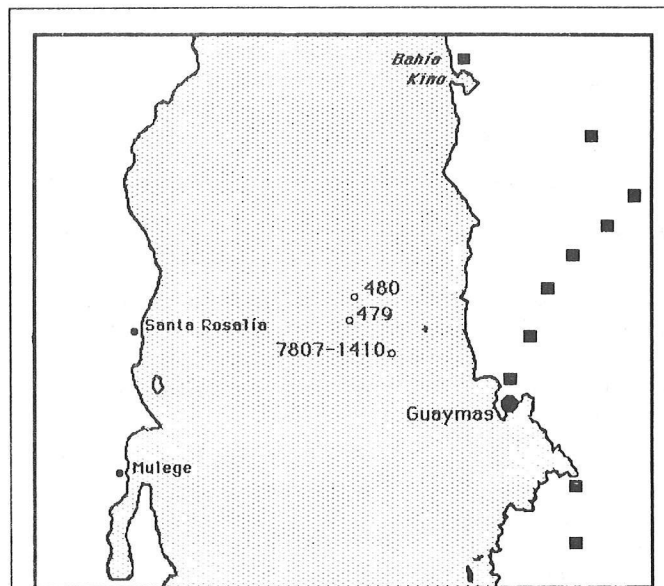


Figure 1. Map of central Gulf of California showing sites referred to in text. Squares mark mainland sample sites within map area.

the samples were too small, given the relatively low pollen concentrations of uncompacted near-surface sediments; two samples were abandoned, and many others were combined. Samples as counted contained 2 to 10 varves.

Pollen counts reported here were made by L.D. Wright after a preliminary series of calibration counts by both Wright and R. Byrne. Discussion in this paper is limited to major taxa, for which discrepancies between analysts are least likely to occur. Sample size limited count totals in some cases (average count was 204, with four counts below 100 and eight others below 200), so the diagram must be regarded as preliminary; comparisons will be based on summed counts (Table 1).

RESULTS

The uppermost sample on the diagram (Figure 2; horizontal units are grains per square centimeter per year) extends through 1967, and individual varves have been accurately dated as far back as 1907 despite non-conformities, by cross-correlating varve patterns with other local cores (Baumgartner et al., 1988a). Using the reconstructed varve sequence, the base of the 18.5 cm sample corresponds approximately to June 1908. A

In J.L. Betancourt and A.M. MacKay, editors, 1990. Proceedings of the Sixth Annual Pacific Climate (PACLIM) Workshop, March 5-8, 1989: California Department of Water Resources, Interagency Ecological Studies Program Technical Report 23.

Table 1. Pollen spectra for comparison; see text. N is total pollen counted in samples; other values are within-table percentages (rows sum to 100) to facilitate comparison of material from different studies.

	N	<i>Pinus</i>	T-C-T	<i>Quercus</i>	<i>Dodo- nea</i>	<i>Celtis</i>	<i>Arte- misia</i>	Low-Sp. Comp.	Hi-Sp. Comp.	E-R-A	Gramin- eae	Cheno- Am.
Core 1410, Post-1958:	834	15.5	0.0	13.8	1.5	0.2	0.6	21.2	6.2	1.4	8.9	30.8
Core 1410, Pre-1908:	2,316	17.0	0.0	9.9	0.9	0.5	1.3	27.2	4.2	1.9	9.9	27.3
Site 480, 0-160 cm:	2,140	9.2	1.9	9.8	0.0	1.0	1.4	28.0	4.1	1.3	13.3	30.1
Adjacent Mainland:	6,042	0.7	0.1	0.5	0.0	2.7	0.0	2.6	13.9	15.6	40.2	23.7
Bahía Kino Sample:	446	0.6	0.0	0.0	0.0	2.7	0.0	45.0	10.9	21.9	3.8	15.1
Core 1410, Semi-homogen.:	451	10.3	0.0	9.8	0.1	0.2	1.2	42.1	4.4	0.7	5.6	25.5

major discontinuity prevents accurate dating farther down, but ^{210}Pb dating suggests that this and several minor discontinuities represent relatively few lost years, and the 85 varves in the lower samples probably place the bottom of the diagram near 1800.

The diagram is far from complacent, exhibiting marked change on two scales. Adjacent samples often differ, suggesting the record is sensitive to short-term changes in pollen production, transport or deposition; and longer-term trends are evident as well. For example, *Pinus*, *Quercus*, and Gramineae are relatively prominent at the top and bottom and much less so in the center, while low-spine Compositae and Cheno-Am (Chenopodiaceae/Amaranthaceae) remain very prominent in the center.

Absent from the diagram is any evidence of influx diminution. In fact, the top two samples, which include material deposited from 1958-1967 after lower-basin dams were in place on all major central Gulf rivers (Baumgartner et al., 1988b), exhibit the highest and third highest overall influx rates, at 3,337 and 2,650 grains per cm^2 per year. These rates are due in part to high influxes of Cheno-Am, which on the adjacent mainland is typically associated with human disturbance, especially irrigated agriculture (Orvis, 1985), which expanded greatly following completion of the dams.

Even with the rise in Cheno-Am, the averaged pollen spectrum of the two uppermost samples closely resembles that of the pre-1908 samples, while both resemble that of the upper 160 cm of DSDP Site 480 (Table 1; see also Byrne et al., this volume).

None of these, however, closely resembles the spectrum averaged from adjacent mainland samples (Table 1 and Figure 1). Many of the contrasts between the marine and mainland spectra can be expected — *Pinus* and *Quercus* percentages tend to increase offshore due to their excellent transport characteristics, for instance — but the high marine concentration of low-spine Compositae is difficult to explain. The nearest mainland region with commonly comparable low-spine concentrations lies over 250 km to the northeast (Orvis, 1985; compare also Hevly et al., 1965).

One single lowland sample, from near Bahia Kino to the north of the core sites (Figure 1; see Orvis, 1985), yielded a low-spine Compositae concentration comparable to that of the marine spectra (Table 1). Interestingly, the sample site was located in a narrow northern mainland coastal band within which — and nowhere else on the mainland — many of the unique floristic elements endemic to central Baja California can be found. Thus it is conceivable, if the endemism is climatically induced, that low-spine Compositae may be an important pollen constituent in central Baja California.

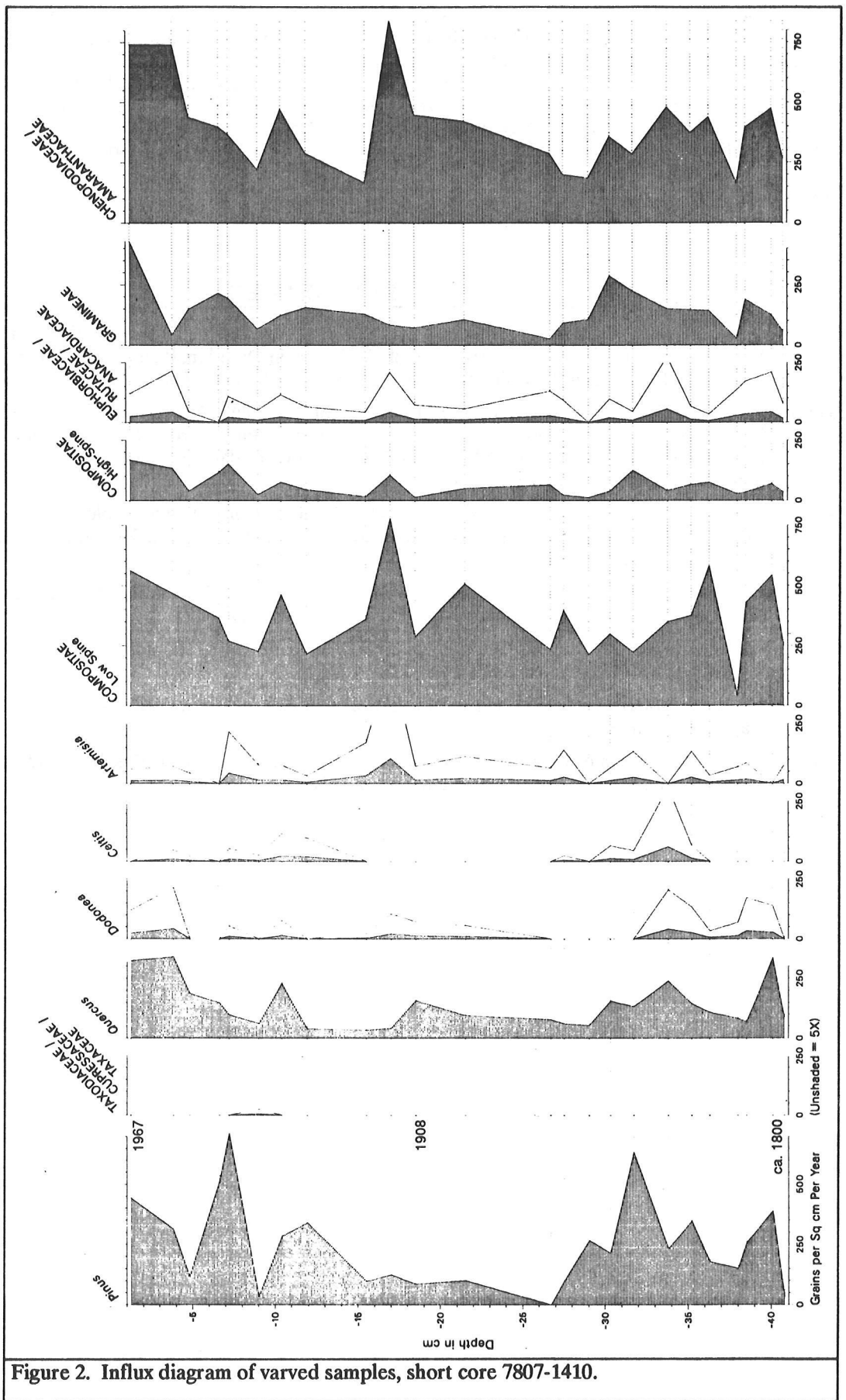
In addition to the varved material, the core contained “lenticular or tabular bodies” (Baumgartner et al., 1988a) of homogeneous material. Pollen concentrations in this material were extremely low: one pure sample could not be counted at all, while two others yielded concentrations of 536 and 1,776 grains per gram wet weight respectively (the mean for varved samples was 6,787, with a standard deviation of 2,179). Samples of or containing homogeneous material were excluded from the diagram, but all such counts have been summed in the last line of Table 1; the very limited data obtained suggest the contrast with the spectra of varved samples would be more striking in pure homogeneous material.

DISCUSSION

Each of the stated objectives of the study was served admirably, in spite of poorer stratigraphic resolution and some lower counts than expected. The short-term variability observed (even among very robust counts) augurs well for the pollen record's utility as a proxy climate record; a high resolution study of the most recent century could be very rewarding.

In any future study, stratigraphic resolution should be as high as possible and the sequence as complete as possible, making full use of the reconstructed varve sequence (see Baumgartner et al., 1988a). Varved samples must contain at least 5-7 g of wet sediment to ensure statistically robust counts, and homogeneous samples at least 15-20 g.

The impact of human disturbance on the Gulf of California pollen record is reassuringly limited and, in



fact, surprisingly so. Beginning with Hoover Dam on the Colorado River in 1936, dams and the attendant use of water for irrigation have drastically cut fluvial sediment transport to the Gulf, yet pollen influx at the core site remained as strong as before, with a virtually unchanged pollen spectrum. This serves as strong independent corroborating evidence for Baumgartner's conclusion (Baumgartner et al., 1988b) that much of the terrigenous flux at the core site is aeolian rather than fluvial.

The high concentrations of low-spine Compositae pollen in the Gulf cannot be adequately explained by differential long distance transport or other sorting of pollen originating on the mainland. The alternative hypothesis, obliquely supported by the pollen spectrum of the Bahia Kino mainland sample, is that a significant fraction of the cores' pollen influx originates in Baja California. This should be tested.

REFERENCES

- Baumgartner, T.R., Ferreira-Bartrina, V., Cowen, J., and Soutar, A., 1988a, Reconstruction of a Twentieth Century Varve Chronology from the Central Gulf of California, in Dauphin, P., and Simoneit, B., editors, *The Gulf of Peninsular Province of the Californias: American Association of Petroleum Geologists, Memoirs* (in press).
- Baumgartner, T.R., Ferreira-Bartrina, V., and Moreno-Hentz, P., 1988b, Varve Formation in the Central Gulf of California: A reconsideration of the Origin of the Dark Laminae from the Twentieth Century Varve Record, in Dauphin, P., and Simoneit, B., editors, *The Gulf and Peninsular Province of the Californias: American Association of Petroleum Geologists, Memoirs* (in press).
- Byrne, R., 1982, Preliminary Pollen Analysis of Deep Sea Drilling Project Leg 64, Hole 480, Cores 1-11, in Curran, J.R., Moore, D.G., et al., *Initial Reports of the Deep Sea Drilling Project, v.LXIV, pt.2*, Washington DC, U.S. Government Printing Office, p.1225-1237.
- Cross, A.T., Thompson, G.G., and Zaitzeff, J.B., 1966, Source and Distribution of Palynomorphs in Bottom Sediments, Southern Part of Gulf of California: *Marine Geology*, v.4, p.467-524.
- Hevly, R.H., Mehringer, P.H. Jr., and Yocum, H.G., 1965, Modern Pollen Rain in the Sonoran Desert: *Journal of the Arizona Academy of Science*, v.3, p.123-135.
- Orvis, K.H., 1985, Modern Surface Pollen and the Tropical Margin of the Sonoran Desert: Master's thesis, University of California at Berkeley, 82pp.
- Soutar, A., 1978, Collection of Benthic Sediment Samples: Southern California Baseline Study Benthic Year II, Final Report to Bureau of Land Management, v.2, pt.4, No.2, 54pp.

A Pollen/Dinoflagellate Chronology for DSDP Site 480, Gulf of California

Roger Byrne, Peta Mudie, and Andrew Soutar

ABSTRACT: DSDP Site 480 in the Gulf of California represents a paleoclimatic record of great potential significance. Much of the 152-meter section is varved, which means that proxy records of climatic change can be analyzed with unusual precision on a variety of time scales. In this paper we present pollen and dinoflagellate evidence that suggests that the base of the section is much older than was previously thought. We propose a basal date of between 300,000 and 350,000 YBP.

INTRODUCTION

In December 1978, the Glomar Challenger entered the Gulf of California as part of Leg 64 of the Deep Sea Drilling Project. Two of the coring sites produced cores of potential paleoclimatic significance: Site 479 and Site 480 on the Guaymas Slope. Together they provide a virtually complete record extending back at least a million years (Curry and Moore et al., 1982).

Most of the Site 480 section is varved. It therefore provides an unusual opportunity to reconstruct the history of climatic change on a variety of time scales. However, this potential has not been fully realized because of uncertainty as to the chronology of the pre-Holocene section. The basic problem has been that the limited number of calcareous foraminifers in the varved sections has prevented establishment of an oxygen isotope chronology.

PREVIOUS CHRONOLOGICAL ESTIMATES

Speculation as to the period of time represented by Site 480 began onboard ship, when it was recognized that it included a sequence of laminated and nonlaminated sections. Preliminary varve counts suggested that the upper 10 meters represented the Holocene, and that the preceding nonlaminated section must, therefore, date to the late-Pleistocene. On the assumption that laminated = interglacial and nonlaminated = glacial, several attempts were made to correlate the sequence with dated oxygen isotope curves. Schrader et al. (1980) concluded that the whole section might represent the last 300,000 to 400,000 years. They also suggested that 250,000 years would be a minimum basal date, and that Isotope Substage 5e was located between Cores 11 and 13. Soutar et al. (1982) slabbed and x-radiographed most of the section and made some preliminary varve counts. On this basis, they concluded that the upper

100 m was approximately equivalent to the last 100,000 years and that the base of the section would date to about 210,000 YBP.

Diatoms are particularly abundant in the Guaymas Slope sediments, and several investigators have used them in an attempt to date the Site 480 section. Schrader (1982) noted the presence of the diatom *Nitzschia fossilis* in core 29 (ca. 140 m) and accordingly made a tentative age estimate of ca. 260,000 years for that level. LeClaire and Kelts (1982) took the Schrader and Soutar estimates to produce a composite age/depth graph on which the basal date estimates range from 163,000 to 250,000 years. They also speculated that a silt and sand layer and a diagenetic carbonate layer in Cores 20 and 21 corresponded to an early part of Isotope Substage 5e.

Bromble and Burckle (1982) also used diatoms in an attempt to provide a chronology. They used size changes in *Coscinodiscus nodulifer* as a general index of climatic change, the assumption being that a low ratio of small to large diatoms is indicative of interglacial conditions. The *Coscinodiscus* index located Isotope Stage 2 in Core 4, Section 1 (ca. 15 m) and the Stage 3/2 boundary in Core 5, Sections 1-2 (ca. 20 m). There was no clear indication of Isotope Substage 5e, but extrapolation of sedimentation rates placed it in Core 22 at 105m.

In the Leg 64 Initial Reports volumes, both Byrne (1982) and Heusser (1982) dealt with the Site 480 pollen record. Both reported the presence of potentially useful climatic indicators, such as *Picea* and *Artemisia*; however, no detailed interpretations were made because of the dating problem. Byrne's diagram covered the upper 50 m of the section and appeared to represent a large part of the last glacial cycle. A chronology based on pollen concentration and influx rates suggested that the base of the diagram was ca. 75,000 YBP. Byrne also concurred with Schrader et al. (1980) that Isotope Substage 5e was probably located somewhere in the unrecovered section of Cores 11 and 12.

A COMPOSITE POLLEN RECORD (Site 479 + Site 480)

Site 479 is located 6.8 km to the southeast of Site 480 on a deeper part of the Guaymas Slope (Figure 1). It was drilled with the conventional DSDP rotary drill; recovery for the upper 50 m was, therefore, poor. The overall stratigraphy of the two sites is generally comparable, although some discrepancies are apparent (Curry and Moore et al., 1982).

In J.L. Betancourt and A.M. MacKay, editors, 1990. Proceedings of the Sixth Annual Pacific Climate (PACLIM) Workshop, March 5-8, 1989: California Department of Water Resources, Interagency Ecological Studies Program Technical Report 23.
Geological Survey of Canada Contribution No. 35290.

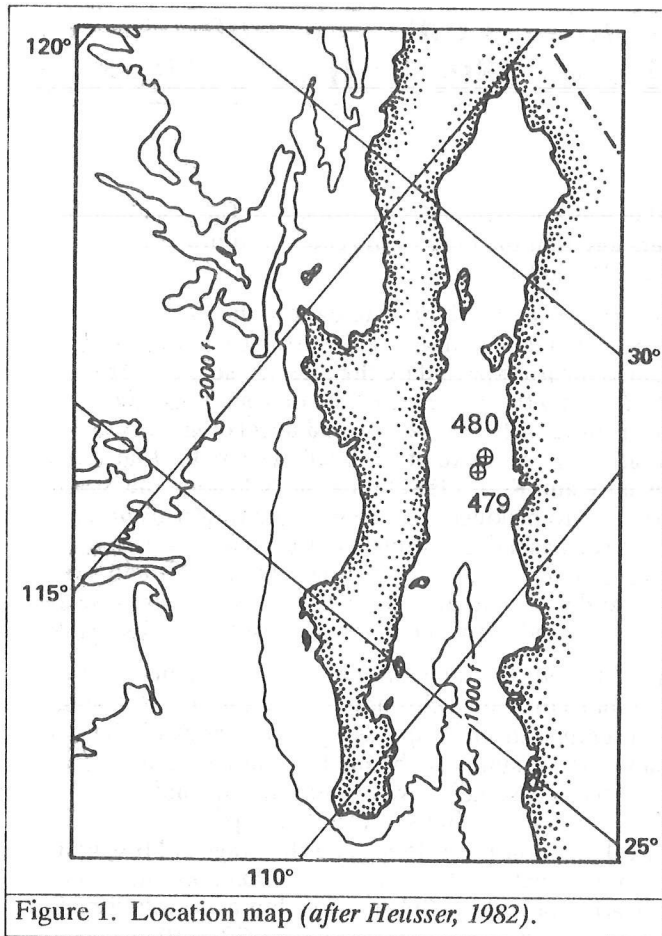


Figure 1. Location map (after Heusser, 1982).

Sirkin (1982) analyzed the pollen content of a series of samples from Site 479 and found some evidence of significant climatic change; for example, spruce and juniper pollen in Core 17 Section 3. The record as a whole, however, was a complacent one. Insofar as Byrne's relatively close interval sampling of the upper 50 m of Site 480 had uncovered what appeared to be a large part of the last glacial cycle, it was decided to resample the upper 150 m of the Site 479 section at 2-meter intervals. Initial counts showed that the prominent Chenopodiaceae/Amaranthaceae peak that was encountered in Core 10 (43.07 m) at Site 480 was located in Core 5 (34.76 m) at Site 479, and in this way it was possible to combine the two records (Figure 2).

Six paleoclimatically sensitive pollen types are shown in Figure 2. The three cool climate indicators are *Picea*, *Artemisia*, and the *Juniperus*-type. All three are rarely encountered in surface samples from the Gulf, which is not surprising in view of their present distribution. *Picea* has a very restricted range in the Sierra Madre; *Artemisia* is mainly restricted to the northern part of Baja and the higher parts of the Sierra Madre; and *Juniperus* is likewise more important in the north and in cool and xeric habitats in the Sierra.

Three pollen types are included as warm climate indicators: Gramineae, the ERA-type, and Chenopodiaceae/Amaranthaceae. These pollen types are more difficult to categorize geographically. The ERA-type is as yet

unidentified but most likely is referable to the Euphorbiaceae, Rutaceae, or Anacardiaceae. Gramineae pollen in the Gulf area is more common to the south (Orvis 1985), which suggests it is primarily a reflection of increasing summer rainfall; however, it is impossible to say which taxa are involved. The Chenopodiaceae/Amaranthaceae group is often thought of as an indicator of desert salt flats, but in this case coastal salt marshes could also have been an important source area.

The pollen record suggests that the glacial/interglacial cycles have not all been of the same wavelength or amplitude. It is tempting to try to correlate a curve such as this with the oxygen isotope stratigraphy, but the problem is that pollen evidence alone cannot distinguish between interglacial and interstadial events. For example, the prominent Chenopodiaceae/Amaranthaceae peak at ca. 43 m appears to be very similar to the mid-Holocene peak at 4 m, and one might therefore assume that it is equivalent to Isotope Stage 5; however, another interpretation would be that it is simply Isotope Stage 3, the mid-Wisconsin interstadial.

On a more positive note, Site 479 has been useful insofar as it has clarified the status of the Site 480 gap (49 m to 61.75 m), which had been proposed by several investigators as being the likely location of Isotope Substage 5e (Schrader et al., 1980; Byrne, 1982). The high values of *Artemisia* and *Juniperus*-type pollen in the equivalent section of Site 479 indicate quite clearly that it corresponds to a glacial stage, not an interglacial.

THE DINOFLAGELLATE RECORD

As we indicated above, the pollen record alone cannot resolve the Site 480 chronology problem because of uncertainty as to what is an interglacial versus an interstadial signal. The dinoflagellate record provides valuable supplementary evidence that helps resolve the problem. Little attention was paid to dinoflagellates in the Initial Reports volumes of Leg 64. Heusser (1982) quantified the total abundance of gonyaulacoid cysts (i.e., spinose hystrichosphaeres), but did not count peridinioid cysts (pers comm, 1989). The latter are indicators of upwelling conditions on some continental margins (Wall et al., 1977). According to Heusser (1982), in some parts of the section (for example, between 120 m and 152 m sub-bottom) the concentration of gonyaulacoid cysts is so high as to decrease the relative frequency of pollen.

On the assumption that changes in the frequencies of indicator dinoflagellate species might help resolve the Site 480 chronology problem, Mudie counted all the dinoflagellate cysts and acritarchs in 51 productive samples from both Sites 479 and 480, at levels where the pollen record indicated either probable glacial or interglacial conditions.

The most important initial results are shown in Figure 3 as percentage diagrams for total peridinioid cysts (P-type dinocysts) and for *Hemicystodinium zoharyi*, a gonyaulacoid cyst that is a well known indicator of warm, saline tropical/subtropical waters (Wall and

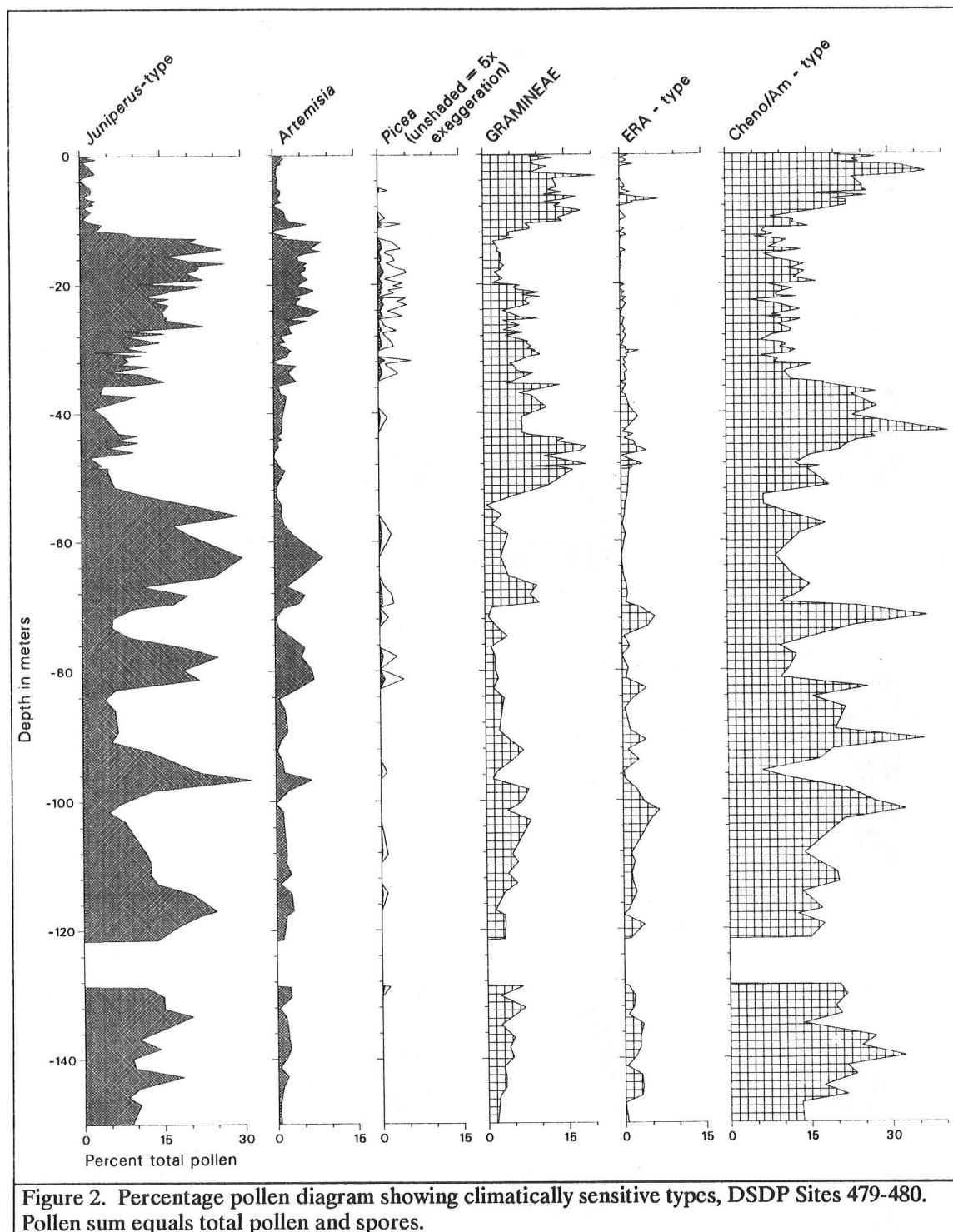


Figure 2. Percentage pollen diagram showing climatically sensitive types, DSDP Sites 479-480. Pollen sum equals total pollen and spores.

Dale, 1969; Wall et al., 1977; Morzadec-Kerfourn, 1979). *H. zoharyi* is the cyst-form of the bioluminescent phytoplankton species *Pyrodinium bahamense*, which causes red tides, shellfish poisoning, and fish kills due to anoxia in tropical estuaries (Maclean, 1979).

The pollen index in Figure 3 is the sum of the interglacial indicators as a percentage of themselves plus the glacial indicators. The proposed correlation with the global oxygen isotopic stratigraphy is given on the left. Of particular interest here is the occurrence of *H.*

zoharyi in high concentrations at depths of 48 m and 145 m.b.s.f. *H. zoharyi* is generally indicative of warm, saline surface water (ca. 24-30°C, 36-38 ppt salinity). A peak of this dinocyst also occurs at 14-16 m.b.s.f., in the Stage 2/1 transition, which has a C-14 age of 16,820 ± 340 YBP (Spiker and Simoneit, 1982). Similar spikes of *H. zoharyi* at the Stage 2/1 transition have been reported for Mediterranean Sea cores (Morzadec-Kerfourn, 1979), and a series of interglacial peaks were found in Red Sea Pleistocene cores (Wall and Dale,

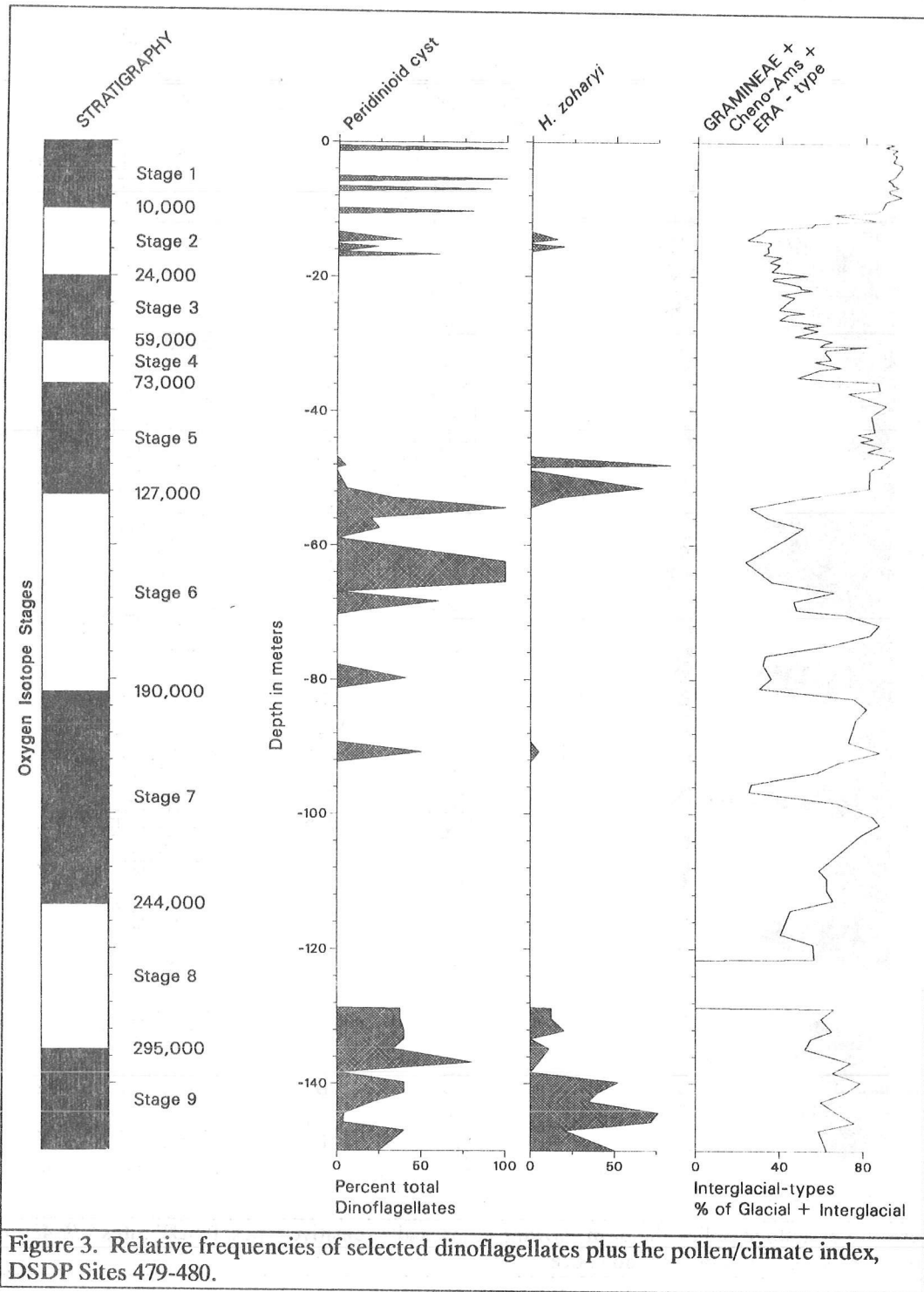


Figure 3. Relative frequencies of selected dinoflagellates plus the pollen/climate index, DSDP Sites 479-480.

1969). The high percentages of warm climate pollen indicators at the same levels or just above the dinocyst peaks strongly supports the idea that these were interglacial rather than interstadial intervals. The 48 m peak is, therefore, almost certainly equivalent to Isotope Substage 5e. This age pick is further supported by the last common occurrence of the dinoflagellate *Achomosphaera andalusiense* in this interval (at 55.9 m), and a high percentage of other gonyaulacoid cysts in addition to *H. zoharyi* and *A. andalusiense*. Of particular note is

the presence of large percentages of *Spiniferites mirabilis*, which is known to be a marker of Stage 5e in Mediterranean and Atlantic Ocean cores (Mudie, 1986; Aksu et al., 1988).

If our identification of Stage 5e is correct, it follows that the largely non-varved section from 43 m to 13.5 m includes not only Stages 2, 3, and 4, but also Substages 5b, 5c and 5d. If we further assume there is no erosional hiatus, it follows that the sedimentation rate was ca. 0.30 m/1000 years. This is significantly less than the

varve deposition rate for the Holocene of 0.8 m/1000 years, but it agrees quite well with an average sedimentation rate of 0.43 m/1000 years, which is obtained by assuming the first appearance (FAD) of the coccolith *Gephyrocapsa oceanica* at 250.15 m.b.s.f. at Site 479 corresponds to an age of 0.6 million years (Aubrey, 1982). The coccolith age pick also gives an age of ca. 115,000 years for 50 m.b.s.f., which is clearly much closer to the age of interglacial Stage 5e than interstadial Stage 3.

The age of the *H. zoharyi* peak at 145 m is more problematic in that the warm climate pollen index shows three peaks in the overlying interval, at 70 m, 90 m and 100 m, whereas *H. zoharyi* only shows small peaks at 90 m and ca. 110 m. One possibility is that all four pollen peaks represent interglacials; i.e., Isotopic Stages 7 (70 m), 9 (90 m), 11 (100 m), and 13 (145 m). This chronology would date the lower peak as ca. 0.478 million years, which seems much too old relative to estimated sedimentation rates and the FAD of *G. oceanica*. It seems more likely, therefore, that the pollen and dinoflagellate peaks represent Isotope Stages 7a (90 m) and 7c (100 m) and that the series of peaks around 145 m correspond to Stage 9. The short-lived pollen peak at 70 m would then correspond to an interstadial within glacial Stage 6, several of which have been found in the North Atlantic (Ruddiman et al., 1986).

There are several reasons we prefer this interpretation. The Site 480 core descriptions show that below the washed-out sandbed, there is a predominantly non-laminated section from 61.75 to 76.0 m. Most likely this bioturbated zone, plus the missing section, represents glacial Isotope Stage 6. The Site 479 pollen record clearly shows this interval is dominated by cool climatic indicators. The dinoflagellates are mostly dominated by low numbers of peridinioids, which also characterize upper Stage 6 in the North Atlantic (Mudie and Aksu, 1984; Aksu et al., 1988).

Good evidence of the preceding glacial (Stage 8) may be missing at both Site 480 and Site 479 because of gaps at Core 24 (114-119 m.b.s.f.) and Core 13 (122-128 m), respectively. Most of the lower half of the Site 480 section (76 to 152 m) is varved. Detailed measurements of the varves have not yet been made, but shipboard counts (Curry and Moore et al., 1982) indicate that individual varve thickness varies from 0.2 to 1.0 mm. Assuming an average varve thickness of 0.5 mm (probably minimal because photographic data from the base shows an aver-

age of 0.5 mm; [Kelts and Niemitz, 1982, p.1204]), then the 60-meter varved section from 76 to 140 m would only represent ca. 120,000 years of sedimentation. This is clearly not enough to make the interglacial peak at 145 m the equivalent of Isotope Stage 13, even allowing for an additional 50,000 years for the missing part of Stage 8.

The most plausible explanation for the sequence of warm climate pollen and dinoflagellate indicators below 50 m is that the 145 m interglacial interval is equivalent to Isotope Stage 9. This suggests that the three warm pollen index peaks at 70, 90, and 100 m represent an interstadial in Isotopic Stage 6 (e.g., Stage 6.4, 151,000-171,000 YBP, of Ruddiman et al, 1986) at 70 m, and Isotope Stages 7a and 7c at 90 and 100 m, respectively. This interpretation is supported by several different lines of evidence:

- The occurrence of a short interval of varved sediments in the stratigraphic equivalent Stage 6 interstadial at Site 480;
- The appearance of a small peak in gonyaulacoid dinocysts at about 70 m in Site 480 (Heusser, 1982)
- A small peak of *H. zoharyi* at 90 m in Site 479, together with the presence of the gonyaulacoid species *Achomosphaera andalousiense*, which is a marker for Isotope Stage 7 in the western North Atlantic (de Vernal and Mudie, in press).

At Site 479, *A. andalousiense* has its last acme at 134.8 m.b.s.f. If this depth is close to the Stage 9/8 boundary, then this datum would be roughly correlative with the chronostratigraphy of Harland (1988) for boreholes in the North Sea, where the last major peak of *A. andalousiense* occurs in lower Isotope Stage 8.

CONCLUSIONS

Paradoxically, the chronology presented here is broadly equivalent to one of the first proposals of the shipboard party, namely that the base of the Site 480 section would date to between 300,000 and 400,000 years before present (Schrader et al., 1980). However, it differs from all of the subsequent estimates in that Isotope Substage 5e is placed in Core 10 and in that the base of the section is assumed to date to between 300,000 and 350,000 years before present; that is, between Isotope Stages 9 and 10.

REFERENCES

- Aksu, A.E., Mudie, P.J., Macko, S.A., and de Vernal, A., 1988, Upper Cenozoic history of the Labrador Sea, Baffin Bay, and the Arctic Ocean: a paleoclimatic and paleoceanography summary: *Paleoceanography*, v.3, p.519-538.
- Aubrey, M.P., 1982, Calcareous nanofossil biostratigraphy, Leg 64, in *Initial Reports Deep Sea Drilling Project*, v.64, Washington, DC, U.S. Government Printing Office, p.955-971.
- Bromble, S.L., and Burckle, L.H., 1983, A Late Quarternary stratigraphy for DSDP Site 480, Gulf of California: *Marine Micropaleontology*, v.7, p.541-543.
- Byrne, R., 1982, Preliminary pollen analysis of Deep Sea Drilling Project Leg 64, Hole 480, Cores 1-11, in *Initial Reports Deep Sea Drilling Project*, v.64, Part 2: Washington, DC, U.S. Government Printing Office, p.1225-1237.

- Curray, J.R., and Moore, D.G., et al., 1982, Guaymas Basin Slope: Sites 479 and 480, *in* Initial Reports Deep Sea Drilling Project, v.64, Part 1: Washington, DC, U.S. Government Printing Office, p.417-504.
- de Vernal, A., and Mudie, P.J., Late Pliocene to Recent palynostratigraphy at ODP Sites 646 and 647, eastern and southern Labrador Sea, *in* Initial Reports ODP 105, Part B.
- Harland, R., 1988, Quarternary dinoflagellate cyst biostratigraphy of the North Sea: *Paleontology*, v.31, p.78-82.
- Heusser, L.E., 1982, Pollen analysis of laminated and homogeneous sediment from the Guaymas Basin, Gulf of California, *in* Initial Reports Deep Sea Drilling Project, v.64, Part 2: Washington, DC, U.S. Government Printing Office, p.1217-1223.
- Kelts, K., and Niemitz, J., 1982, Preliminary sedimentology of Late Quarternary diatomaceous muds from Deep Sea Drilling Project Site 480, Guaymas Basin Slope, Gulf of California, *in* Initial Reports Deep Sea Drilling Project, v.64, Part 1: Washington, DC, U.S. Government Printing Office, p.417-504.
- LeClaire, J.P., and Kelts, K., 1982, Calcium carbonate and organic carbon stratigraphy of Late Quarternary laminated and homogeneous diatom oozes from the Guaymas Slope, HPC Site 480, *in* Initial Reports Deep Sea Drilling Project, v.64, Part 2: Washington, DC, U.S. Government Printing Office, p.1263-1275.
- Maclean, J.L., 1979, Indo-Pacific red tides, *in* Taylor, D.L., and Seliger, H.H., eds., Toxic dinoflagellate blooms: Developments in Marine Biology, v.1, p.173-178.
- Morzadec-Kerfourn, M.T., 1979, Les kystes de Dinoflagelles: *Geologie Mediterranee*, v.6, p.221-246.
- Mudie, P.J., 1986, Palynology and dinoflagellate biostratigraphy of DSDP Leg 94, Sites 607 and 611, North Atlantic Ocean, *in* Initial Reports Deep Sea Drilling Project, v.94: Washington, DC, U.S. Government Printing Office, p.785-812.
- Mudie, P.J., and Aksu, A.E., 1984, Paleoclimate of Baffin Bay from 300,000-year record of foraminifera, dinoflagellates and pollen: *Nature*, v.312, p.630-634.
- Orvis, K.H., 1985, Modern surface pollen and the tropical margin of the Sonoran Desert: Unpublished master's thesis, University of California, Berkeley, 82p.
- Ruddiman, W.F., Shackleton, N.J., and McIntyre, A., 1986, North Atlantic sea-surface temperatures for the last 1.1 million years, *in* Summerhayes, S.P., and Shackleton, N.J., eds., North Atlantic Paleooceanography, Geological Society Special Publication No. 21, p.155-173.
- Schrader, H., 1982, Diatom biostratigraphy and laminated diatomaceous sediments from the Gulf of California, Deep Sea Drilling Project Leg 64, *in* Initial Reports Deep Sea Drilling Project, v.64, Part 2: Washington, DC, U.S. Government Printing Office, p.973-981.
- Schrader, H., et al., 1980, Laminated diatomaceous sediments from the Guaymas Basin Slope (Central Gulf of California): 250,000 year climate record: *Science*, v.207, p.1207-1209.
- Sirkin, L., 1982, Preliminary palynology of Pleistocene sediments from Deep Sea Drilling Project Sites 474 and 479, *in* Initial Reports Deep Sea Drilling Project, v.64, Part 2: Washington, DC, U.S. Government Printing Office, p.1211-1215.
- Soutar, A., Johnson, S.R., Taylor, E., and Baumgartner, T.R., 1982, X-Radiography of Hole 480: Procedures and results, *in* Initial Reports Deep Sea Drilling Project, v.64, Part 2: Washington, DC, U.S. Government Printing Office, p.1183-1190.
- Spiker, E.C., and Simoneit, B.R.T., 1982, Radiocarbon dating of Recent sediments for Leg 64, Gulf of California, *in* Initial Reports Deep Sea Drilling Project, Washington, DC, U.S. Government Printing Office, p.757-758.
- Wall, D., and Dale, B., 1969, The "Hystriochosphaerid" resting spore of the dinoflagellate *Pyrodinium bahamense*, Plate, 1906: *Journal of Phycology*, v.5, p.149-149.
- Wall, D., Dale, B., Lohmann, G.P., and Smith, W.K., 1977, The environmental and climatic distribution of dinoflagellate cysts in modern marine sediments from regions in the north and south Atlantic Oceans and adjacent seas: *Marine Micropaleontology*, v.2, p.121-200.

Can a Climate Record Be Extracted from Giant Sequoia Tree Rings?

M.K. Hughes, B.J. Richards, T.W. Swetnam, and C.H. Baisan

ABSTRACT: Extreme low growth events in giant sequoia ring-width index series coincide with severe droughts in the San Joaquin drainage, on whose eastern flank the sequoia groves stand. Comparison with a network of 102 largely moisture-sensitive tree-ring chronologies from western North America suggests that this relationship has been stable for at least 380 years. The twentieth century is not unusual in the frequency of these events. We expect the growth record will soon be well replicated for over 2000 years at two locations.

BACKGROUND

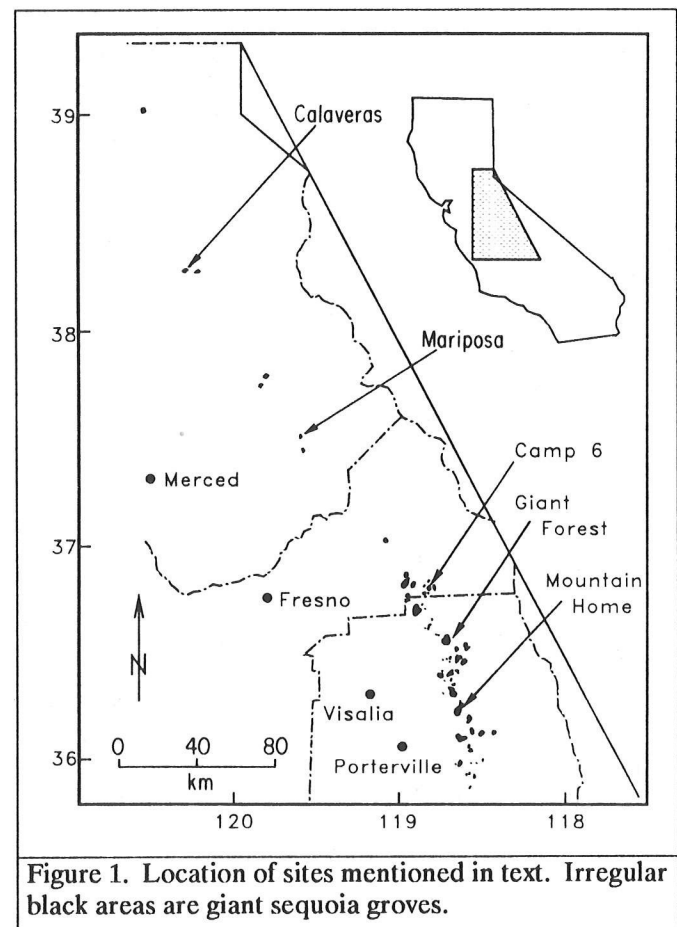
Giant sequoia [*Sequoiadendron giganteum* (Lindl.) Bucholtz] was one of the first tree species to attract the attention of Andrew Ellicott Douglass, the founder of the field of dendrochronology. The potential for long tree-ring records and the opportunity provided by hundreds of recently cut stumps drew Douglass and others to investigate these remarkable trees. In the early decades of this century, Ellsworth Huntington established a relative record of the growth of this species by ring counting and measuring 10-ring increments on hundreds of giant sequoia stumps.

Douglass took the more difficult route of precisely cross-dating all of the annual rings. He worked out inconsistencies between patterns of broad and narrow rings among radii of individual trees, between neighboring trees, and between groups of trees at different sites. He identified AD 1580, for example, as a year in which many giant sequoias failed to produce a growth ring, at least in the lower part of the bole, where most of his samples came from. This painstaking work led to a 3,200-year tree-ring chronology.

Douglass (1919, 1928), Huntington (1914), and Antevs (1925) all sought to establish correlations between series of giant sequoia ring widths and meteorological records from stations such as Fresno in the Central Valley and others more distant, such as San Francisco. They examined complicated model structures involving multi-year influences of precipitation and temperature on giant sequoia ring growth, with but limited success.

In the middle decades of this century little attention was given to this species by dendrochronologists, other than some examination by Schulman (1956) of the relationship between Douglass' giant sequoia chronology and other chronologies from California. The failure of the early studies to establish the kind of strong and simple

link to climate found in conifer chronologies in the interior southwest may have discouraged those seeking to develop records of past climate from tree rings. Indeed, giant sequoia acquired a reputation for being relatively unsuitable for dendroclimatology on grounds of irregular variations of rings around the tree and growing in mesic environments (Brubaker, 1982). Nevertheless, Douglass had managed to find sufficient common variation, primarily in fairly rare marker or *signature* years, to apply his technique of cross-dating throughout the range of this species. This applied from the area now known as Mountain Home State Park to Camp Six, northeast of Grant Grove, and as far north as the Mariposa and Calaveras Groves over 250 km away (Figure 1). The cross-dating indicates that regional climate had a common effect on radial increment of giant sequoia across this part of the central Sierra Nevada, at least in the signature years.



Douglass' success in developing a tree-ring chronology of regional applicability for giant sequoia led one of us (Swetnam) to initiate a program of research in fire history, in which fire scars in the wood of the lower part of giant sequoia stumps are dated using Douglass' chronology. In this research, samples are taken from close to the ground with the intention of acquiring the most complete record possible of fire scars. For the work reported here, we followed Douglass' example and took samples from higher up the trees to minimize the effects of fire scars.

By using Douglass' original measurements, by remeasuring some of his original samples, and by collecting new samples, it has been possible to greatly strengthen the replication of the Douglass chronology. Most of the new material has been collected in the area of Giant Forest in Sequoia National Park. This new material extended the series to 1987, and facilitated the present comparison of giant sequoia growth in relation to the instrumented record of drought.

CHRONOLOGIES

Separate chronologies were established for two sites, Giant Forest and Camp Six. The Camp Six chronology (301 BC to AD 1915) is based on material collected and dated by Douglass, whereas that for Giant Forest (571 BC to AD 1987) is based on more recently sampled materials. In the case of each site, a chronology was produced from dated series of ring-width measurements that were:

- Selected to exclude gross surges or depressions in growth that were unique to individual trees;
- Detrended so as to remove biological growth trend and disturbance-related low frequency change;
- Prewhitened to remove persistence represented by a time-series model; and
- Combined into a mean series for each site using a biweight mean procedure.

Steps 2 through 4 were performed using program ARSTAN, developed by Cook (1985). Options within the program were chosen to produce series that were residuals left when a parsimoniously chosen autoregression time series model was fitted to the detrended measurements. The desired effect was to retain high frequency common variability and discard low frequency changes that are likely to this species to be the result of within-stand effects such as fire and competition, rather than regional climate. The resulting site mean series will be referred to as residuals chronologies in this report.

The two residuals chronologies overlap by 2220 years, over which period their simple correlation coefficient is 0.534 ($p < 0.001$), suggesting they are strongly similar. The Camp Six residuals chronology is based on multiple measurements from each of eight long-lived individual trees, whereas the Giant Forest residuals chronology is based on many more trees in recent centuries and a number of very old individuals. For the purposes of this

exploratory exercise, material from the two sites has been combined into a single residuals chronology extending from 571 BC to AD 1987 (Figure 2), so as to achieve better replication.

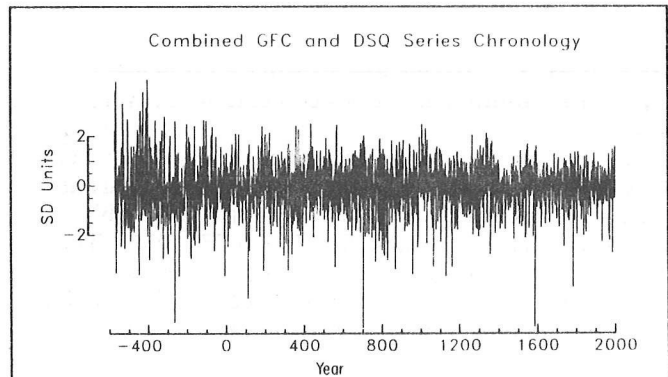


Figure 2. Combined residuals chronology derived from giant sequoia samples from Camp Six and Giant Forest. Units are standard deviation units.

Much the best replication is available for the period since AD 1400. Experience suggests that no use should be made of the early part of the chronology where sample number is less than eight; i.e., before about AD 500. We already have a sufficient number of samples from these and other sites awaiting analysis to give excellent replication (about 30 trees) for more than 2,000 years.

THE SEARCH FOR A CLIMATE SIGNAL

The strong similarity of two site chronologies from about 30 km apart, along with the existence of regional cross-dating, suggests some climate influence on giant sequoia ring growth. Correlations were calculated between the combined residuals chronology and monthly mean temperatures and monthly total precipitation from the Grant Grove and Giant Forest meteorological stations combined into single series 51 years long (see Graumlich, this volume). These stations are located close to or within giant sequoia stands.

A best subsets regression approach yielded a linear regression model accounting for 44 percent (adjusted R^2) of the tree-ring chronology variance using as the major predictors:

- Monthly precipitation for months in the fall and winter prior to growth and for the spring and summer of the growth year
- Monthly mean temperatures for spring of the growth year.

The sign of the coefficients was not consistent between months in the same season, so it is unlikely that this tree-ring chronology could be used to reconstruct the past course of any of these individual monthly variables with any confidence. This was consistent with the experience of Douglass and the other earlier investigators.

The climate at elevations on the west slope of the Sierra Nevada at which giant sequoia is found is such that radial growth is unlikely to be directly limited by low

summer temperatures. Given that most precipitation falls in winter and spring, it is much more likely that growth is limited by soil moisture during the growing season.

As a first approximation to the inter-annual variation in soil moisture in the giant sequoia groves, we examined the Palmer Drought Severity Index (PDSI) calculated for the San Joaquin drainage (Karl and Koscielny, 1982) for extreme low values; that is, intense drought. Taking July as representative of the period of wood formation, the lowest values of PDSI coincide with the lowest values of the combined residuals chronology to a remarkable degree (Figure 3).

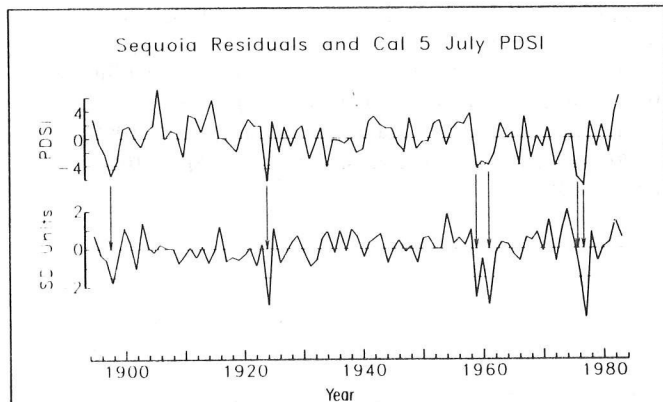


Figure 3. Upper line: July Palmer Drought Severity Index (PDSI) for California Division 5 (San Joaquin drainage) for 1894-1983. Lower line: Giant sequoia combined residuals chronology for the same period.

It is evident there is little or no relationship between these two variables when PDSI is greater than -4. This suggests that radial growth is not limited by moisture availability except during periods of severe lack of soil water sustained over many months; for example, the winters and spring preceding the 1976 and 1977 growth seasons. Similar effects are apparent for the growth seasons of 1897, 1898, 1924, and 1959 through 1961. The negative effect on the trees would appear to be most reliable when low PDSI values occur in two or more consecutive summers. Indeed, slightly less severe droughts may have an accumulated effect as severe as a single extreme event (see Figure 3). This relationship requires further investigation.

If this interpretation is substantially correct, it follows that extreme low values in the combined residuals chronology probably represents a record of such droughts for the last 2½ millennia. There are marked changes of the frequency of low growth events of this severity and, by inference, of droughts as severe as those preceding the growth seasons of 1924, 1961, and 1977. Focusing on the best replicated part of the chronology since AD 1490 (Figure 4), there are periods, such as the second halves of the seventeenth and nineteenth centuries when such events were uncommon, and others, such as the sixteenth century, where they were more frequent.

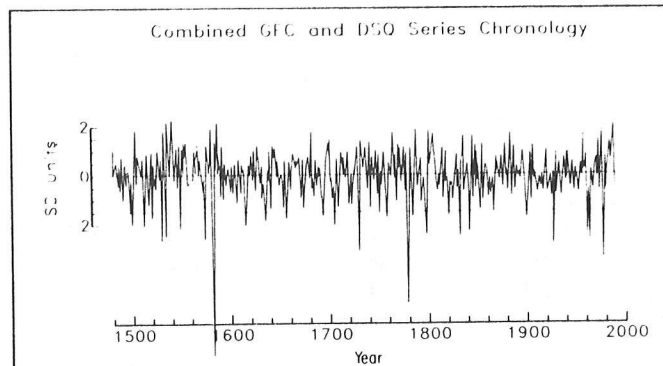


Figure 4. Giant sequoia combined residuals chronology for 1490-1987. The broken line is at 1.5 standard deviation units below the mean, the same level as the broken line in the lower part of Figure 3.

Did this relationship between giant sequoia low-growth events and severe drought hold over a longer period? To test this, we used a network of 102 tree-ring chronologies, largely good recorders of moisture availability. A superposed epoch analysis was conducted in which the difference was calculated for each chronology of the mean ring index for the giant sequoia low-growth years (lowest decile) and the mean index for the period 1601-1963 (Figure 5). Giant sequoia low-growth years were found to be strongly associated with significantly low growth and, hence, drought throughout the area west of the Rocky Mountains.

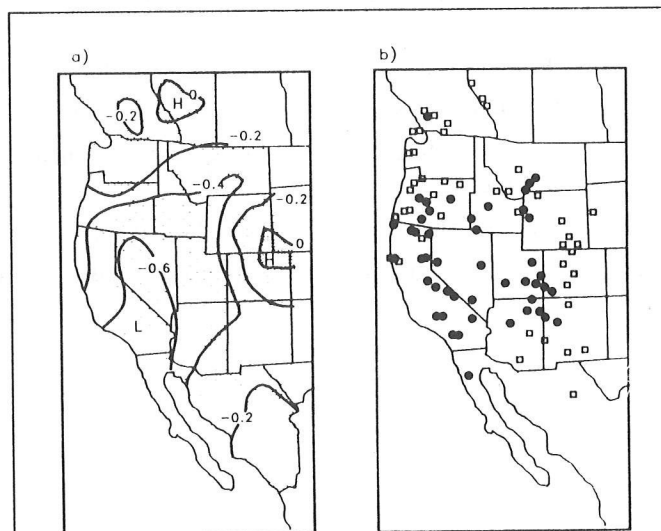


Figure 5. Growth anomaly in 102-chronology network for years of giant sequoia low growth. a) Contoured growth anomaly (normalized departures from full-period mean) for these years against the period 1601-1963. Growth was low in almost all sites. b) Locations of the 102 chronologies, indicating with a closed circle those where the growth anomaly was significant at $p < 0.05$. Giant sequoia low-growth years were those in this period from the first decile of the whole length of the chronology: 1612, 1632, 1653, 1691, 1703, 1729, 1748, 1756, 1777, 1783, 1795, 1818, 1829, 1841, 1864, 1898, 1924, 1959, 1961.

The effect is strongest in the region of California and Nevada on either side of the central and southern Sierra Nevada. This pattern is also found when the 19 giant sequoia low-growth years are split into two groups of nine and ten (odd and even in the sequence) and the analysis repeated. This indicates that not only is the relationship between giant sequoia low-growth events and severe drought consistent since AD 1601, but that the low-growth events may well be good indicators of drought over a large area. This, in turn, implies they may record the occurrence of synoptic-scale circulation anomalies.

CONCLUSION

There is a climate record to be extracted from the growth rings of giant sequoia. Rather than acting as a continuous recorder of precipitation or temperature, the rings act as event recorders for a class of extreme conditions, *viz.* severe drought.

Is there anything unusual about the twentieth century in this record? Restricting the comparison to the last 500 years until a better replicated giant sequoia chronology exists for earlier times, it would appear that frequency of droughts in the region centered on the mid-Sierra Nevada is greater than in the late nineteenth century, but similar to that in the 1500s and 1700s.

ACKNOWLEDGEMENT

Permission to collect materials in Sequoia National Park was granted to T.W. Swetnam by the Superintendent of the Park. Thanks are due to Nate Stephenson for access to increment cores from Giant Forest. We are indebted to Harold Fritts, Linda Brubaker, Lisa Graumlich, and Richard Holmes for access to the 102 chronology network used in Figure 5 and to Harold Fritts for use of the software with which that figure was prepared. T.W. Swetnam and C.H. Baisan were supported by the National Park Service under Cooperative Agreement CA 8018-1-002.

REFERENCES

- Antevs, E., 1925, The big tree as a climatic measure: Carnegie Institution of Washington Publication, v.352, p.115-153.
- Brubaker, L.B., 1982, Western North America in Hughes, M.K., Kelly, P.M., Pilcher, J.R., and LaMarche, V.C. Jr., editors, *Climate from Tree Rings*: Cambridge, University Press, p.118-126.
- Cook, E.R., 1985, A time-series analysis approach to tree-ring standardization: Ph.D. Dissertation, University of Arizona, 171p.
- Douglass, A.E., 1928, Climatic cycles and tree-growth: Carnegie Institution of Washington Publication, v.289, no. II, 166p.
- _____, 1919, Climatic cycles and tree-growth: Carnegie Institution of Washington Publication, v.289, no. I, 127p.
- Huntington, E., 1914, The climatic factor as illustrated in arid America: Carnegie Institution of Washington Publication, v.192, 341p.
- Karl, T.R., and Koscielny, A.J., 1982, Drought in the United States: 1895-1981: *Journal of Climatology*, v.2, p.313-329.
- Schulman, E., 1956, *Dendroclimatic changes in semiarid America*: Tucson, University of Arizona Press, 142p.

Interactions Between Climatic Variables Controlling Subalpine Tree Growth: Implications for Climatic History of the Sierra Nevada, California

Lisa J. Graumlich

ABSTRACT: Tree-ring records from foxtail pine (*Pinus balfouriana*) and western juniper (*Juniperus occidentalis*) growing near tree line in the eastern Sierra Nevada, California, show strong correlations with summer temperature and winter precipitation. Response surfaces portraying tree growth as a function of summer temperature and winter precipitation indicate a strong interaction between these variables in controlling growth. In both species, growth response to summer temperature is positive when precipitation is above normal. When precipitation is below average, growth shows a curvilinear relationship with temperature for foxtail pine and a negative relationship with temperature for western juniper. Above average growth for both foxtail pine and western juniper from AD 1480 to 1570 can be interpreted as indicating an extended period of warm, moist conditions unequalled during the 20th century.

INTRODUCTION

Tree-ring records from trees growing at elevational tree line have long been recognized as a source of proxy climatic data. Long-period variation in such records has been interpreted as reflecting variation in temperature (LaMarche, 1974, 1978; Scuderi, 1987). In addition, precipitation may play an important role in controlling high-frequency variation in growth at tree line (LaMarche and Stockton, 1974; Graumlich and Brubaker, 1986). Understanding the relative role of different climatic variables in controlling growth is a critical preliminary step before either qualitative inferences or quantitative reconstructions of climate based on tree-ring data can be made.

In this paper I describe how temperature and precipitation variables interact in controlling growth of two long-lived subalpine conifers, foxtail pine (*Pinus balfouriana*) and western juniper (*Juniperus occidentalis*), growing along the eastern crest of the Sierra Nevada. I then discuss how the differences in growth response between these two species can be used to elucidate climatic conditions associated with periods of above average tree growth previous to the 20th century.

DATA AND METHODS

Two increment cores were extracted from 20 to 25 individual foxtail pines at each of three sites located on the easternmost crest of the Sierra Nevada between Kearsarge Pass and Mt. Whitney (Table 1). All cores were processed, cross-dated, and measured using standard methods (Swetnam et al., 1985). Cores proving difficult to cross-date or having visible indication of damage were removed from the analysis.

Table 1. Site and chronology characteristics of tree-ring data.

Site	Species	Lat. ($^{\circ}$ N)	Long. ($^{\circ}$ W)	Elev. (m)
West Tyndall	Foxtail pine	36 $^{\circ}$ 39'	118 $^{\circ}$ 23'	3450
Bighorn	Foxtail pine	36 $^{\circ}$ 36'	118 $^{\circ}$ 22'	3430
Crabtree	Foxtail pine	36 $^{\circ}$ 35'	118 $^{\circ}$ 22'	3350
Kaiser Pass	Western juniper	37 $^{\circ}$ 17'	119 $^{\circ}$ 05'	2700

Age-related trends in core measurements were removed by fitting negative exponential growth curves to individual measurement series. Site chronologies were then developed by averaging standardized measurements within each site (Graumlich, in prep). The western juniper "standard" chronology from Kaiser Pass was developed by Richard Holmes of the University of Arizona using similar techniques (Table 1; Holmes et al., 1986).

Monthly temperature and precipitation data used for the foxtail pine analyses are from Giant Forest (1927-1968; 36 $^{\circ}$ 34'N, 118 $^{\circ}$ 46'W, 1943 m) and from Grant Grove (1944-1986; 36 $^{\circ}$ 46'N, 118 $^{\circ}$ 58'W, 2012 m). Regression equations were used to predict Grant Grove monthly temperature and precipitation from the corresponding Giant Forest data and thus extend the Grant Grove record. During the 25-year period of overlap, the regression equations accounted for 41-97% of the variance of the Grant Grove data (Graumlich, in prep). The predictive power of the Giant Forest/Grant Grove calibration equations was high for the summer temperature and winter precipitation variables discussed below ($R^2 = 85\%$ and 93% , respectively). Climate data used for the western juniper analyses are from Yosemite Park Headquarters (1906-1981; 37 $^{\circ}$ 45'N, 119 $^{\circ}$ 35'W, 1236 m).

Response surfaces portraying graphically annual tree growth as a function of two climatic variables were constructed by:

- Using an inverse distance weighting algorithm to interpolate between observed data points, resulting in a regularly spaced grid of tree-ring data, and
- Smoothing the resultant grid by averaging adjacent points with a center-weighted smoothing matrix.

The resulting response surfaces show general trends of growth response to climatic variation and can be interpreted to indicate the presence of nonlinearities or interactions between two variables as they influence tree growth (Graumlich, in prep; Graumlich and Brubaker, 1986).

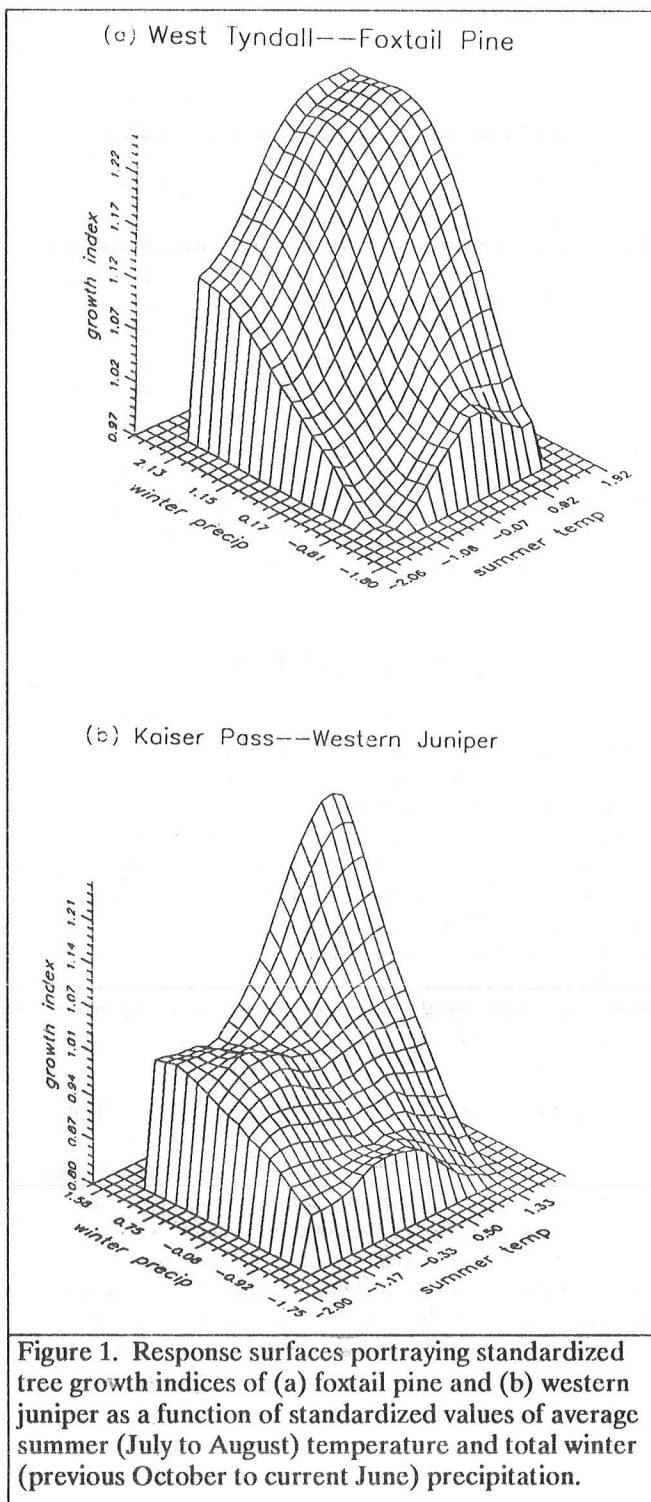
In the analyses presented here, total winter (previous October to current June) precipitation and average summer (July to August) temperature were selected for the response surface analysis based on preliminary analyses of scatter plots between climate and tree-ring variables. The low correlation between summer temperature and winter precipitation results in a wide scatter of values over the X-Y plane formed by these two variables and thus allows a response surface to be calculated over the entire range of both variables. Standardized values of the climatic variables were used to facilitate comparisons between response surfaces.

GROWTH RESPONSE TO CLIMATE

The response surface for the West Tyndall foxtail pine site (Figure 1a) is typical of the foxtail pine response surfaces in indicating that growth is maximized when both summer temperatures and winter precipitation values are high. The response surface is also typical of those for this species in indicating that summer temperature and winter precipitation interact in controlling tree growth. For example, when precipitation is above average, the response to summer temperature is positive; when precipitation is below average, the response to summer temperature is depressed under both very cool or very warm conditions. A positive response to temperature in these subalpine conifers thus depends on the availability of adequate moisture supplies, a result that is not surprising given the coarse soils, warm temperatures, and low precipitation totals on the lee side of the Sierra Nevada.

The response surface for the Kaiser Pass western juniper site (Figure 1b) is similar to that of the foxtail pine sites in indicating maximum growth under conditions of high summer temperatures and high winter precipitation. The previously observed interactions between temperature and precipitation in controlling tree growth can also be seen in the change from a positive response to temperature when precipitation is above average to a negative response to temperature when precipitation is below average. The response surface for western juniper displays a higher degree of non-linearity than does

the foxtail response surface. Without additional western juniper sites, it is difficult to determine if the climatic response surface derived for Kaiser Pass is typical of western juniper. Analysis of recently collected western juniper cores from similar tree-line sites in the Sierra Nevada will allow such a determination.



LONG-TERM GROWTH TRENDS

Growth trends at the three foxtail pine sites and one western juniper site are strongly coherent over time at both high and low frequencies (Figure 2). Particularly intriguing are the extended periods of above average growth for foxtail pine from AD 1400 to 1450 and from AD 1480 to 1570. If climatic inferences were to be drawn from the foxtail pine record, one would conclude that the periods from 1400 to 1450 and from 1480 to 1570 were long warm, moist episodes during the 20th century (e.g., 1951-1952, 1969-1970, 1978, 1980).

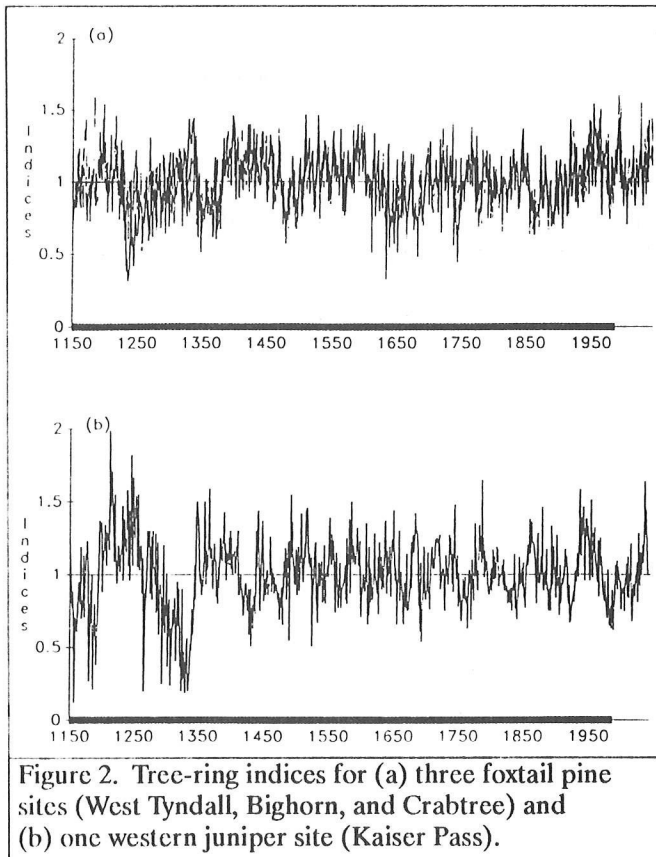


Figure 2. Tree-ring indices for (a) three foxtail pine sites (West Tyndall, Bighorn, and Crabtree) and (b) one western juniper site (Kaiser Pass).

When a detailed comparison is made between foxtail pine and western juniper growth (Figure 3), the previous interpretation of climatic significance of a portion of the AD 1400 to 1570 period breaks down. If conditions were uniformly warm and moist, then we would expect to observe greater than average values of both foxtail pine and western juniper. While the two species vary coherently from 1480 onward, from AD 1400 to 1450, levels of foxtail pine growth are substantially higher than those of western juniper.

There are several possible interpretations of the differing growth patterns observed between the two species from AD 1400 to 1450. One could argue that the response surfaces indicate the greatest contrast in growth between the two species when temperatures are below average and precipitation is above average and

that growth during the period in question could reflect such a climatic scenario. Alternatively, climatic conditions during the period from 1400 to 1450 might not have analogs during the period of observed climate, and our inferences based on analogy are thus inadequate. Finally, sample size of the western juniper chronology during this period is small enough ($n=6$) that non-climatic factors could be responsible for the low frequency variation in the early part of the chronology.

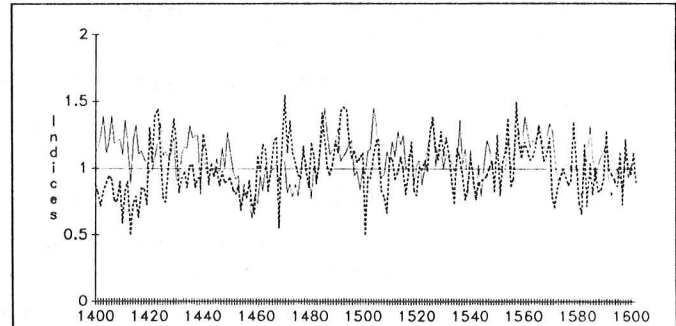


Figure 3. Tree-ring indices for foxtail pine at West Tyndall site (solid line) and western juniper at Kaiser Pass site (dashed line).

Ongoing work, including further sampling of subalpine conifers, investigation of the possibility of no-analog climatic conditions in the past (Graumlich and Brubaker, 1986), and development of maximum likelihood approaches to reconstructing climate directly from response surfaces (Bartlein et al., in prep) should resolve these and similar questions.

CONCLUSIONS

Analyses of foxtail pine and western juniper chronologies from the Sierra Nevada clearly indicate that:

- Both summer temperature and winter precipitation are important factors governing subalpine tree growth in the Sierra Nevada;
- Summer temperature and winter precipitation interact strongly in controlling growth in these subalpine environments; and
- Given the complex nature of the growth response to climate, use of alternative reconstruction strategies involving response surfaces from multiple species will be necessary to reconstruct quantitatively climate from subalpine tree-ring chronologies in this region.

ACKNOWLEDGEMENTS

I thank Ayre Blank, Mike Kiernan, and especially Hollis Gillespie for field and laboratory assistance. Malcolm Hughes, Dave Meko, Henri Grissino-Mayer, and Paul Sheppard provided helpful editorial comments on an early draft of the paper. This work was supported by a grant from the UCLA Academic Senate.

REFERENCES

- Bartlein, P.J., Prentice, I.C., and Webb, T. III, in prep, Evidence for climatic equilibrium in the long-term vegetation dynamics of eastern North America.
- Graumlich, L.J., in prep, Subalpine tree growth, climate variation, and increasing atmospheric carbon dioxide: an assessment of recent growth trends in the Sierra Nevada and Transverse Ranges.
- Graumlich, L.J., and Brubaker, L.B., 1986, Reconstruction of annual temperature (1590-1979) for Longmire, Washington, derived from tree rings: *Quaternary Research*, v. 25, p. 223-234.
- Holmes, R.L., Adams, R.K., and Fritts, H.C., 1986, Tree-ring chronologies of western North America: California, eastern Oregon and northern Great Basin: Laboratory of Tree-Ring Research, University of Arizona, Chronology Series VI, 182p.
- LaMarche, V.C. Jr., 1978, Tree-ring evidence of past climatic variability: *Nature*, v.27, p.334-338.
- _____, 1974, Paleoclimatic inferences from long tree-ring records: *Science*, v.183, p.1043-1048.
- LaMarche, V.C. Jr., and Stockton, C.W., 1974, Chronologies from temperature-sensitive bristle-cone pines at upper treeline in western United States: *Tree-Ring Bulletin*, v.34, p.21-45.
- Scuderi, L.A., 1987, Glacier variations in the Sierra Nevada, California, as related to a 1200-year tree-ring chronology: *Quaternary Research*, v.27, p.220-231.
- Swetnam, T.W., Thompson, M.A., and Sutherland, E.K., 1985, Using dendrochronology to measure radial growth of defoliated trees: *Agriculture Handbook No. 639*, U.S. Department of Agriculture, Forest Service, 39p.

Holocene Fossil Pollen Records of Douglas Fir in Northwestern California: Reconstruction of Past Climate

G. James West

ABSTRACT: Douglas fir is one of the most important trees in northwestern California. Regional pollen records suggest that it has become prominent only in the late Holocene. The primary cause for this change is probably southward stabilization of the mean airstream.

INTRODUCTION

Results of pollen analysis of sediments from marshes, ponds, and lakes are used here to examine the Holocene spatial history of Douglas fir, an important arboreal component of three vegetation associations in northwestern California, and to infer past climatic conditions.

LOCATION AND DESCRIPTION

The study region is shown in Figure 1. The terrain consists of a nearly parallel series of mountain ranges trending obliquely to the coast in a northwesterly direction. Most of the ridges and summits are between 600 and 1500 meters above sea level, whereas several peaks north of Clear Lake and east of the Middle Fork Eel River rise above 2100 meters. All major drainages tend to run parallel to the mountain ranges.

As in the rest of the Pacific Northwest, the climate of northwestern California varies considerably as a consequence of interplay between maritime and continental air masses and mountain ranges (Waring and Franklin, 1979). Immediately along the coast, where the maritime influence is strongest, mild temperatures with narrow diurnal and seasonal fluctuation, extremely wet winters (>2000 mm/year) and cool, dry summers characterize the climate. Valleys in the lee of the Coastal Ranges are drier and subject to greater temperature extremes. With elevation, precipitation increases to >1500 mm/year, and temperatures decrease about 0.6°C/100m (Major, 1977). East of the mountains is the Central Valley, with a more arid continental climate. This steep climatic gradient from the coast inland is a major factor contributing to the vegetational diversity of the region.

DOUGLAS FIR

Douglas fir (*Pseudotsuga menziesii* [Mirb.] Franco var. *menziesii*) is an important conifer in the Pacific Northwest. In California, extensive stands continue southward from Oregon through the Klamath and Coast Ranges as

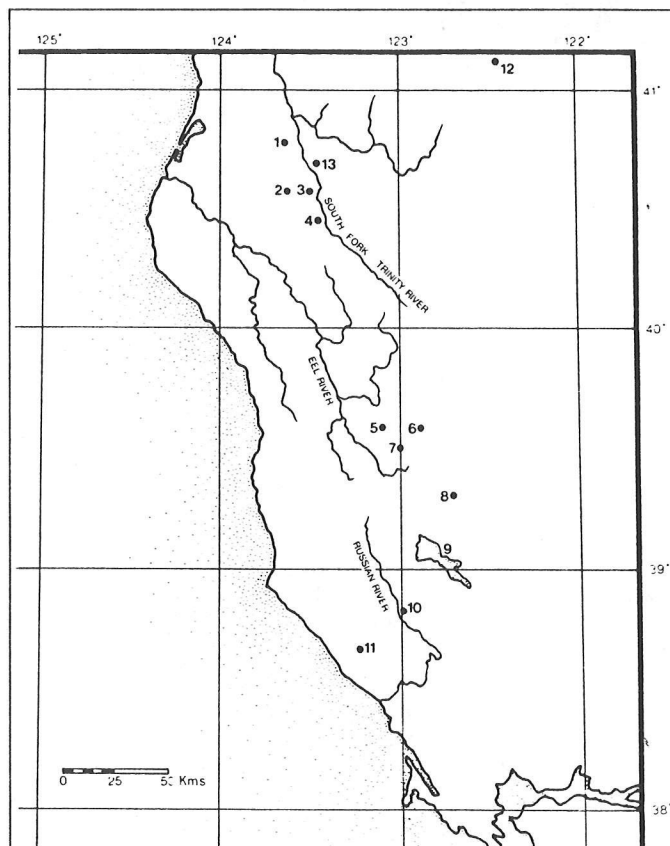


Figure 1. Grid map of pollen records. 1: Big Lake, 2: Hum-558, 3: McKay Spring, 4: Lemonade Spring, 5: Men-1633, 6: Barley Lake, 7: Tule Lake, 8: Lily Pond, 9: Clear Lake, 10: Preston Lake, 11: Plantation, 12: Cedar Lake, 13: Dead Man's Point Pond.

far as the Santa Cruz Mountains (Griffin and Critchfield, 1972; Figure 2). Douglas fir mixes into the eastern portion of the redwood forest, is a major component of the Coast Range montane, and dominates the mixed evergreen forest. Scattered, disjunct groves extend as far south as northwestern Santa Barbara County, but they are not important elements of the vegetation. In the Sierra Nevada, Douglas fir is restricted primarily to forests west of the crest and is associated commonly with the mixed conifer forest. In the southern part of its range, it occurs mainly on northerly slopes and moist canyon bottoms.

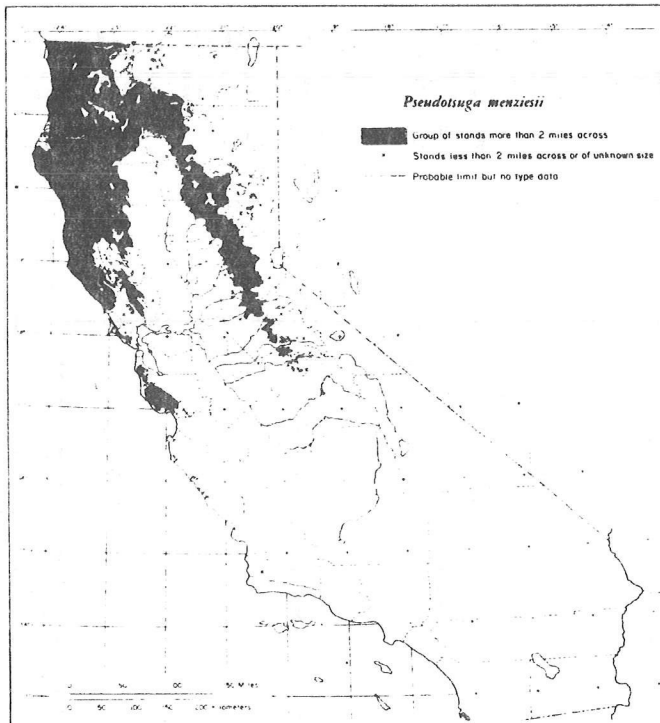


Figure 2. Distribution map. Adapted from Griffin and Critchfield (1972).

The coastal variety of Douglas fir grows best in a mild and humid maritime climate with dry summers, characterized as superhumid or humid (Thornthwaite, 1931). Average annual temperature varies from about 7° to 13°C, with an absolute maximum of 44°C and a minimum of about -34°C (Fowells, 1965). At higher elevations, mainly in the Sierra Nevada, a large part of winter precipitation is snow. In coastal areas, the frost-free period averages > 200 days/year.

Climatic data close to the southern limit of significant stands of Douglas fir are found inland of Santa Cruz (37°N, 122°W). Average annual precipitation is 750 to 1500 mm, and the area is classed by Thornthwaite (1931) as humid. Average length of freeze-free period is > 300 days, and annual temperature range is 9° to 12°C (Donley et al., 1979).

Pollen in Douglas fir, as in other conifers, is dispersed by wind. Douglas fir pollen is large (90-110 μm), relatively heavy (Tsukada, 1982) and, unlike most other conifers, lacks wings or bladders. As a result, it normally has a relatively short dispersal distance.

Empirical and theoretical analyses demonstrate that Douglas fir pollen rapidly falls and declines in concentration as the depositional point moves away from the source (Silen, 1962; Tsukada, 1982). Silen (1962) found that the most marked drop in pollen count occurs in the first 100 meters from the tree, and only a small fraction of the pollen is dispersed a distance farther than 5 to 10 times the height of the tree. Tsukada (1982) concluded that in large bogs and lakes, the pollen influx of Douglas

fir is much smaller than that of other species. In contrast with this, in a small catchment basin (< 500 meters in diameter), the majority of the pollen is derived from trees that grow around the basin. Contemporary pollen rain percentages (Heusser, 1983) exhibit a good correspondence with regional distribution of various arboreal species and, in particular, Douglas fir (West, unpublished reports).

HOLOCENE FOSSIL POLLEN RECORD

The thirteen regional fossil pollen records examined range in age from < 2000 to > 10,000 YBP, and all but one are from four major vegetation associations – the redwood forest, mixed evergreen, Coast Range mountain, and blue oak/digger pine forest. Cedar Lake, on the far northeastern margin of the region, is the one exception, and it is located in the Klamath mountain forest with yellow pine (Küchler, 1977).

The varying pollen frequencies of the regional pollen studies suggest significant vegetation changes have occurred at the local and regional scale. Like the region's vegetation, the pollen records are diverse and complex, with varying species assemblages and temporal patterns (Figure 3); however, some trends are evident.

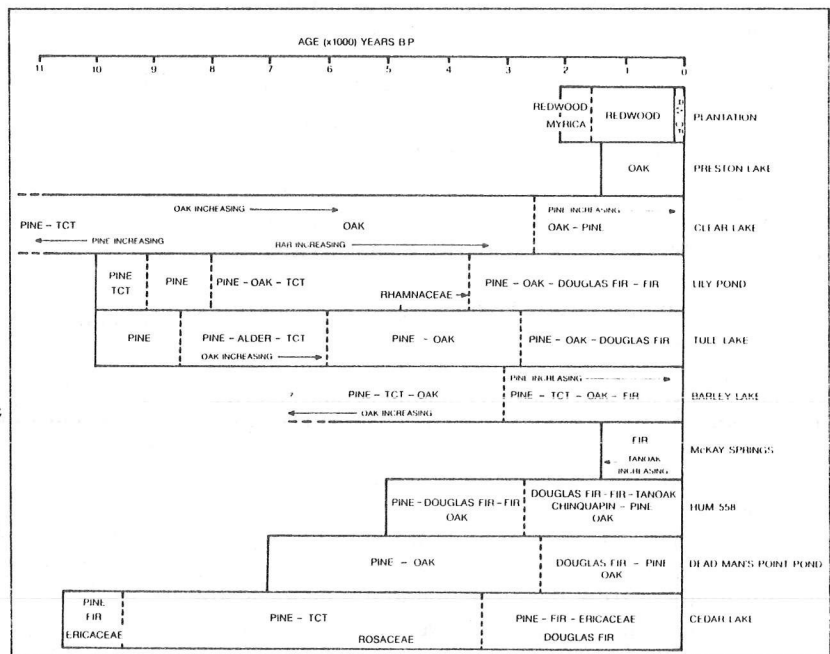


Figure 3. Generalized vegetational reconstruction from pollen data. Sources: Adam, 1988; Baker, 1983; West, 1989.

Prior to about 8500 YBP, pine and, at some localities, pine and TCT (Taxodium, Cupressaceae, and Taxaceae) pollen grains are the dominant types, with relative values > 65 percent. After 8500 YBP, the pollen records exhibit considerably more species and temporal diversity. At Cedar Lake, decreases in pine with corresponding increases in TCT characterize the early part of the mid-Holocene. In this instance, it is likely that a large fraction of the TCT pollen was

derived from Port Orford cedar, which had expanded onto the lake margins in response to lower water levels (West, 1986). At other localities, maximum oak values are reached at mid-Holocene times, peaking about 5000 YBP. Oaks must have expanded their range considerably throughout the region at this time.

Throughout the early and middle Holocene, of the records examined, Douglas fir pollen is conspicuous by its absence or low values. At Hum-558, a marsh on Pilot Ridge in a Douglas fir forest, average Douglas fir pollen values prior to 4000 YBP were about 10 percent; after 4000 YBP, they were almost 20 percent. Nearby and to the east across the South Fork of the Trinity River at Dead Man's Point Pond, average Douglas fir pollen values were <6 percent from 2300 to >7000 YBP. To the south, at Tule Lake, Douglas fir pollen is present continuously at low levels (2 percent) from about 2500 to 6000 YBP. At the other localities, where the fossil record extends back to the early and mid-Holocene, Douglas fir is absent or only sporadically present at values of <2 percent.

In the last third of the Holocene, modern pollen values, including those for Douglas fir, were attained. This change began, depending on the locality, from about 2300 to almost 6500 YBP, but the relative proportions of the pollen taxa did not stabilize until after 2500 YBP. Generally, when Douglas fir pollen values increased, oak or pine values decreased and tanoak values increased.

The pollen record suggests that there have been no permanent plant communities. Instead, species populations collected in habitats for which their adaptations were suited and when local histories brought them within dispersal range (cf. Colinvaux, 1987). Douglas fir was a much less important tree in the region during the early and mid-Holocene and has only become a dominant arboreal species in part of the region during the late Holocene.

PALEOCLIMATIC INTERPRETATION

Using an indicator species model (Birks and Birks, 1981; Barnosky, 1984) for interpreting the fossil pollen record, at least three climatic periods are evident (West, 1989). The earliest period (8500 YBP), with very high pine pollen values, is indicative of a climate cooler and more continental than at present. High oak values, except at Cedar Lake, mark the next period, from about 8500 to 2500 YBP, which was warmer and possibly drier, more Mediterranean. Adam and West (1983), using a transfer function based on the ratio of modern pine and oak pollen values, estimated mid-Holocene temperatures were 1.4° to 2.1°C warmer than today. At Cedar Lake during this period, TCT and Rosaceae pollen values reach their maximum, probably reflecting lower lake levels and warmer temperatures. Declining oak values and increasing values for Douglas fir, most evident after 2300-3800 YBP for five of the pollen records, indicate stronger maritime conditions.

At Clear Lake (Adam, 1988) and Barley Lake, oak pollen shows a slight decline with increasing pine pollen values during the late Holocene. Clear Lake is large (114 km²) and — because of its size, relatively low elevation (404 m), and interior location — does not show an increase in Douglas fir pollen. Barley Lake is high (1658 m) and has an open southern exposure not conducive to Douglas fir growth.

DISCUSSION AND CONCLUSIONS

According to COHMAP's (1988) atmospheric general circulation model (GCM), the paleoclimate of the eastern North Pacific and western North America was characterized by a weak subtropical high in July and a very strong westerly flow at 12,000 YBP. Temperatures were colder than at present. From 9000 to 6000 YBP, the subtropical high was stronger in July than it is today. At 9000 YBP, the mean airstream flow arched farther northward, away from northwestern California. In the Pacific Northwest, July was warmer and drier than today. The mean airstream flow attained its current position by 6000 YBP.

Comparison of COHMAP's GCM and the climatic interpretation of the regional pollen records suggests similar trends, but temporal differences are present. In the early Holocene, change may be time transgressive with the shift from colder, more continental conditions to warmer, more Mediterranean conditions evident first in the north, at Cedar Lake. There are probably a number of causes for the temporal discrepancies between the GCM and the fossil record.

- First, the GCM does not have the resolution to account for local variability and factors other than climate that may be significant.
- Second, each taxon responds individually to climatic change, according to its own tolerances, going in its own direction, and at its own pace.
- Third, the apparent time transgressive pattern of vegetation change may be related to the position of the main airstream. Shifts in the mean airstream flow of even tens of kilometers would have a significant effect on the region's climate and vegetation.

This third cause may explain the expansion of Douglas fir in the late Holocene. The fossil pollen record of Douglas fir may reflect a climatic pattern in which the position of the mean airstream during mid-Holocene was more variable and did not stabilize in a more southerly position until late Holocene times.

Possible future warming as a result of the greenhouse effect of increased carbon dioxide and methane concentrations in the atmosphere (Ramanathan, 1988) may have a significant effect on the region's vegetation. Based on the fossil pollen record, warming with less effective moisture will lead to a decrease in conifers, particularly Douglas fir, and an increase in oaks and chaparral. Predicted changes will take place in decades, and some local extinction of taxa with limited tolerances is likely.

REFERENCES

- Adam, D.P., 1988, Pollen zonation and proposed climatic units for Clear Lake, California, Cores CL-73-4 and CL-73-7, in J.D. Sims, editor, Late Quaternary Climate, Tectonism, and Sedimentation in Clear Lake, Northern California Coast Ranges, Geological Society of America Special Paper 214, Boulder, CO, p. 63-80.
- Adam, D.P., and West, G.J., 1983, Temperature and precipitation estimates through the last glacial cycle from Clear Lake, California, pollen data: *Science*, v.219 P.168-170.
- Baker, R.G., 1983, Holocene vegetational history of the western United States, in H.E. Wright, Jr., editor, Late Quaternary environments of the United States, v.2, The Holocene: Minneapolis, University of Minnesota Press, p.109-127
- Barnosky, C.W., 1984, Late Pleistocene and early Holocene environmental history of southwestern Washington, U.S.A.: *Canadian Journal of Earth Sciences*, v.21, p.619-629.
- Birks, H.J.B. and Birks, H.H., 1981, Quaternary Paleocology: Baltimore, University Park Press, p.289.
- COHMAP, 1988, Climatic changes in the last 18,000 years: Observations and model simulations: *Science*, v.214, p.1043-1052.
- Colinvaux, P.A., 1987, The changing forests: Ephemeral communities, climate and refugia: *Quarterly Review of Archaeology*, v.8, n.1.
- Donley, M.W., Allen, S., Caro, P., and Patton, C.L., 1979, Atlas of California: Portland, Academic Book Center, p.191.
- Fowells, H.A., 1965, Silvics of the forest trees of the United States, Agricultural handbook No. 271, U.S. Department of Agriculture, Forest Service, Washington, DC, p.762.
- Griffin, J.R., and Critchfield, W.B., 1972, The distribution of forest trees in California: Berkeley, Pacific SW Forest & Range Exp. Stn., USDA Forest Service Research Paper PSW-82 (reprinted with supplement, 1976), p.114.
- Heusser, L., 1983 Contemporary pollen distribution in coastal California and Oregon, *Palynology*, v.7, p.19-42.
- Küchler, A.W., 1977, Map of natural vegetation of California, in Barbour, M.G., and Major, J., eds., Terrestrial vegetation of California, New York, John Wiley & Sons.
- Major, J., 1977, California climate in relation to vegetation, in Barbour, M.G., and Major, J., eds., Terrestrial vegetation of California, New York, John Wiley & Sons, p.11-74.
- Ramanathan, V., 1988, The greenhouse theory of climate change: A test by an inadvertent global experiment, *Science*, v.240, p.293-299.
- Silen, R.R., 1962, Pollen dispersal considerations for Douglas fir, *Journal of Forestry*, v.60, p.790-795.
- Thorntwaite, C.W., 1931, The climates of North America according to a new classification, *Geographical Review*, v.21, p.633-655.
- Tsukada, M., 1982, *Pseudotsuga menziesii* (mirb.) Franco: Its pollen dispersal and late Quaternary history in the Pacific Northwest, *Japanese Journal of Ecology*, v.32, p.159-187.
- Waring, R.H., and Franklin, J.F., 1979, Evergreen coniferous forests of the Pacific Northwest, *Science*, v.204, p.1380-1386.
- West, G.J., 1989, Late Pleistocene-Holocene climate and vegetation of California's north Coast Ranges: the pollen record, in press.
- _____, 1983, Pollen analysis of sediments from Lily Pond, lower Letts Valley, Mendocino National Forest, California: A record of Holocene vegetation and climate, ms. on file, U.S. Forest Service, Mendocino National Forest, Willows, CA.

Inferences from Tree Rings on Low Frequency Variations in Runoff in the Interior Western United States

David M. Meko

ABSTRACT: Low frequency variations in runoff, AD 1700-1964, in the interior western United States are inferred from smoothed tree-ring series averaged over north, central, and south regions. Main inferences drawn from visual comparison of smoothed curves are that: (1) observed declines in the first half of the 20th Century have been the most severe back to at least AD 1700 in all regions, (2) low-flow periods have been more synchronous from north to south than high-flow periods, and (3) longer wavelength (60-70 years) variations have been more prevalent in the north than in the central and south regions. The central regional tree-growth series was found to track reasonably well the important low frequency variations in the Colorado River, 1906-1964. Relative locations of peaks and troughs in streamflow, precipitation, temperature, and tree-ring series suggest that annual precipitation and warm season evapotranspiration variations may both be important to low frequency fluctuations in tree growth and in streamflow.

INTRODUCTION

Historical streamflow anomalies have been recognized for some time as containing useful information on climate fluctuations over the United States (Hoyt and Langbein, 1944). A common feature in adjusted annual flow records of the Colorado River at Lee Ferry and the Columbia River at The Dalles is a relatively large low frequency component, manifested primarily by steep downward trends over several decades beginning in the late 19th or early 20th Century (Meko, 1985). Given the large size of the two drainage basins, it seems reasonable to conclude that runoff summed over large areas of the interior western United States also has a large low frequency component. Existing streamflow records are too short, however, for an adequate representation of low frequency variability.

In this paper, an attempt is made to gain a long-term perspective on the regional low frequency runoff variations of the past century using tree rings. The quality of the runoff signal in tree-ring data from various parts of the interior western United States was first demonstrated by Schulman (1951) using graphical methods

and simple correlations. Subsequently, modern statistical transfer/function methods have been used in streamflow reconstructions (e.g., Stockton, 1975; Smith, 1979).

The present study is closer to the graphical approach in that no quantitative reconstruction of specific streamflow records are made using transfer functions. It differs from previous studies, however, in geographical extent, density of tree-ring coverage and manner of treatment of tree-ring data, and emphasis on the low frequency component of variability. Smoothed growth series from northern, central, and southern parts of the interior western United States are examined for relative magnitude of variations in the current century and for synchrony in timing of major wet and dry anomalies.

TREE-RING DATA

Regional tree growth series were formed from 146 drought-sensitive ring-width chronologies collected and developed between 1962 and 1984 by researchers at the University of Arizona Tree-Ring Laboratory (TRL). The study area reaches from central Montana and Idaho to southern Arizona and New Mexico. Methods of sampling and development of chronologies are described in detail elsewhere (Fritts, 1976).

A method of reducing the tree-ring data was adopted that would use all available drought-sensitive chronologies, deemphasize those not co-varying with nearby chronologies, and yield regional average series that could be compared without unduly weighting variations in areas of intense tree-ring collection. The 146 sites were first grouped on considerations of natural clustering and site density into the 20 groups shown in Figure 1. Principal components analysis was then done separately on the chronologies in each group, and the amplitude series of the first principal components were defined as "group" tree-ring series. Each group series was then converted to "Z-scores" by subtracting the mean and dividing by the standard deviation. Finally, the group tree-ring series were averaged into northern, central, and southern regional tree-ring series according to the boundaries shown by the heavy dashed line in Figure 1.

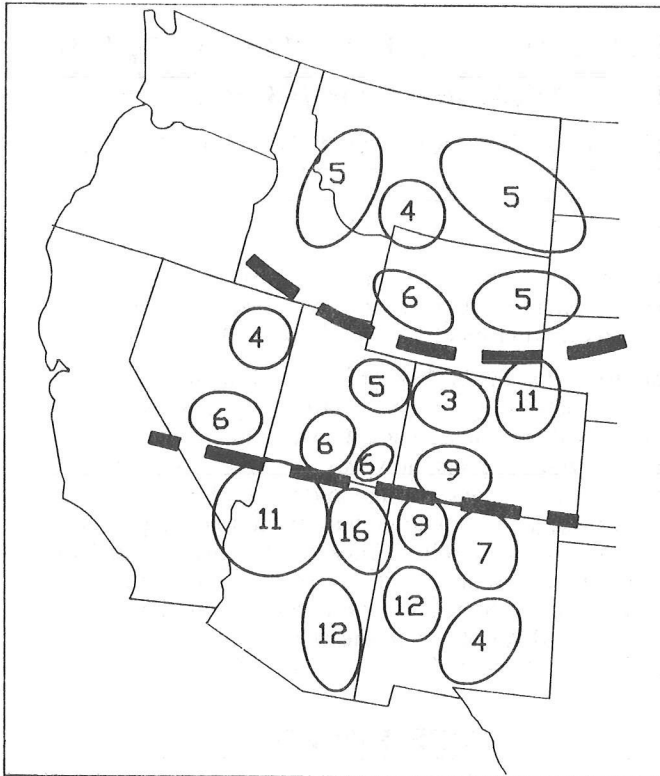


Figure 1. Locations of groups of tree-ring chronologies and number of chronologies in each group. Heavy dashed line shows division into northern, central, and southern regions.

STREAMFLOW DATA

A time series, 1906-1985, of *natural* annual flow of the Colorado River at Lee Ferry, Arizona, was obtained from the U.S. Bureau of Reclamation. The series represents flow adjusted for removal of anthropogenic influences such as withdrawals for irrigation and storage by reservoirs. Time variations in this series as they relate to streamflow variations in other parts of the West have been discussed by Meko and Stockton (1984) and Meko (1985).

CLIMATE DATA

Annual time series of **water year total precipitation and precipitation-weighted, warm season average temperature** averaged over the latitude/longitude range 36-40N, 106-109W, were computed using monthly station data from the F.T. Quinlan's Historical Climate Network (HCN) from the National Climatic Data Center. Both series are averages over 12 stations with records covering the period 1907-1984. Temperature was used — for lack of a better alternative — as an indicator of interannual variations in evaporation. May through October is defined as the *warm season*, and the computed temperature series is the average over those months weighted by the proportion of warm season precipitation falling in each month. This particular grouping and weighting was intended to emphasize interannual temperature variations in the warmer months of the year,

when potential evapotranspiration is relatively high, and in the wetter months, when variations in potential evapotranspiration are most likely to translate into variations in actual evapotranspiration.

SMOOTHING

The tree-ring, streamflow, and climate series were each smoothed by the same low-pass filter before plotting to emphasize low frequency variations. This 11-weight, raised-cosine filter (Hamming, 1983) has a frequency response such that the amplitude of a sine wave with a period of 12 years would be reduced by half. Waves with periods less than 6 years would be eliminated entirely.

RESULTS

The single dominant feature of the smoothed tree growth plots (Figure 2) is the period of high growth about 1905-1920. The long-term anomalous nature of this period was noted previously by Fritts (1965) from spatial patterns of decadal average deviations in tree growth over the West and later by Stockton (1975) in a tree-ring reconstruction of the annual flow of Colorado River. All three regional tree-ring series in Figure 2 reached their record high levels in this period. The growth anomaly was most severe relative to previous anomalies in the central region, indicating an increase in storminess in that area relative to areas to the north and south. The north/south extent of the anomaly, at least in the early part of the 1905-1920 period, may reflect anomalous central development of storms, with precipitation increases extending north and south, or possibly a more longitudinal component rather than zonal orientation to storm tracks.

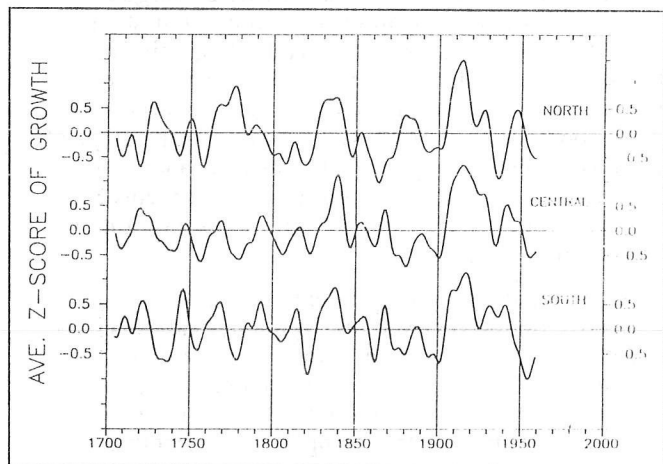


Figure 2. Smoothed annual series of regionally averaged tree growth.

Cayan and Peterson (1989) suggest that high streamflows from 1906-1910 in the northern part of the interior western United States were caused by an anomalous southern displacement of the winter storm track into the western United States associated through teleconnections with anomalously high sea level

pressure (SLP) south of the Aleutian Islands. They also suggest increased activity from storms moving southward from Canada and Alaska east of the Cascades, a pattern that would be consistent with the exceptionally cold winter temperature anomalies in the interior West in the first two decades of the 20th Century (temperature curves in Bradley et al., 1982).

Longer wavelength fluctuations are more evident in the north than in the other two regions. An irregular periodicity of about 60-70 years is suggested by growth peaks in the north anchored near 1780, 1840, and 1915.

Growth peaks near these years were also major components contributing to a significant spectral peak found previously in tree-ring data from the northwestern fringe of the Great Plains (Meko, 1982). The latter two peaks in the sequence also show up in the central and southern region plots, but the 1780 peak is conspicuously absent there. Instead, an irregular occurrence of about two peaks every 40 to 50 years is characteristic in the central and southern regions.

In spite of the obvious coincidence of the major growth peaks near 1838 and 1915 across regions, a close look at Figure 2 suggests that growth peaks generally were not synchronous from the southern to northern regions. A peak in one region was judged to coincide with a peak in another region if the year of the peak in the first region fell no more than a third of the way from a peak to the adjacent trough in the second region. Of the twelve largest peaks in the south, ten coincided with peaks in the central region, but only three coincided with peaks in the north. Low-growth anomalies were somewhat more coherent in space.

By a similar criterion as used for peaks, all of the ten identified deepest troughs in the south coincided with troughs in the central region, but only five of the ten coincided with troughs in the north. The results are consistent with meteorological data in that coherence of moisture anomalies decreases over distance, and dry periods appear to be more spatially coherent than wet (Julian, 1970).

The lack of synchrony between north and south at times deteriorated into a latitudinal contrast in sign of anomalies. Periods with a wet north and dry south are centered at 1778, 1880, and the late 1940s. Periods of marked opposite contrast — wet south and dry north — are centered at 1722, 1815, and 1868. The existence of north/south contrasts in both precipitation (Sellers, 1968) and streamflow (Langbein and Slack, 1982; Meko and Stockton, 1984) have been noted previously. Such periods of contrast may reflect unusual clustering of years with specific modes of anomalous atmospheric circulation. The wet south/dry north contrasts, for example, could be related to the El Niño phase of the Southern Oscillation (SO). The synoptic regime, as described by Cayan and Peterson (1989), is for low mid-latitude storms tapping moisture from the subtropical jet and bringing heavy precipitation to the Southwest.

Lough and Fritts (1985) list 1867, 1868, and 1869 as three of the most extreme low-index years in the period 1852-1900 by the winter SO index of Wright (1975).

Interestingly, while the smoothed regional tree growth plots of Figure 2 are consistent with a low-index SO clustering at 1868, Lough and Fritts' (1985) SO tree-ring reconstruction based on a 65-station grid of pre-whitened tree-ring chronologies does not point out those years as anomalous.

Two possible explanations for the discrepancy are:

- Contamination of the SO signal at times from tree-ring sites outside the area of strongest related climate signal, and
- De-emphasis of clustering periods of SO anomalies due to the use of tree-ring series that have been pre-whitened in the reconstruction model.

The 20th Century stands out for the magnitude of the swing from high to low growth — starting at about 1915 in all regions, but ending in the 1930s in the northern region and the 1950s in the central and southern regions. Corresponding large streamflow trends in the study area in this century (Meko and Stockton, 1984) are, therefore, inferred to be at least 250-year extremes.

This conclusion cannot be generalized to include rivers with significant runoff-producing areas outside the interior western United States. For example, the period of generally highest annual flows on the Columbia River at The Dalles was centered near 1896 (Meko, 1985), which from the northern region tree-ring series (Figure 2) would be inferred as a period of low runoff. The Columbia at The Dalles receives significant contributions of runoff from Canada and the U.S. Pacific Northwest. Apparently these areas and the northern region in Figure 1 were experiencing greatly contrasting runoff anomalies in the 1890s. As another example of the greater spatial coherence of dry relative to wet anomalies, however, the bottoming out of the growth curve for the north near 1940 does coincide with the record low-flow period for the Columbia at The Dalles.

How well do the regional tree-ring series reflect variations in runoff for specific watersheds? Ideal series for verification of the regional tree-ring series (actual runoff, summed regionally) simply do not exist, although it may be possible to eventually derive suitable regional runoff indices by adjusting streamflow records.

For present purposes, the natural flow series of the Colorado River at Lee Ferry was used as a preliminary attempt at rough verification for the central region growth series. Smoothed plots of Colorado River flow and central region tree growth (Figure 3, bottom) show that low frequency variations in growth generally track variations in flow. The major peaks and troughs in the tree-growth series all match up (though not in perfect timing) with similar features in annual flow. The major discrepancies are related to the early 1900s high runoff period, which is somewhat underestimated in magnitude relative to the wet period in the early 1940s. The year of peak runoff in the earlier period is also off by a few years.

The associated smoothed annual precipitation and weighted warm season average temperature are plotted at the top of Figure 3. The peak in the growth curve at

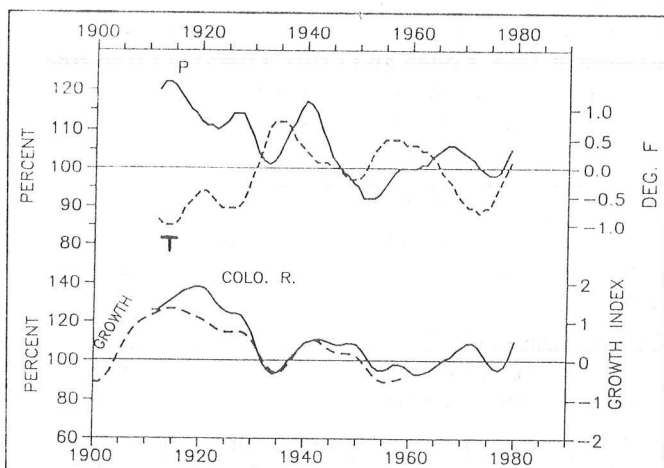


Figure 3. Comparison of selected streamflow, climate, and tree growth data for Colorado basin.

Bottom: Smoothed central region tree growth and annual virgin flow of the Colorado River at Lee Ferry, Arizona.

Top: Smoothed time series of water year total precipitation and precipitation-weighted warm season average temperature for area covering Colorado River basin. Precipitation and streamflow are given as percentages of 1951-1980 mean; temperature is given as departure from 1951-1980 mean.

about 1915 is seen to coincide with both the wettest annual and the coolest warm-season conditions in the instrumental record. From seasonal temperature and precipitation plots (Bradley et al., 1982), the period 1910-1920 was exceptionally cool and generally wetter than normal in fall, winter, and spring in Colorado and Utah. The snowpack was, therefore, probably anomalously heavy and retained unusually long into the warm season, giving ideal conditions for tree growth: gradual release of snowmelt to keep soil moisture high well into the growing season and low evaporative stress associated with cool spring and summer temperatures, probably with unusually cloudy conditions and high relative humidity.

Comparison of timing of peaks and troughs in the four series in Figure 3 suggests that low frequency variations in tree growth and runoff are associated with anomalies in annual precipitation and possibly warm season temperature. Tree growth peaks and troughs in Figure 3 are most extreme when temperature and precipitation anomalies are large and of opposite sign. Evidence of temperature (through evapotranspiration) influence comes mainly from difficulty in explaining magnitude or location of some growth peaks from precipitation alone. For example, growth minima near 1934 and 1956 both coincide with warm season temperature peaks and are deeper than growth anomalies in other periods with comparable precipitation anomalies. Support for a temperature effect on runoff is somewhat weaker: the relative severity of the streamflow minimum in 1934 appears to be greater than implied by the precipitation anomaly alone, and streamflow peaks centered at 1950 and 1972 coincide with temperature minima.

A more rigorous search for evidence of a relationship between annual runoff and temperature would require detailed examination of climate data at the seasonal resolution. A shift to a higher proportion of the annual precipitation falling in the cooler months, for example, would favor reduced net evapotranspiration and increased runoff. The increasing *winter* precipitation shown by Bradley et al. (1982) for Colorado over the period 1914-1920 is one possible explanation for the streamflow peak lagging a few years behind the annual precipitation peak at 1915 in Figure 3.

CONCLUSIONS

Recognizing that rigorous statistical tests have not been done here to establish the reliability of the runoff/tree growth signal, the following inferences are made on runoff variations in the interior western United States to AD 1700:

- Low runoff anomalies are more synchronous from north to south than high runoff anomalies.
- Longer wavelength variations (60-70 years) are more noticeable in the northern than in the central and southern regions.
- Downward trends in streamflow over the first half of the 20th Century are at least 250-year extremes.
- Periods of contrasting anomalies in the north and south are common, but exceptional periods of same-sign anomaly over a broad latitude range have occurred. The most prominent of these by far is the wet anomaly 1905-1920, which was most anomalous in the central latitudes.

Changes in seasonal distribution of annual precipitation are likely to distort the tree growth/annual runoff relationship. Fortunately for accuracy of reconstructions, development of a heavy snowpack favors both high annual flows and increased tree growth. Basins with a relatively large snowmelt component may be most amenable to accurate reconstruction of high annual flows. More research is needed on the statistical relationship of snowpack variations and tree growth.

Although low frequency variations in annual flow of the Colorado River are closely related to precipitation, interannual variations in evapotranspiration may help explain some of the details involved in the magnitude and timing of peaks and troughs.

The approach used here can be extended in time by studying subsets of longer length tree-ring series after first establishing that they retain the low frequency variations shown by the relatively dense network used in this study. Another possible extension is to concentrate field collections in areas where streamflow and climate data appear to be most sensitive to circulation indices (e.g., Southern Oscillation) to maximize the climatic value of the tree-ring data.

ACKNOWLEDGEMENTS

I thank Lisa Graumlich and Thomas Swetnam of the University of Arizona Tree-Ring Laboratory for their helpful comments on the manuscript. This work was supported by the National Science Foundation, Climatic Dynamics Program, through grant ATM-88-14675.

REFERENCES

- Bradley, R.S., Barry, R.G., and Kiladis, G., 1982, Climatic fluctuations of the western United States during the period of instrumental records: Contribution No. 42, Department of Geology and Geography, University of Massachusetts at Amherst.
- Cayan, D.R., and Peterson, D., 1989, The influence of North Pacific atmospheric circulation on streamflow in the West, in Peterson, D.H., Editor, Aspects of climate variability in the Pacific and western Americas: American Geophysical Union Monograph V.55, p.325-398.
- Fritts, H.C., 1976, Tree rings and climate: Academic Press.
- _____, 1965, Tree-ring evidence for climatic changes in western North America: Monthly Weather Review, v.93, n.7, p.421-443.
- Hamming, R.W., 1983, Digital filters: Prentice-Hall, Inc., Englewood Cliffs, NJ, 257p.
- Hoyt, W.G., and Langbein, W.B., 1944, The yield of streams as a measure of climatic fluctuations: Geographical Review, v. XXXIV, n.2, p.218-234.
- Julian, Paul R., 1970, An application of rank-order statistics to the joint spatial and temporal variations of meteorological elements: Mon. Wea. Rev., v.98, n.2, p.142-153.
- Langbein, W.B., and Slack, J.R., Yearly variations in runoff and frequency of dry years for the conterminous United States, 1911-79: U.S. Geological Survey Open File Report 82-751, 85p.
- Lough, J.M., and Fritts, H.C., 1985, The southern oscillation and tree rings: 1600-1961: Journal of Climate and Applied Meteorology, v.24, n.9, p.952-966.
- Meko, D.M., 1985, Climatic inferences from adjusted streamflow records of the Columbia and Colorado rivers: in Extended Abstracts Volume, Third Conference on Climate Variations and Symposium on Contemporary Climate 1850-2100, American Meteorological Society, Boston, p.76-77.
- _____, 1982, Drought history in the western Great Plains from tree rings: Proceedings of International Symposium on Hydrometeorology, American Water Resources Association, p.321-326.
- Schulman, Edmund, 1951, Tree-ring indices of rainfall, temperature, and river flow: Compendium of Meteorology, American Meteorological Society, p.1024-1029.
- Sellers, W.D., 1968, Climatology of precipitation patterns in the western United States, 1931-1966: Monthly Weather Review, v.96, p.585-595.
- Stockton, C.W., 1975, Long-term streamflow records reconstructed from tree rings: Papers of the Laboratory of Tree-ring Research, University of Arizona Press, Tucson.
- Wright, P.B., 1975, An index of the Southern Oscillation. CRU RP4, Climate Research Unit, Norwich, England, 22p.

El Niño-Southern Oscillation (ENSO) Phenomena and Forest Fires in the Southwestern United States

Thomas W. Swetnam and Julio L. Betancourt

ABSTRACT: Fire statistics (area burned) and fire-scar chronologies from tree rings show reduced fire activity during El Niño-Southern Oscillation (ENSO) in forests of Arizona and New Mexico. This relationship probably stems from increased fuel moisture after a wet winter and spring, but also could involve climatic controls on lightning activity at the onset of the monsoon season.

INTRODUCTION

Fire plays an important role in plant communities worldwide, yet one of the more uncertain impacts of climatic change is an altered fire regime. Traditionally, fire research has emphasized meteorology in predicting fire intensity and rate of spread given short-term weather conditions. Early efforts to determine the synergistic influence of climate and fuel accumulation on fire occurrence were mostly unsuccessful (Hardy, 1983).

Renewed interest in fire climatology is partly a response to the emerging science of global change and to recent catastrophic fires, such as those in Indonesia and Australia during the 1982-1983 El Niño (Gill, 1983; Leighton, 1984) and at Yellowstone Park, USA, in 1988. A possible link between fire activity and climatic variability due to ENSO phenomena, implied in the recent literature, could have forecasting value. Not only is the onset of an El Niño sometimes predictable months in advance (Barnett et al., 1988), but also the significant teleconnections for fire climatologies may lag the onset by more than one season.

In the southeastern United States, Simard et al. (1985a) found that fire activity decreased significantly during ENSO events of the last 50 years. There, cool season precipitation is positively correlated with ENSO indicators, such as the Southern Oscillation Index and Line Island rainfall (Douglas and Englehart, 1980; Ropcewski and Halpert, 1986, also this volume). More recently, Simard and Main (1987) developed a regression model for predicting variability of fire activity in the southeast. The regression is derived from the relationships of fire with the quasi-biennial oscillation and the frequency and intensity of ENSO.

ENSO also may influence fire activity in the southwestern United States, where the annual march of precipitation produces a distinctly seasonal fire regime (Figure 1). An extremely arid foresummer follows a highly variable winter and spring. The dryness of May

and June ends abruptly in early July with synoptic-scale surges of moist tropical air that continue into September. Commonly referred to as the Arizona monsoon, this is the season of maximum frequency of thunderstorms and cloud-to-ground lightning strikes.

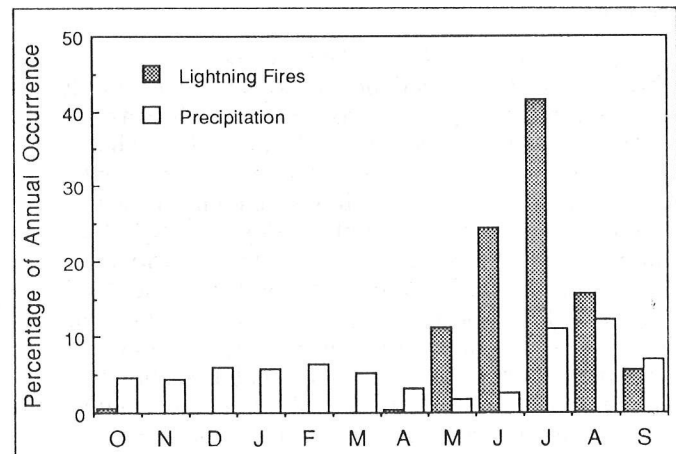


Figure 1. Percentage of mean annual occurrence for lightning fires and precipitation in Arizona and New Mexico (1940-1975). Note peak fire activity just before or at the onset of the rainy season in July.

The fire season closely tracks the rainfall regime. Lightning fires begin in the arid foresummer and peak in July, with a significant decrease as the rainy season progresses (Figure 1). Interannual differences in fire occurrences (area burned or number of fires) may result from the influence of winter-spring precipitation on the accumulation and moisture content of the fuel load. Alternatively, these differences can be attributed to short-term weather conditions, particularly high surface winds and the frequency, intensity, and timing of lightning strikes at the beginning of the summer rainy season.

Correlations between ENSO and fall, winter, and spring precipitation in the southwestern states are well known (Douglas and Englehart, 1984; Andrade and Sellers, 1988). All three seasons tend to be wetter during warm ENSO events. Increased winter/spring precipitation stems from a deep and intensified Aleutian low (a southerly displacement of the North Pacific storm track) and a stronger subtropical jet stream that brings moisture directly from the Intertropical Convergence Zone (ITCZ) in the eastern and central Pacific. Relationships with summer rainfall are less clear. Opposition of

winter/spring and summer precipitation was first noted by Sellers (1960). Reyes and Cadet (1988) suggest that, during ENSO summers, the ITCZ moves south, the South Pacific high weakens, and low-level moisture advection into the southwestern United States is reduced. Rainfall may increase during the following summer due to persistence of warm surface waters off the west coast of Mexico and northward penetration of the subtropical high ridge over the western United States (Carleton et al., in press). Summer teleconnections may have an uneven expression across the southwestern United States, depending on proximity to the different sources of moisture (Gulf of Mexico and Pacific Ocean/Gulf of California).

In this paper, we identify an ENSO teleconnection in archival and tree-ring evidence of fire activity primarily affecting ponderosa pine (*Pinus ponderosa*) forests in the southwestern United States. Because of its thick bark, ponderosa pine is one of the more fire-resistant species of western conifers. Slow-spreading surface fires encourage regeneration of ponderosa pine in forest openings and result in an uneven-aged forest with trees growing in even-aged cohorts (Schubert, 1974; see White, 1985 for opposing view). A better understanding of long-term fire-climate relationships is paramount to wise management of southwestern ponderosa pine forests. These forests provide most of the region's lumber and form the predominant cover in the headwaters of the Rio Grande and Colorado River basins.

METHODS

Reports of the U.S. Forest Service provide records of fire after 1900. The Forest Service keeps annual records of number of fires and area burned on more than 8 million hectares under its jurisdiction (U.S. Department of Agriculture, 1975-1986; see summary in Barrows, 1978). A reliable chronology of fire activity for Arizona and New Mexico is readily available since 1940. Longer records may be gleaned from district offices at individual forests. For Gila National Forest, in southwestern New Mexico (Figure 2), the chronology can be extended from 1909.

Evidence for pre-1900 fires was compiled from fire-scar chronologies developed at the University of Arizona's Laboratory of Tree-Ring Research. Fifteen fire-scar chronologies are available from Arizona (7), New Mexico (5 of 6 in Gila National Forest), west Texas (1), and Sonora, Mexico (1) (Figure 2). Full or partial cross sections were collected from both live and dead fire-scarred trees, the annual rings were cross-dated, and the position of fire scars within annual rings were noted (Dieterich and Swetnam, 1984). Fire-scar dates from 315 trees are included in the fifteen chronologies.

Eleven of the fire-scar chronologies span the period from about 1700 to 1900, three of them extend from about 1750 to 1900, and one chronology extends from 1800 to the mid-1980s (Swetnam, in press). The dearth of fire scars after 1900 reflects reduction of fire due to removal of fine fuels by heavy grazing and a vigorous program of fire suppression by government agencies.

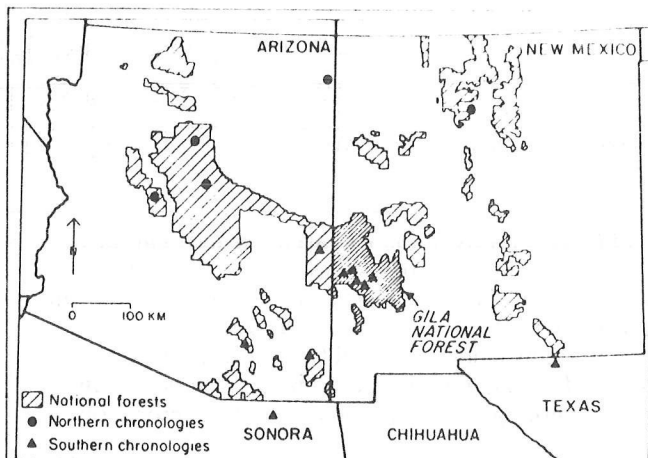


Figure 2. Map of Arizona and New Mexico showing boundaries of National Forests and locations for fire-scar chronologies. Northern Arizona chronologies discussed in the text include all four sites north of 34° latitude. The southern Arizona and New Mexico group includes ten sites south of 34°. The single site in northern New Mexico was used only in compiling overall statistics.

Only the chronology from Mexico extends into the 1980s, probably because fire suppression either was not practiced or was ineffective. In general, the fire-scar chronologies document the timing of episodic, low intensity surface fires that burned unchecked through the understory of ponderosa pine and mixed-conifer forests. Both fire-scar and archival evidence show years in which fires were widespread (Swetnam, in press). In the twentieth century, these events include some of the driest years of record (e.g., 1946, 1956, 1971, 1974, and 1989).

FIRES AND ENSO

Figures 3 and 4 show the average Southern Oscillation Index (SOI) in the Northern Hemisphere winter (December-February) (Ropelewski and Jones, 1987) with annual area burned since 1909 in Gila National Forest (both lightning and person-caused fires) and since 1940 in Arizona and New Mexico (lightning fires only). In both cases, SOI is significantly correlated with mean area burned (Gila: $r = 0.35$, $p < 0.01$; Arizona and New Mexico: $r = 0.48$; $p < 0.01$). These correlations are comparable with those obtained between SOI or other ENSO indicators and cool season precipitation in the southwest (Douglas and Englehart, 1984; Andrade and Sellers, 1988).

As with precipitation, the correlations are significant but normally explain less than one-fourth of the variance. The closest association is that of minimal fire activity during strong and very strong ENSO events (1912, 1926, 1932, 1941, 1957-58, 1972-73, 1982-83 [event strength is defined by Quinn et al., 1987]). There is a weaker tendency for severe fire years to occur during La Niña years (cold water events in the equatorial Pacific). A prime example is the current fire season.

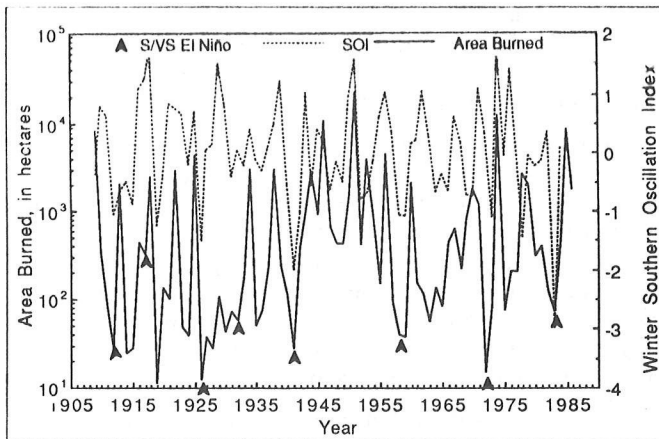


Figure 3. Mean annual area burned in Gila National Forest (lightning- and person-caused fires, 1909-1986) and average December-February Southern Oscillation Index (1909-1984). The Pearson correlation coefficient between log. mean annual area burned and the winter SOI is $r = 0.35$ ($p < 0.01$). Strong and very strong (S/V) El Niño events, as defined by Quinn et al. (1987), are indicated by arrows.

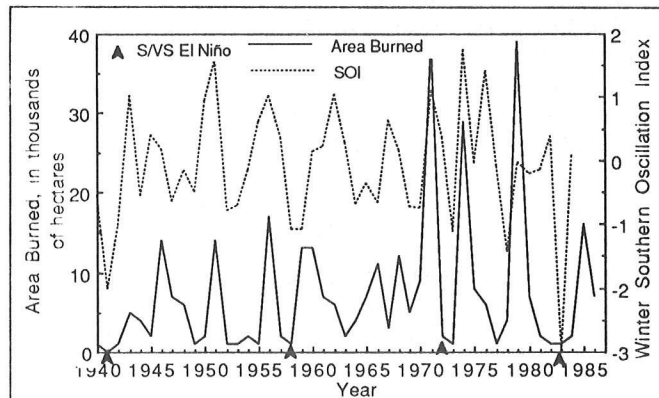


Figure 4. Mean annual area burned in all National Forests in Arizona and New Mexico (lightning fires only, 1940-1986) and average December-February Southern Oscillation Index (1940-1984). The Pearson correlation coefficient between log. mean annual area burned and the winter SOI is $r = 0.48$ ($p < 0.01$). Strong and very strong (S/V) El Niño events, as defined by Quinn et al. (1987), are indicated by arrows.

Very little precipitation fell in Arizona and New Mexico between February and July, 1989. By mid-July, tens of thousands of hectares had burned in the region. In addition, many shrubs in the Arizona chaparral died during the 1989 drought and will provide fuel for the 1990 fire season.

Differences in mean area burned per year during ENSO vs. non-ENSO events were evaluated using the Mann-Whitney test. Mean area burned (387 ha) in Gila National Forest during 14 strong and very strong ENSO events is significantly different than for 52 non-ENSO events (1,582 ha) ($p < 0.001$, 2-tailed probability level). Mean area burned (1,412 ha) during 26 ENSO events of all intensities between 1909 and 1986 also was signifi-

cantly different than for non-ENSO years (1,582 ha). Weak ENSO events apparently are not closely associated with fire activity; Andrade and Sellers (1988) also found that the correlation between ENSO and southwestern precipitation decreases with event intensity.

For Arizona and New Mexico, mean area burned (957 ha) during 8 strong and very strong ENSO events was significantly less than during non-ENSO years (8,676 ha; $p < 0.001$). For 13 ENSO events of all intensities, mean area burned (3,013 ha) was considerably lower than for non-ENSO years ($p < 0.001$).

Comparisons between SOI and southwestern fire activity can be extended to before the turn of the century using fire-scar records. Figure 5 relates percentage of trees scarred in Arizona and New Mexico to the annual SOI for the period 1866-1900. Percentage of trees scarred was computed as the number of sampled trees scarred in a given year relative to the number of sampled trees at the site that had been scarred previously. This percentage was calculated for each of the chronologies and then averaged for the region. The percentage of trees scarred in Arizona and New Mexico was positively correlated with the annual SOI between 1866 and 1900 ($r = 0.50$, p). This is a better correlation than that obtained with twentieth century observational data (area burned). This is because area burned can be affected by a large local fire, whereas percentages of trees scarred reflect fire activity throughout the region.

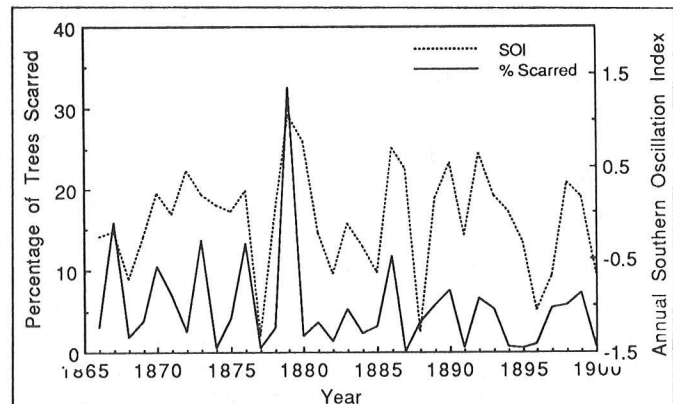


Figure 5. Percentage of trees scarred per year in fire-scar chronologies from Arizona and New Mexico (see text and Figure 1) and the average annual Southern Oscillation Index (1866-1900, both series). The Pearson correlation coefficient is $r = 0.50$ ($p < 0.01$).

Table 1 lists results of contingency analyses for the time series of mean area burned since 1909 in Gila National Forest and percentage of trees scarred in the southwest between 1700 and 1900 (Quinn, et al., 1987, only note strong and very strong ENSO events prior to 1800). The number of strong to very strong El Niños above and below the median area burned were compared using chi-square statistics.

Contingency results show that ENSO events are clearly associated with below median area burned in Gila National Forest. Fire-scar data, however, show mixed

Table 1. Results of contingency analysis of numbers of strong and very strong El Niño-Southern Oscillation (ENSO) events above and below (A/B) the median values of fire occurrence in four time series. The Gila National Forest series is mean annual area burned, and the fire-scar series is percentage of trees scarred each year. ENSO groupings with (-) exclude first years of 2- or 3-year ENSO events. Yates correction of chi-square and P levels are shown in parentheses for groupings with expected frequencies less than or equal to 10.

	Number of Events		Chi-Square	P Level
	Expected A/B	Observed A/B		
<i>Gila National Forest (1909-1985)</i>				
ENSO	7/7	2/12	8.756 (7.092)	0.004 (0.008)
ENSO (-)	4/4*	1/7	5.029 (3.493)	
<i>Northern Arizona Fire-Scar Chronologies (1700-1900)</i>				
ENSO	13.5/13.5	8/19	5.181	0.022
ENSO (-)	10/10	5/15	5.556 (4.500)	0.018 (0.032)
<i>Southern Arizona & New Mexico Fire-Scar Chronologies (1700-1900)</i>				
ENSO	13.5/13.5	10/17	2.098	0.144
ENSO (-)	10/10	6/14	3.556 (2.722)	0.056 (0.095)
<i>All Fire-Scar Chronologies (1700-1900)</i>				
ENSO	13.5/13.5	10/17	2.098	0.144
ENSO (-)	10/10	6/14	3.556 (2.722)	0.056 (0.095)

* The chi-square critical value for $p \leq 0.05$ is 3.84. The chi-square (non-Yates) exceeds the critical value in this case; however, since expected cell frequency (4) is too low for this test, the significance level is suspect.

results. From 1700 to 1900 fire occurrence during ENSO years was lowest in northern Arizona, suggesting that fire/ENSO relationships may be more coherent to the north. Note that earlier analyses by Simard et al. (1985b) showed that in the western states the highest correlations between fire and ENSO were in Colorado — not in Arizona and New Mexico, as might be expected. This pattern may stem from higher incidence of cloud-to-ground lightning strikes and more common lightning fires in northern parts of the Southwest. (In the western United States, the greatest number of cloud-to-ground lightning strikes for the 1983 and 1984 summers was in the Four Corners area [Reap, 1986]). Alternative explanations may involve some aspect of

climate/fuel dynamics, especially the role of winter grasses, or simple geography. The largest contiguous forests, which are vulnerable to large fires during dry years, occur in the northern parts of the southwest.

Though there is an association between annual fire occurrence in the southwest and ENSO occurrence and intensity, the relative dependence on long-term processes (e.g., seasonal drought) versus short-term weather (e.g., lightning) is uncertain. Hypothetically, increased fuel moisture during a wet, cool season discourages the spread of fires. By raising soil moisture, the buildup of moist litter also forestalls normal dieoff of plants during the arid spring and foreshummer.

Interannual variability of lightning and its relationship to fire occurrence are virtually unexplored. Reliable lightning data for the western United States are only available since 1976, when the Bureau of Land Management established an extensive lightning detection network (Kridge et al., 1980). An important factor may be the incidence of "dry lightning" storms just before or at the onset of the monsoon season. One possible source is early summer hurricanes in the Gulf of Mexico. As the hurricanes dissipate over land, some of the moisture gets caught in the normal southeasterly flow. When the limited moisture reaches the southwest, strong thermal heating may form isolated thunderstorms that produce enough lightning to ignite fires but not enough rain to put them out. Gray (1984) found a significant decrease in the number of hurricane days during moderate to strong El Niños. Tropical cyclone activity is inhibited by the anomalous increase in upper tropospheric westerly winds characteristic of warm ENSO events.

Obviously, the relationship between the synoptic climatologies of ENSO versus non-ENSO events and early summer lightning activity needs further investigation.

TRENDS IN FIRE ACTIVITY

Unlike annual area burned and percentage of trees scarred, the total number of fires per year has no apparent relationship to ENSO. Simard et al. (1985a) also found no apparent relationship in the southeast.

In the southwest, annual number of fires has increased significantly, partly because fire detection has improved with time (Swetnam, in press). For example, in the early part of the century, four or five mounted rangers patrolled Gila National Forest and reported about 40 fires each year. Increase of personnel and the use of aircraft now accounts for detection of about 350 fires per year. Most of the additional fires detected were small (less than 0.25 acre [0.09 ha]). Notwithstanding, there is an increase in the number of large fires reported in southwestern forests. Considering only those fires greater than 10 acres (3.6 ha) in Gila National Forest, an average of five fires per year occurred between 1909 and 1939, compared with eleven fires per year from 1960 to 1980 (Swetnam, in press). Such fires would not have escaped the attention of even a few mounted rangers. The apparent increase in number of lightning-caused

fires greater than 100 acres (35.9 ha) throughout Arizona and New Mexico (Figure 6) began in the late 1950s, when most of the technological advances and commitment of resources were already in effect.

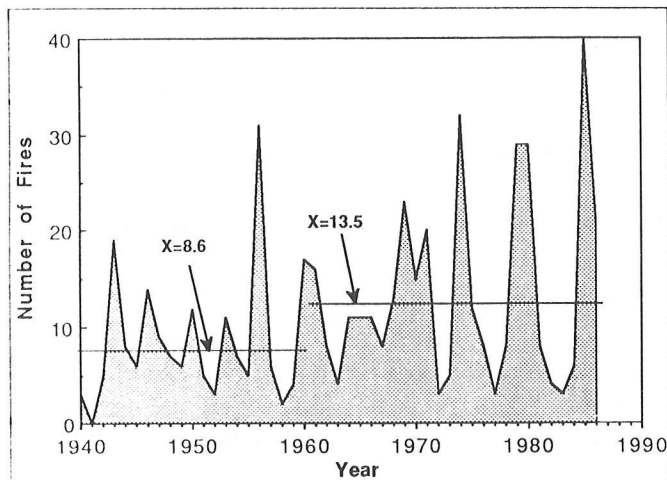


Figure 6. Annual number of lightning-caused fires with an area of more than 100 acres (35.9 ha) in Arizona and New Mexico (1940-1986). Fires allowed to burn under prescribed fire programs were excluded. The mean number of fires from 1940 to 1960 (8.6) was less than the mean from 1961 to 1986 (13.5) ($p = 0.064$).

A climatic explanation for the increasing number of fires is unlikely; cool seasonal precipitation increased after the 1960s, partly in response to more frequent ENSO events. A greater number of large fires per year probably has its origin in fire suppression and increasing fuel loads. When fires are suppressed, dead fuel high in ether extractives continues to accumulate until it is released by fire. Also, without the thinning effect of frequent fires, dense and quite flammable stands of stunted ponderosa pine trees may develop in the understory of mature forests.

Suppression of small fires and greater flammability due to increased accumulation of both dead and live fuel shifts the fire regime from episodic surface burns to infrequent crown fires. Thus, fire regimes in ponderosa pine are becoming more like those in mixed-conifer and spruce/fir forests that consist of fire-susceptible and shade-tolerant trees.

Natural regeneration of ponderosa pine has slowed during the past 70 years (Schubert et al., 1970). This may portend profound changes in the structure and composition of southwestern forests in centuries to come. An interesting analog is the last ice age, when ponderosa pine was much reduced in range and dominance throughout the region. Explanations include a different seasonal distribution of rainfall (and possibly heavy grazing by animals now extinct) that favored a lower fire recurrence than during the Holocene (Betancourt and Van Devender, 1981).

CONCLUSIONS

Correlations comparable to those found for cool season precipitation exist between low values of the Southern Oscillation Index and reduced fire activity in the southwestern United States. The environmental factors responsible for this relationship are undetermined, but they may involve a decrease in the fuel load due to a wet winter and spring and/or the lack of lightning activity before the onset of the monsoon season. Successful forecasting of an El Niño (or La Niña) and its delayed teleconnections could improve fire readiness and scheduling of prescribed burning in the southwest.

Superimposed on the highly variable annual fire occurrence is a trend of increasing number of large fires since 1960. We attribute this trend to systematic fire suppression and the unnatural accumulation of fuel loads. Such manipulation of fire regimes, if they persist, could drive large-scale changes in the composition and structure of southwestern ponderosa pine forests.

REFERENCES

- Andrade, E.R., and Sellers, W.D., 1988, El Niño and its effect on precipitation in Arizona and western New Mexico: *Journal of Climatology*, v.8, p.403-410.
- Barnett, T.P., Graham, N., Cane, M., Zebiak, S., Dolan, S., O'Brien, J., and Legler, E., 1988, On the prediction of El Niño of 1986-87: *Science*, v.241, p.192-196.
- Barrows, J.S., 1978, Lightning fires in southwestern forests: Fort Collins, Colorado, U.S. Department of Agriculture, Forest Service, Rocky Mountain Forest and Range Experiment Station.
- Betancourt, J.L., and Van Devender, T.R., 1981, Holocene vegetation of Chaco Canyon, New Mexico: *Science*, v.214, p.656-658.
- Carleton, A.M., Carpenter, D.A., and Weser, P.J., in press, Mechanisms of interannual variability of the southwest U.S. summer rainfall maximum: *Journal of Climate*.
- Dieterich, J.H., and Swetnam, T.W., 1984, Dendrochronology of a fire-scarred ponderosa pine: *Forest Science*, v.30, p.238-247.
- Douglas, A.V., and Englehart, P.J., 1984, Factors leading to the heavy precipitation regimes of 1982-1983 in the United States: *Proceedings of the Eighth Annual Climate Diagnostics Workshop, Downsview, Ontario 42, 54 (INTIS PB84-192418)*.

- _____, 1980, On a statistical relationship between autumn fall in the central equatorial Pacific and subsequent precipitation in Florida: *Monthly Weather Review*, v.109, p.2377-2382.
- Gill, A.M., 1983, Forest fire and drought in eastern Australia: *Proceedings of Colloquium on the Significance of the Southern Oscillation-El Niño Phenomena and the Need for a Comprehensive Ocean Monitoring System in Australia*, Australia Marine Sciences and Technologies Advisory Committee.
- Gray, W.M., 1984, Atlantic seasonal hurricane frequency: *Monthly Weather Review*, v.112, p.1649-1683.
- Hardy, C.E., 1983, The Gisborne era of forest fire research, legacy of a pioneer: U.S. Department of Agriculture, Forest Service, FS-367.
- Krider, E.P., Pifer, A.E., and Vance, D.L., 1980, Lightning direction finding systems for forest fire detection: *Bulletin of the American Meteorological Society*, v.61, p.980-986.
- Leighton, M., 1984, The impact of one of the world's worst forest fires: World Wildlife Fund, Monthly Report, June, p.117-123.
- Quinn, W.H., Neal, V.T., Antunes de Mayolo, S.E., 1987, El Niño occurrences over the past four and a half centuries: *Journal of Geophysical Research*, v.92 (C13), p.14,449-14,461.
- Reap, R.M., 1986, Evaluation of cloud-to-ground lightning data from the western United States for the 1983-84 summer seasons: *Journal of Climate and Applied Meteorology*, v.25, p.785-799.
- Reyes, Sergio, and Cadet, D.L., 1988, The southwest branch of the North American monsoon during 1979: *Monthly Weather Review*, v.116, p.1175-1187.
- Ropelewski, C.F., and Halpert, M.S., 1986, North American precipitation and temperature patterns associated with El Niño/Southern Oscillation (ENSO): *Monthly Weather Review*, v.114, p.2,352-2,362.
- Ropelewski, C.F., and Jones, P.D., 1987, An extension of the Tahiti-Darwin Southern Oscillation Index: *Monthly Weather Review*, v.115, p.2,161-2,165.
- Schubert, G.H., 1974, Silviculture of southwestern ponderosa pine, the status of our knowledge. U.S. Department of Agriculture, Forest Service Research Paper RM-123.
- Schubert, G.H., Heidmann, L.J., and Larson, M.M., 1970, Artificial reforestation practices for the southwest: U.S. Department of Agriculture, Agriculture Handbook, v.370, Washington, DC.
- Sellers, W.D., 1960, Precipitation trends in Arizona and western New Mexico: *Proceedings, 28th Annual Western Snow Conference*, Santa Fe, New Mexico.
- Simard, A.J., and Main, W.A., 1987, Global climate change, the potential for changes in wildland fire activity in the southeast, *Proceedings of the Symposium on climate change in the southern United States, Future impacts and present policy issues*, May 28-29, 1987, New Orleans: U.S. Environmental Protection Agency, Washington, DC, p.280-308.
- Simard, A.J., Haines, D.A., and Main, W.A., 1985a, Relations between El Niño/Southern Oscillation anomalies and wildland fire activity in the United States: *Agricultural and Forest Meteorology*, v.36, p.93-104.
- _____, 1985b, El Niño and wildland fire, an exploratory study, in *Weather – The drive train connecting the solar engine to forest ecosystems* (Donoghue, L.R., and Martin, R.E., eds), p.88-95: Bethesda, MD, Society of American Foresters.
- Swetnam, T.W., in press, Fire history and climate in the southwestern United States, *Proceedings of Symposium on effects of fire in management of southwestern natural resources*, Tucson, AZ, November 14-17, 1988: U.S. Department of Agriculture, Forest Service, General Technical Report.
- U.S. Department of Agriculture, Forest Service 1975-1986, Annual Reports: Washington, DC.
- White, A.S., 1985, Presettlement regeneration patterns in a southwestern ponderosa stand: *Ecology*, v.66, p.589-594.

Tropical and Subtropical Moisture and Southerly Displaced North Pacific Storm Track: Factors in the Growth of Late Quaternary Lakes in the Mojave Desert

Yehouda Enzel, Roger Y. Anderson, William J. Brown, Daniel R. Cayan, and Stephen G. Wells

ABSTRACT: Historical flood events produced lakes in the Mojave River watershed in southeastern California and represent climatic conditions similar to those in the late Quaternary when perennial lakes formed in the Mojave Desert. Historical lakes are related to tropical and subtropical sources of moisture and an extreme southward shift of storm tracks. It is suggested that this atmospheric pattern occurred frequently during earlier periods with perennial lakes in the Mojave River drainage basin.

INTRODUCTION

Perennial lakes occupied Silver Lake playa (Figure 1) in the Mojave Desert, not only in late Pleistocene (Ore and Warren, 1971; Wells et al., 1984, 1989), but also for brief intervals in the middle and late Holocene (Wells et al., 1989). Ephemeral lakes have filled Silver Lake playa at least eight times during the historical period (Enzel et al., 1989). This paper pursues one of the goals of PACLIM (Moores et al., 1986) by presenting the hypothesis that extreme modern hydrological events that

produced the historical ephemeral lakes in Silver Lake playa, and their related climatic conditions, can be used as analogs for perennial lakes of the middle to late Holocene and perhaps the late Pleistocene.

MODERN EVENTS AND ATMOSPHERIC PATTERNS

Silver Lake playa is the terminus of the Mojave River, located in the hyperarid Mojave Desert, in the southern Great Basin (Figure 1). Based on instrumented and historical records, eight relatively long-standing (2 to 18 months), ephemeral lakes are documented in Silver Lake playa since AD 1892 (Wells et al., 1989; Enzel et al., 1989). These ephemeral lakes were formed as a result of heavy winter storms in the headwaters of the Mojave River, in San Bernardino Mountains. The winter storms are related to distinctive patterns of circulation and pressure over the North Pacific Ocean. North Pacific sea level pressure (SLP) patterns include:

- Weak eastern North Pacific subtropical high,
- Shifts of the central North Pacific low to the south and east, resulting in anomalously low pressure over the west coast of the United States,
- Tendency for a "split" Aleutian low, and
- In few cases, occurrence of blocking high pressure in the eastern Aleutian.

Extreme southerly displacement of storm tracks was detected during the historical ephemeral lake events (Enzel et al., 1988; 1989; also see Weaver, 1962; Pyke, 1972; Kline and Bloom, 1987; Namias, 1980; Cayan and Peterson, 1989).

Although high elevation atmospheric pressure data are available for only four of eight lake-building flood events (1969, 1978, 1980, and 1983), inspection of these data show the following pattern:

- A trough or cutoff low pressure over off-shore California,
- Southerly displacement of the maximum zonal winds, and
- In some cases, blocking high pressure in the Gulf of Alaska and/or the northwestern United States (e.g., Wagner, 1969; Bonner et al., 1971; Namias et al., 1988).

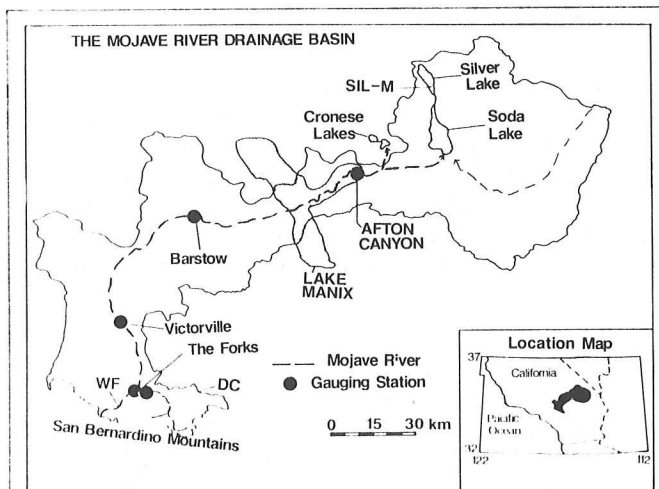


Figure 1. Location map of the Mojave River and its terminal basins, Silver Lake and Soda Lake playas. SIL-M is a drilled core that contains Holocene lake deposits. DC (Deep Creek) and WF (West Fork) are the main tributaries to the Mojave River.

In J.L. Betancourt and A.M. MacKay, editors, 1990. Proceedings of the Sixth Annual Pacific Climate (PACLIM) Workshop, March 5-8, 1989: California Department of Water Resources, Interagency Ecological Studies Program Technical Report 23.

Namias (1980) identified the similarities between sea surface temperature (SST) and the 700-millibar height patterns between the winters of 1969, 1978, and 1980. During the January 1969 event, clouds extended from the Intertropical Convergence Zone (ITCZ) to southern California, and the subtropical jet shifted northward from its normal position over Baja California, directing tropical moisture to southern and central California (Bonner et al., 1971). This specific event was apparently accompanied by a merging of the polar jet, and the subtropical jet occurred over central and southern California. Tropical and subtropical moist warm air was directed into southern and central California during the other three lake-building flood events (1978, 1980, and 1983). In these events, the North Pacific storm track was at an extremely southern position along the western coast.

Present cyclogenesis and precipitation maxima are normally under the axis of the jet (Starret, 1949; Pyke, 1972), with rapid decreases in precipitation to the south and more gradual decreases to the north of the jet axis. This configuration is the basis for the regional-scale interpretations of proxy-climatic data in paleoclimatologic studies.

HOLOCENE LAKES

Modern climatic conditions during the ephemeral lake-building events appears to be analogous to conditions that produced permanent lakes in Silver Lake basin 390 ± 90 and 3620 ± 70 YBP (Beta-25341 and 25634, respectively). These lake stands were interpreted from alternating millimeter-scale laminated lake deposits, found in drilled core Sil-M (Figure 1) (Wells et al., 1989). Climatic conditions that support a lake in the "Little Ice Age" are reflected in tree-ring analyses in southern California (Schulman, 1947; Fritts et al., 1979; Haston and Michaelsen, 1988). Reconstructions of climatic patterns from tree rings show more streamflow, a high frequency of extreme annual precipitation, and persistent SLP patterns during the late 1500s and early 1600s. This shift to more frequent events of precipitation is contemporaneous with the youngest lake stand in the Mojave River drainage basin (390 ± 90 YBP).

Smith et al. (1979, p.187) suggested that "the climate represented by the 1968-69 winter and spring might resemble the typical climate of this area during the Pleistocene". They observed lower temperatures and abnormal amounts of snow accumulation in the Sierra Nevada (more than 1 m water content) during the January 1969 event (Smith et al., 1979).

Other indicators of climatic patterns during periods that supported Holocene lakes are reflected in early 1600s ("Little Ice Age") and early Neoglacial moraines in the Sierra Nevada (LaMarche, 1974; Burke and Birkeland, 1983). This suggests concurrence of snow accumulation in the Sierra Nevada in central California, large precipitation and streamflow in southern California, and lake stands in the Mojave River basin during both historical and prehistorical periods.

LATE PLEISTOCENE LAKES

Evidence for Holocene lakes in Silver Lake basin raises the issue of type of circulation systems that supported larger lakes in the late Pleistocene. Is the Holocene moisture directed from new sources, or is it a vestige of a pattern that has persisted since the Pleistocene?

Late Pleistocene Lake Mojave

During the late Pleistocene, Lake Mojave occupied both Silver Lake and Soda Lake basins (Figure 1) during high stands of the lake. Detailed analysis of cored lake deposits and mapping of dated shoreline features indicate that Pleistocene Lake Mojave formed in Silver Lake basin by 22 ka and possibly earlier in the deeper Soda Lake basin (Wells et al., 1989). Prior to this time discharge from the Mojave River fed paleo-lake Manix (Jefferson, 1985) (Figure 1).

Two major high stands occurred in Lake Mojave 22 to 8.5 ka (Figure 2): Lake Mojave I (18.4 to 16.6 ka [thousands of years ago]), and Lake Mojave II (13.7 to 11.5 ka). Both lakes reached the elevation of the spillway and were separated by periods with rapid fluctuations and total drying of at least the shallower Silver Lake basins. Sedimentation in the two lake basins between

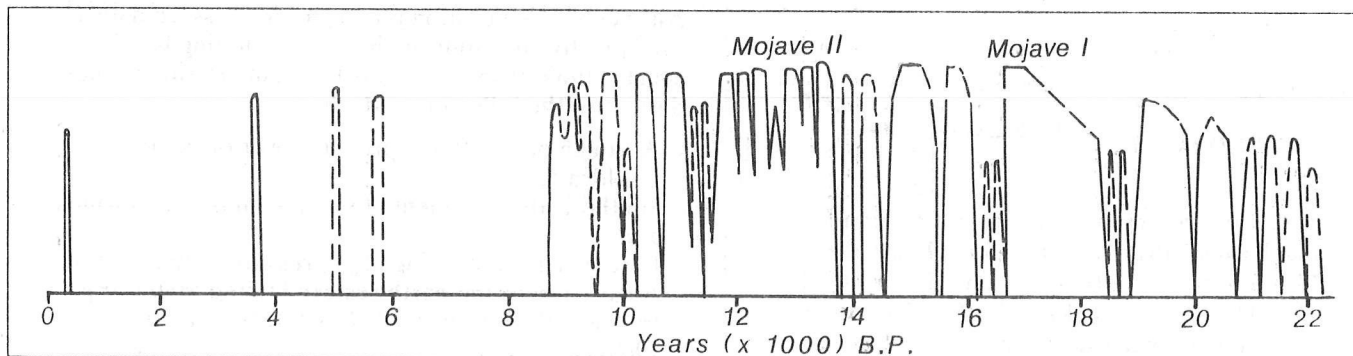


Figure 2. Lake-level fluctuations in Lake Mojave since 22 ka. It is based on dated deposits from drilled cores and stratigraphy of shore features from Silver Lake playa (Wells et al., 1989). Dashed lines represent lack of either age or elevation data. The ordinate is interpreted relative elevation of water surface above the lake floor. The abscissa represents elevation of Silver Lake basin floor. This elevation increased with time (see text) as the result of sedimentation. The maximum water surface elevation decreased as a result of lowering of the lake spillway elevation.

the beginning of Lake Mojave I and 8.5 ka resulted in more than 50 percent reduction in the lake's storage capacity, thus producing a more sensitive system. Based on this, Lake Mojave I appears to have been sustained by an equal if not greater amount of river discharge than occurred during Lake Mojave II. During the glacial maxima (18 ka) Lake Mojave contained a larger volume of water and fluctuated less than it did during the interval from 13.7 to 11.5 ka (Figure 2).

Paleoclimatic Conditions

Kutzbach (1987) presented results of climatic simulations since the glacial maxima. He suggested that at 18 ka the polar jet was split and the mean position of the southern split of the polar jet was at 30°-35°N (Figure 3). Based on spatial variations in lake-level fluctuations, Harrison and Metcalfe (1985), suggested that from 18 to

13 ka the mean westerly storm track was 35°-36°N (Figure 3). They also concluded that their compilation supports latitudinal migration of major features of the general atmospheric circulation. Benson and Thompson (1987) suggested that since paleo-Lake Lahontan was at its highest stand between 14 and 12.5 ka, the storm track and, hence, the mean polar jet position must have been at 39°-42°N during this time (Figure 3).

In the same period (13.7 ka-11.5 ka) Lake Mojave, 5° to the south, was fluctuating at and just below its highest stand (Figure 2). This suggests more frequent episodic input of water to the relatively shallow and, hence, sensitive Lake Mojave. For the same period, 5° north at Lake Lahontan, Barnosky et al. (1987) interpreted relative dry and cold conditions. This suggests the mean position of the storm track should be somewhat farther south than the one proposed by Benson and Thompson (1987), possibly at the latitude proposed by Harrison and Metcalfe (1985) or Kutzbach (1987).

The synchronicity between Lake Lahontan and Lake Mojave might be explained either by:

- Southward migration during the wet season of the storm track, which is similar to the present situation (Pyke, 1971) or
- A subtropical moisture source directed to the southern Great Basin by a northward shift of the subtropical jet.

During the historical Mojave Lake events, the zone of maximum wind velocity was at 33°-35°N (Figure 3) over the proposed range of latitudes (Bonner et al., 1971; Namias et al., 1988; U.S. Department of Commerce, 1969, 1978, 1980, 1983).

The North Pacific SLP for both the simulation output for 18 ka (Kutzbach, 1987) and the composite SLP for the eight historical lake events (Enzel et al., 1989) show a generally similar pattern of deviation from the modern mean SLP. This pattern includes a shift to the south and east of the central Pacific low, and higher pressures over Canada and the Pacific Northwest. These features are evident in both the 18 ka model simulation and in the historical lake-producing events.

SUMMARY

Modern and Holocene lakes in the Mojave River drainage basin serve as an analog for climate conditions during earlier and larger lake stands. During the historical events, the polar jet (and the North Pacific storm track) was at an extremely southern position. Persistent similar patterns can explain the building of the Holocene and the larger late-Pleistocene lakes. As the subtropical jet played a role in directing moist air masses into the southern Great Basin in some of the modern lake-building events, it is also conceivable that the subtropical jet may have been deflected toward more northern latitudes in the late Pleistocene. This position of the subtropical jet could contribute moisture to the much larger paleolakes in hyperarid basins in the southern Great Basin, which were already fed by North Pacific storms.

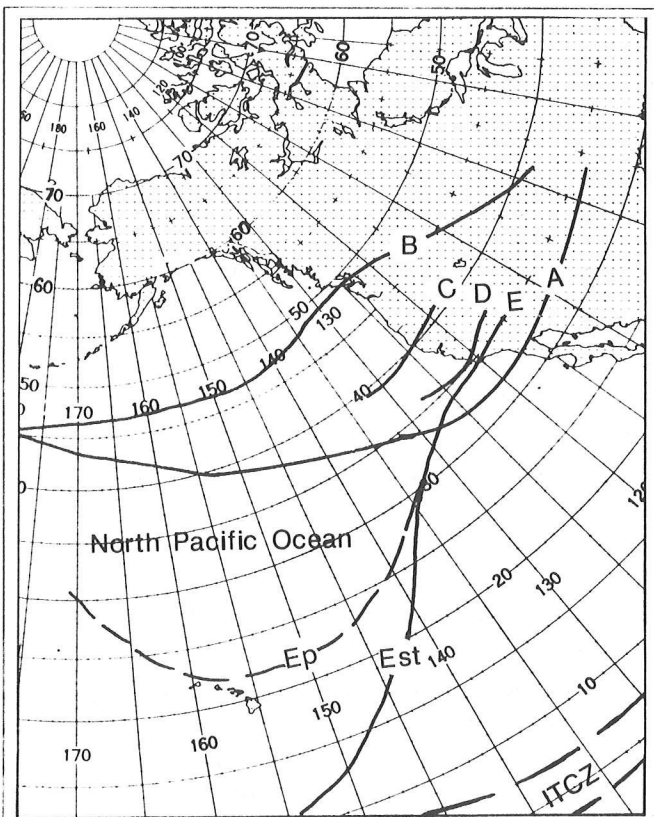


Figure 3. Proposed winter jet stream positions for the eastern North Pacific.

- A = Average for 18 to 15 ka;
 - B = Average for 12 to 0 ka (Kutzbach, 1987).
 - C = Average for 14 to 12.5 ka (Benson and Thompson, 1987).
 - D = Average for 18 to 13 ka (Harrison and Metcalfe, 1985).
 - E = Merging of the polar jet (Ep) and subtropical jet (Est) during the 1969 event; the polar jet was at similar latitudes over the west coast during the 1978, 1980, and 1983 events.
- ITCZ = Intertropical Convergence Zone.

ACKNOWLEDGEMENTS

For helpful discussions we thank Bruce Allen, Robert G. Balling Jr., Thomas F. Bullard, and Bruce Harrison. Support for this study was partially provided by New Mexico WRRI and U.S. Geological Survey Project No. 1423686 to S.G. Wells, R.Y. Anderson, and L.D. McFadden.

REFERENCES

- Barnosky, C.W., Anderson P.M., and Bartlein, P.J., 1987, The northwestern U.S. during deglaciation; Vegetational history and paleoclimatic implications, *in* Ruddiman, W.F., and Wright, H.E. Jr., eds., North America and adjacent oceans during the last deglaciation: Boulder, CO, Geological Society of America, v.K-3, p.289-321.
- Benson, L.V., and Thompson, R.S., 1987, Lake-level variations in the Lahontan basin for the past 50,000 years: *Quaternary Research*, v.28, p.69-85.
- Bonner, W., Pyke, C., and Hickey, R., 1971, A study of the California rainstorm of January 1969, Final Report, National Environmental Satellite Center, National Oceanographic and Atmospheric Administration, Contract E-3270(N), 29p. and 29 figures.
- Burke, R.M., and Birkeland, P.W., 1983, Holocene glaciation in the mountain ranges of western United States, *in* Wright H.E. Jr., ed., Late-Quaternary environments of the United States, v.2: Minneapolis, MN, The Holocene, University of Minnesota Press, p.3-11.
- Cayan, D.R., and Peterson, D.H., 1989, The influence of North Pacific atmospheric circulation on streamflow in the west, *in* Peterson, D.H., Editor, Aspects of climate variability in the Pacific and western Americas: American Geophysical Union Monograph v.55, p.325-398.
- Enzel, Y., Cayan, R.D., Anderson, R.Y., and Wells, S.G., 1989, Atmospheric circulation during Holocene lake stands in the Mojave Desert: Evidence of regional climate change: *Nature*, v.341, p.44-47.
- Enzel, Y., Cayan, R.D., Balling, R.S., Wells, S.G., Anderson, R.Y., Brown, W.J., 1988, Large-scale "anomalous" Northern Pacific storm patterns recorded in the Mojave River hydrologic system: *EOS, Transactions, American Geophysical Union*, v.69, no.44, p.1220.
- Fritts, H.C., Lofgren, R.G., and Gordon, G.A., 1979, Variation in climate since 1602 as reconstructed from tree rings: *Quaternary Research*, v.12, p.18-46.
- Harrison, S.P., and Metcalfe, S.E., 1985, Spatial variations in lake levels since last glacial maximum in the Americas north of the equator: *Zeitschrift fur Gletscherkund und Glazialgeologie*, Band 21, p.1-15.
- Haston, L., and Michaelsen, J., 1988, Spatial and temporal components of precipitation variability in California as derived from tree-ring chronologies: *EOS, Transactions, American Geophysical Union*, v.69, no.44, p.1061.
- Jefferson, G.T., 1985, Stratigraphy and geological history of the Pleistocene Manix Formation central Mojave Desert, California, *in* Reynolds, R.E., *Geologic investigations along Interstate 15; Cajon Pass to Manix Lake, California: Redlands, CA, San Bernardino County Museum*, p.157-170.
- Kline, W.H., and Bloom, H.J., 1987, Specification of monthly precipitation over the United States from the surrounding 700 mb height field: *Monthly Weather Review*, v.115, p.2118-2132.
- Kutzbach, J.E., 1987, Model simulation of the climatic patterns during the deglaciation of North America, *in* Ruddiman, W.F., and Wright, H.E. Jr., eds., North America and adjacent oceans during the last deglaciation: Boulder, CO, Geological Society of America, The Geology of North America, v.K-3, p.425-446.
- LaMarche, V.C., 1974, Paleoclimatic inferences from long tree-ring records: *Science*, v.183, p.1043-1048.
- Moores, C.N.K., Peterson, D.H., Cayan, D.R., 1986, The Pacific Climate Workshop: *EOS, Transactions, American Geophysical Union*, v. 67, no. 52, p. 1404-1405.
- Namias, J., 1980, The heavy California winter rains of 1979-80 as a manifestation of macroscale air/sea-coupling, *Proceedings of the Fifth Annual Climate Diagnostic Workshop: U.S. Department of Commerce, National Oceanographic and Atmospheric Administration*, p.35-50.

- Namias, J., Yuan, X., and Cayan, D.R., 1988, Persistence of North Pacific sea surface temperature and atmospheric flow patterns: *Journal of Climate*, v.1, p.682-703.
- Orc, H.T., and Warren, C.N., 1971, Late Pleistocene-early Holocene geomorphic history of Lake Mojave, California: *Geological Society of America Bulletin*, v.82, p.2553-2562.
- Pyke, C.B., 1972, Some meteorological aspects of the seasonal distribution of precipitation in the western United States and Baja California: University of California, Water Resources Center, Contribution 139.
- Schulman, E., 1947, Tree-ring hydrology in southern California, Tucson, Arizona: Tucson, AZ, University of Arizona, Laboratory of Tree-Ring Research Bulletin 4, 36p.
- Smith, G.I., Friedman, I., Klieforth, H., Hardcastle, K., 1979, Areal distribution of Deuterium in eastern California precipitation, 1968-1969: *Journal of Applied Meteorology*, v.18, p.172-188.
- Starret, L.G., 1949, The relation of precipitation patterns in North America to certain types of jet streams at the 300-millibar level: *Journal of Meteorology*, v.6, p.347-352.
- U.S. Department of Commerce, 1969, 1978, 1980, 1983, Daily Weather Maps.
- Wagner, A.J., 1969, The weather and circulation of January 1969; Continued strong high-latitude blocking and flood-producing rains in California: *Monthly Weather Review*, v.97, p.351-358.
- Weaver, R.L., 1962, Meteorology of hydrologically critical storms in California: U.S. Weather Bureau, Hydrometeorological Report 37, 207p.
- Wells, S.G., McFadden, L.D., Dohrenwend, J.C., Bullard, T.F., Feilberg, B.F., Ford, R.L., Grimm, J.P., Miller, J.R., Orbock, S.M., and Pickle, J.D., 1984, Late Quaternary geomorphic history of the Silver Lake area, eastern Mojave Desert, California, in Dohrenwend, J.C., ed., *Surficial geology of the eastern Mojave Desert, California: Geological Society of America 1984 Annual Meeting Field Trip 14 Guidebook*, p.69.
- Wells, S.G., Anderson, R.Y., McFadden, L.D., Brown, W.J., Enzel, Y., and Miossec, J.L., 1989, Late Quaternary paleohydrology of the eastern Mojave River drainage, southern California: Quantitative assessment of the late Quaternary hydrologic cycle in large arid watershed: New Mexico Water Resources Research Institute, Technical Completion Report, Project 1423686.

Holocene History of the El Niño Phenomenon As Recorded in Flood Sediments of Northern Coastal Peru

L.E. Wells

ABSTRACT: The Holocene history of flooding in northern coastal Peru is believed to be a proxy record for the El Niño phenomenon. A recently completed set of 30 radiocarbon dates on overbank flood deposits and a tsunami deposit from the Casma region (Figure 1 and Table 1) establishes a chronology for the largest events that have occurred during the last 3500 years. The El Niño phenomenon is an episodic event that perturbs the ocean/climate system of the Pacific basin and is believed to be related to anomalous weather patterns worldwide (Rasmusson and Wallace, 1983). An increased understanding of the magnitude variations and the long-term frequency of the El Niño phenomenon will provide a better understanding of the nature and causes of the El Niño/Southern Oscillation phenomenon. The data presented here indicate that events much larger than the one in 1982-1983 may occur with a frequency of about once every 1000 years.

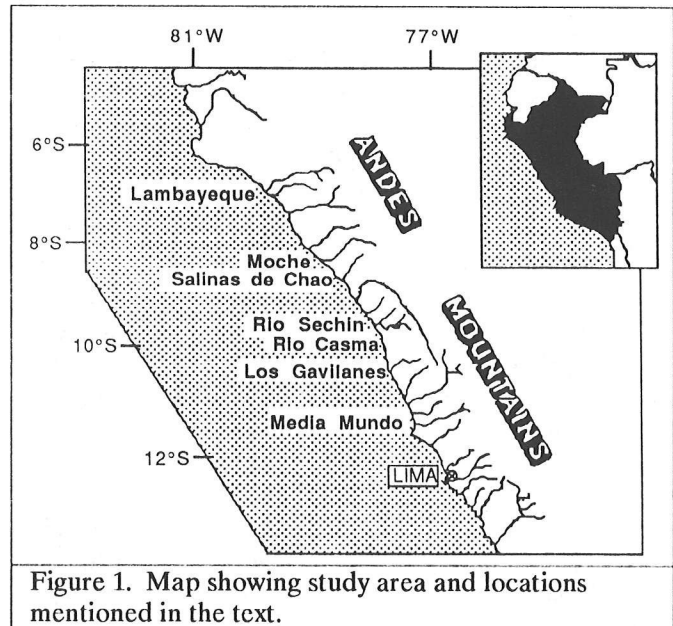
INTRODUCTION

The desert climate of the Peruvian coast is responsible for a direct correspondence between flood events and the El Niño phenomenon. The hyperarid climate is controlled by the location of the South Pacific anticyclone, the rain-shadow effect of the Andes, and the location of the cold Peru/Chile Current. It is only during El Niño events, when the South Pacific anticyclone weakens and the northern boundary of the Peru/Chile current migrates south (Rasmusson and Wallace, 1983), that significant precipitation is able to reach the coastal zone.

At Casma (Figure 1), annual precipitation has averaged 4.2 ± 2.0 mm during the last 20 years; during 1983 an annual precipitation of 42.4 mm was recorded here. There is a large orographic gradient to the precipitation during the El Niño events, and most of the flooding is induced by precipitation that falls upstream of the area studied. There is also a latitudinal gradient of rainfall, with more northerly areas receiving more frequent and larger rainfall than areas to the south. At Casma (9.5°S) precipitation data indicates that flooding occurs during all events of the magnitude of 1982-1983 or larger.

FLOOD SEDIMENTS

Flood sediments of the 1982-1983 El Niño event were studied to characterize an El Niño alluvial deposit



(Wells, 1987). Sedimentary structures indicate that depositional processes ranged from sheet floods to debris flows. The 1982-1983 deposits were recognized by the pristine preservation of surface textures, burial of live trees and plants, and burial and reworking of recent artifacts or of recently plowed fields. Field comparison of the surface geomorphology before and after flooding showed that about 30 percent of the flood plain was reworked during the winter of 1983.

Pre-1982-1983 deposits of the overbank flood plain are sedimentologically identical to 1982-1983 deposits, indicating similar depositional origins (Wells, 1987, 1988). Individual flood deposits are typically fining-upward silty-sand beds separated by mud-cracked silt layers, agricultural soils, and/or eolian sand sheets. The sediments bury archaeological sites and include reworked prehistoric artifacts and abundant charcoal. Deposits were tentatively dated in the field on the basis of the included artifacts and the inset stratigraphy of the fluvial terraces. Conventional and atomic mass spectrometer radiocarbon dates, together with field relationships, resulted in the stratigraphy presented in Table 1 and Figure 2. The radiocarbon dates have been corrected for $\delta^{13}\text{C}$ variations and calibrated using the dendrochronologic time scale.

Table 1. Radiocarbon-dated El Niño events.

Location	Laboratory Number	Material	Calibrated Age ¹	Event Date
Rio Casma	SMU-1861	Wood	139.2% Modern	1957-1958 ²
Rio Casma	ETH-3483	Charcoal	136.6% Modern	1957-1958 ²
Rio Casma	SMU-1955	Peat	129.2% Modern	1957-1958 ²
Que. Tomeque	ETH-3924	Charcoal	101.8% Modern	1957-1958 ²
Rio Sechin	ETH-3919	Charcoal	100.3% Modern	1957-1958 ²
Rio Casma	ETH-3922	Charcoal	AD 1880-1980	AD 1925 ²
Rio Casma	SMU-1860	Wood	AD 1813-1919	AD 1891 ²
Rio Casma	ETH-3920	Charcoal	AD 1680-1880	AD 1828 or 1878 ²
Rio Casma	ETH-3917	Charcoal	AD 1660-1860	AD 1791 ²
Rio Casma	ETH-3921	Charcoal	AD 1640-1840	AD 1791 ²
Rio Casma	ETH-3484	Charcoal	AD 1631-1810	AD 1728 ²
Rio Casma	ETH-3918	Charcoal	AD 1670-1870	AD 1728 ²
Rio Casma	SMU-1938	Charcoal	AD 1665-1808	AD 1728 or 1791 ²
Que. Rio Seco	SMU-1694	Wood	AD 1662-1801	AD 1728 or 1791 ²
Que. Rio Seco	SMU-1696	Wood	AD 1638-1810	AD 1728 or 1791 ²
Rio Sechin	ETH-3485	Charcoal	AD 1651-1813	AD 1728 or 1791 ²
Rio Sechin	ETH-3482	Charcoal	AD 1651-1886	AD 1728 or 1791 ²
Salinas de Chao	A-3279	Driftwood	AD 1508-1655	AD 1618 ²
Los Gavilanes	SMU-1752	Driftwood	AD 1470-1627	AD 1618 ²
Media Mundo	SMU-1753	Driftwood	AD 1521-1658	AD 1618 ²
Rio Sechin	ETH-3486	Charcoal	AD 1486-1668	AD 1578 ^{2,3}
Rio Casma	SMU-1693	Wood	AD 1434-1474	~ AD 1450
Rio Casma	SMU-1935	Charcoal	AD 1441-1483	~ AD 1450
Rio Sechin	SMU-2002	Charcoal	AD 1296-1453	~ AD 1450
Rio Casma	ETH-3916	Charcoal	AD 1270-1390	AD 1325 ⁴
Rio Casma	SMU-1940	Charcoal	AD 1282-1389	AD 1325 ⁴
Que. Rio Seco	SMU-1669	Wood	AD 1220-1460	AD 1325 ⁴
Rio Casma	SMU-1963	Charcoal	130 BC-AD130	~ AD 0
Que. Rio Seco	SMU-1692	Wood	1211-1315 BC	~ 1200 BC ⁵
Rio Casma	ETH-3915	Charcoal	1140-1400 BC	~ 1200 BC ⁵

¹ Post-modern radiocarbon dates calibrated according to curve in Baker et al. (1985). Other radiocarbon dates corrected for $\delta^{13}C$ variations and calibrated according to the dendrochronologic time scale.

² Corresponds to event dated by Quinn et al. (1987).

³ Corresponds to event dated by Rowe (1948).

⁴ Corresponds to event dated by Pozorski (1987).

⁵ Corresponds to event dated by Wells (1987, 1988).

FLOOD STRATIGRAPHY AND EL NIÑO HISTORY

A total of 34 samples were submitted for radiocarbon dating. Samples included detrital charcoal and wood, buried plant material from between individual flood sheets, and organic material from buried agricultural soil horizons. Three of the radiocarbon dates are from driftwood samples, collected over 3° of latitude (8-11°S). These samples were deposited by a tsunami during the 1618 AD El Niño (Wells and DeVries, 1987). Four of the 31 fluvial samples were determined to yield inappropriate dates, demonstrated by stratigraphic reversals. The anomalously old dates probably result from inclusion of old detrital carbon.

Event dates for historical times (post-AD 1578) were determined by comparing the precision of the calibrated radiocarbon ages with the historical dates compiled by Quinn (1987) and then choosing the largest event that occurred within the 1 σ error range. Five of these eight events yielded multiple dates from samples collected at different locations within the flood plain. Four prehistoric events are dated, three of which yielded multiple dates. The AD 1325 event is probably the same event recorded ethnohistorically and referred to as Nyamlaps flood (Rowe, 1945; Pozorski, 1987). Multiple dates from widely separated regions of the flood plain and the close correspondence of these dates with the historical record indicate that radiocarbon dating is a valid way of determining dates for prehistoric El Niño events.

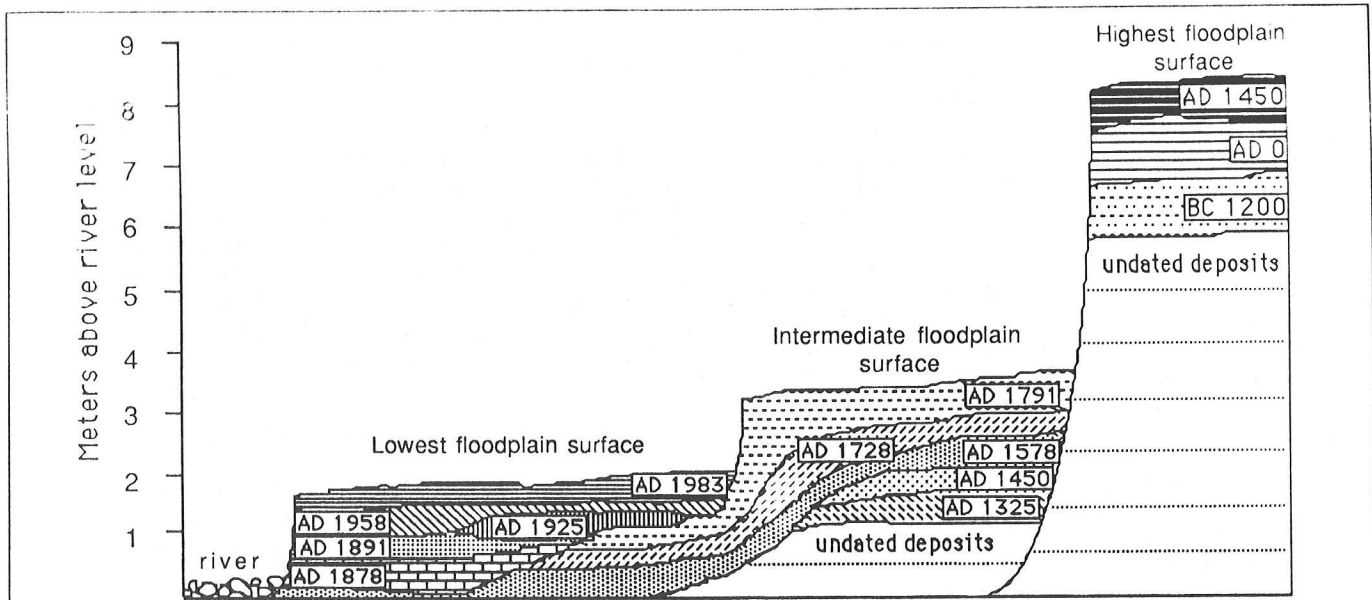


Figure 2. Flood plain surfaces and deposits of the Rio Casma area. The dates shown are hypothesized event dates (see Table 1) for individual flood events. Note overlapping stratigraphy for lowest to intermediate surface. Base of the section below highest flood plain surface is believed to be ~ 7500 years old (Wells, 1988).

The apparent change in the frequency of El Niño events (Figure 3) is most likely due to the nature of the stratigraphic record rather than to an actual frequency change. Three distinct flood plain levels have been identified on the Holocene flood plain (Figure 2):

- The youngest surface (average height 2.0 m) includes sediments of the eight most recent flood events and yields a frequency of one event every 36 years.
- The middle surface (average height 3.5 m) records events 6 through 11 (sans event 10) and yields a frequency of one event every 100 years.
- The oldest surface (average height 7.5 m) records events 10 through 12 (sans event 11), and yields a frequency of one event every 1060 years.

The difference in the height of the flood plain surfaces indicates that a threshold water level must be reached before new deposition takes place on each progressively higher surface. We are looking, therefore, through a geomorphologic filter that separates the stratigraphic record of events with different magnitudes. The largest events (1/1000 years) probably destroy the record of younger events. The basal and undated stratigraphy of the highest flood plain surface includes a minimum of seven large flood events prior to AD 1450. The base of the section is believed to correspond to Holocene stabilization of sea level that initiated backfilling of river valleys at c. 7500 YBP. This sequence, therefore, further indicates an average recurrence interval of about once every 1000 years for the largest Holocene flood events.

The cause of these large flood events is not clear. The 1982-83 El Niño event was the largest during recorded history. It left deposits on only the youngest flood plain surface. Two scenarios can be envisioned that could explain the frequency of the largest events:

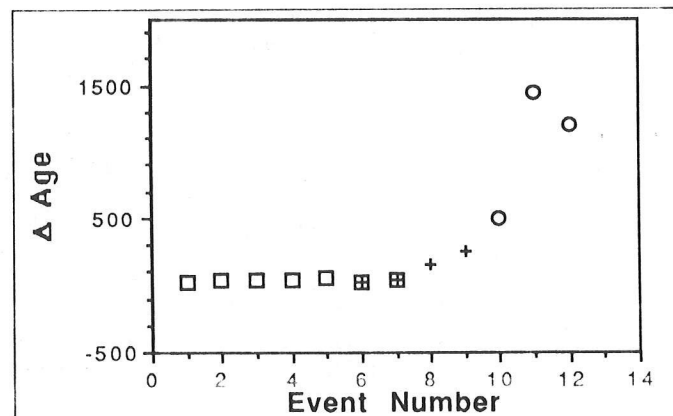


Figure 3. Change in frequency of flood events with time. Change in event frequency from c. 1/1000 years to c. 1/36 years is believed a result of the geomorphologic filter that separates events of various magnitudes. Events represented with: (○) are preserved on the highest terrace; (+) are on the intermediate terrace; (□) are on the lowest terrace (see text and Figure 2). Δ age refers to difference in years between sequential flood events. Event numbers are used rather than actual age dates on the abscissa: event 1 represents time difference between the two most recently dated events (AD 1983 and AD 1958); event 12 represents the time between the two oldest events (AD 0 and 1200 BC).

- “Mega El Niño events” exist that cause major devastation in coastal Peru and perhaps worldwide, and
- Once every 1000 years rainfall associated with El Niño events concentrates in the Casma area, causing large-scale flooding.

If the largest El Niño events recorded at Casma are global-scale events, they would have caused major societal impacts. These events would result in a loss of most of the agricultural area in coastal Peru as well as any human development on the flood plain. In comparing the flood date list (Table 1) with archaeological record, it appears the two oldest El Niño events occur at about the times of the transitions between major archaeological periods:

- The 1200 BC event occurs during the transition from the Initial Period to the Early Horizon (c. 900-1400 BC) (Lanning, 1967; Rowe and Menzel, 1948) when the Chavin culture spread its influence from the highlands into the coastal zone.
- The AD zero event occurs near the estimated transition from the Early Horizon to the Early Intermediate Period (c. 200-400 BC) (Lanning, 1967; Rowe and Menzel, 1948); during this time a large coherent culture broke down and the coastal zone became controlled by small political entities.
- The AD 1325 event is believed to correspond to Nyamlaps flood (Rowe, 1945; Pozorski, 1987). This ethno-historically recorded flood caused the breakdown of the Dynasty of Nyamlap and the subsequent invasion of the Lambayeque region by the Chimu Dynasty, a large power base centered to the south, in the Moche valley.

All of these societal changes record a region outside the area of flood devastation gaining political control over regions affected by the floods or in the breakdown of a large political entity in the flooded zone. These data indicate that the flood events recorded here are large-scale disasters that affected the entire northern coastal zone of Peru and that, if repeated, may have global implications. A crucial test will be the dating of a sequence of flood deposits from other coastal valleys in Peru to document the regional nature of contemporaneous flooding and the correlation of these large events with extreme climate events, as recorded historically or geologically, in other regions of the globe.

ACKNOWLEDGMENTS

This work was supported by NSF, Division of Earth Sciences, under grant EAR-8503886 and by the National Center for Atmospheric Research. I thank Professor Herb Haas for the radiocarbon analysis. El Servicio Nacional de Meteorología e Hidrología del Perú provided the precipitation data. I acknowledge Professor Tjeerd van Andel and Jay Noller for their critiques and support in this project, and would like to thank Larry Benson for his thorough review of the manuscript.

REFERENCES

- Baker, V.R., Pickup, G., and Polach, H.A., 1985, Radiocarbon dating of flood events, Katherine Gorge, Northern Territory: *Geology*, v.13, p.344-347.
- Lanning, E.P., 1967, *Peru Before the Incas*: New Jersey, Prentice-Hall, p.216.
- Pozorski, T., 1987, Changing priorities in the Chimú state: The role of irrigation agriculture, in Haas, J., Pozorski, S., and Pozorski, T., editors, *The Origins and Development of the Andean State*: Cambridge, Cambridge University Press, p.111-120.
- Quinn, W.H., Neal, V.T., and Antunez de Mayolo, S.E., 1987: El Niño occurrences over the past four and a half centuries: *Journal of Geophysical Research*, v.92, p.14,449-14,461.
- Rasmusson, E.M., and Wallace, J.M., 1983: Meteorological aspects of the 1982/1983 El Niño/Southern Oscillation episode: *Science*, v.222, p.1195-1202.
- Rowe, J.H., 1945: Absolute chronology in the Andean area: *American Antiquity*, v.10, p.267-284.
- Rowe, J.H., 1948: The kingdom of Chimor: *Acta Americana*, v.6, p.26-59.
- Rowe, J.H., and Menzel, D., 1967: Introduction, in Rowe, J.H. and Menzel, D., editors, *Peruvian Archaeology, Selected Readings*: Palo Alto, CA, Peek Publications, p. v-x.
- Wells, L.E., 1987, An alluvial record of El Niño events from northern coastal Peru: *Journal of Geophysical Research*, v.92, p.14,463-14,470.
- Wells, L.E., 1988, Holocene fluvial and shoreline history as a function of human and geological factors in arid northern Peru: Ph.D. dissertation, Stanford University, Stanford, CA, 381pp.
- Wells, L.E., and DeVries, T.J., 1987, Driftwood deposits of the AD 1618 tsunami, northern coastal Peru: *Geological Society of America Abstracts with Programs*, v.19, p.885.

Changes in Mid-Troposphere Snow Accumulation on Mt. Logan, Yukon, over the Last Three Centuries

Gerald Holdsworth

ABSTRACT: A net snow accumulation time series is presented. It is derived from a 102.5 m ice core retrieved from Mt. Logan at an altitude of 5340 m a.s.l. Annual increments are identified using stable isotopes, trace chemistry, and beta activity. An absolute time scale is constructed using the chemical signatures of volcanic events. Annual layers are converted to water equivalent using the measured density profile. Corrections are applied for ice deformation and the surface snow accumulation gradient. The resulting time series of nearly 300 years seems to indicate a lower mean accumulation from AD 1700 to the mid-19th century than after that time. The last 100 years of the series correlates significantly with certain instrumental station records at mid-northern latitudes.

INTRODUCTION

In 1980, a 102.5 m glacier core was retrieved from a site at 5340 m on Mt. Logan (60°35'N; 140°35'W; 5951 m), Yukon, Canada. With update to 1987, the core spans almost 300 years. The data are in the form of:

- $\delta^{18}\text{O}$ (δD) time series, usually assumed to represent proxy temperature information, and
- The net snow accumulation time series.

To correctly interpret the results, particular attention must be paid to the fact that the core site is located in the middle troposphere above the lower frictional boundary layer. An initial ice flow model time scale for the core was calibrated using the chemical signatures of volcanic events as time markers. Isotopic and certain trace chemical signatures were used to identify seasonal and, hence, annual layers. Beyond the depth where stable isotopes become unreliable (60 m), seasonal signatures are solely identified by nitrate ion variations.

STABLE ISOTOPE TIME SERIES

Vertical profiles of stable isotopes on Mt. Logan and nearby Mt. Steele over an altitude range of 4100 m define the upper limit of the lower boundary layer to be at about 3350 m. Above this is a mixed (iso- δ) layer reaching to the upper plateau at about 5300 m. This mixed layer is evidently created by wind shear, which blends boundary layer moisture with moisture from the free troposphere (geostrophic flow region) that begins at the level of the upper plateau. Upper air wind data

have been used to arrive at this interpretation. Vertical variations in this precipitation structure will cause a spurious signal to be built into the $\delta^{18}\text{O}$ time series. This will be added to signals due to storm track length variations (Covey and Haagenson, 1984), the rate of delivery of precipitation to the site, and the temperature effect (Dansgaard et al., 1973).

As a result, the time series is difficult to interpret, although sections of it appear to be closely related to air temperature by comparing it with a tree-ring width time series from the northern Yukon (Jacoby and Cook, 1981). This series correlates with regional air temperature. The two dendro-climatological coldest periods virtually coincide with two isotopic minima at ca. AD 1715-1725 and ca. AD 1850-1855. The latter period probably includes the year of "two winters" recorded in Indian legend throughout the Yukon (Cruikshank, 1981). A substantial volcanic acid signal at 70 m depth in the core is believed to correspond to the eruption of Chikurachki-Tartarinov in the Kurile Islands in 1850-1855 (Simkin et al., 1981). In the same way that the "year without a summer" in 1816 was linked (Stommel and Stommel, 1983) to a volcanic event (the eruption of Tambora), it is possible that the "two winters" episode was a result of reduced surface isolation caused by the dust and acid gas cloud from the North Pacific rim eruption in 1853-1855. Paleoclimatic evidence for the "year without a summer" (1816) is not seen in either the Mt. Logan stable isotope record or in the northern tree ring chronology of Jacoby and Cook (1981), even though the acid signal from Tambora is quite clear in the ice core data. These results emphasize the fact that such events may affect only certain regions, rather than being uniformly distributed throughout a hemisphere.

NET ACCUMULATION TIME SERIES

Annual increments identified in the core have been corrected for effects of ice deformation and for an accumulation gradient across the core site. Below a depth of 97 m (AD 1736) annual increments become difficult to define using current methods of sampling. Figure 1 shows the net accumulation time series. It is of great importance to know the reliability of this series before it is used for climatological or hydrological modeling.

An estimated error from AD 1950 to 1987 is 0.01 m. The corrections for ice deformation are negligible until a depth of about 65 m is reached. At this depth, grain

In J.L. Betancourt and A.M. MacKay, editors, 1990. Proceedings of the Sixth Annual Pacific Climate (PACLIM) Workshop, March 5-8, 1989: California Department of Water Resources, Interagency Ecological Studies Program Technical Report 23.

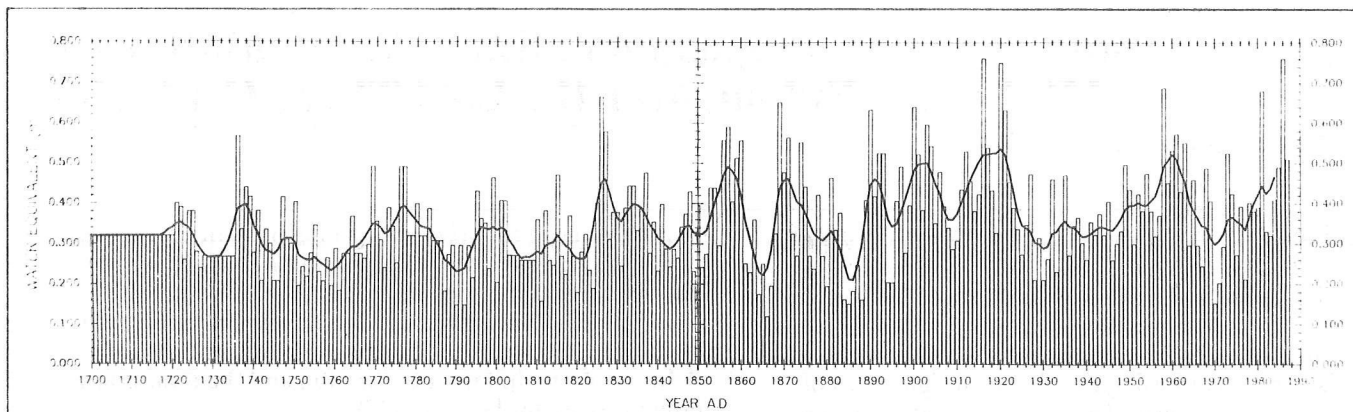


Figure 1. Time series of net snow accumulation, in meters of water equivalent, at 5340 m altitude on Mt. Logan.

compaction and diagenesis have caused layer thinning and have produced "ice" of density 0.83 mg m^{-3} . Further slow densification occurs as the ice flows outward to cause progressive creep thinning of layers. The layer thinning correction, the largest one to be applied, together with corrections for layer tilt and for the gradient of accumulation across the core site, account for a total error of about 0.04 m at a depth of about 101 m (AD 1700). To this must be added the estimated error (0.01 m) for layer misidentification. Thus a total estimated error of 0.05 m applies at the lower end of the series.

Calibration against Instrumental Data

Cross correlation with low level Yukon and Alaska station data yields statistically insignificant results. On the other hand, several significant, positive long-distance correlations (teleconnections) exist. These include parts of the western prairie region of North America, the steppe region of the Soviet Union (Budyko, 1977), and Japan, where the mean of five major station precipitation time series — when compared with the Mt. Logan accumulation series from AD 1890 to 1985 — show a correlation coefficient $r = 0.6$, significant at the 95% level. Such a result may be due to:

- Location of the core site in the middle troposphere,
- Proximity of these sites to the limits of the circumpolar vortex,
- Their proximity to the preferred tracks of Rossby waves, and
- The trajectories of major cyclones.

An ocean/atmosphere interaction is also implied.

Figure 2 shows some elements of the north Pacific climate system that are likely to be responsible for the climate of Mt. Logan. Significant positive correlations between sea surface temperatures and the snow accumulation series exist over extensive peripheral regions of the north Pacific.

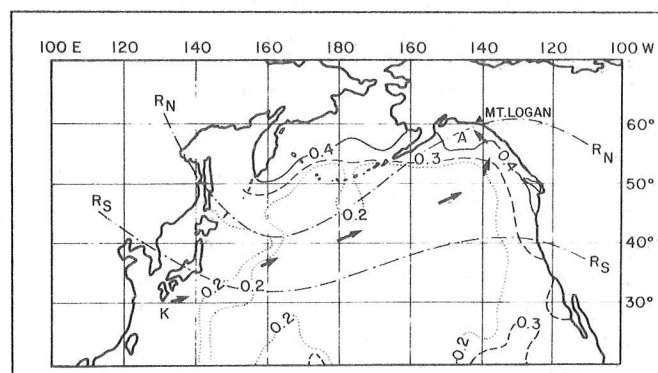


Figure 2. North Pacific sector showing approximate position of the northern and southern limits (R_N , R_S respectively) of the preferred Rossby wave tracks, the Kuroshio current (K), Alaska current (A), and iso-lines of the cross correlation coefficients (0.2 to 0.4) between Mt. Logan net accumulation series and sea surface temperature series.

Spectral Analysis

Power spectra have been produced for the full (250-year) time series and its two halves. Several physically significant peaks occur at frequencies corresponding to periods of 3.8, 10.9, and 15 to 22 years. These periods may be associated with the El Niño/Southern Oscillation (Quinn et al., 1987), the quasi-periodic sunspot cycle, and possibly the lunar M_N tidal period (Currie, 1984) and/or the 20-year period signal of Hibler and Johnsen (1979). The statistical significance of these peaks is marginal at the 90% level, but the integrity of at least the 10.9-year peak has been verified by generating the waveform in the time domain and comparing it with the Zurich sunspot number waveform. For such results to occur, the time scale of Figure 1 must be essentially correct. This implies also that the snow accumulation data are essentially correct.

DISCUSSION OF RESULTS

For the early half of the series, some uncertainty does exist in identification of some individual annual layers; therefore, a safer series would be one produced by using a 2-year filter. The 7-year triangular filter applied to the original data set (Figure 1) more than compensates for the +1 year error in occasional layer misidentification.

Two immediate observations can be made:

- The mean net accumulation rate for the early half of the series (0.31 m yr^{-1}) is significantly lower than the corresponding value (0.37 m yr^{-1}) for the more recent half.
- The variance of the early half is significantly less than that of the more recent half.

These changes took place over the latter half of the 19th century, which may coincide with the end of the Little Ice Age (LIA) for this region. According to Denton and Stuiver (1969), late Neoglacial advances in the St. Elias Mountains terminated during this period. Evidence from a drowned forest in Lake Kluane (Bostock, 1969), northeast of the St. Elias Mountains, indicates lake levels were substantially lower during the LIA than now. This implies that snow and ice melt runoff was lower during the LIA than it has been this century. Whereas such a result can be attributed to lower air temperatures during the LIA, it could also be attributed to lower snowfall in the St. Elias Mountains region. This, in turn, can be linked to lower north Pacific sea surface temperatures.

REFERENCES

- Bostock, H.S., 1969, Kluane Lake: Its drainage and allied problems. Ice-field Ranges Research Project: Scientific Research, v.1, p.149-160.
- Budyko, M.I., 1977, Climatic changes: Washington, DC, American Geophysical Union.
- Covey, C., and Haagenson, P.L., 1984, A model of oxygen isotope composition of precipitation: Implications for paleoclimate data: *Journal of Geophysical Research*, v.89, (D3), p.4647-4655.
- Cruikshank, J., 1981, Legend and landscape: convergence of oral and scientific traditions in the Yukon Territory: *Arctic Anthropology*, v. XVIII-2, p.67-93.
- Currie, R.G., 1984, Periodic (18.6-year) and cyclic (11-year) induced drought and flood in western North America: *Journal of Geophysical Research*, v.89, (D5), p.7215-7230.
- Dansgaard, W., Johnson, S.J., Clausen, H.B., and Gundestup, N., 1973, Stable isotope glaciology: *Medd. om Grønland*, v.197 (2), København, C.A. Reitzels Forlag.
- Denton, G.H., and Stuiver, M., 1969, Neoglacial chronology, northeastern St. Elias Mountains, *in* Icefield ranges research project: Scientific Research, v.1, p.173-186.
- Hibler, W.D., and Johnsen, S.J., 1979, The 20-year cycle in Greenland ice core records: *Nature*, v.280, p.481-483.
- Jacoby, G.C., and Cook, E.R., 1981, Past temperature variations inferred from a 400 year tree ring chronology from Yukon Territory, Canada: *Arctic and Alpine Research*, v.13, p.409-418.
- Quinn, W.H., Neal, V.T., and Antunez de Mayola, Santiago E., 1987, El Niño occurrences over the past four and a half centuries: *Journal of Geophysical Research*, v.92, (C13), p.14449-14461.
- Simkin, T., Sieberg, L., McClelland, L., Bridge, D., Newhall, C., and Latter, J.H., 1981, *Volcanos of the world*: Stroudsburg, PA, Hutchinson Ross Publishing Company.
- Stommel, H., and Stommel, E., 1983, *Volcano weather: The story of the year without a summer, 1816*: Newport, RI, Seven Seas Press.

1. The first part of the document discusses the importance of maintaining accurate records of all transactions. It emphasizes that every entry should be supported by a valid receipt or invoice to ensure transparency and accountability.

2. The second section outlines the procedures for handling discrepancies between the recorded amounts and the actual cash flow. It suggests a systematic approach to identify the source of the error and correct it promptly to avoid any financial misstatements.

3. The third part of the document addresses the role of internal controls in preventing fraud and misappropriation of assets. It highlights the need for a strong internal control system that includes segregation of duties and regular audits.

4. The fourth section discusses the impact of external factors, such as market fluctuations and regulatory changes, on the organization's financial performance. It advises the management to stay informed and adapt their strategies accordingly to mitigate risks.

5. The fifth part of the document focuses on the importance of communication and reporting. It stresses that clear and concise financial reports are essential for providing stakeholders with the information they need to make informed decisions.

6. The sixth section discusses the role of technology in modern financial management. It highlights how software solutions can streamline processes, reduce errors, and provide real-time insights into the organization's financial health.

7. The seventh part of the document addresses the importance of ethical considerations in financial reporting. It emphasizes that honesty and integrity are fundamental to building trust and maintaining the organization's reputation in the market.

8. The eighth section discusses the role of the board of directors in overseeing the organization's financial performance. It highlights the board's responsibility to ensure that the management is acting in the best interests of the shareholders and the organization as a whole.

9. The ninth part of the document addresses the importance of continuous improvement in financial management. It suggests that the organization should regularly review its financial processes and seek opportunities for optimization to enhance efficiency and effectiveness.

10. The final section of the document provides a summary of the key points discussed and offers some concluding thoughts on the importance of sound financial management for the long-term success of the organization.

CONVERSION FACTORS

Quantity	To Convert from Metric Unit	To Customary Unit	Multiply Metric Unit By	To Convert to Metric Unit Multiply Customary Unit By
Length	millimetres (mm)	inches (in)	0.03937	25.4
	centimetres (cm) for snow depth	inches (in)	0.3937	2.54
	metres (m)	feet (ft)	3.2808	0.3048
	kilometres (km)	miles (mi)	0.62139	1.6093
Area	square millimetres (mm ²)	square inches (in ²)	0.00155	645.16
	square metres (m ²)	square feet (ft ²)	10.764	0.092903
	hectares (ha)	acres (ac)	2.4710	0.40469
	square kilometres (km ²)	square miles (mi ²)	0.3861	2.590
Volume	litres (L)	gallons (gal)	0.26417	3.7854
	megalitres	million gallons (10 ⁶ gal)	0.26417	3.7854
	cubic metres (m ³)	cubic feet (ft ³)	35.315	0.028317
	cubic metres (m ³)	cubic yards (yd ³)	1.308	0.76455
	cubic dekametres (dam ³)	acre-feet (ac-ft)	0.8107	1.2335
Flow	cubic metres per second (m ³ /s)	cubic feet per second (ft ³ /s)	35.315	0.028317
	litres per minute (L/min)	gallons per minute (gal/min)	0.26417	3.7854
	litres per day (L/day)	gallons per day (gal/day)	0.26417	3.7854
	megalitres per day (ML/day)	million gallons per day (mgd)	0.26417	3.7854
	cubic dekametres per day (dam ³ /day)	acre-feet per day (ac-ft/day)	0.8107	1.2335
Mass	kilograms (kg)	pounds (lb)	2.2046	0.45359
	megagrams (Mg)	tons (short, 2,000 lb)	1.1023	0.90718
Velocity	metres per second (m/s)	feet per second (ft/s)	3.2808	0.3048
Power	kilowatts (kW)	horsepower (hp)	1.3405	0.746
Pressure	kilopascals (kPa)	pounds per square inch (psi)	0.14505	6.8948
	kilopascals (kPa)	feet head of water	0.33456	2.989
Specific Capacity	litres per minute per metre drawdown	gallons per minute per foot drawdown	0.08052	12.419
Concentration	milligrams per litre (mg/L)	parts per million (ppm)	1.0	1.0
Electrical Conductivity	microsiemens per centimetre (µS/cm)	micromhos per centimetre	1.0	1.0
Temperature	degrees Celsius (°C)	degrees Fahrenheit (°F)	(1.8 × °C) + 32	(°F - 32) / 1.8

